New modeling and control strategies for reducing disease impact in greenhouses

Ph.D. in Computer Science

UNIVERSITY OF ALMERÍA

Author:
Ran Liu
Supervisors:
Prof. José Luis Guzmán Sánchez

Almería, November 2022

Ph.D. Thesis

New modeling and control strategies for reducing disease impact in greenhouses

Nuevas estrategias de modelado y control para la reducción del impacto de enfermedades en invernaderos

University of Almería

Department of Informatics

Ph.D. in Computer Science (RD99/11)

Author:

Ran Liu

Supervisor:

José Luis Guzmán Sánchez

Almería, November 2022

Acknowledgment

When I was studying for a master's degree in NERCITA, Beijing, Prof. Yang and Li Ming invited José Luis Guzmán for a visit. I was asked to wait for José Luis and his wife Aurelia at the airport with a driver. There were many people and I held a piece of blank paper with his name on it, to avoid missing it. But in the end, I could easily identify him according to the photo. He gave lectures for several days and I was deeply impressed by his introduction to UAL and the group TEP-197. We went to the Great Wall, the Summer Palace, the Forbidden City, etc. At that time, I realized he was a young and promising academic with a good personality. When I graduated from my master's degree, I decided to go to UAL to be his Ph.D. student.

During my three years as a Ph.D. student, my supervisor José Luis never lost his temper with me. He always encouraged me and made me think that I am excellent. When one manuscript was rejected, he used to say me that this is a very common situation, and we should continue working and try again in a new journal. He pays for coffee every time. I was invited to Gádor for a visit. I was very grateful because the route was carefully planned. When I encountered the problem of applying for residence, he told me not to have any worries, and that he would take care of everything. When doing the research, I often put forward models that are difficult to implement. He helped me to solve the technical problems in MATLAB with very high efficiency. I respect his every idea and try to make them come true. Finally, we published all the ideas as good journal papers. These experiences were very cool. I hope to see him and his family, Aurelia, Jimena and Julieta soon in China.

Thanks to Prof. Li Ming in NERCITA (National Engineering Research Center for Information Technology in Agriculture) for his full support of my research. He gave me great freedom and authority in the arrangement of the experiments. He likes to introduce me to his life experience in Almería. Near graduation, he often sent me recruitment information to help me find the best job. I am very lucky that the tutors I met are all kind and simple people. With their support, I can study with ease. They are my wealth.

Thanks to Manuel Berenguel for his support. I could ask him any questions every time we have met. He is used to answering me very patiently. I felt his kind heart and encouragement to us. Thanks to Fernando Bienvenido for helping me to solve a series of problems concerning admission, registration, and visa. With his help, I can study and work in Spain without any worries as a foreigner. The first time I applied for a NIE card, Fernando drove me to the immigration office. There were many people there. We waited for a long time, and he was sweating all over. I'm very sorry. Thanks to Francisco Rodríguez Díaz and Jorge Antonio Sánchez, I have the honor to discuss research with them. We have similar research fields. They are experts in this field. I can learn a lot from them.

Thanks to Ángeles Hoyo Sánchez, Pablo Otálora Berenguel, Francisco García

Mañas, Marta Barceló Villalobos, Igor Pataro, Juan Diego Gil, Jerónimo Ramos, and María for their help in my life. Because of the language problem, I was worried about many things, including renting a house, making an appointment for a vaccine, handling residence, making an appointment for a doctor, and recommending food. Whenever I ask them for help, they always give me the best help. Thanks to NERCITA's colleagues Zhang Chunhao, Liu Jian, and Liu Kaige for their support of my experimental data. I would like to thank Wang Hui for telling me about her experience studying in Spain. Thanks to my family for their support in my Ph.D. I have been abroad for many years and my family never complains and often asks me about difficulties in life and study. Thanks to my girlfriend Zhang Chenyang for taking care of me in Spain. She always supports my work and accompanies me when I was sad. Thanks for the financial support of the China Scholarship Council. Finally, I would like to thank Liu Huiying and Shi Weimin, my first teachers at Shihezi University, who inspired me to be very interested in agricultural models and taught me the basic knowledge.

Thank you very much to all,

Liu Ran

Agradecimientos

Cuando estaba estudiando para una maestría en NERCITA, Beijing, los profesores Yang y Li Ming invitaron al profesor José Luis Guzmán. Me pidieron que esperara a José Luis y su esposa Aurelia en el aeropuerto con un chofer. Había mucha gente y sostuve un papel en blanco con su nombre para no perderle. Pero al final, pude identificarlo fácilmente según la foto. Impartió diversas conferencias durante varios días y me impresionó mucho su introducción sobre la UAL y el grupo TEP-197. Fuimos a la Gran Muralla, el Palacio de Verano, la Ciudad Prohibida, etc. En ese momento, pensé que era un académico joven y prometedor con una buena personalidad. Cuando terminé mi maestría, opté por ir a la UAL para ser su estudiante de doctorado.

Durante mis tres años como doctorando, mi tutor José Luis nunca perdió los estribos conmigo. Siempre me animó y me hizo pensar que soy excelente. Cuando un artículo era rechazado, él solía decir que esta es una situación muy común y que deberíamos continuar intentándolo después de revisarlo. Él siempre me invita a café. Fui invitado a Gádor para una visita. Estuve muy agradecido porque la ruta fue cuidadosamente planeada. Cuando me encontré con el problema de solicitar la residencia, me dijo que no me preocupara, que él se encargaría de todo. Durante mi investigación, obtuve modelos que son difíciles de implementar. Me ayudó a resolver los problemas técnicos en MATLAB con una eficiencia muy alta. He respetado todas sus ideas y he tratado de hacerlas realidad. Finalmente, todas han sido publicadas artículos en revista de prestigio. Estas experiencias fueron muy fructíferas e inspiradoras. Espero verlo pronto a él y su familia, Aurelia, Jimena y Julieta, en China.

Gracias al Prof. Li Ming en NERCITA (Centro Nacional de Investigación de Ingeniería para la Tecnología de la Información en la Agricultura) por su total apoyo a mi investigación. Siempre me ha dado gran libertad y autoridad en la organización de los experimentos. Le encanta hablarme y presentarme su experiencia de vida en Almería. Cerca de la graduación, a menudo me enviaba información de reclutamiento para ayudarme a encontrar el mejor trabajo. Tengo mucha suerte de que los tutores que conocí son todos gente amable y sencilla. Con su apoyo, puedo estudiar con tranquilidad. Ellos son mi riqueza.

Gracias a Manuel Berenguel por su apoyo. Desde que lo he conocido he podido preguntarle cualquier cuestión y siempre me ha respondido con mucha paciencia. Sentí su corazón bondadoso y su ánimo hacia nosotros. Gracias a Fernando Bienvenido por ayudarme a resolver una serie de problemas relacionados con la admisión al doctorado, el registro y la visa. Con su ayuda puedo estudiar y trabajar en España sin preocupaciones como extranjero. La primera vez que solicité una tarjeta NIE, Fernando me acompañó a la oficina de inmigración. Había mucha gente allí. Esperamos mucho tiempo y estaba sudando por todas partes. Lo siento mucho. Gracias a Francisco Rodríguez Díaz y Jorge Antonio Sánchez, con quienes tuve el honor de discutir sobre investigación. Tenemos campos de investigación similares. Son expertos en este campo. He podido aprender mucho de ellos.

Gracias a Ángeles Hoyo Sánchez, Pablo Otálora Berenguel, Francisco García Mañas, Marta Barceló Villalobos, Igor Pataro, Juan Diego Gil, Jerónimo Ramos y María por su ayuda en mi vida. Por el problema del idioma, me preocupaban muchas cosas, entre ellas alquilar una casa, solicitar una cita para una vacuna, gestionar la residencia, solicitar una cita para el médico y buscar sugerencias de alimentos. Cada vez que les he pedido ayuda, siempre han estado allí para apoyarme. Agradezco a los colegas de NERCITA Zhang Chunhao, Liu Jian y Liu Kaige por su apoyo a mis datos experimentales. Me gustaría agradecer a Wang Hui por contarme sobre su experiencia estudiando en España. Gracias a mi familia por su apoyo en mi tesis. He estado en el extranjero durante muchos años y mi familia nunca se ha molestado al respecto y, a menudo, me han preguntado sobre las dificultades en la vida y el estudio. Agradecer a mi novia Zhang Chenyang por cuidarme en España. Ella siempre ha apoyado mi trabajo y me ha acompañado cuando he estado triste. Gracias por el apoyo financiero del Consejo de Becas de China. Finalmente, me gustaría agradecer a Liu Huiying y Shi Weimin, mis primeros profesores en la Universidad de Shihezi, quienes me inspiraron a interesarme mucho en los modelos agrícolas y me enseñaron los conocimientos básicos.

Muchas gracias a todos,

Liu Ran

Abstract

The main contribution of this thesis is focused on the reduction of the infection of crop fungal diseases in greenhouses through the use of modeling and control approaches. To complete this task, three independent studies have been developed, namely, a greenhouse climatic model, a greenhouse fungal disease estimator, and a greenhouse climate control algorithm. Finally, combining these models and algorithms, a hierarchical optimization control strategy is proposed to maintain the optimum temperature for cucumber production, but providing priority to the control of disease apparencies. Compared with the current disease management schemes in literature, this new strategy maximizes the accumulated temperature under the condition of reducing diseases, contributing so to reduce the application of chemical pesticides.

For the climatic greenhouse modelling, a transient greenhouse model was developed in 2019 and 2020, which uses a mechanism method to estimate the temperature and humidity in typical Chinese solar greenhouses. A novel and easy-to-use wall temperature estimation method based on the energy balance was adopted for the environment model rather than using boundary temperature measurements. In this way, the number of model inputs is considerably reduced, and the proposed model is able to predict future greenhouse climate conditions by using only the weather forecast. The model validation was performed in two different greenhouses (each with different sizes and physical parameters, such as the greenhouse volume, the roof and wall areas, the wall materials and so on) on three typical days in 2019 and 2020, and over four consecutive weeks in different seasons during 2016 and 2019. Promising results were obtained and the model performed well in different operating modes; these included having the vents completely closed, opening the vents, and completely closing the vents in the cold season with an additional thermal insulation blanket covering. The validation results demonstrated that the proposed model can be widely adapted to different sizes of typical Chinese solar greenhouses, as well as to different weather conditions. Thus, the developed model is a flexible and valuable tool that can be used for greenhouse climate simulation, temperature and humidity control, and as a decision-making support system to help in the management of solar greenhouses.

To improve the natural ventilation model for the previous greenhouse climate model, a regression-trees natural ventilation model was developed using results from one thousand samples by Computational Fluid Dynamics (CFD) calculations. This model perfectly deals with the combined effect of wind pressure and thermal gradients. This regression-trees natural ventilation model was embedded in the greenhouse climate model and was validated for a 7-day simulation study with promising results.

For disease predictions, taking cucumber downy mildew as an example, a new approach was proposed by combining the mechanism greenhouse climate model and a disease model for the forecast of diseases occurrence in greenhouses. The method was evaluated in NPADB (National Precision Agriculture Demonstration Base), Beijing,

China using data collected from transplanting to the primary infection occurred in the greenhouse, in the spring season of 2021. First, the dynamic climatic model is used to predict the greenhouse indoor climate 72 hours ahead. Then, this prediction is used as input to the disease model in order to detect disease occurrence in advance. The predictions for the greenhouse downy mildew were compared using real-time measured data for two months. After several false positive reports, one positive report by both methods fitted the first observation in the greenhouse on April 24, 2021. Thus, a relevant contribution was developed in this topic where the early warning cucumber downy mildew was obtained via coupling climate and disease models, where only transient inputs from weather forecast are required.

Regarding the control contributions, first, a selective event-based control approach was proposed to regulate the temperature and the humidity by using the natural ventilation as unique actuator. A temperature PI controller was studied with an event-based approach. Different values with $\delta = [0, 0.1, 0.2, 0.5, 1]$ relating to the event occurrence were tested. The results show that $\delta=0.5$ is the optimum value, which significantly reduces the number of vent movements by 43.8%, while only increasing the temperature error by 1.13%. Secondly, comparative studies of humidity controllers (tracing relative humidity, TRH and tracing absolute humidity, TAH) are conducted independently. The results show that TRH performs ideal when the RH set-point is not high. However, the controller lost robustness when RH is over 70%. Comparatively, TAH keeps reasonable robustness with all the RH set-points, but it lacks sensitivity so that the accuracy is lower than TRH method when RH is lower than 60%. Finally, a selective temperature control strategy with a humidity priority control scheme was demonstrated through a simulation study. This control strategy constantly keeps the relative humidity below 80% while controlling the temperature to the set-point, which not only prevents high humidity damaging the crops, but also greatly avoids the loss of energy.

For climate control in greenhouses, increasing yield and preventing fungal diseases are contradictory processes, because fungal pathogens and hosts are necessarily stay in the same niche. Therefore, a new hierarchical optimization control strategy was proposed to maintain the optimum diurnal and nocturnal temperature for cucumber production, but giving priority to the disease control. The hierarchical optimization control scheme provides the optimal temperature set-point in each transient step. In the lower layer, the previously developed event-based PID controller keeps the optimum temperature for cucumber production. In the upper layer, an optimizer provides a suggested set-point looking to avoid the ongoing infection. For this, the disease infection model (given by the combination of the greenhouse climate model together the disease model previously discussed) is simulated by a three-day prediction using weather forecast. The new set-point is calculated by a cost function, which ensures the minimum integration of absolute error between the current set-point and the greenhouse temperature. This novel study is of great significance for precise control of greenhouse fungal diseases.

Based on these results, further studies were explored to improve control efficiency. Classical closed-loop control takes the temperature in the center of the greenhouse as the

current temperature. This temperature comes from the greenhouse model output or the sensor placed in the center of the greenhouse. However, there are remarkable non-uniformities in leaf microclimate within the canopy in a greenhouse, with implications for variable heat and mass exchange, and the heterogeneity distribution of greenhouse climate. The future closed-loop control may calculate the optimal feedback temperature according to the temperature distribution in each transient step. It may be costly to install many sensors in the greenhouse. So, a practical solution is to develop a distribution model based on the current weather condition and greenhouse structure. CFD technique is one of the powerful tools to achieve this goal.

According to the previous reason, the following CFD studies were conducted relating to greenhouse climate models. Two-dimensional and three-dimensional transient CFD models were developed for the temperature and humidity distribution in the greenhouse and the LWD (Leaf Wetness Duration) distribution leading to disease infection. The RMSE of the temperature, relative humidity and leaf temperature during the two nights were 1.24 °C, 3.31%, and 1.32 °C, respectively. The leaf condensation results were manually observed for comparison with the simulated results. Leaf condensation always occurred first in the area near the semi-transparent roof, both in the observations and the simulation. The LWD was simulated by considering the duration of the simulated leaf condensation at each point. The evaluation was conducted on 216 pairs of samples. The True Negative Rate (TNR), True Positive Rate (TPR), and Accuracy (ACC) were 1, 0.66, and 0.89, respectively. This study serves as a reference for an early warning model of disease based on the temporal and spatial distribution of leaf condensation. However, CFD simulation is time-consuming, and the current computing power is insufficient to provide transient feedback for the feedback controller. In the near future, the feedback control based on the transient distribution of temperature and humidity will greatly improve the control efficiency.

To conclude, this summary ends by depicting the structure of this document, which has been divided into three parts according to those described in the University of Almería regulation for Ph.D. theses presented in the compendium modality:

i. Chapter 1 describes the framework of the thesis and introduces the main methodologies used. In addition, this chapter describes the development structure of the thesis and indicates the publications dealing with each of the topics covered.
ii. Chapter 2 presents the scientific publications that support the work done.
iii. Chapter 3 summarizes the conclusions derived from the different publications as well as the recommendations for future work.

Resumen

La principal contribución de esta tesis se centra en reducir la infección de enfermedades fúngicas en los cultivos bajo invernadero a través del uso de metodologías de modelado y control. Para completar esta tarea, se han llevado a cabo tres estudios independientes, correspondientes al desarrollo del modelo de clima de un invernadero, modelo de predicción de enfermedades fúngicas en cultivo bajo invernadero y un algoritmo de control climático para invernaderos. Finalmente, estos modelos y algoritmos han sido combinados para proponer una estrategia de control jerárquica con el objetivo de mantener la temperatura óptima para la producción de pepino, pero dando prioridad al control de enfermedades. En comparación con los esquemas de gestión de enfermedades actuales, esta nueva estrategia maximiza la temperatura acumulada bajo la condición de reducir la presencia de enfermedades, contribuyendo así a la reducción del uso de pesticidas para este fin.

El modelo climático de invernadero se desarrolló durante los años 2019 y 2020, y utiliza un método mecanicista para estimar la temperatura y la humedad en los invernaderos solares típicos de China. Se adoptó un método de estimación de temperatura de pared novedoso y fácil de usar basado en el balance de energía para el modelo ambiental en lugar de usar mediciones de temperatura límite. De esta forma, la cantidad de entradas del modelo se reduce considerablemente y el modelo propuesto puede predecir las condiciones climáticas futuras del efecto invernadero utilizando solo el pronóstico de las condiciones medioambientales externas. La validación del modelo se realizó en dos invernaderos diferentes (cada uno con diferentes tamaños y parámetros físicos, como el volumen del invernadero, las áreas del techo y las paredes, los materiales de las paredes, etc.) en tres días típicos en 2019 y 2020, y durante cuatro semanas consecutivas en diferentes épocas del año durante 2016 y 2019. Se obtuvieron resultados prometedores y el modelo funcionó adecuadamente en diferentes modos de operación; que incluyeron tener las ventanas de ventilación completamente cerradas, completamente abiertas, y considerando el uso de una cubierta de manta de aislamiento térmico adicional. Los resultados de la validación demuestran que el modelo propuesto se puede adaptar ampliamente a diferentes tamaños de invernaderos solares chinos típicos, así como a diferentes condiciones climáticas. Por lo tanto, el modelo desarrollado es una herramienta flexible y valiosa que se puede utilizar para la simulación climática de invernaderos, el control de la temperatura y la humedad, y como un sistema de apoyo a la toma de decisiones para ayudar a gestionar los invernaderos solares.

Para mejorar el modelo de ventilación incluido en el modelo climático anteriormente descrito, se desarrolló un modelo de ventilación natural basado en árboles de regresión utilizando los resultados de más de mil muestras obtenidas mediante cálculos de dinámica de fluidos computacional (CFD). Este modelo trata perfectamente el efecto combinado de la presión del viento y los gradientes térmicos. Dicho modelo de ventilación natural se incorporó al modelo climático del invernadero mejorando considerablemente el efecto de ventilación y demostrando su efectividad mediante un simulación de 7 días consecutivos.

Para las predicciones de enfermedades, tomando como ejemplo el cultivo del pepino, se propuso un nuevo enfoque mediante la combinación del modelo climático de invernadero desarrollado en esta tesis y un modelo de enfermedad para el pronóstico de la aparición de enfermedades en los invernaderos disponible en la literatura. El método se evaluó en NPADB (Base Nacional de Demostración de Agricultura de Precisión), Beijing, China, utilizando datos recopilados desde el trasplante del cultivo hasta la infección primaria ocurrida en el invernadero, en la temporada de primavera de 2021. En esta metodología, primero el modelo dinámico se utiliza para predecir el clima interior del invernadero 72 horas hacia delante haciendo uso de previsiones climáticas. Posteriormente, esta predicción se usa como entrada al modelo de enfermedades para detectar la ocurrencia de la enfermedad por adelantado. Las predicciones obtenidas se compararon utilizando datos reales medidos en un invernadero durante un periodo de dos meses. Después de varios informes de falsos positivos, un informe positivo por ambos métodos se ajustó a la primera observación en el invernadero el 24 de abril de 2021. Por lo tanto, la principal contribución de este trabajo es la alerta temprana de enfermedades (del pepino en este estudio) a través de modelos de clima y enfermedad acoplados, donde solo las predicciones de clima exteriores son necesarias.

Con respecto a las contribuciones de control, en primera instancia se desarrolló un algoritmo de control selectivo basado en eventos para el control simultáneo de temperatura y humedad. El control de temperatura se basó en un controlador PI de temperatura con un enfoque basado en eventos. Se probaron diferentes valores con $\delta = [0, 0.1, 0.2, 0.5, 1]$ relacionados con la ocurrencia del evento. Los resultados mostraon que $\delta=0.5$ es el valor óptimo, cuyo valor permite reducir significativamente el número de movimientos de ventilación en un 43.8 %, mientras que solo aumenta el error de temperatura en un 1.13 %. En segundo lugar, se realizaron de forma independiente estudios comparativos de controladores de humedad (rastreo de humedad relativa, TRH y rastreo de humedad absoluta, TAH). Los resultados muestran que TRH funciona de manera ideal cuando el punto de referencia de HR (humedad relativa) no es alto. Sin embargo, el controlador pierde robustez cuando la HR es superior al 70 %. Comparativamente, TAH mantiene una solidez razonable con todos los puntos de ajuste de HR, pero carece de sensibilidad, por lo que la precisión es menor que el método TRH cuando la HR es inferior al 60 %. Finalmente, se demuestra una estrategia de control de temperatura selectiva con un esquema de control de prioridad de humedad a través de un estudio de simulación. Esta estrategia de control mantiene constantemente la humedad relativa por debajo del 80% mientras controla la temperatura cercana al valor de referencia, lo que no solo evita que la alta humedad dañe los cultivos, sino que también evita en gran medida la pérdida de energía.

Para el control del clima en los invernaderos, aumentar el rendimiento y prevenir las enfermedades fúngicas son procesos contradictorios, ya que los hongos patógenos y los huéspedes permanecen necesariamente en el mismo nicho. Para abordar este problema, se propuso un mejor esquema para mantener la temperatura óptima diurna y nocturna para la producción de pepino, pero dando prioridad al control de enfermedades, utilizando para ello una estrategia de control de optimización jerárquica. La estrategia de control de

optimización jerárquica proporciona el mejor punto de ajuste de temperatura en cada paso transitorio. En la capa inferior, el controlador PID mencionado anteriormente mantiene la temperatura óptima para la producción del cultivo. En la capa superior, el optimizador hace uso del sistema de predicción de enfermedades desarrollado como parte de esta tesis para estimar la posibilidad de aparición de infecciones en las próximas 72 horas y determinar la referencia de temperatura óptima que permita reducir el número de infecciones. Dicha decisión se apoya en una función objetivo que asegura la mínima integración de error absoluto entre la referencia sugerida y la temperatura del invernadero. Este nuevo estudio es de gran importancia para el control indirecto de las enfermedades fúngicas en invernaderos permitiendo reducir la aplicación de pesticidas basado únicamente en un sistema de control de clima.

Con base en estos resultados anteriormente expuestos, se exploraron más estudios para mejorar la eficiencia de los sistemas de control. El control clásico de circuito cerrado toma la temperatura en el centro del invernadero como la temperatura actual. Esta temperatura proviene de la salida del modelo de invernadero o del único sensor típicamente colocado en el centro del mismo. Sin embargo, existen notables faltas de uniformidad en el microclima de las hojas dentro del dosel de un invernadero, con implicaciones para el intercambio variable de calor y masa, y la distribución heterogénea del clima del invernadero. Por tanto, una mejora sustancial sería la aplicación de un control de circuito cerrado puede calcular la temperatura de retroalimentación óptima de acuerdo con la distribución de temperatura en cada paso transitorio. Para este fin, la instalación múltiples sensores distribuidos en el invernadero sería altamente costa, por lo que una solución práctica consiste en desarrollar un modelo de distribución basado en las condiciones climáticas actuales y la estructura del invernadero. Para ello, en esta tesis se ha hecho uso de la técnica CFD como una herramienta con gran potencial para lograr este objetivo.

Los siguientes estudios CFD se realizaron en relación con los modelos climáticos de invernadero previamente mencionados como pare de esta tesis. Se desarrollaron modelos CFD transitorios bidimensionales y tridimensionales para la distribución de la temperatura y la humedad en el invernadero y la distribución LWD (duración de la humedad de la hoja) que conduce a la infección por enfermedades. El RMSE de la temperatura, la humedad relativa y la temperatura de la hoja durante las dos noches fue de 1.24 °C, 3.31 % y 1.32 °C, respectivamente. Los resultados de la condensación de la hoja se observaron manualmente para compararlos con los resultados simulados. La condensación de hojas siempre ocurrió primero en el área cercana al techo semitransparente, tanto en las observaciones como en la simulación. La LWD se simuló considerando la duración de la condensación foliar simulada en cada punto. La evaluación se realizó sobre 216 pares de muestras. La tasa de verdaderos negativos (TNR), la tasa de verdaderos positivos (TPR) y la precisión (ACC) fueron 1, 0.66 y 0.89, respectivamente. Este estudio sirve como referencia para un modelo de alerta temprana de enfermedades basado en la distribución espacial y temporal de la condensación de las hojas. Sin embargo, la simulación CFD requiere mucho tiempo y la potencia informática actual es insuficiente para proporcionar retroalimentación transitoria con fines de control. En un

futuro cercano, el control de retroalimentación de circuito cerrado basado en la distribución transitoria de temperatura y humedad mejorará en gran medida la eficiencia del control.

Para concluir, este resumen termina describiendo la estructura del presente documento, el cual se ha dividido en cuatro partes de acuerdo a las descritas en la normativa de la Universidad de Almería para tesis presentadas en la modalidad por compendio:

i. En el capítulo 1 se describe la unidad temática de la tesis y se introducen las principales metodologías empleadas. Además, se indica la estructura de desarrollo de la tesis y las publicaciones que tratan cada uno de los temas abordados.
ii. En el capítulo 2 se presentan las publicaciones científicas que avalan el trabajo realizado.
iii. En el capítulo 3 se recogen las conclusiones que se derivan de las diferentes publicaciones así como las recomendaciones para trabajos futuros.

Financial support:

I am most grateful for the financial support given by the China Scholarship Council for this project (no. 201909505002).

This project has been funded by Project PID2020-112709RB-C21 (HYCO2BIO) of the Spanish Ministry of Science, Innovation and Universities, and by ERDF funds.

This project has been funded by the FP7 Framework Program (PIRSES-GA-2013-612659); Science and Technology Innovation Capacity Building Project of Beijing Academy of Agricultural and Forestry Sciences (No. KJCX20211002); and by the National Natural Science Foundation of China (31401683).

Contents

List of Acronyms

ARX	Auto Regressive with Extra Input
CFD	Computational Fluid Dynamics
CSG	Chinese Solar Greenhouse
DPD	Dew Point Depression
LWD	Leaf Wetness Duration
ME	Mean Error
MAE	Maximum Error
MPC	Model Predictive Control
NN	Neural Network
PID	Proportional, Integral and Derivative
RBF	Radial Basis Function
RH	Relative humidity
RMSE	Root Mean Square Error
TAH	Tracing Absolute Humidity
TRH	Tracing Relative Humidity
TLWD	Mean Temperature in LWD
UDF	User Defined function

1 INTRODUCTION

1 Introduction

This section aims to provide the reader with a general overview of the research work carried out. Section 1.1 describes the main interest and the motivation of the Ph.D. thesis. Section 1.2 introduced the pathogenesis of greenhouse fungal diseases. Taking cucumber downy mildew as an example, a disease model for predicting infection and onset time is proposed and evaluated in a greenhouse. Based on this work, a journal paper was published (Liu et al., 2022a). Section 1.3 makes a brief review of the current state of art of greenhouse climate models, emphasizing the advantages and disadvantages the mechanism models and machine learning models. Then, a novel one-dimensional transient mechanism model for predicting greenhouse temperature and humidity is proposed and evaluated. This work was published in Computers and Electronics in Agriculture (Liu et al., 2021a). Section 1.4 presents the work in greenhouse control, including a study of event-based PID controller for greenhouse temperature and humidity, which was published in RIAI (Liu et al., 2022c); and a hierarchical control scheme for reducing the greenhouse fungal disease, which is under review in Journal of Cleaner Production (Liu et al., 2022d). Section 1.5 introduces those works on the modelling of the spatial and temporal distribution of the greenhouse microclimate. The two-dimensional and three-dimensional models were developed using CFD (Computational Fluid Dynamics) methods for simulating the transient distribution of greenhouse temperature, humidity and leaf condensation. The obtained results were published in two journal papers and one international conference (Liu et al., 2020; Liu et al., 2021b; Zhang et al., 2022). In addition, this section introduces a virtual wind tunnel experiment in order to develop a regression trees model for predicting the greenhouse natural ventilation rate, which is currently under review (Liu et al., 2022e).

1.1 Context and motivation

Section 1.1.1 and 1.1.2 introduces the significance of the protected agriculture and current existing environmental problems during greenhouse production. Finally, the aim of this work is illustrated in section 1.1.3, which is to reduce the occurrence of fungal diseases through a hierarchical optimization control strategy. The proposed method tries to solve the overdose of fungicide and pesticide in the soil, meanwhile, keeps the optimal climate for crop production.

1.1.1 Protected agriculture

By the end of the century, the global population will be over 10 billion (Roser et al., 2013). The climate types in 31.3%–46.3% of global land area are estimated to change. It is approximately 5.7% of Earth's surface has become drier and hotter (Guan et al., 2021). The barren land that was considered as uncultivated area will be used for agricultural production (Fig. 1.1). Approximately 128 million ha of the global agriculture land has changed to other types since 2000 (FAO and IIASA, 2021). Several factors that restrict the current greenhouse development will disappear, such as operating costs, sensors, electromechanical equipment, models, etc. The protected agriculture production may become dominant.

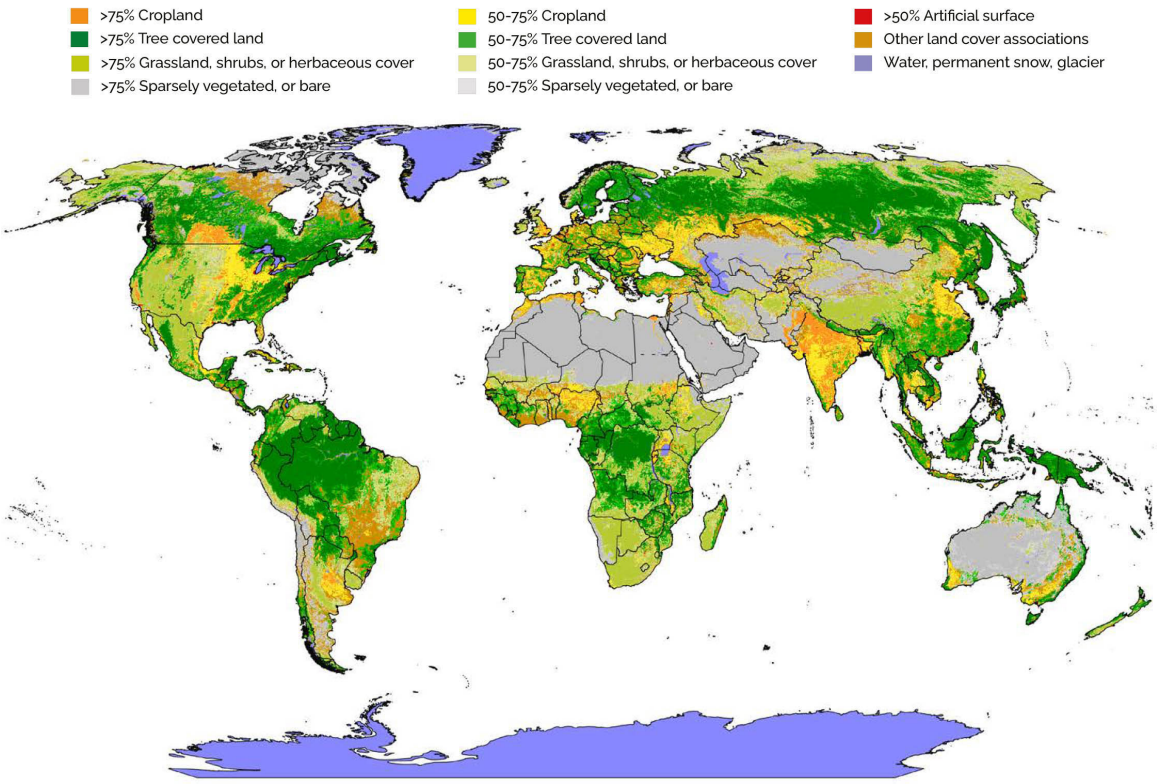

Fig. 1.1. Map of global agricultural land use (FAO and IIASA, 2021).

According to the latest statistics, the area of greenhouses worldwide was estimated as 3.64 million hectares (Guo et al., 2021). In particular, the greenhouse cultivation area in China has approached to 2 million ha, and among them, the area of Chinese solar greenhouse (CSG) is 0.6 million and that of plastic tunnel is approximately 1.2 million (Wang et al., 2017). Solar greenhouses and plastic tunnels are the main types of horticulture facilities in northern provinces of China. The production of vegetables in solar greenhouse is a major way for farmers to conduct overwintering production.

The CSG is a semi-fan shaped tunnel greenhouse with a transparent polyethylene film roof facing south and brick or soil walls on other sides (Fig. 1.2). The lengths varying from 30 to 100 meters and spans (widths) varying from 7 to 20 meters.

Natural ventilation is realized by rolling the film at the roof vent (upper vent) and side vent (lower vent). According to the investigation, one of the devices most widely adopted by farmers is the thermal insulation blanket rolling machine, this has reached an application rate of more than 90% in Shandong province, the main protected vegetable production area in China, (Wen et al., 2019). Another common approach adopted by most farmers is to use natural ventilation to cool and dehumidify their crops (Li et al., 2018); this is because of the interaction between the energy cost and market prices, which will continue far into the future.

Fig. 1.2. Semi-fan shaped solar greenhouses.

1.1.2 Environmental risks in CSGs

In recent years, environmental problems in CSG have received increasing attention, relating to the intensive application of agrochemicals (Kalkhajeh et al., 2021). The main reason is the overdose of fungicide and pesticide in the soil. Another important factor is that the application of soilless culture has not been popularized (Fig. 1.3). A large amount of agrochemicals have accumulated in the soil with continuous cultivation year after year, due to imprecise crop management and imperfect promotion of soilless culture.

Fig. 1.3. A photo inside the greenhouse.

In the past, agrochemical dosage was generally estimated based on the farmer's own experience, which causes chemical residues, excessive expenditure and pollution. For cucumber production, the environmental risks are mostly related to excessive fertilizers (nitrogen, phosphorus and potassium), fungicides and pesticides inputs (Hu et al., 2017; Guan et al., 2022). For the fungal disease treatment, the objections are mostly downy mildew (*Peronospora sparsa*), botrytis (*Botrytis cinerea*) and powdery mildew

(*Sphaerotheca pannosa*), which are three common fungal plant diseases in greenhouses, always resulting in damages on the foliage and fruit, and bringing great economic losses. Thus, new solutions to predict the occurrence of diseases and to reduce the application of chemical pesticides is a relevant research line on this topic. For that reason, this thesis is focused on the use of model-based control methods to contribute in the reduction of crop diseases by improving the environmental impact.

1.1.3 Using hierarchical optimal control strategy to reduce greenhouse diseases

Automatic control application has received considerable attention in greenhouse climate control and management in recent years. Whether for agronomic or financial purposes, the main objective of the climate control problem is to maintain the temperature and relative humidity within the ranges suitable for crops (Rodríguez et al., 2008; Ramírez-Arias et al., 2012).

At present, the applications of optimization control are mostly about improving the energy utilization and crop production. This approach has been studied in various greenhouses, including the Venlo, Almería type greenhouses, and CSGs. They focus on higher productivity, better thermal utilization and lower economic consumption (Körner et al., 2004; Montoya et al., 2016; Xu et al., 2018a; Lin et al., 2020; Zhang et al., 2020). Much of the works designed to enhance productivity or energy efficiency have been done without considering its implications in making crops susceptible to diseases infections (Jewett and Jarvis, 2001). Few previous control approaches focus on plant fungal disease, which causes severe economic losses every year throughout the world, leading to environmental pollution caused by fungicide. Because the host plant necessarily stays the same ecological niche as fungal pathogens, consciously control to avoid infection without damaging the host plant requires precise theoretical support.

The aim of this project is to develop a control system for the management of greenhouse diseases. Specifically, on the one hand, taking cucumber downy mildew as an example, the system performs early warning of fungal disease infection based on temperature and humidity. On the other hand, the system maintains the optimum diurnal and nocturnal temperature control for cucumber production, but giving priority to disease control, everything based on a hierarchical optimization control strategy.

1.2 Crop fungal disease in greenhouse

This section introduces the main fungal diseases threatening greenhouse production. Afterwards, the pathogenesis and prediction methods for the infection and symptom appearance of cucumber downy mildew are introduced.

1.2.1 Pathogenesis of Fungal Diseases in Greenhouse

Downy mildew (*Peronospora sparsa*), Botrytis (*Botrytis cinerea*) and Powdery mildew (*Sphaerotheca pannosa*) are three common fungal plant diseases in greenhouses.

Among others, water stains on leaves are typical symptoms of downy mildew, which significantly affect photosynthesis (Fig.1.4). There are four common ways for fungal spores to get into the greenhouse: with the air flow through vents; carried through the clothes and shoes of the farmer; hidden in the soil for overwintering; infected plant tissue in the last cultivation remain in the greenhouse (Liu et al., 2022a). In fact, it is very difficult to completely remove spores in a greenhouse where fungal diseases have ever occurred. However, it is significant to avoid high humidity and moderate temperature in the greenhouse to reduce disease occurrence.

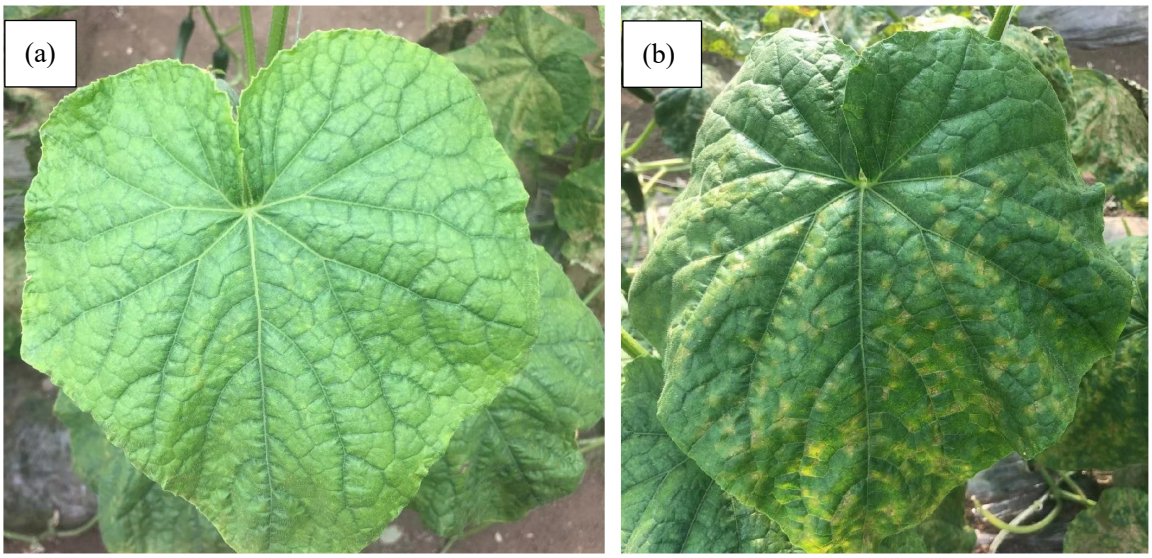

Fig. 1.4. Photos of healthy (a) and diseased leaves (b).

Avoiding infection is the key step to prevent disease. On the premise of minimizing pathogens as far as possible, the optimum to prevent the occurrence of disease is to avoid placing its host in a suitable environment for inoculation. This idea was widely used in fungal disease management, as it has a characteristic of rapidly spreading and extremely breakout when it meets medium temperature and high humidity conditions (Ojiambo et al., 2015).

Sufficient LWD (Leaf Wetness Duration) in hours and ideal temperature threshold (medium or high temperature) are considered as required conditions for several common fungal conidia infection by most of the previous studies (Zhao et al., 2011; Mashonjowa et al., 2013; Wang et al., 2019). LWD is the core parameter for infection modelling. Studies have shown that it plays an important role in the infection of downy mildew, botrytis and powdery mildew (Table 1).

Table 1. Summary of the symptoms and optimum conditions of the common fungal diseases in greenhouse roses (Mashonjowa et al., 2013).

Disease	Symptoms	Optimal conditions		
		RH	Temperature	Leaf wetness
Downy mildew (Peronospora sparsa)	Distorted shoots and deformed flowers; Grey coloured spore masses on the abaxial surface of leaves, which eventually die and abscise, resulting in severe defoliation.	High humidity (~80%) for spore germination and disease spread.	15-20 °C for spore germination; 20-25 °C for disease development and spread.	2 h of LW for spore germination; Minimum LWD of 8.4 h per day over a 10-day period for disease development.
Botrytis (Botrytis cinerea)	Spotted flower petals; Tips and edges of petals turn soft and brown; Flower buds droop and remain closed.	RH >/93% is necessary for development and infection.	Temperaturs between 9 and 21 °C.	Minimum LWD of 7 h per day for growth and development.
Powdery mildew (Sphaerotheca pannosa)	Irregular shaped blistered areas on the adaxial surface of expanding leaves, followed by yellowing and dropping off; Deformed flowers with discoloured petals and blooms with a very short vase-life.	RH rising from 40-70% in daylight hours and exceeding 90% at night.	High daytime temperatures (~35 °C). followed by cool humid nights (~5 °C).	Leaf wetness inhibits spore germination.

In general, LWD can result from dew, fog, rain and overhead irrigation (Hornero et al., 2017). In a greenhouse, LWD mainly comes from dew on leaf surface and dew dripping down from the roof. From this point of view, one of the main meteorological problems in greenhouses is crop wetting caused by the interaction of high humidity and low temperature. The above are the environmental preparations that the infection process depends on. The latter factors can be avoided through adequate management. At present, most of the research on LWD modelling focuses on the simulation of leaf condensation.

Once the pathogen spores are successfully infected on the leaves of the plant, the disease is inevitable. The period from infection to the onset of symptoms is called the incubation period (Fig. 1.5). Its duration depends on the accumulated temperature, usually two to three days.

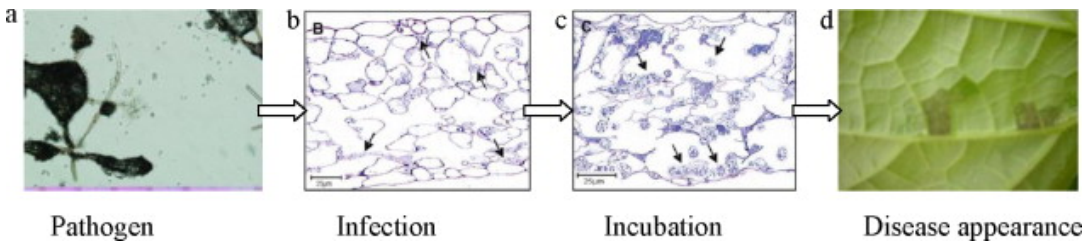

Fig. 1.5. The primary infection mechanism of cucumber downy mildew (Zhao et al., 2011).

1.2.2 Primary infection model for cucumber downy mildew

Taking cucumber downy mildew as an example, the lower limit for infection is 20°C with 2 h of wetness (Cohen, 1977). The infection condition therefore depends on a favourable combination of LWD (Leaf Wetness Duration) and mean temperature in LWD (TLWD). The minimal threshold is 2 h × 20 °C = 40 h °C (Zhao et al., 2011),

$$LWD \times TLWD \geq 40\ h℃\ (LWD \geq 2\ h, 5\ ℃ \leq TLWD \leq 30\ ℃) \quad (1)$$

Once infection is done, incubation period starts. It usually needs a couple of days when incubation period finishes. It is an integration of hourly contribution rate (i, Eq. 2), which is calculated by an equation of hourly average temperature (T_h, ℃). The deadline of incubation period is the hour when the integration of i ≥ 1, when leaves are predicted to be symptomatic. For example, if T_h is a constant value as 20 ℃, then the contribution rate i is calculated as 0.015 in each hour. The i takes 67 hours to progress to 1, which means that that symptoms will appear in less than 3 days.

$$i = \frac{0.0165}{1+10389.2\times exp\ (-0.5743\times T_h)} \quad (2)$$

Measuring and estimating LWD are the commonly used ways to obtain the leaf wetness data (Hornero et al., 2017). The measurement of LWD is to trace the electric resistance on an artificial leaf (Fig. 1.6 (a)). Dew condensation on the leaves can change the resistance. The LWD can also be estimated by many methods. Dew point depression relative to canopy temperature (DPD_c) and dew point depression of the air (DPD_a) are two methods to evaluate whether the leaves are wet, according to the difference between the dew point temperature and the canopy temperature or air temperature (Sentelhas et al., 2008). There are upper and lower limits thresholds to define onset and dry-off, usually about 2 ℃. Relative humidity threshold estimation is another common method to simulate the LWD. Depending on geographical location and climatic conditions, this threshold changes from 80% to 95% (Wang et al., 2019).

In this thesis, three methods are adopted to obtain LWD data: sensor measurement, model estimation and manual observation. The measurements inside the greenhouse are respectively air temperature (range, -40 - +65 ℃; accuracy, ±0.5℃), relative humidity (range, 0-100%; accuracy, ±3%, Fig. 1.6 (b)) and leaf wetness duration (artificial leaf with electricity resistance, range, 0 dry – 15 saturated wetness, Fig. 1.6 (a)) at a height of 1 m. With LWD and air temperature, infection data can be predicted. Then, according to Eq. 2, the deadline of incubation period is estimated according to accumulated temperature. There are usually several false positives and then true positives. The above is the whole process of early warning of cucumber downy mildew.

In this thesis, an experiment in a greenhouse for a complete growing season was conducted, with the purpose of using the above models to carry out early warning of cucumber downy mildew. See Liu et al., 2022a for detailed information. The advantage

of this method is that it quantifies the climate parameters of downy mildew infection, so that the control measures can be used to eliminate the factors leading to positive reports.

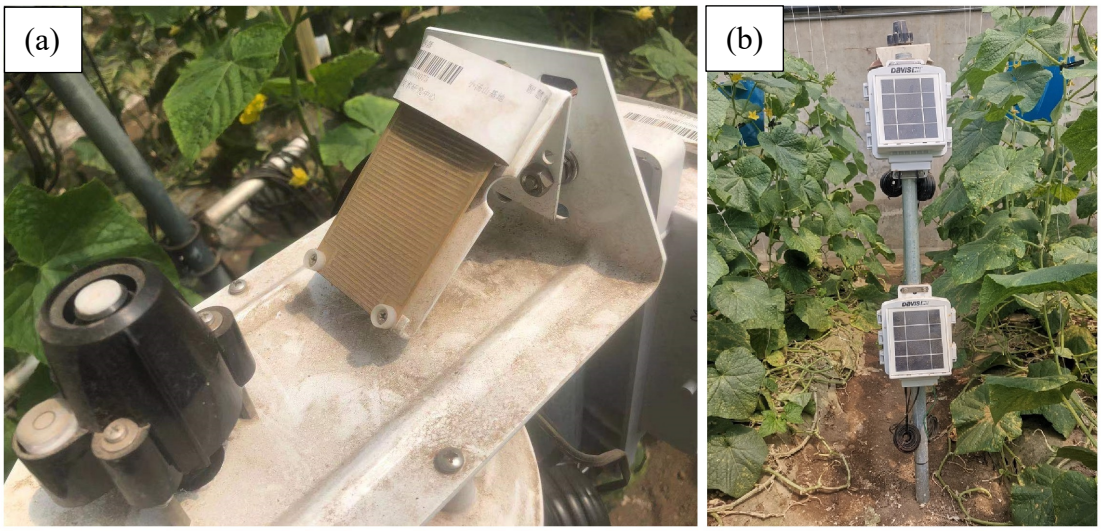

Fig. 1.6. LWD sensor (a) and air temperature-humidity sensor (b), Davis-6162, Davis Instruments, Hayward, USA.

1.3 Greenhouse climate model

LWD and temperature data obtained by sensors placed in the greenhouse can be used for early warning of downy mildew. Similar experiments have been published (Zhao et al., 2011; Wang et al., 2019). Both of the monitoring or estimating ways rely on sensors sending out current signals to identify whether the leaf is wet or not and have limited abilities in sending warning massages for future LWD. The infection may have occurred when LWD appeared by monitoring or simulating.

For those reasons, data-based disease warning models were widely developed and applied in recent decades, including wheat stripe rust (El Jarroudi, et al., 2017), rice blast (Wang et al., 2021), tomato and potato blight (Chelal et al., 2015; Andrade-piedra et al., 2005), etc. Some of these methods have been well applied in the open field condition by using weather forecasts (Kim et al., 2020). However, in greenhouses, the prediction lacks the link between the weather forecast and the infection model, which is given by the inside greenhouse climate, and thus, a greenhouse climate model is required. For that reason, the climate model for CGS in China has been developed to be connected with the LWD model. So, the following sections present and short state of art of greenhouse climate models, and then, the developed model is summarized.

1.3.1 Review of greenhouse climate models

Greenhouse model is a mathematical and logical relationship describing the internal and external environmental parameters of greenhouse, which is divided into dynamic or

transient model and steady-state model (Fig. 1.7). The earliest greenhouse model can be traced back to 1958 (Katzin et al., 2022). Most of the early models are systems composed of multiple equations. Their parameters are visible so that they are called mechanism models or white box models.

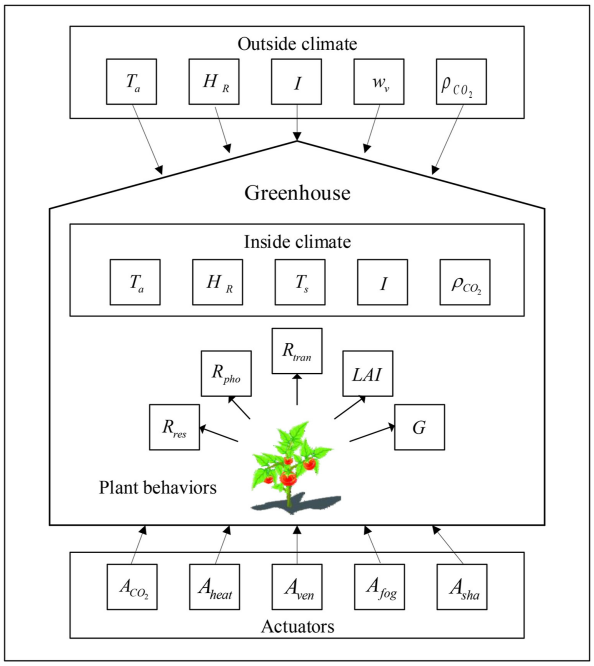

Fig. 1.7. Influence factors for modelling agricultural greenhouse system (Guo et al., 2021).

With the improvement of computing power, black box models or time-series models are established by training multiple inputs and outputs data (Guo et al., 2021). An easily determined one of the black box models is autoregressive models (Ljung, 1999). The ARX (auto-regressive with exogenous inputs) model is selected to simulate the greenhouse temperature (Montoya-Ríos et al., 2020; García-Mañas et al., 2021). The limitation of ARX model is that the training results of continuous sample data in long seasons are not accurate. Therefore, developers usually establish and adopt models for different time periods.

In the 21st century, deep learning models and big data makes the prospect of complex nonlinear simulation optimistic (Jung et al., 2020; Moon and Son, 2021). Although in the past 5 years, the deep learning model has gradually become the mainstream, one-third of the greenhouse models are NN (Neural Network) models, its application and promotion in agricultural greenhouses have made slow progress (Guo et al., 2021). This is because data loss caused by sensor failure is a common problem in agricultural environment. In addition, widely data collection, irregular and discontinuous sample data format is currently still a challenge. This shows that standardization for greenhouse is of great significance to the progress of an industry.

For mechanism models, many published greenhouse models require very complex real-time measurement parameters, which makes it almost impossible to obtain the

greenhouse microclimate only using weather forecast data, e.g., temperature, humidity, solar radiation, wind speed and direction. See for instance, (Chen et al., 2022), where a one-dimensional greenhouse model for temperature and humidity was published. For the temperature, the following equation is usually considered,

$$\rho V Cp \frac{dT}{dt} = q_{sol} + q_{pipe} + q_{light} - q_{cover} - q_{vent} - q_{pad} \quad (3)$$

where ρ is the air density, V is the greenhouse volume, Cp is the air specific heat capacity, T is the greenhouse air temperature, q_{sol} is the net solar radiation, q_{pipe} is the heat flux from the heating pipe, q_{light} is the heat flux from supplemental lighting, q_{cover} is the heat flux through the cover, q_{vent} is the heat flux from ventilation, and q_{pad} is the heat flux from the pad. For the humidity, the typical equation is,

$$\rho V \frac{dh}{dt} = m_{vent} + m_{trans} + m_{fog} \quad (4)$$

where h is the absolute humidity, m_{vent} is the water vapor source term from ventilation, m_{trans} is the water vapor source term from transpiration of the plants, and m_{fog} is the water vapor source term from the fogging system (Fig. 1.8).

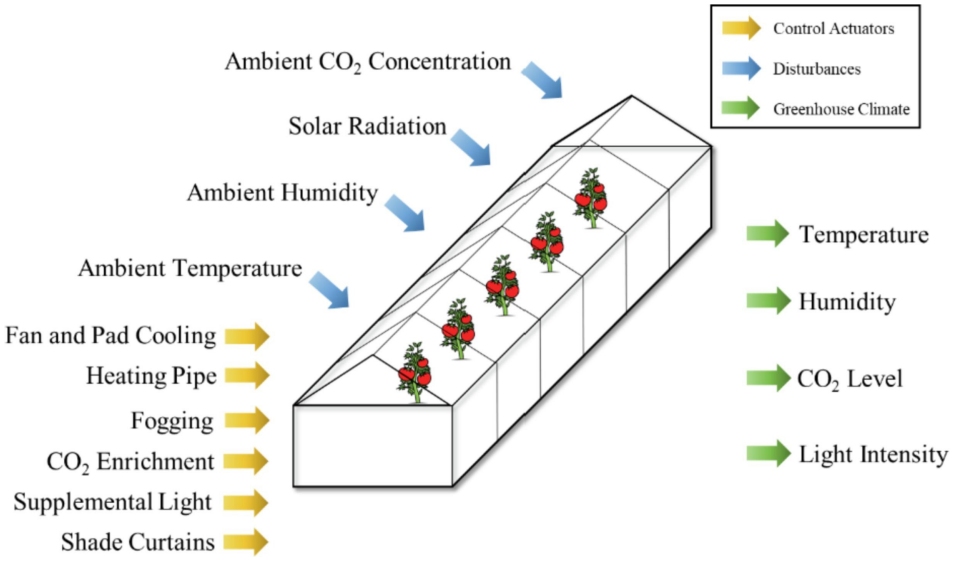

Fig. 1.8. Semi-closed greenhouse structure model that shows control actuators (yellow arrows), disturbances (blue arrows), and greenhouse climate system states (green arrows) (Chen et al., 2022).

Each source term is calculated by multiplying the difference between internal and external air temperature or humidity by a coefficient: $(T-T_o)\times Coe_1$, $(h-h_o)\times Coe_2$. For example, in this case,

$$q_{cover} = A_s K_c (T - T_o) \quad (5)$$

where A_s is the surface area of the greenhouse; K_c is the coefficient of the cover equation, and T_o is the outdoor temperature. Then, the problem is that K_c is a professional convection heat transfer parameter, which is not a constant. The greenhouse climate model cannot run when only inputting weather forecast. Similar questions also exist in other source terms. This case adopted mechanical ventilation when calculating the ventilation source term, which makes the modelling easier. For example,

$$q_{vent} = \rho C p u_{fan,max}(T - T_o)u_{fan} \tag{6}$$

$$m_{vent} = \rho C p u_{fan,max}(h - h_o)u_{fan} \tag{7}$$

where $u_{fan,max}$ is the maximum fan speed in the greenhouse, and u_{fan} is the control input of the fan speed ranging from 0 to 1, h_o is the outdoor absolute humidity. When natural ventilation is used in greenhouse, the calculation of natural ventilation rate will make the problem more complicated. In addition, the crop transpiration humidity source term is the famous Penman-Monteith equation (Widmoser et al., 2009). The parameters used in these equations are very complex. When the data is only weather forecast, the parameters are often missing. Another example comes from Lin et al. (2021), the parameters α_1, α_2 and g_v from the following equations are not given by a calculation method,

$$Q_{sun} = \alpha_1(1 - s_r)I_{rad} \tag{8}$$

$$Q_{cov} = \alpha_2(T - T_o) \tag{9}$$

$$Q_{vent} = g_v \rho C p(T - T_o) \tag{10}$$

where Q_{sun}, Q_{cov}, Q_{vent} are respectively heat source terms of solar, roof convection heat transfer and ventilation. α_1 is the transmission coefficient of the cover material; s_r is the shading rate and is adjusted by the greenhouse shading system; I_{rad} is the solar radiation; α_2 is the heat transfer coefficient of the cover; g_v is the ventilation rate of a ventilation fan. The above equations are simple, but how to determine the core parameters is extremely important.

Comparatively, the black-box models are easier to apply. Yue et al. developed a neural network greenhouse model (2018) (Fig. 1.9). This neural network input is the state of the thermal screen, the state of the shading net, heating valve opening, outdoor temperature, illumination, and wind speed. The outputs were respectively the indoor temperature and humidity (Yue et al., 2018). This means that only six inputs are needed to simulate the temperature and humidity of the greenhouse.

The maximum relative error of temperature and humidity prediction inside greenhouse does not exceed 0.5%. This model is undoubtedly very user-friendly. However, the 1440 training sample data used in this experiment are all from the same greenhouse. Besides, the training data and validation data are both collected in March. The errors may be greatly increased when the model is applied in another greenhouse or

in different seasons. This is a common problem of the black box model. In the future, big data may be the solution. At present, the use of big data to train the neural network model has some major difficulties, such as widely data collection, irregular and discontinuous sample data format. This also shows that standardization is of great significance to the progress for an industrial point of view.

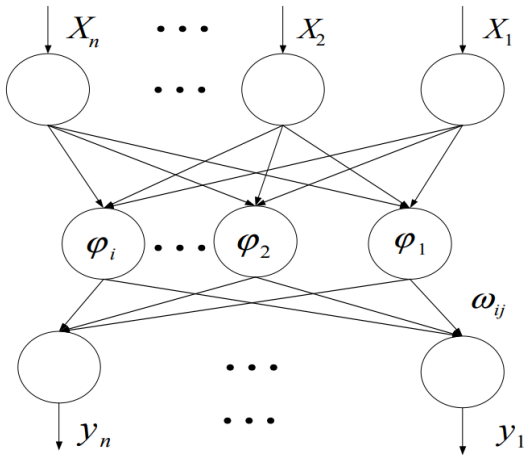

Fig. 1.9. A three layers RBF neural network structure (Yue et al., 2018).

1.3.2 The greenhouse climate model developed in this thesis

Such as mentioned above, many of the mechanistic greenhouse models were designed using the traditional energy-balance-based modeling method. However, the traditional modeling method usually requires multiple inputs such as the wall temperature, roof temperature and soil temperature, to simulate the resulting air temperature; this limits its applicability to real greenhouses where farmers need to predict the future greenhouse climate. In this thesis, a new, simple model is introduced. Its simplicity derives from embedding a group of conservation equations relating to the boundary conditions. The steady-state equation series is solved in each transient simulation step to simplify the user's input conditions. To obtain the boundary conditions for each step, a feasible assumption is made to simulate the wall's future temperature distribution with the help of a weather forecast based on the finite difference method or finite volume method (Zhang et al., 2019). However, for the greenhouse energy budget, only the temperature on both sides of the wall is needed, otherwise it would take up too much computational load. Therefore, a novel, easy-to-use wall temperature estimation method based on the energy balance was adopted for the environment model. It should be pointed out that few models have been developed to date that employ a mechanistic method combining temperature and humidity for use in Chinese solar greenhouses.

The main contributions of the proposed models are (Liu et al., 2021a):

1. A new greenhouse climate model is proposed that includes a novel and easy-to-use wall temperature estimation method based on the energy balance. With the

help of the embedded group of conservation equations, the greenhouse boundary temperatures can be simulated rather than having to measure the boundary temperature at each time step. Therefore, the number of model inputs is reduced, and the model can estimate the future greenhouse climate using only the current or predicted weather variables.

2. Several typical management measurements were considered and then validated, such as: arbitrarily defining the vents' opening angle and the time they remain open, the time the greenhouse vents are completely closed, and whether to use the thermal insulation blanket as a roof covering. These aspects are not usually considered in climate models for Chinese solar greenhouses.
3. The model is computationally light and fast, and was calibrated and validated using data from different seasons and from different years
4. The validation can be carried out in greenhouses of different sizes (and constructed from different materials) by switching the physical parameters; thus, the model is flexible and widely applicable. This was demonstrated by validating the proposed model in two greenhouses, each having a different size and located at different sites.
5. The greenhouse temperature and humidity are simulated together using a mechanistic model – this is the first study to do so for Chinese solar greenhouses.

A schematic description a CSG can be seen in Fig. 1.10. The south side of the CSG is a translucent fan-shaped roof, usually made of polyethylene cover. The north side is brick wall, concrete wall or compacted soil wall. The vents are opened by rolling the PE film.

The CSG are being innovated year after year. The half fan-shaped greenhouses of various materials and sizes can be seen everywhere in northern China. The wide of the CSG ranges 7 m to 20 m, and the length of the CSG could be 50 to 100 m. Some CSGs are built below the ground for 0.5 m to 1 m. This design is to better isolate the heat conduction between the greenhouse and the surrounding soil.

In general, the biggest reason for the difference in the appearance and heat performance of the greenhouse is the north wall. Sun et al. compared the greenhouse temperature with three different wall materials. The north walls of these CSGs are respectively built with the ordinary clay brick (greenhouse W_1), lightweight aggregate concrete block (greenhouse W_2) and a row of sand-filled cement pipes (greenhouse W_3) (Sun et al., 2022). The measurements show that greenhouse W_3 has the best heat storage performance in sunny days and the best heat release performance at night. Besides, the yield of tomatoes was the highest in greenhouse W_3. Although the continuous optimization of the structure and materials of the greenhouse is of positive significance, from the perspective of control, the lack of standardization makes the extensive application of the algorithm very difficult. This also reduces the enthusiasm of control algorithm developers. Usually, after a certain material or structure is adjusted, the greenhouse model needs to be recalibrated, and the control algorithm need to be redeveloped.

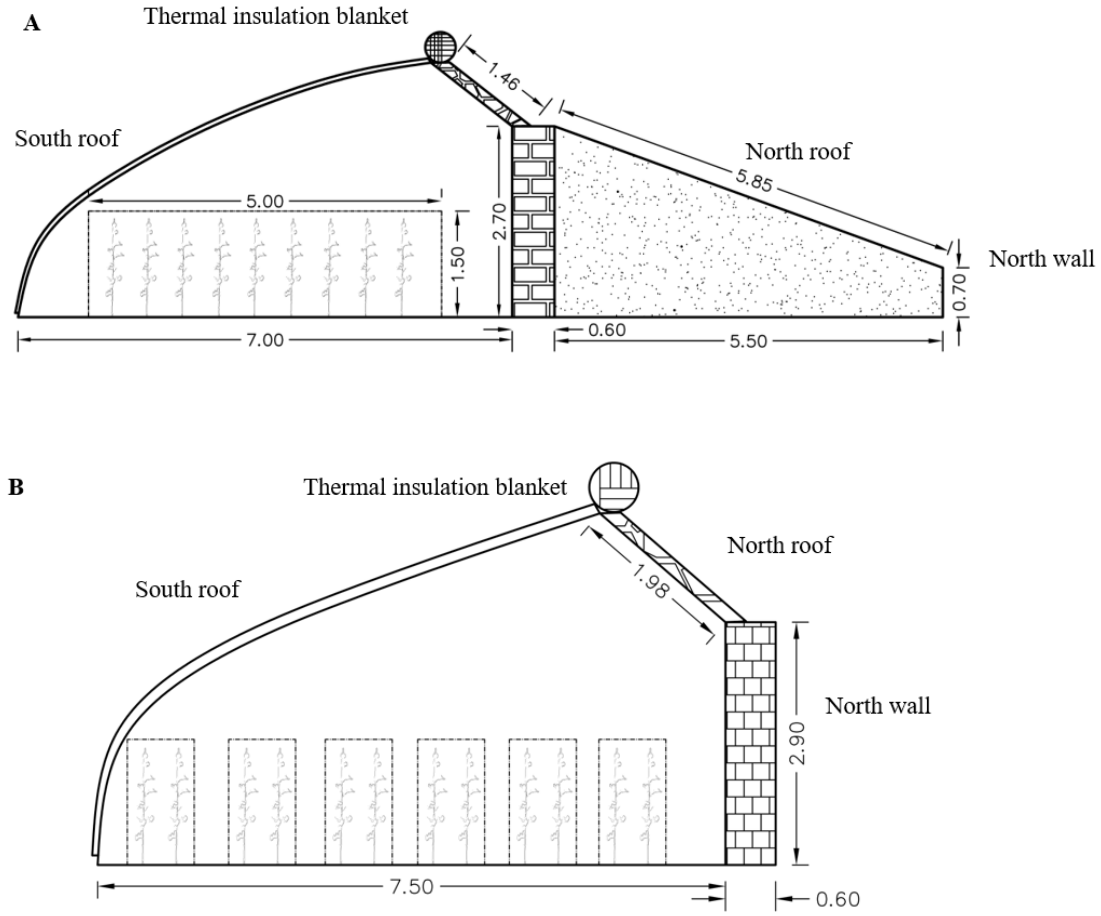

Fig. 1.10. Diagram of the structural dimensions (in meters) for greenhouses A and B.

Based on the above situation, this thesis takes two common CSGs in Beijing as an example, to develop and introduce a general modelling and calibration method for greenhouse temperature and humidity. This method is introduced in detail in a journal paper (Liu et al., 2021a). It is a flexible modelling method, even if the size or material of the greenhouse is different, developers can to reproduce the process by following the steps descripted in the paper.

The governing equations of this model for the greenhouse air temperature and relative humidity is a basic equation similar to Eq. 3 and Eq. 4., but summarized in the following

$$\frac{dT(t)}{dt} * \rho * c_p * v + h(t) * \rho * c_{pw} * v * \frac{dT(t)}{dt} = q_v(t) + q_{lea}(t) + q_c(t) + q_{liq}(t) + q_p(t) \quad (11)$$

which can be simplified as,

$$\frac{dT(t)}{dt} = \frac{q_v(t)+q_{lea}(t)+q_c(t)+q_{liq}(t)+q_p(t)}{\rho*v*(c_p+c_{pw}*h(t))} \quad (12)$$

where, T is the indoor air temperature, K; h is the indoor absolute humidity, kg kg^{-1}; t is time, s; ρ is the air density, (1.293) kg m^{-3}; c_p is the specific heat capacity of the air, (1005) J kg^{-1} K^{-1}; c_{pw} is the specific heat capacity of the water vapor, (1850) J kg^{-1} K^{-1}; and v is the greenhouse volume, m^3. The source terms are respectively the ventilation energy source term, $q_v(t)$, W; the air leakage energy source term, $q_{lea}(t)$, W; the convective energy source term, $q_c(t)$, W; the water vapor liquidation energy source term, $q_{liq}(t)$, W; and the plant energy source term, $q_p(t)$, W.

The humidity equation was obtained by mass conservation. The greenhouses' humidity source terms come from the ventilation humidity source term, $s_v(t)$, kg kg^{-1} s^{-1}; the air leakage humidity source term, $s_{lea}(t)$, kg kg^{-1} s^{-1}; and the plant humidity source term, $s_p(t)$, kg kg^{-1} s^{-1}. The equation is given as follows,

$$\frac{dh(t)}{dt} = s_v(t) + s_{lea}(t) + s_p(t) \tag{13}$$

The output of the model is relative humidity, RH. It is worth noting that the conversion between relative humidity and absolute humidity is widely used in the modeling process. Absolute humidity (AH) is often used when writing the mass conservation equation. However, some threshold discrimination algorithms in the middle links and the output of the model are regarding to the relative humidity. Since it is used everywhere, I prefer to package it into a block and assemble it when necessary.

The equations in the AH-RH block are as follows,

$$P_w(t) = \frac{h(t) * P}{0.622 + h(t)} \tag{14}$$

$$RH(t) = \frac{100 * P_w(t)}{610.78 * e^{\left(\frac{T(t)-273.15}{T(t)-34.85} * 17.2694\right)}} \tag{15}$$

The equations in the RH-AH block are as follows,

$$P_w(t) = 610.78 * \frac{RH(t)}{100} * e^{\left(\frac{T(t)-273.15}{T(t)-34.85} * 17.2694\right)} \tag{16}$$

$$h(t) = 0.622 * \frac{p_w(t)}{p - p_w(t)} \tag{17}$$

where P_w is the water vapor pressure, Pa; P is the atmospheric pressure, Pa. RH is the relative humidity, %.

A major innovation of this model is that in each transient step, a steady-state operation is performed to obtain the temperature and heat flux of the greenhouse shells, that are surface1, 2, 4, 5 and interior 3 (Fig. 1.11).

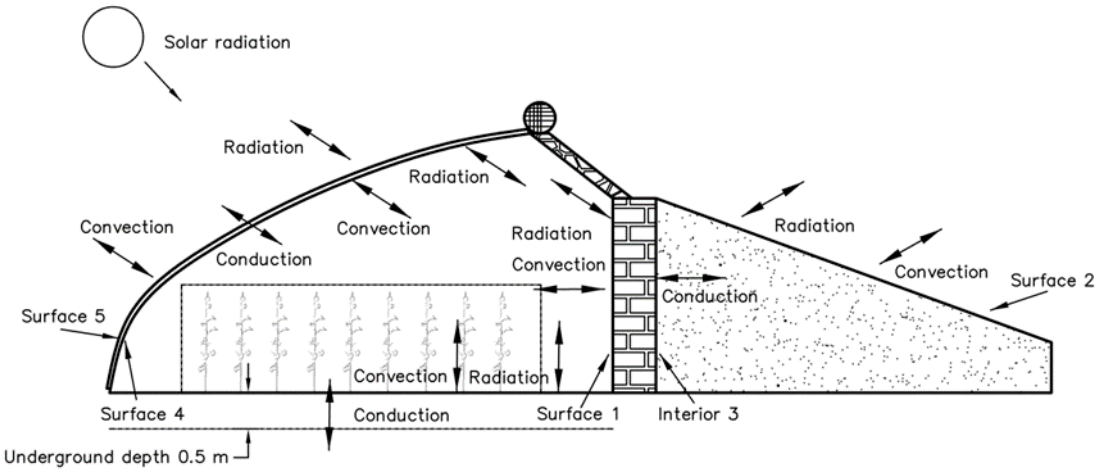

Fig. 1.11. Heat transfer liquidation of the greenhouse, convection, conduction and radiation.

The equations for the boundary conditions are a group of energy conversation functions, for the wall surface 1 in Fig. 1.11, the energy balance belongs to the convective term, the conduction term, and the long-wave and solar radiation term:

$$A_{s1} * c_{wi}(t) * \left(T(t) - T_1(t)\right) + \frac{(T_3(t) - T_1(t)) * Cd_{w1}}{Th_{w1}} * A_{s1} + \sigma * e_{wr} * (T_4(t)^4 - T_1(t)^4) * A_{s1} * x_{wr} + \sigma * e_{ws} * \tau_l * (T_o(t)^4 - T_1(t)^4) * A_{s1} * x_{wr} + \tau * R_s(t) * A_r * x_{rw} * a_{s1} = 0 \quad (18\text{-}1)$$

for surface 2, the equation terms are similar to Eq. (18-1), with the addition of the solar radiation term:

$$A_{s2} * c_{wo}(t) * (T_o(t) - T_2(t)) + \frac{(T_3(t) - T_2(t)) * Cd_{w2}}{Th_{w2}} * A_{s3} + \sigma * e_{ws} * (T_o(t)^4 - T_2(t)^4) * A_{s2} = 0 \quad (18\text{-}2)$$

for interior 3:

$$\frac{(T_1(t) - T_3(t)) * Cd_{w1}}{Th_{w1}} * A_{s1} + \frac{(T_2(t) - T_3(t)) * Cd_{w2}}{Th_{w2}} * A_{s3} = \frac{dT_3(t)}{dt} * \rho_{wall} * c_{pwall} * v_{wall} \quad (18\text{-}3)$$

for the transparent roof surface 4:

$$A_r * c_{ri}(t) * (T(t) - T_4(t)) + \frac{(T_5(t) - T_4(t)) * Cd_r}{Th_r} * A_r + \sigma * e_{rw} * (T_1(t)^4 - T_4(t)^4) * A_r * x_{rw} = 0$$

(18-4)

and for surface 5:

$$A_r * c_{ro}(t) * \left(T_o(t) - T_5(t)\right) + \frac{(T_4(t) - T_5(t)) * Cd_r}{Th_r} * A_r + \sigma * e_{rs} * (T_o(t)^4 - T_5(t)^4) * A_r = 0$$

(18-5)

T_1, T_2, T_3, T_4 and T_5, are the temperatures of surface 1, 2, 4, 5 (S. 1, 2, 4, 5) and interior 3 (I.3) (in K), respectively; A_{s1}, A_{s2}, A_{s3} and A_r are the area of walls and the roof (in m^2), respectively; Cd_{w1} is the thermal conductivity of the wall material close to S.1,W m^{-1} K^{-1}; Th_{w1} is the wall thickness between S.1 and I.3, m; Cd_{w2} is the thermal conductivity of the wall material close to S.2, W m^{-1} K^{-1}; Th_{w2} is the wall thickness between S.2 and I.3, m; σ is the Boltzmann constant, (0.0000000567) W m^{-2} K^{-4}; e_{ws}, e_{wr}, e_{rw} and e_{rs} are the long-wave radiation exchange coefficients from the wall to the sky, from the wall to the south roof, from the south roof to the wall and from the south roof to the sky, respectively; x_{wr} is the view factor from the wall to the south roof; x_{rw} is the view factor from the south roof to the wall; τ is the short-wave transmissivity of the south roof; τ_l is the long-wave transmissivity of the south roof; a_{s1} is the absorbed solar radiation coefficient of surface 1; and c_{wo} and c_{ro} are the convective transfer coefficients of the external wall and roof surfaces, W m^{-2} K^{-1}. ρ_{wall} is the density of wall, kg m^{-3}. c_{pwall} is the specific heat capacity of the wall, J kg^{-1} K^{-1}; v wall is the wall volume, m^3.

There are five unknows (T_1, T_2, T_3, T_4, T_5) in the equation group (Eq. 18), so that the equations are closed. See (Liu et al., 2021a) for the calculation of the other parameters, e.g. view factors and convective transfer coefficients.

To solve the above equations in Matlab, a nonlinear solve was used using the nonlinear programming toolboxes within Matlab (MATLAB, 2021).

1.3.3 Calibration and validation of greenhouse climate model

The model was validated during different seasons with data from Greenhouse A and Greenhouse B (see Fig. 1.10). Note that the accuracy of the model is demonstrated not only by validating the model in different seasons and in different years, but also by calibrating it in one greenhouse and validating it in the other. The calibration process was performed in MATLAB implementing the Monte Carlo method to estimate the global model parameters.

In a first step, the simulated indoor solar radiation gain was validated with the measurement (Fig. 1.12). Several intermediate variables that are difficult to measure are

also displayed and compared with the previous literatures to ensure that they are within a reasonable range. The air leakage rate varies from 0.2 h^{-1} to 0.6 h^{-1} and reaches its peak at noon. The convective heat transfer coefficients used in this model have been proven to be applicable to other scenarios (De Halleux, 1989; Papadakis et al., 1992; Walton, 1983; Mirsadeghi et al., 2013). Transpiration in cucumber varies from 0 to 160 W m^{-2} with the LAI ranging from 2 to 3.5. It began to rise after 6:00 a.m. and reached its peak at noon. Then, the transpiration rate gradually dropped to 0 after 18:00. Similarly, more internal indicators are tested independently (e.g. wall temperature; wall heat flux) to make sure the greenhouse climate model is designed properly.

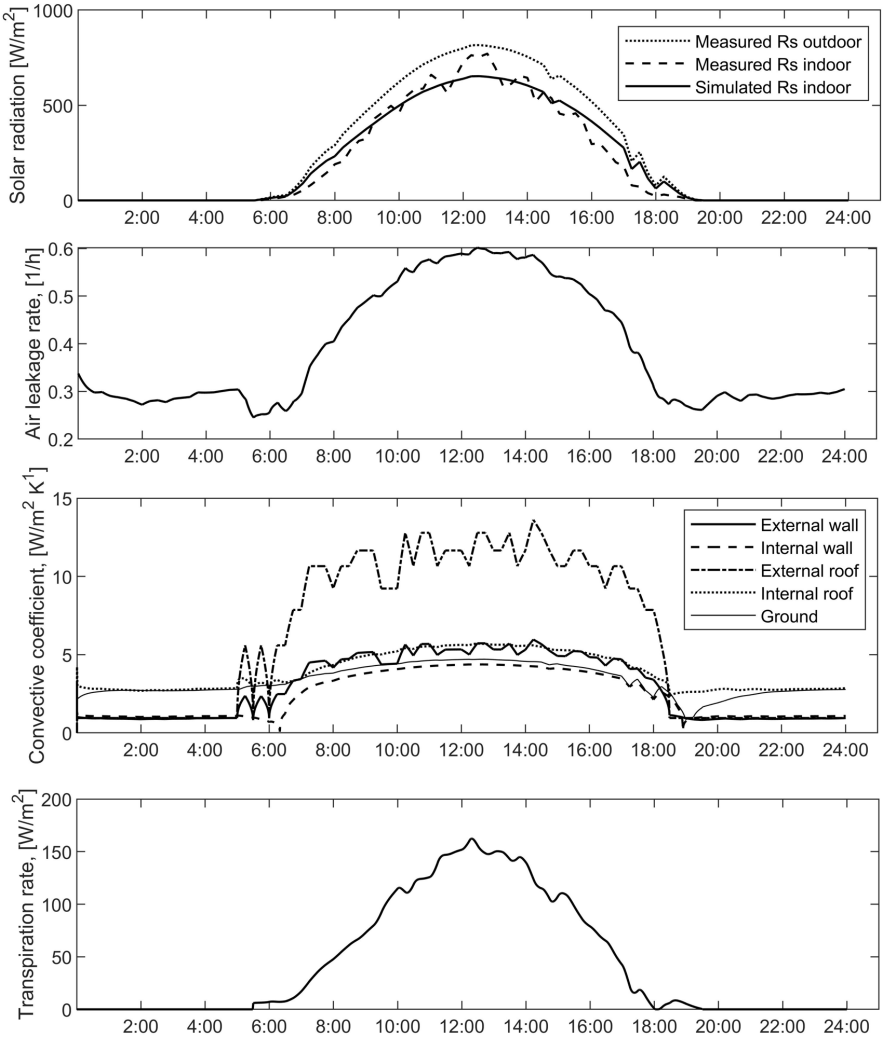

Fig. 1.12. Data set for the simulated solar radiation, air leakage rate, convective transfer coefficient and crop transpiration rate in a CSG.

In the next step, the model was calibrated and validated separately under fully closed and proportionally ventilated conditions. In this case, the thermal and mass (humidity) performance was validated on a single day when the vents are closed (Fig. 1.13). The curve fluctuation and peak value of the temperature and absolute humidity are consistent with the real situation, although the relative humidity error is striking due to the

temperature difference. This shows that the model is able to properly estimate the energy budget and water vapor gain of the greenhouse under fully closed condition.

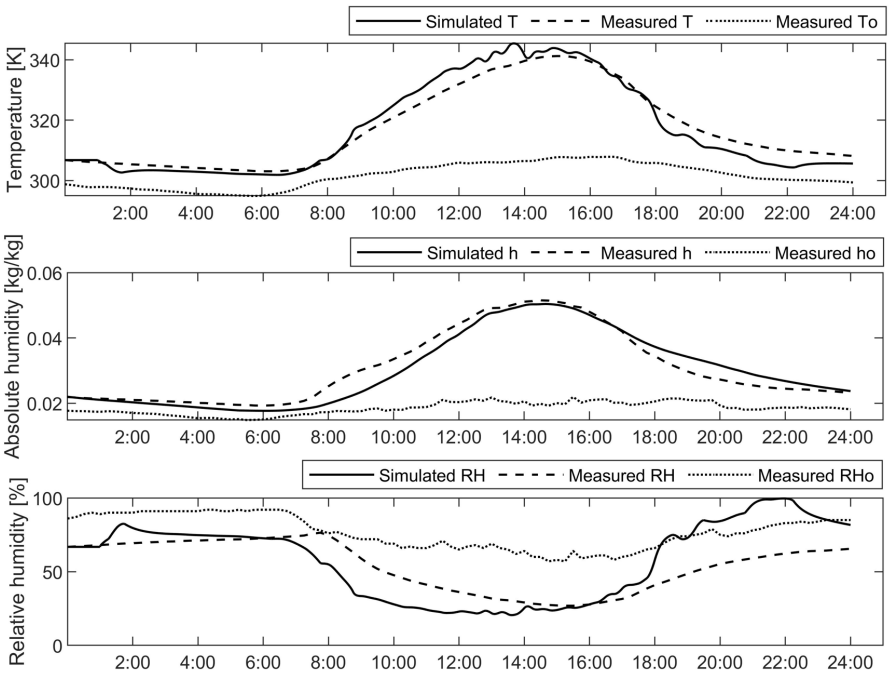

Fig. 1.13. Data set for the temperature and humidity under closed-vent conditions in a CSG.

Natural ventilation is an important part in modelling greenhouse climate, since most greenhouses rely on natural ventilation to conduct air exchange between indoor and outdoor. However, measurement of ventilation rate relies on a great deal of labour force. Then, validating the temperature and humidity response of the greenhouse under proportionally ventilated conditions could be an indirect way to test the natural ventilation modular, provided that the energy and mass gain have already been tested under fully closed condition. Fig. 1.14 shows the model's ventilation performance for different vent opening areas, in which the temperature curve and the absolute humidity curve indicate the energy and mass responses to the ventilation, respectively. The agreement between the measured and the simulated curves demonstrates the accuracy of the simulated ventilation rate. After passing the above tests, a good model should also maintain good robustness in different seasons and weather conditions, so it needs to be validated in stages for consecutive days. See Fig. 1.15 for an example (see Liu et al., 2021a for detailed information and more validation results).

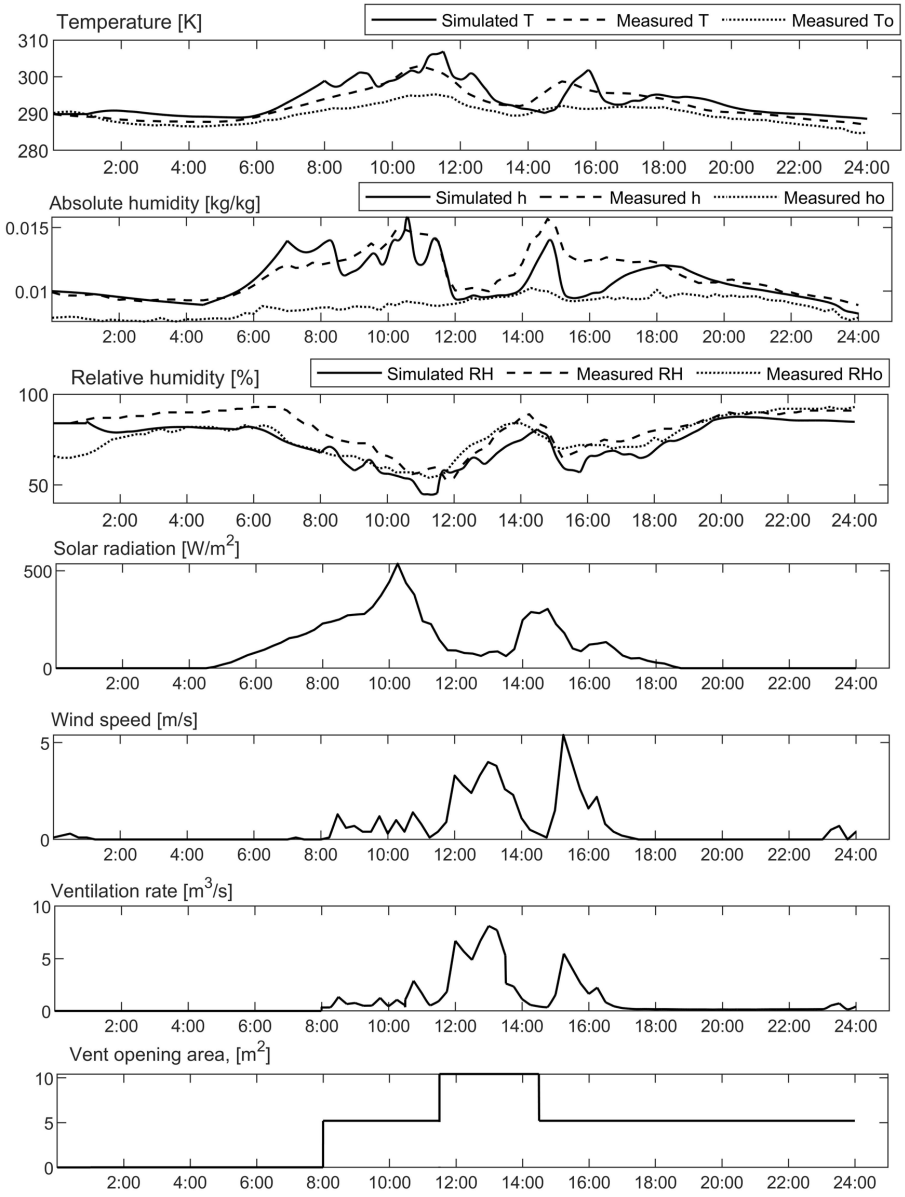

Fig. 1.14. Data set of the temperature, humidity, outdoor solar radiation, wind speed, simulated ventilation rate and the vent opening area under natural ventilation in a CSG.

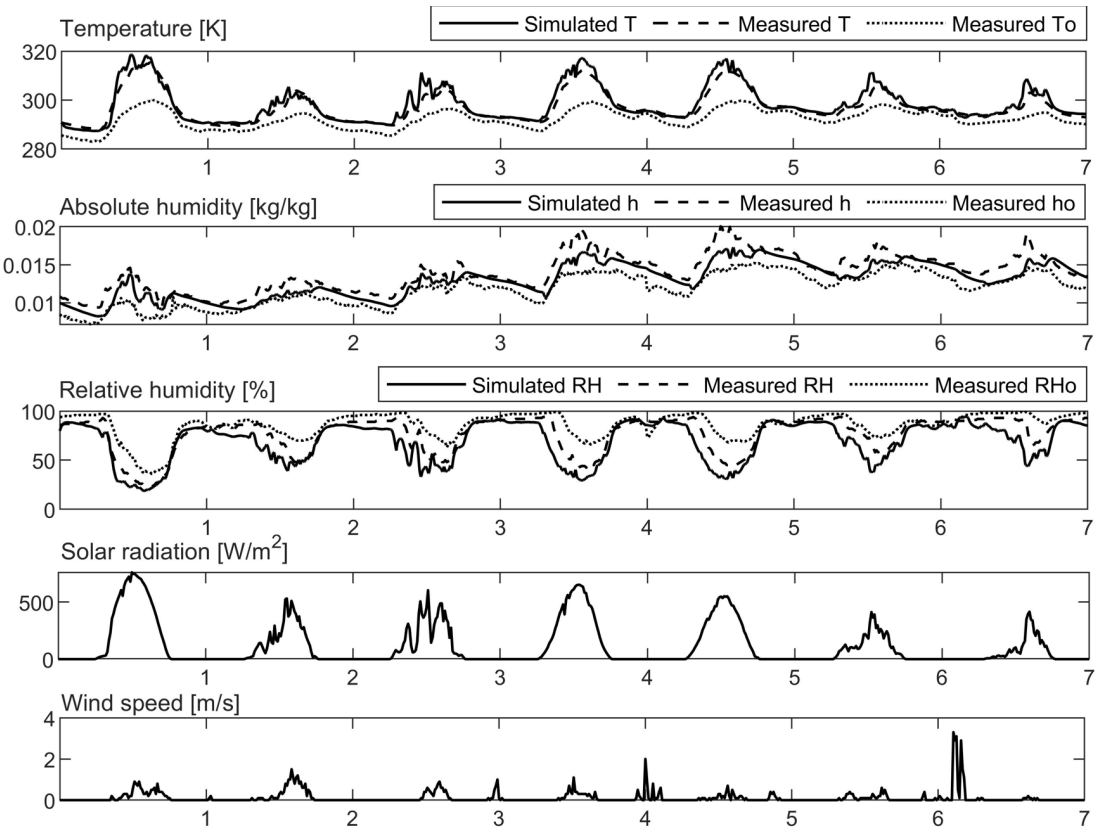

Fig. 15. Data set used for the model validation with the temperature and humidity, recorded on 20-26 September 2016 in Greenhouse A.

1.4 Greenhouse control

This section introduces the proposed control algorithm for the simultaneous control of the air temperature and humidity by using ventilation as the single actuator. First, a system identification methodology is performed to obtain low-order models for control purposes. This methodology consists in calculating high-order linear models based on ARX descriptions, and then, the simplificaions of those models for control design. Afterwards, an event-based control algorithm is proposed for the temperature control. Finally, a selective control scheme for the combined control of temperature and humidity is presented with a humidity priority control approach.

1.4.1 System identification methodology

The micro-climate inside a greenhouse is a highly complex process that involves multiple variables, phenomena, time scales and non-linear dynamics. System identification techniques allows to represent complex systems by using linear models based on data collected from input-output experiments performed in the real process. In a greenhouse, the inside micro-climate variables are strongly affected by the outside environmental conditions (disturbances) and the state of the actuators. For this work, the

inside air temperature and the humidity were the desirable variables to be controlled by only using the natural ventilation system. Therefore, simple models were required to capture the effect of the main disturbances and the natural ventilation on the greenhouse inside air temperature and the humidity. Notice that low-order models are required to design the control approach. However, due to the complexity of the greenhouse dynamics, first, a high-order linear model is obtained to capture the process behaviour, and afterwards, the model is reduced to a low-order model for control purposes.

As an initial step, some tests were carried out on the non-linear model described in (Liu et al., 2021a) to register data from various days for the system identification procedure. In each test, the natural ventilation system was programmed to offer a changing signal with different ventilation opening percentages during the day. Hence, the effect of the natural ventilation on the inside air temperature could be properly reproduced by the model to be identified.

For this work, an auto-regressive with exogenous input (ARX) model was selected to obtain the high-order empirical model for the inside air temperature and the humidity of the greenhouse.

In particular, the implemented ARX model for this work is a Multiple-Input and M-Output (MISO) model (one for temperature and another for humidity) that can be mathematically represented in discrete-time form by the following expression:

$$A(z)y(t) = \sum_{i=1}^{nu} B_i(z)u_i\,(t - nk_i) + e(t) \tag{19}$$

where y is the output, u_i are the inputs, e is the white noise, nu is the total number of inputs and nki is the number of samples corresponding to each input time delay. A(z) and Bi(z) are polynomials with the following structure:

$$A(z) = 1 + a_1 z^{-1} + \cdots + a_{na} z^{-na} \tag{20}$$

$$B(z) = b_{0_i} + b_{1_i} z^{-1} + \cdots + b_{nb_i} z^{-nb_i} \tag{21}$$

where na and nb are the order for polynomial A and B, respectively, and a and b are the coefficients to be determined in the identification procedure with real data of the process.

Once the high-order ARX model was obtained, a model reduction stage was accomplished for control purposes as commented above. In this model reduction stage, the relationship for each input with the output was modelled as a first-order model described by a transfer function expressed in Laplace domain for continuous time as follows:

$$G_i(s) = \frac{Y(s)}{U_i(s)} = \frac{k_i}{\tau_i s + 1} e^{-L_i s} \tag{22}$$

where k_i is the static gain, τ_i is the time constant and L_i is the time delay (dead time), all referred to the ith input. Thanks to transfer function models, the development of automatic control strategies can be easily achieved as explained in the following Section 1.4.2.

For the temperature model, the output of the ARX model is the greenhouse internal air temperature and the input is a set of randomly generated vent opening (Fig. 1.16). External air temperature, solar radiation and wind speed are considered as disturbances. The equation is described below,

$$y(t) = \frac{B_1(z)}{A(z)}u(t) + \frac{B_2(z)}{A(z)}v_1(t) + \frac{B_3(z)}{A(z)}v_2(t) + \frac{B_1(z)}{A(z)}v_3(t) + e(t) \quad (23)$$

where, y is the output, indoor temperature, °C; u is the vent opening, %; v_1 is the outdoor temperature, °C; v_2 is the solar radiation, W m^{-2}; v_3 is the wind speed, m s^{-1}; e is error, °C.

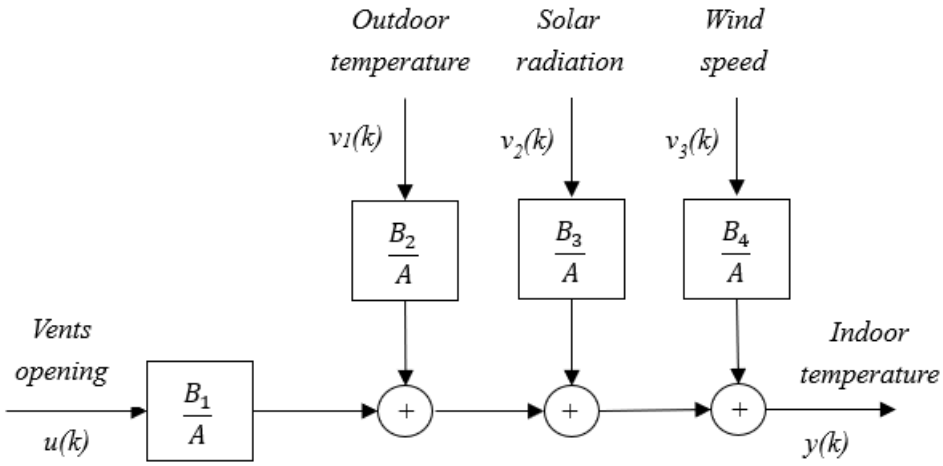

Fig. 1.16. ARX model for vents opening and internal air temperature with disturbances.

For the humidity model, two methods are compared to control the humidity. One is to directly trace the response of RH with the vents opening, the other one is to follow a dynamic set-point of AH derived from a desired RH and current temperature. For the first method, ARX models are developed respectively for the diurnal and nocturnal RH (Fig. 1.17 (a)). For the second method, the model output is current AH, kg kg^{-1} (Fig. 1.17 (b)). The AH is a quantification of the water vapor content in the greenhouse, which is significantly correlated with internal-external climate exchange, light and crop activities. The equations for RH and AH are similar to Eq. 23, see (Liu et al., 2022c) for more information.

Fig. 1.18 shows the developed ARX models and their inputs. The experiment is mainly conducted near noon of the day to reduce the disturbance caused by changes in solar radiation. The proportion of vents opening area is suggested to cover all control ranges from 0% to 100%. Finally, the ARX model is validated with real data to make sure

the model will work properly. With the linear models, transfer functions for temperature and humidity are easily obtained from the step responses. See PAPER RIAI for more information.

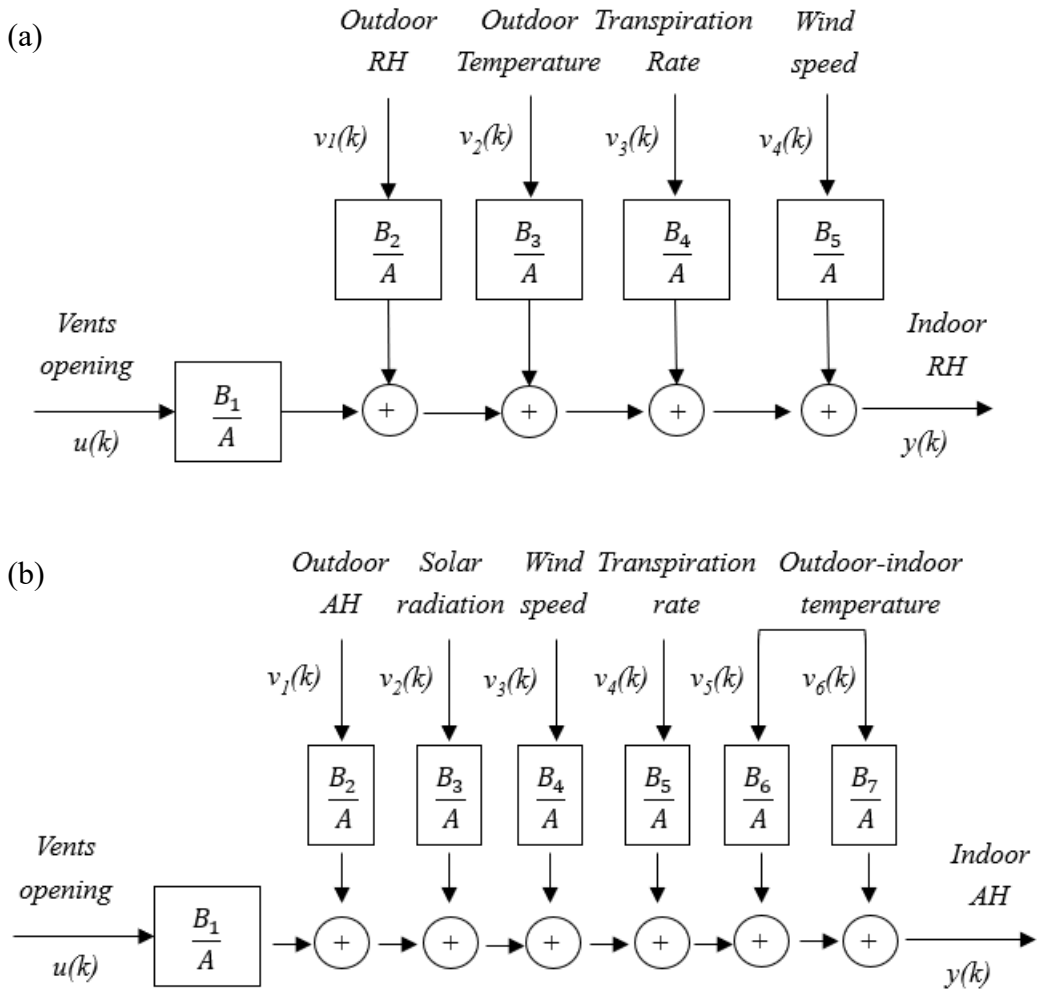

Fig. 1.17. ARX models for vents opening and internal humidity with disturbances. (a) for relative humidity and (b) for absolute humidity.

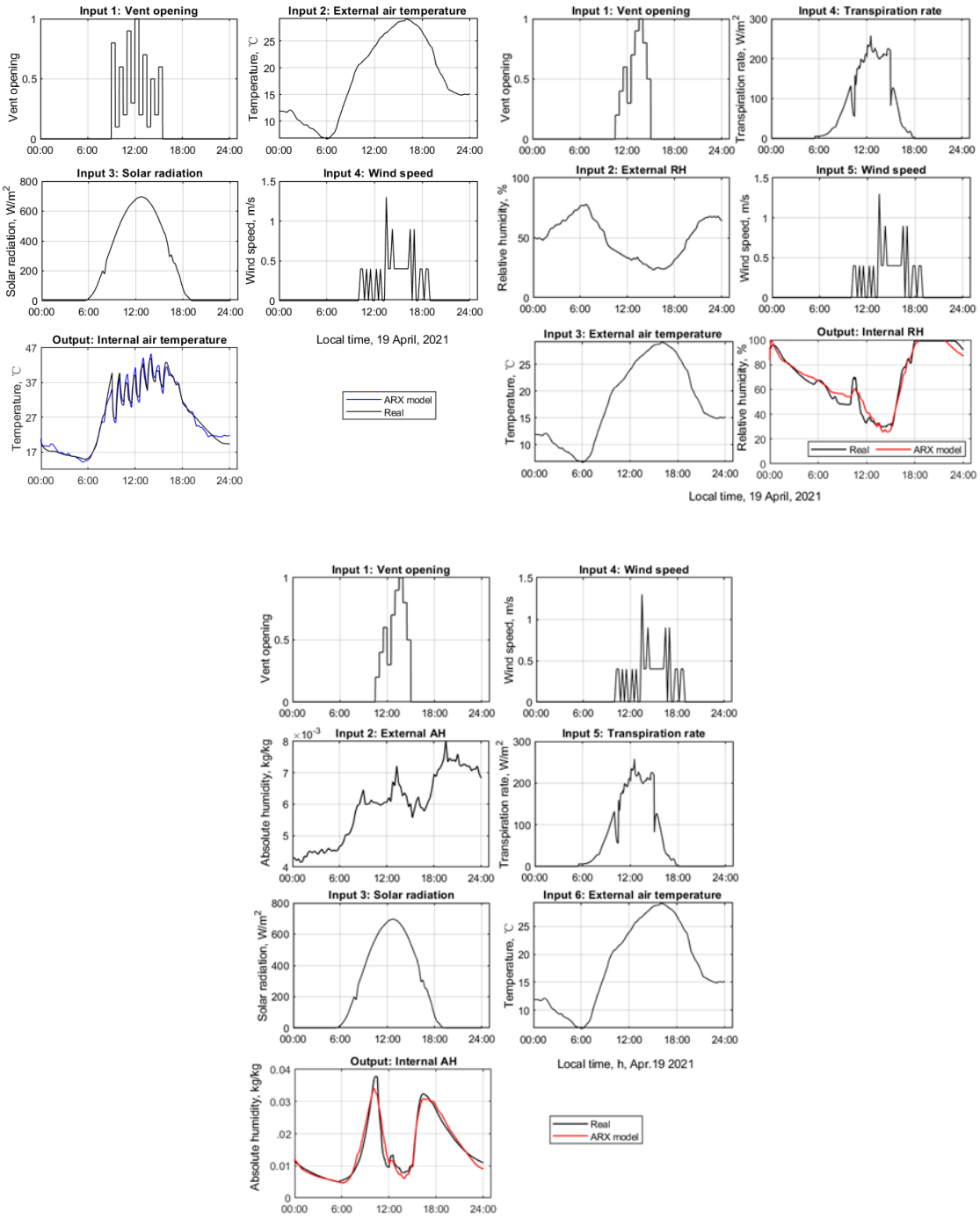

Fig. 1.18. ARX model identifications respectively for temperature, RH and AH.

1.4.2 PID control

The Proportional-Integral-Derivative (PID) controller is the most extended feedback control technique in most industrial processes (and particulary in greenhouses, (Montoya-Ríos et al., 2020), (Beschi et al., 2014)) and it is the one selected for this work because of its simplicity and high flexibility. The PID controller allows to calculate a control action depending on the existing error between the measured process output and the desired setpoint. A basic PID controller can be mathematically expressed as follows:

PID controllers are the widely used feedback algorithm to control the inside temperature in greenhouses. In a PID control algorithm, the control signal in each step is calculated based on the following equation,

$$u(t) = k_p e(t) + \frac{k_p}{T_i}\int e(t)dt + k_p T_d \frac{de(t)}{dt} \quad (24)$$

where where u is the control signal, e is the control error, kp is the proportional gain, T_i is the integral time, and T_d is the derivative time. The values for these parameters can be calculated based on different tuning methods depending on the desired control response and the process dynamics. A common formulation for a PID controller as a transfer function in Laplace domain is presented in the following equation:

$$C(s) = k_p(1 + \frac{1}{sT_i} + sT_d) \quad (25)$$

and a basic feedback control scheme based on a PID controller is shown in Fig. 1.19.

In industry, typically T_d=0 and then, a PI controller is considered, as it is the case in this thesis. The derivative term was omitted mainly because of the noisy signals in the real facilities. An additional modification was made to the basic structure of a PI controller in order to take into account the saturation of the ventilation motors. An anti-windup mechanism based on the back-calculation technique was incorporated to the PI controller to prevent the undesirable "windup" effect of the integral term [REF TO ASTROM BOOK]. When the actuator is saturated, the anti-windup mechanism shown in Fig. 1.20 is designed to reset the integrator value to zero by adding the signal es multiplied by the tacking constant $1/T_t$. The parameter T_t is an adjustable term to regulate how rapidly the integrator is reset.

The lambda (λ) method was selected as the tuning approach to calculate the parameters for the PI controller and to impose a desired behaviour for the feedback control response. According to this method, the PI controller parameters are calculated using the following expressions:

$$T_i = \tau \quad (26)$$

$$k_p = \frac{\tau}{k(t_r+\lambda)} \quad (27)$$

where λ is the tuning parameter representing the desired time constant for the closed-loop response, and k, τ and L are the parameters of the first-order model used to describe the process behaviour presented in section 1.4.1.

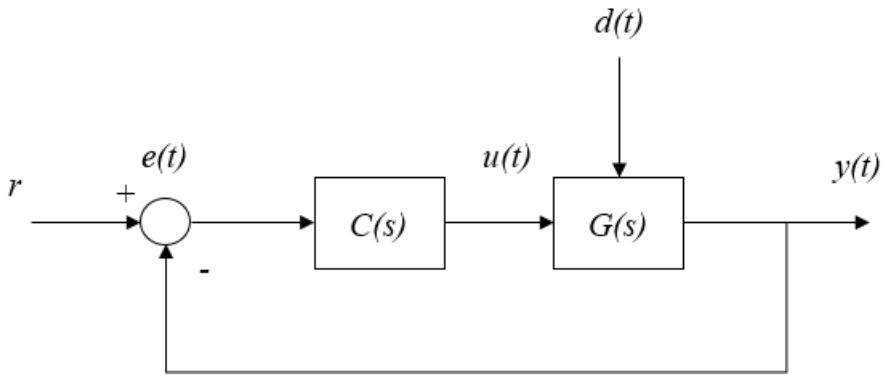

Fig. 1.19. Flow chart of control scheme. r is reference; e is error; u is vents opening; d is disturbances; y is internal greenhouse temperature or humidity.

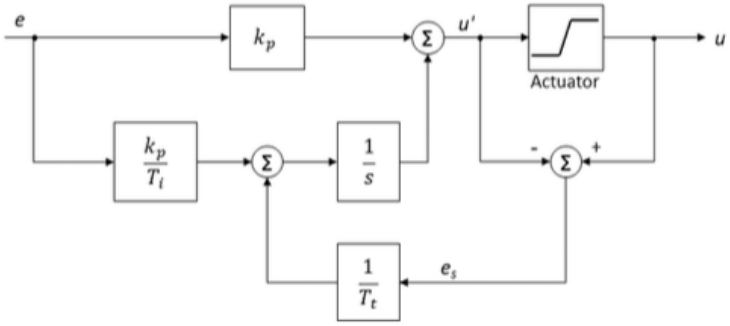

Fig. 1.20. Block diagram of a PI (Proportional-Integral) controller with an anti-windup mechanism.

1.4.3 Event-based control method for temperature control

The standard PID controllers require the actuator to respond continuously and frequently around the set-point, looking for reducing the control error with the highest accuracy. However, a resolution of less than 0.1℃ is too low for farm-oriented greenhouses, inevitably leading to waste of energy. The event-based control methods uses a parameter δ to reduce the control effort (Fig. 1.21). With this method, the controller is only triggered when the error is out of the limits, otherwise, the error is 0. The control method is realized by put the error between ±δ to a dead zone.

For instance, compared to classical PID controller, the number of events of an event-based controller in an Almería-type greenhouse was reduced by 34% when the error increased only by 1%; and the number of events were reduced by 83% when the error increased by 19.8% (Pawlowski et al., 2016). This method is an important contribution to promoting agricultural cleaner production. In this thesis, different values with δ = [0, 0.1, 0.2, 0.5, 1] relating to the event occurrence are tested. The results show that δ=0.5 is the optimum value, which significantly reduces the number of vent movements by 43.8%, while only increasing the temperature error by 1.13% (Table. 2; Fig. 1.22).

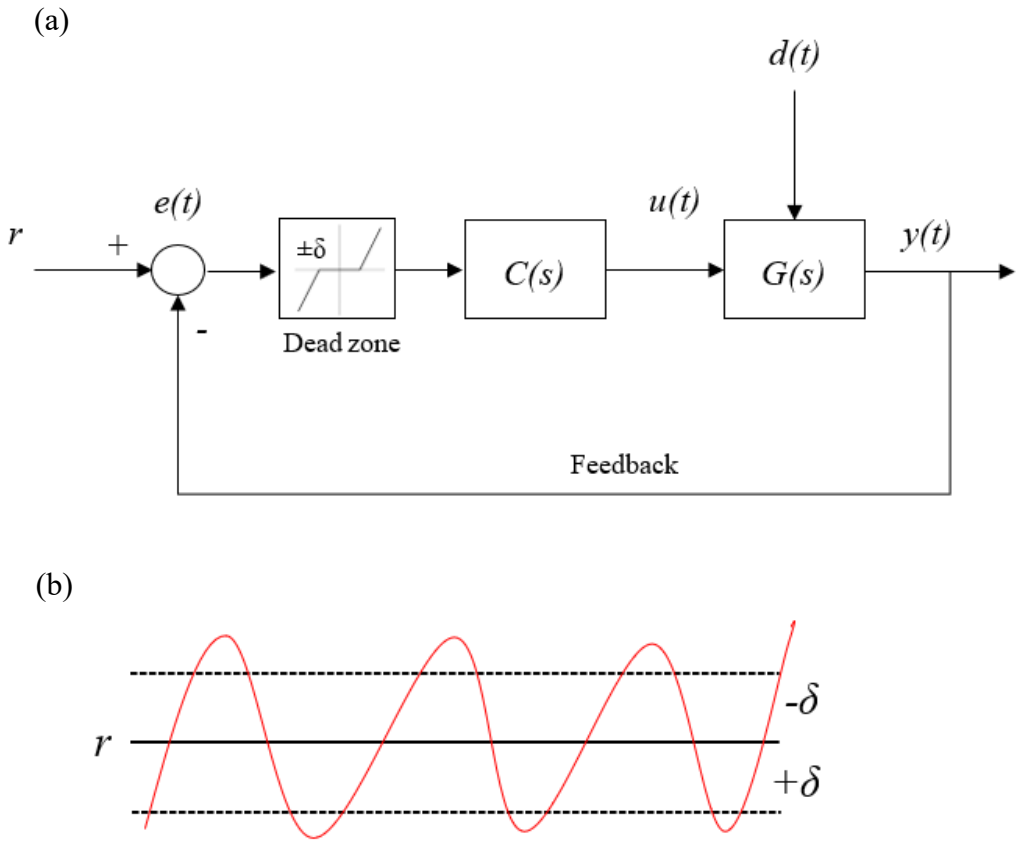

Fig. 1.21. Flow chart of the event-based control scheme (a). Description of event-based control method (b). Solid line in black is the reference; Dotted lines in black are the upper and lower limit; red line is the output y(t).

Table 2. Comparative evaluation of temperature control with different δ values.

δ	IAE (℃)	ΔIAE (%)	E (number)	ΔE (%)	IAU (0-100%)	ΔIAU (%)
0	7.7409e+05	0	22968	0	156.0	0
0.1	7.7593e+05	0.24	19463	15.3	143.1	08.3
0.2	7.7776e+05	0.47	17287	24.7	132.6	15.0
0.5	7.8286e+05	1.13	12913	43.8	116.1	25.6
1	7.9179e+05	2.29	11395	50.4	105.4	32.4

Note:

I. *IAE*, integrated absolute error $IAE = \sum_t(|e(t)|)$;
II. ΔIAE, (IAE - $IAE_{\delta=0}$) / $IAE_{\delta=0}$, in percentage %.
III. *IAU*, integrated absolute control effort $IAU = \sum_t(|u(t) - u(t-1)|)$;
IV. ΔIAU, ($IAU - IAU_{\delta=0}$) / $IAU_{\delta=0}$, in percentage %.
V. *E*, the number of events.
VI. ΔE, ($E_{\delta=0}$ - E) / $E_{\delta=0}$, in percentage %.

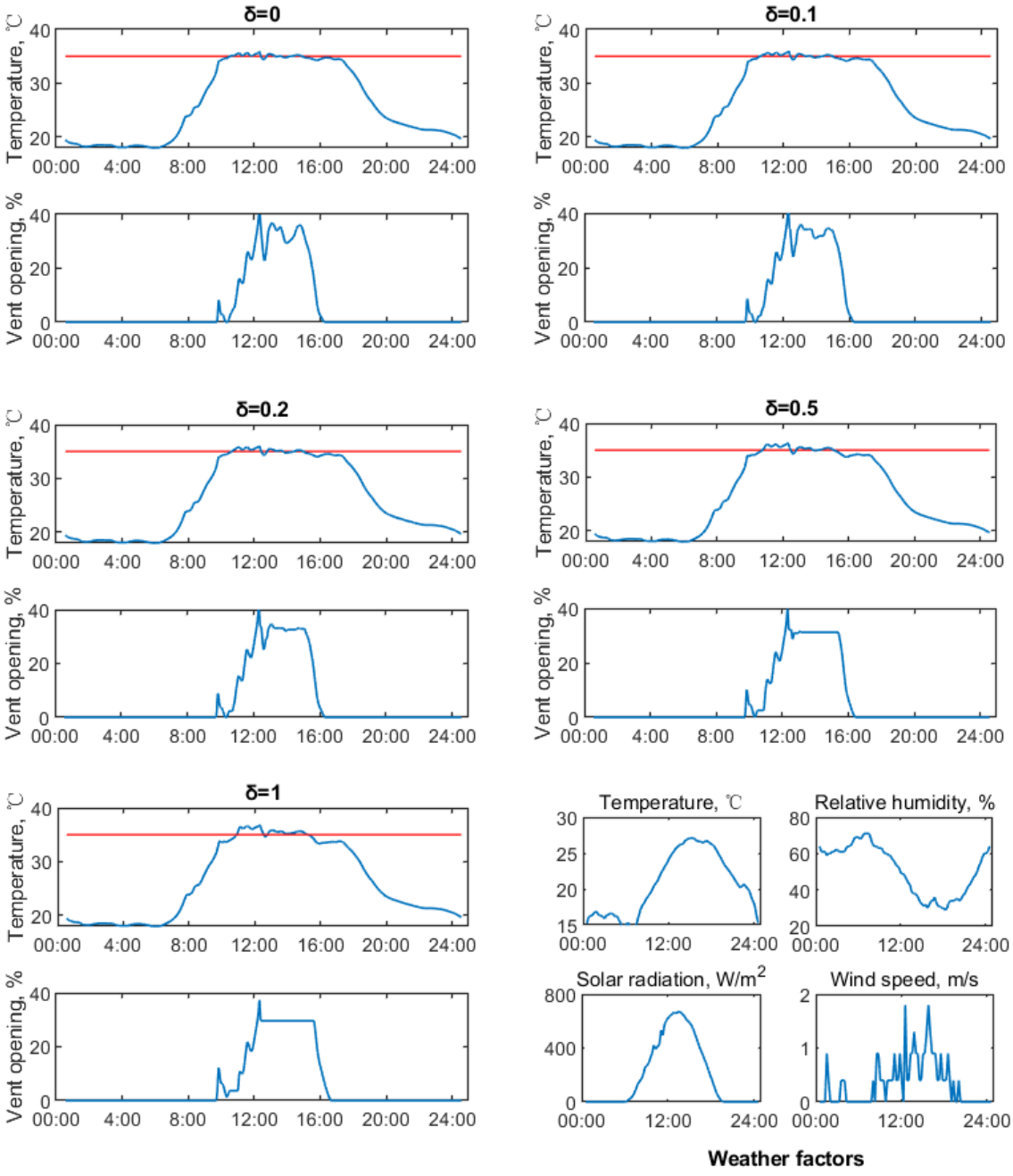

Fig. 1.22. Temperature control with different values of δ and external weather data in a CSG.

1.4.4 Greenhouse control strategies to manage crop fungal disease

In the above sections, we introduced the greenhouse climate model and downy mildew prediction, as well as the design of PID controller in the lower layer. This section describes two strategies to manage crop disease, using the above knowledge. One is to constantly keep the relative humidity below the threshold that leads to leaf wetting. The other one is to maintain the optimum diurnal and nocturnal temperature for cucumber production, but give priority to disease control, using a hierarchical optimization control strategy.

1.4.4.1 Selective algorithm for temperature and humidity control

The first control algorithm is called selective temperature and humidity control strategy with an event-based approach. The primary aim of disease control is to avoid leaf surface condensation caused by high humidity, one of the most common factors. Excessive high absolute humidity, or low temperature that close to the dew point leads to high relative humidity. Currently, the LWD relating to high humidity is studied to be measured or estimated by models. LWD is estimated using relative humidity threshold, usually between 80% and 95%, depending on geographic location and climate.

To control the greenhouse climate, normally, only the temperature PI controller is activated. However, the humidity priority is given. The aim of humidity control regarding to the CSG is usually avoiding high humidity, because excessive low humidity for the CSG is very rare. In this study, the relative humidity is controlled by given an upper limit, when the RH is over that limit, the vent opening is increased. Specifically, two values of 80% and 60% for the RH is designed as the upper limit and the lower limit (Fig. 1.23). When RH is over the upper limit, the humidity PI controller is activated to put the RH to 60%. When RH $\leq$ 60%, switch to the temperature actuator with the original temperature set-point. Note that two cases are different. When the RH rises to this range (60%-80%), the RH controller is not activated. When the RH is over 80% and is controlled to this range, the RH controller needs to be continue activated until the RH is lower than 60%.

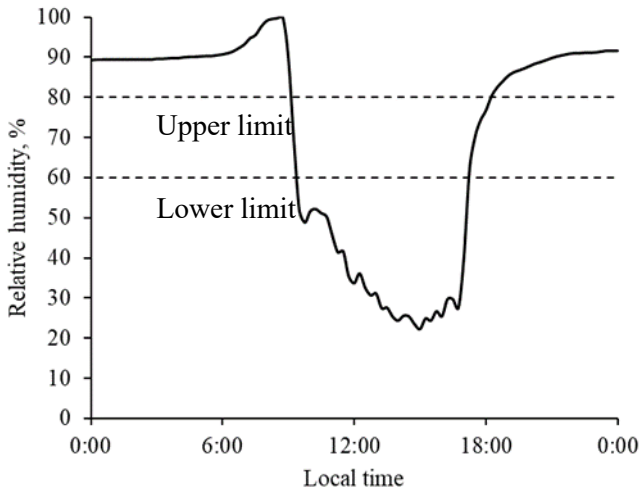

Fig. 1.23. Description of the humidity priority control scheme.

Fig. 1.24 shows a temperature control results in two consecutive weeks in the top graphic. The conventional fixed set-point temperature control is a very common practice in actual production. However, this sometimes leads to high RH, which causes fungal disease and damages the crops, e.g. on days 2, 7, 8 and 9. The application of humidity priority control scheme in Fig. 1.24 shows an ideal performance of dehumidification in these days. The dehumidification action has an uncertain influence on the temperature. High humidity usually occurs in the afternoon or at night. If it happens during the day, the dehumidification behavior has little effect on the temperature, e.g. day 2. When it happens during the night, the controller has to open the vents so that both of the temperature and RH are decreased, e.g. day 8. In any case, this humidity priority control scheme greatly avoids the loss of energy and reach the aim of dehumidification. Note that this approach may cause the nocturnal temperature to fall below 10 ℃, e.g. day 8. It is interesting to design independent dehumidification strategies for a specific crop, regarding to the tolerating low temperature.

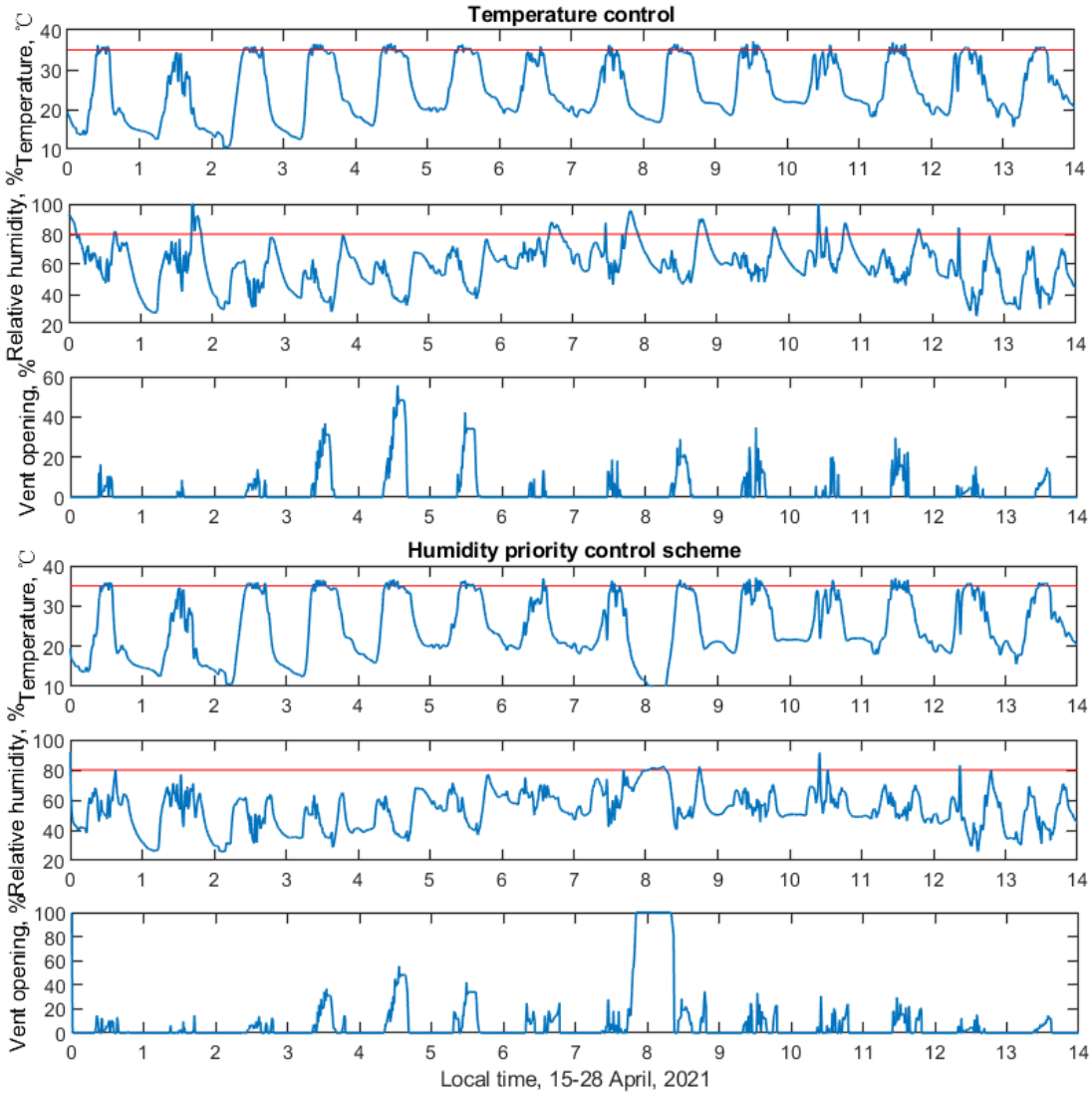

Fig. 1.24. Comparative control results when only controlling the temperature and controlling the temperature with the humidity priority control scheme in consecutive days

The above method indeed eliminates climate factors with fungal disease infection risk, but it has an obvious disadvantage that excessive dehumidification leads to low temperature and low humidity, which obviously affects the growth of crops, because cucumbers are warm and wet loving crops.

1.4.4.2 Hierarchical control strategy to manage crop fungal disease

The second proposed control approach is based on hierarchical optimization control algorithm to keep the optimum temperature for cucumber production, but giving priority to avoiding positive reports for downy mildew infection. From the previous literature review, it is known that the ongoing leaf wetting and disease infection are detected or simulated throw LWD models and primary infection models. When LWD appears, the greenhouse is suggested to conduct ventilation for dehumidification. However, this process leads to heat leakage and reduces the accumulated greenhouse temperature. The hierarchical optimization control strategy provides the optimal temperature set-point in each transient step to contribute to the infection reduction. In the lower layer, a PI controller keeps the optimum temperature for cucumber production throw an expert supporting system (Fig. 1.25). In the upper layer, the optimizer calculates the suggested set-point in order to avoid the ongoing infection. For this, the disease infection model (given by the combination of the greenhouse climate model together the disease model previously discussed) is simulated by a three-day prediction using weather forecast. The new set-point is calculated by a cost function, which ensures the minimum integration of absolute error between the current set-point and the greenhouse temperature.

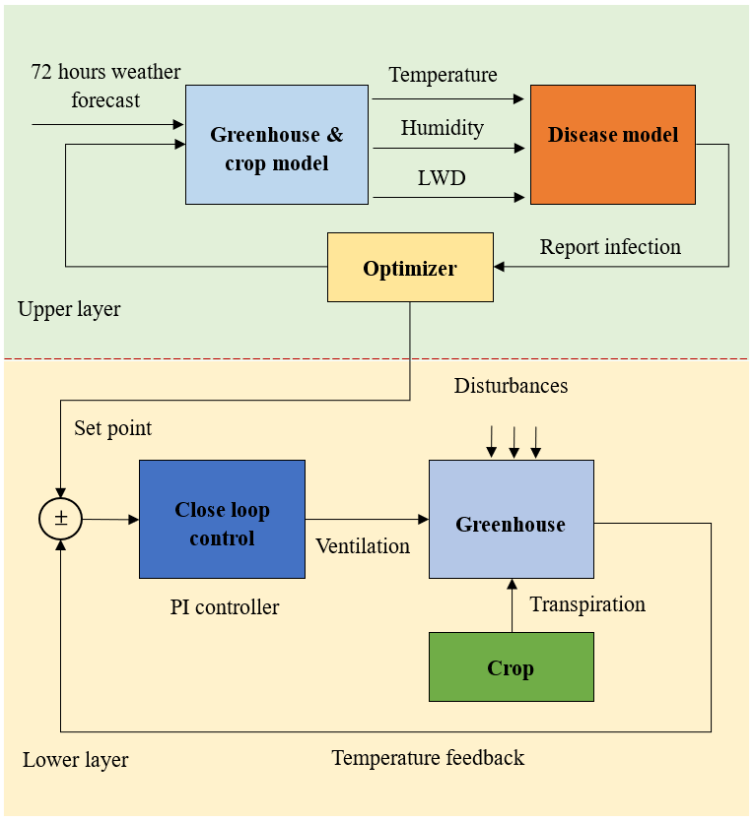

Fig. 1.25. Hierarchical control architecture of greenhouse disease.

For the weather forecast, a web-based model based on a REST API service provided by Weatherbit is used (WeatherBit, 2019). This model allows to obtain weather forecasts in different geographical locations around the world. For this work, that service was used to obtain weather forecasts 72 hours ahead with an hourly sampling period. It is generally within 72 hours from infection to the deadline of incubation. Thus, the 72 hours prediction and climate control are adequate to avoid the occurrence of downy mildew. Temperature, humidity, wind speed and solar radiation forecasts are obtained to be used as inputs to the proposed methodology. This web-based service requires basic parameters such as latitude, longitude, language, key and number of hours for the forecast.

To demonstrate the accuracy of the weather forecast, a local weather station located at the greenhouse facilities was used. Specifically, the Davis Vantage Pro2 Plus (Davis Instruments, Hayward, USA) weather station was installed on an open land near the greenhouse, to measure the total solar radiation (range, 0-1800 W m^{-2}; accuracy, ±5%), wind speed (range, 0-67 m s^{-1}; accuracy, ±5%), air temperature, and relative humidity (see Fig. 1.26).

Fig. 1.26. Photo of the outdoor weather station.

The weather forecast data was downloaded and updated by every hour from 00:00 on April 25 to 00:00 on April 28, 2021. The RMSE (Root Mean Square Error) was used as metric to evaluate the resulting accuracy. The RMSE of temperature and relative humidity between weather forecast and outdoor measurement were evaluated as range 2.5-4.5 ℃ and 25-37% in 73 samples on April 25-30. The temperature prediction was ideal and the weather forecast humidity was a little bit lower than the measurement (Fig. 1.27). The measured wind speed was lower than the weather forecast data, of which, the RMSE ranges 2.5-3 m s^{-1}, because the impacts on wind speed of obstacles and height from the ground were not considered by the weather forecast. The RMSE of solar radiation forecast ranges 182-262 W m^{-2}. Both of the measured and predicted solar

radiation contain the attenuation by clouds. Anyway, the accuracy of the weather forecast was good enough for the objective of this work. To improve the accuracy, a receding horizon approach was used, where inputs to the greenhouse climate simulation were updated hourly, and new prediction for the next 72 hours was obtained every hour.

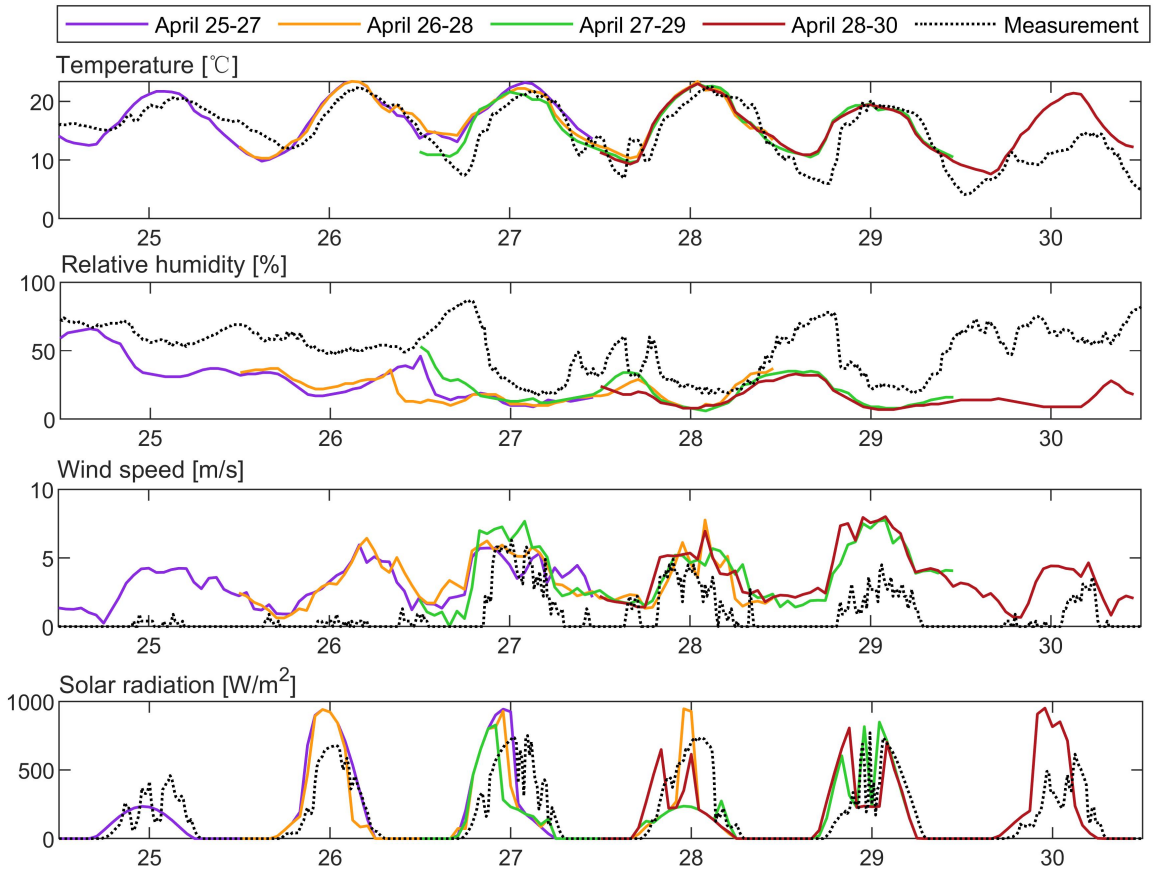

Fig. 1.27. Weather forecast data and outdoor measurements on April 25-30, 2021. Colors represent samples for the next 72 hours collected at 00:00 on each day.

To test the capabilities of the proposed hierarchical control approach, an experimental evaluation was performed using classical disease-detection methods in order to collect enoguth data for this study. The experimental greenhouse is located at the National Precision Agriculture Demonstration Base (40°18' N, 116°47' E, annual average temperature :11.8 °C), Changping District, Beijing. The seedling of fruit cucumber 'Jingyan Mini II' was transplanted on March 4, 2021, in an average of 36 rows. A layer of plastic film was covered on the soil, and the drip irrigation belt was buried under the plastic film for irrigation and fertilization. The harvest season was ended on 7 July 2021.

A weekly observation of downy mildew was conducted since transplanted. Until the early symptoms of downy mildew appear (light yellow water-stained polygonal disease spots on the leaves, Fig. 1.4(b)), the observation frequency was changed to two times a week. The downy mildew symptom and lead area index (LAI) were observed at five fixed locations distributed in the greenhouse for every investigation, according the five-point sampling method (Liu et al., 2022b). Mildewed leaves were scored with a rating (r) of 0,

1, 3, 5, 7 or 9, denoting proportions of disease over the whole leaf area of 0, 1-5%, 6–10%, 11–25%, 26–50% and > 50%, respectively (Liang et al., 2005). Disease index was calculated according to the equation,

$$DI\% = \frac{\sum(n_r * r)}{N \times 9} * 100 \qquad (26)$$

where r is rating value; n_r is number of disease leaves with a rating of r; N = total number of investigated leaves. Fig. 1.28 shows the disease index development along five sampling point, when this greenhouse is managed by the experience of farmers. The disease began to appear after April 20, and then the disease index increased rapidly. The farmers conducted two treatments respectively on May 7 and May 15. These treatments include the use of pesticides (spray of propamocarb hydrochloride, carbamate fungicide for downy mildew) and the removal of diseased leaves.

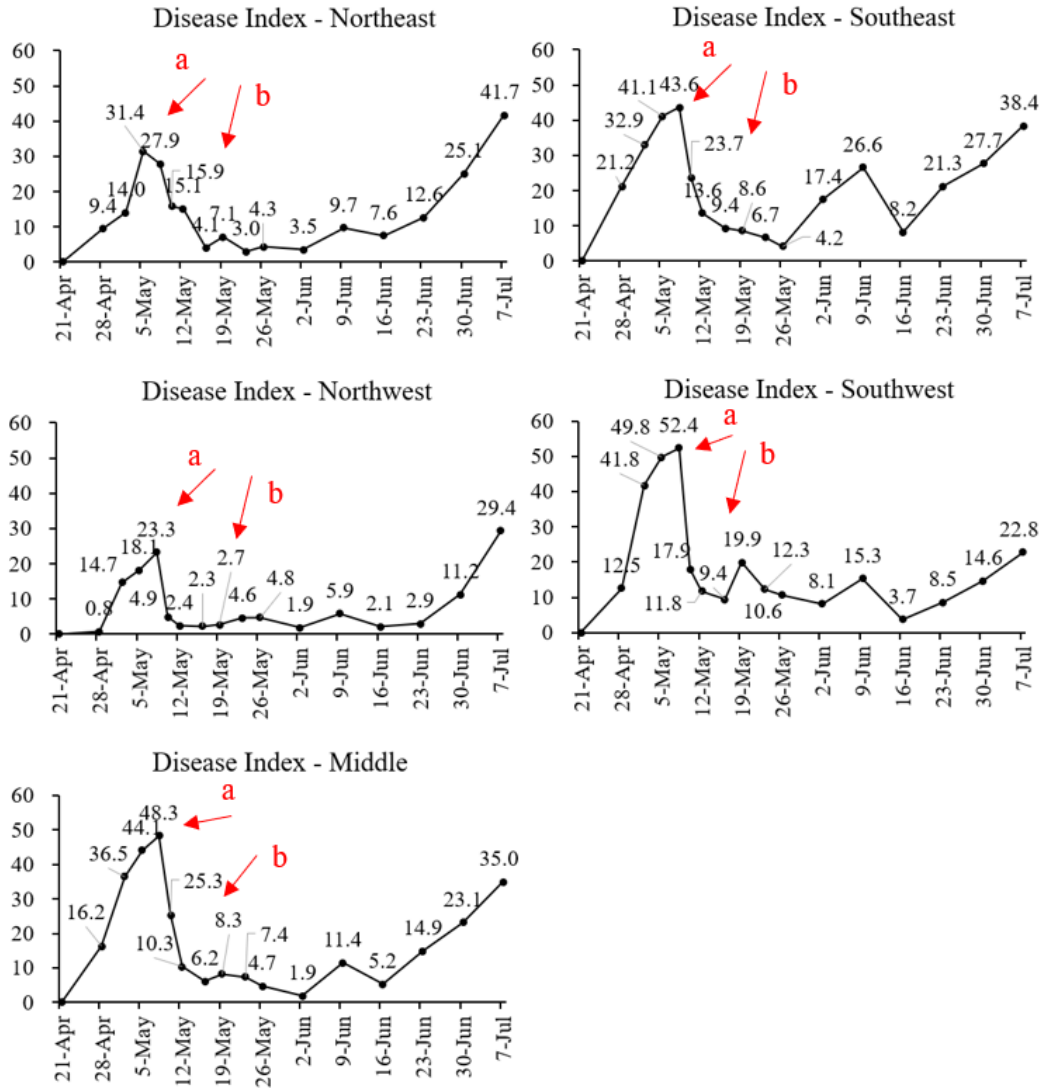

Fig. 1.28. Disease index at five sample point in the greenhouse. a is the first treatment and b is the second treatment.

Let's see the warning messages given by the primary infection model before the disease occurs. The blue bar in Fig. 1.29 shows the positive reports. If the infection factor over 40 h°C, which is calculated by Eq. 1. Then a positive report is issued. It usually takes three days to complete the incubation period after infection, and then symptoms appear. Multiple positive reports before April 23 are the first condition for the rapid development of the following disease index. Therefore, the aim is to remove all of the positive reports derived from the greenhouse climate, as well as keeping the optimum temperature for cucumber production, through the hierarchical control strategy. In this way, the crop disease is suppressed through climate control, not through fungicides, which is relevant for cleaner production.

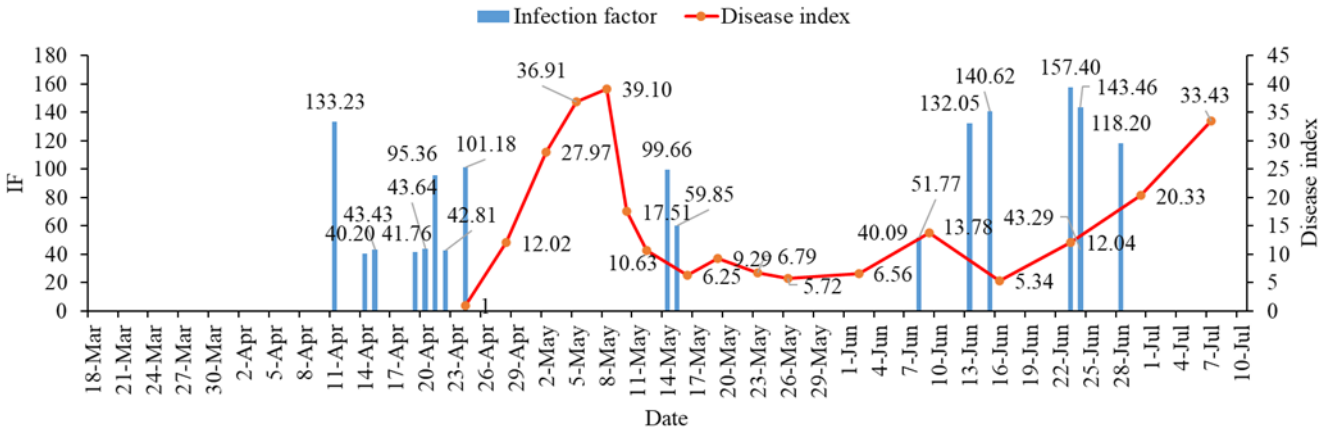

Fig. 1.29. Infection factor (IF) from model prediction of cucumber downy mildew and averaged disease index from investigation.

In the lower layer of the hierarchical control scheme, the PI controller keeps the optimum temperature for cucumber production. Cucumber is a warm season crop, and the temperature is closely related to yield. At germination, average temperature is needed between 25-35 ℃. At growth stage, the optimum temperature is suggested by different researchers (Table 3). The minimum and maximum tolerable temperatures for cucumber are respectively 13 ℃ and 40 ℃ (Pal et al., 2020). In this study, the expert supporting system provides a diurnal temperature set-point as 30 ℃ and suggests closing the vents at night in order to keep the nocturnal temperature as high as possible. The outdoor nocturnal temperature in northern China is usually low. When a positive report for downy mildew is issued, the set-point is modified by the optimizer. Besides, the lower and upper limits of the tolerable temperature for cucumber growth have the highest priority, that are set to 13 ℃ and 40 ℃ in this study. When the set-point given by the optimizer exceeds these two limits, it is changed to the closed boundary value.

Fig. 1.30 shows the closed-loop control in the lower layer. This control result keeps the greenhouse temperature around a constant set-point, which is the optimal temperature for cucumber production. However, it leads to high humidity in the greenhouse, because the vents are closed in order to keep the heat. Finally, two positive reports for the infection

of downy mildew are issued in one day. This demonstrates that in the season of up to 100 days, control only based on crop growth will lead to many risk stages conducive to downy mildew infection.

Table 3. The optimum diurnal and nocturnal temperature for cucumber production suggested by different researchers.

Diurnal temperature	Nocturnal temperature	Literatures
27 ℃	23 ℃	Ding et al., 2019
30 ℃	20 ℃	Hui et al., 2003
28 ℃	≥18 ℃	Singh et al., 2017

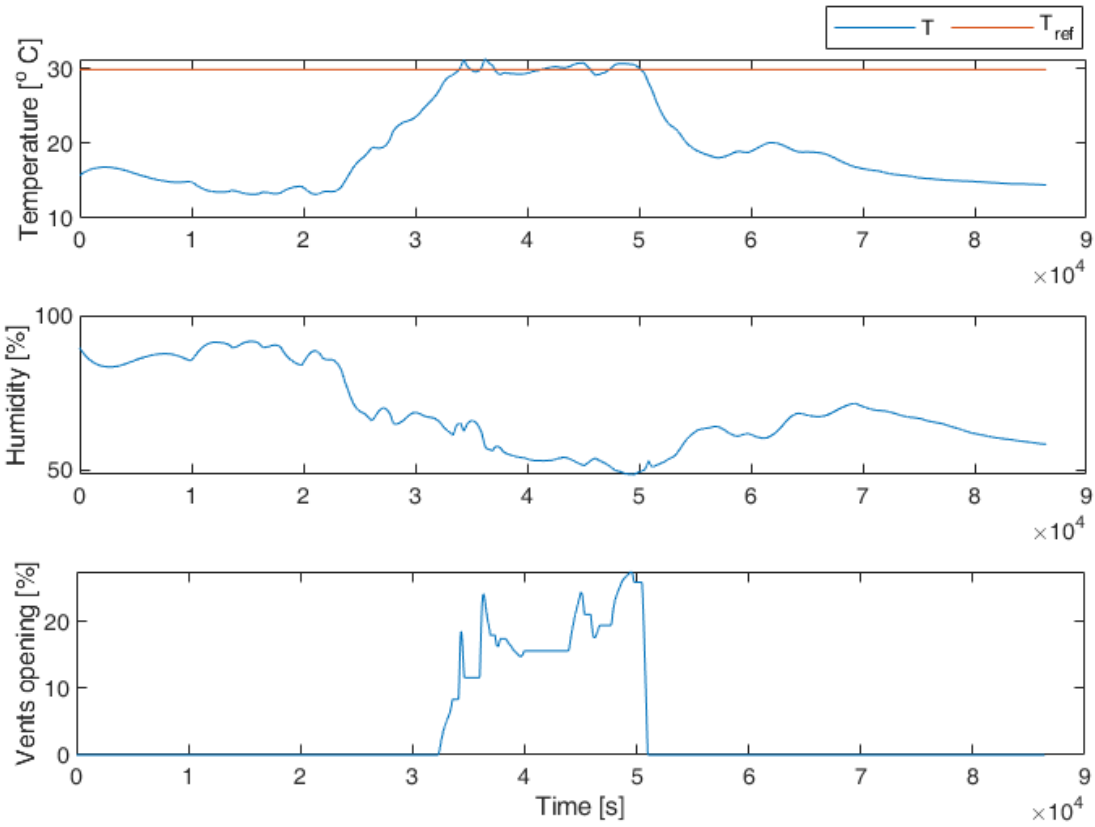

Fig. 1.30. Low level control for cucumber production.

Fig. 1.31 shows that the environmental factors that lead to downy mildew infections are eliminated by a hierarchical control strategy. The optimizer gives an independent optimal set-point by every hour. Then the horizon is moved forward for one hour and repeat the same procedure. The risk of infection can therefore be avoided and the set-point always changes around the optimal temperature for crop growth. Compared with the control strategy of direct cooling and dehumidification to avoid disease, this method contributes with a better solution in production and safety.

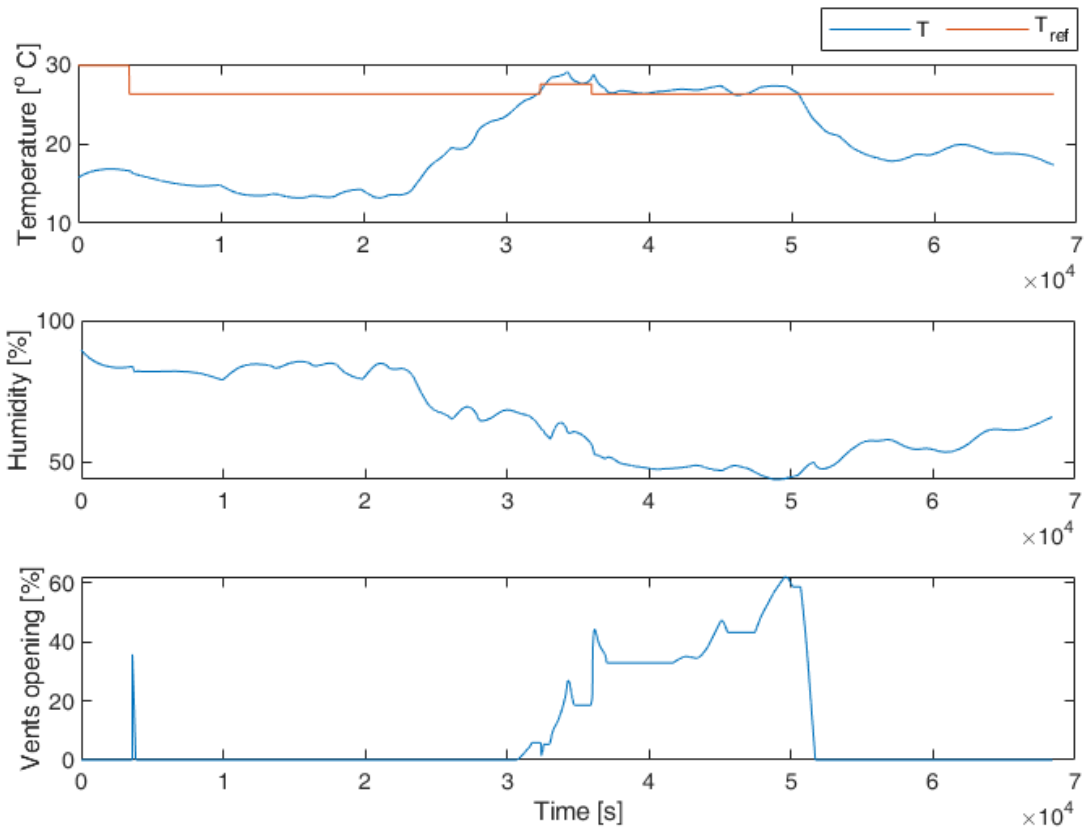

Fig. 1.31. Hierarchical control in order to keep the optimum temperature for cucumber production, but give priority to avoiding positive reports for downy mildew infection.

1.5 CFD (Computational Fluid Dynamics), a further study of greenhouse modelling

Classical closed-loop control takes the temperature in the center of the greenhouse as the current temperature. This temperature comes from the greenhouse model output or the sensor placed in the center of the greenhouse. However, there are remarkable non-uniformities in leaf microclimate within the canopy in a greenhouse, with implications for variable heat and mass exchange, and the heterogeneity distribution of greenhouse climate (Kimura et al., 2020). For the CSGs, its south side is exposed to more light, and the temperature is higher in the daytime and lower at night, due to the asymmetric structure. The future closed-loop control may calculate the optimal feedback temperature according to the temperature distribution in each transient step. It may be costly to install many sensors in the greenhouse. Thus, a practical solution is to develop a distribution model based on the current weather condition and greenhouse structure, and CFD technique is one of the more powerful tools to achieve this goal.

This section describes the development of CFD model for the CSGs, including the wind field, building thermal conduction, and radiation. Moreover, a special function realization relating to the crop zone microclimate, using UDFs (User Defined Functions) is proposed. Developing a CFD model for the greenhouse requires complex steps, such

as geometric modeling, meshing, coding functions, and defining boundary conditions. It also relies on the modeler's skill in mesh design, and problem understanding and formalizing. It usually requires mesh reconstruction and boundary condition redefining when vent configuration or building structures are different, what requires relatively heavy workloads. For the special structure of CSGs, it is challenging to design high-quality boundary layer grids along the arched roof. In this thesis, the problem for three-dimensional CSGs modelling is solved, being the first time proposed in the literature.

1.5.1 Literature review of CFD greenhouse modelling

The continuous flow of air inside a greenhouse, despite the low speed, leads to the exchange of energy and mass. CFD is a method that can develop a model of the flow field. CFD technique has been widely applied in the optimal design and the simulation of ventilation since the 1990s (Mistriotis et al., 1997; Boulard et al., 1997). In the 21st century, more comprehensive models were developed including the interaction between the microclimate and the crop (Boulard and Wang, 2002; Majdoubi et al., 2009; Boulard et al., 2010; Kichah et al., 2012; Chen et al.,2015; Boulard et al., 2017; Liu et al., 2021b; Cheng et al., 2021). By using the CFD method, the impact of wind speed, vent opening configuration, and greenhouse structures on the airflow pattern have been investigated by many researchers (Ould Khaoua et al., 2006; Molina-Aiz et al., 2010; Rocha et al., 2021). Bournet and Boulard (2010) reviewed optimum solutions for designers and analyzed the effect of ventilator configurations on the distributed climate inside greenhouses from CFD simulations published over 25 years. Regarding to advanced simulations (e.g. surface condensation), Tong et al. (2009) developed a numerical model of temperature, which included the influence of roof condensation on the energy budget in a Chinese solar greenhouse. Bouhoun Ali et al. (2014) developed a two-dimensional transient model to assess condensation on roofs in a Venlo glasshouse. Piscia et al. (2012) studied the three-dimensional transient modelling of night-time condensation on a four-span greenhouse plastic cover, but the crop–environment interaction was neglected. Recently, Bournet and Rojano (2022) provides an examination of recent progress (last 2 decades) in CFD studies, mainly applied to greenhouses and livestock buildings with the aim to depict current status and trends and potential research directions. The current status comprises CFD applied to regional and local climate, housing design and operation, and animal or plant interaction with its surroundings.

1.5.2 Development of CFD model using Ansys Fluent

For most greenhouse scenarios, the governing equations to be solved are simulating using low velocity incompressible turbulence flow. The first two equations are partial differential equations based on the conservation of mass and momentum. If temperature and thermal buoyancy effects are simulated, the energy conservation equation is solved in parallel. If another gas other than air is simulated (e.g. CO_2, water vapor), the species transport equation is solved as well. For low velocity incompressible flow, Ansys fluent provides a pressure-based solver (Ansys Inc., PA, USA). For high velocity compressible flow, Ansys fluent provides density-based solver, but it is seldom used in agricultural

scenario. In this project, the equations are as follows,

$$\frac{\partial(\phi)}{\partial t} + \mathrm{div}(\vec{u}\,\phi) = \mathrm{div}(\Gamma\,\mathrm{grad}\phi) + S_\phi \quad (28)$$

where t is the flow time (s) and u is the velocity (m s^{-1}). The variables Φ and S_Φ, and the corresponding adopted conservation equations are shown in Table 4.

Table 4. Φ and S_Φ and the corresponding conservation equations. ρ is the air density (kg m^{-3}); u is the velocity (m s^{-1}); g_i is the gravity acceleration component in the i-direction (m s^{-2}); C_P is the specific heat capacity of air (J kg^{-1} K^{-1}); T is the air temperature (K); C_w is the mass concentration of the water vapour component (kg kg^{-1}); k is the turbulent energy (m^2 s^{-2}); ε is the turbulent dissipation rate (m^2 s^{-3}); and S_m, S_r, S_t, S_w, S_k, and S_ε are the source terms of momentum, radiation, energy, water vapour, k, and ε, respectively, which are calculated by UDFs.

Conservation equation	Φ	S_Φ
Mass	ρ	0
Momentum	$\rho * \vec{u}$	$S_m + \rho * g_i$
Energy	$\rho * C_P * T$	$S_r + S_t$
Water vapour	C_w	S_w
k	$\rho * k$	S_k
ε	$\rho * \varepsilon$	S_ε

Therefore, for CFD models, the equations inside are very similar. So, after identifying the flow, the main task of modelling is to find the simulation domain and define the boundary conditions. For greenhouses modelling, when the outdoor wind field is included in the simulation domain, the length of the upstream portion is suggested to be determined as 3 times the greenhouse ridge height, while the downstream portion is suggested to be determined as 10 times the greenhouse ridge height; since the backflow cannot form inside the computational domain within 10 times of the ridge height (Kim et al., 2017). In addition, for the three-dimensional wind tunnel, the windward cross section of the greenhouse needs to meet the blocking degree of less than 5%. The next step is to build the geometry model, including points, curves and surfaces (Fig. 1.32).

Then, for a complex geometry, the geometric model is suggested to be associated with created blocks to create a high-quality mesh file, including associating Points with Vertex, associating Curves with Edges, associating Surfaces with Faces (Fig. 1.33 (a)). The former is the name corresponding to the geometric model, and the latter is the name corresponding to the block. The next key step is to split the blocks. Note that it is not easy in meshing high-quality boundary layer around the semi fan-shaped south roof. The solution in this case is to use 'Ogrid Block' splitting method along the side wall of the greenhouse (Fig. 1.33 (b)). Finally, it is beneficial to move the vertex in order to find the optimal quality and check the global association (Fig. 1.33 (c)).

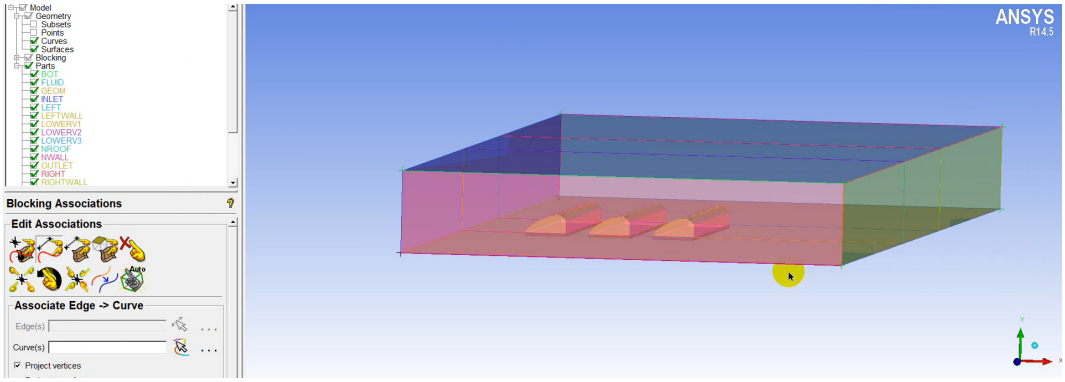

Fig. 1.32. A photo of greenhouse wind field geometry model in Ansys Fluent.

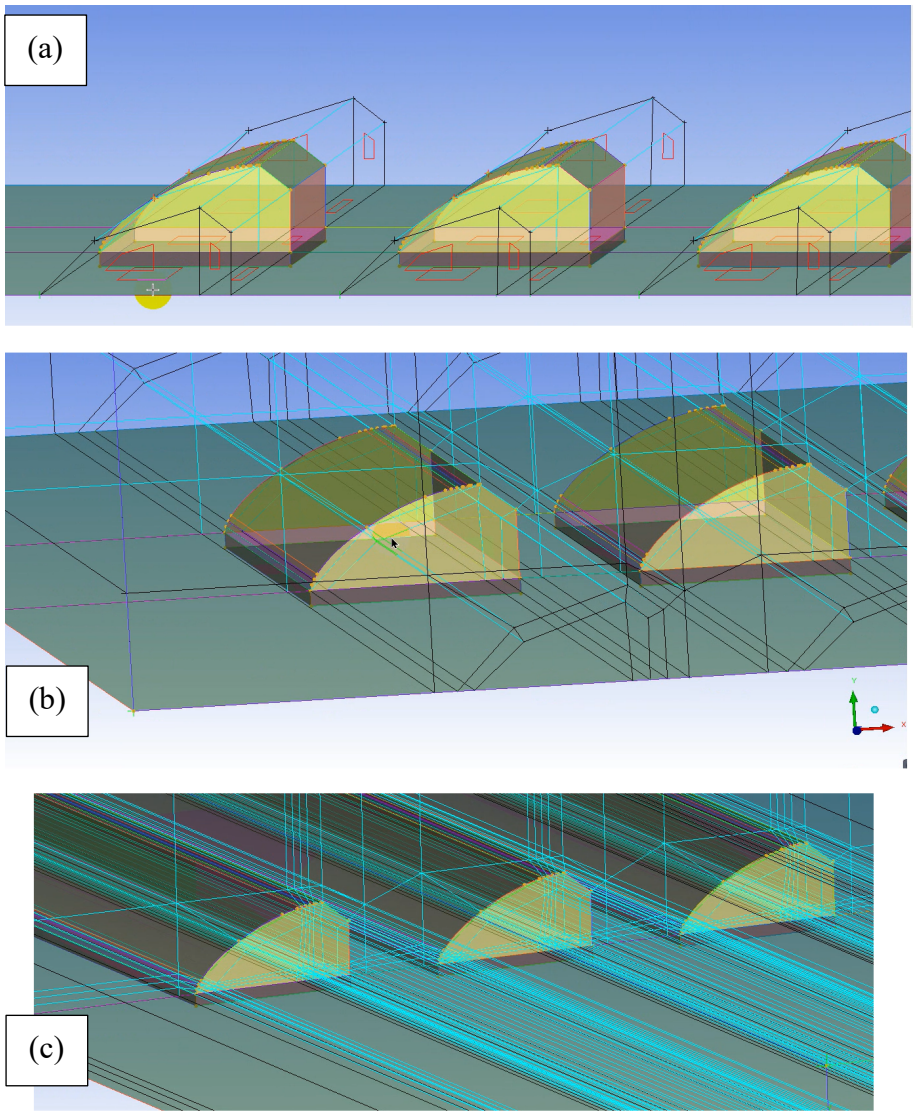

Fig. 1.33. Process of creating a mesh file.

The last step of creating a mesh file is to conduct grid independence tests. The aim is to find the optimal value of the total elements number, in order to keep the balance

between model accuracy and computation load. An important criteria is the wall y^+ solution, which must satisfy $30<y^+<300$ for the Standard Wall Function (Ansys, 2010). The wall y^+ solution is closed related to the first cell height of the boundary layer (Fig. 1.34). The height of the first cell from the wall in the boundary layer was determined by conducting iteration tests of independence of the results regarding the grid density.

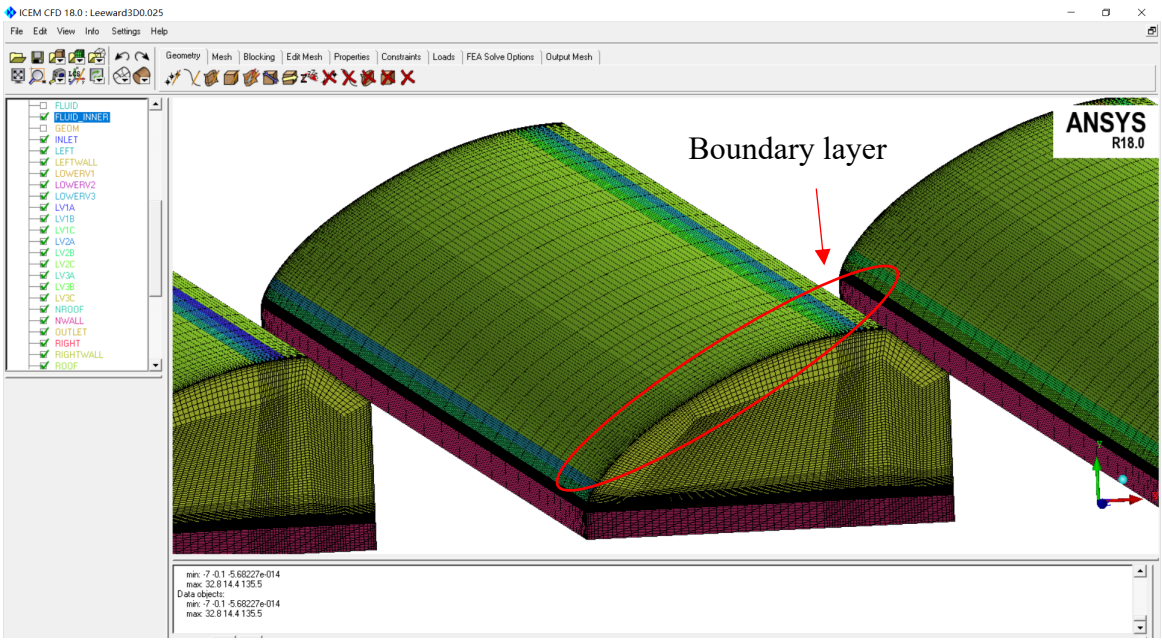

Fig. 1.34. Boundary layer grids along the surfaces

The boundary conditions of the model are determined according to the actual situation. For the external flow field, the velocity inlet and pressure outlet are commonly used (Fig. 1.35), with a log law wind profile (Haxaire, 1999),

$$u = \frac{u_*}{\kappa} ln(\frac{H+H_0}{H_0}) \tag{29}$$

where u is wind speed at the velocity inlet, m s^{-1}. κ is von Karman constant, 0.42; u_* is the friction velocity, m s^{-1}. H is the reference height, m. H_0 is the aerodynamic roughness length, m.

The turbulent kinetic energy k and dissipation rate ε distributions at the entrance are defined by the following equations (Hoxey and Richardson, 1983),

$$k = \frac{u_*^2}{\sqrt{C_\mu}} \tag{30}$$

$$\varepsilon = \frac{{u_*}^3}{\kappa(H+H_0)} \tag{31}$$

For the thermal boundary conditions of the greenhouse walls, Fluent provides fixed temperature boundary, fixed heat flux boundary, coupling wall boundary, etc. Note that the boundary conditions should be appropriately selected according to available data. If the first two are selected, there must be a temperature sensor or a heat flux sensor placed in the wall. When the future climate is simulated, the measured boundary conditions cannot be obtained. Then the wall thermal condition must be simulated in each transient step to get the surface temperature or heat flux.

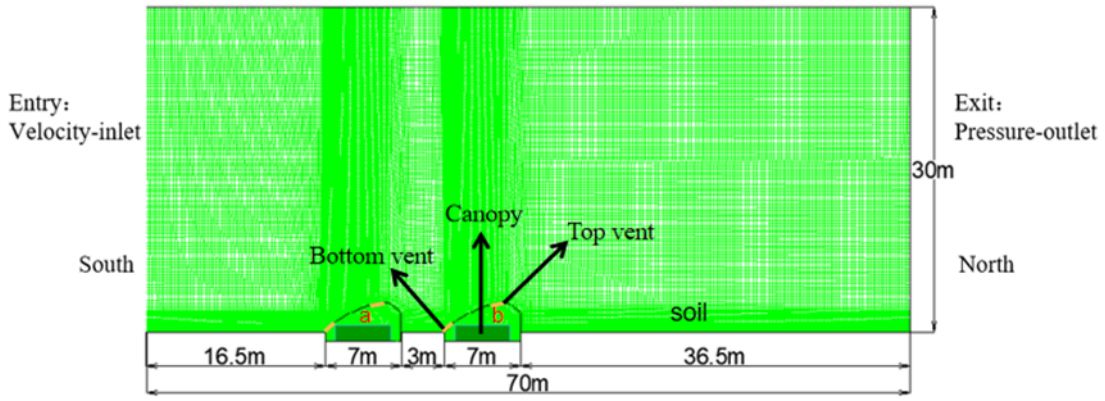

Fig. 1.35. Boundary conditions of CFD model.

1.5.3 CFD simulation of the greenhouse climate model

This section introduces simulation results using the CFD greenhouse model, including wind filed simulation, greenhouse climate simulation, and LWD distribution simulation.

Estimation of ventilation rate is a laborious work and usually requires multiple complex parameters. CFD method provides a theoretical basis for virtual wind tunnel experiments. A huge number of reliable samples can be obtained through virtual wind tunnel experiments. In this project, three-dimensional wind field inside and around CSGs is simulated (Fig.1.36). A regression trees ventilation model was developed from 990 CFD samples. This model applies to a greenhouse in an open area. The output of the model is the area ventilation rate in $m^3\ s^{-1}\ m^{-2}$ (Fig. 1.37). From left to right in this figure, the velocity speed is increased, and from bottom to top, the vent opening area is increased. The points on each short line correspond to the tested temperature differences, which increase from left to right. There are therefore 11 points in each short line, representing the temperature difference between 0 to 10 K. It shows that at low wind speed, the temperature difference makes the lines tilt greatly. But at high wind speeds, all the lines are almost horizontal, which demonstrates that under low wind speed, thermal pressure ventilation becomes predominant, and vice versa. From bottom to top, the vents opening areas are increased. There are 18 rows at each wind speed. This shows that choosing a larger vent area at high wind speed is more positive for increasing the ventilation rate than at low wind speed. The RMSE of the regression trees model is 0.002. This model can perfectly deal with the combined effect of wind pressure and thermal gradients.

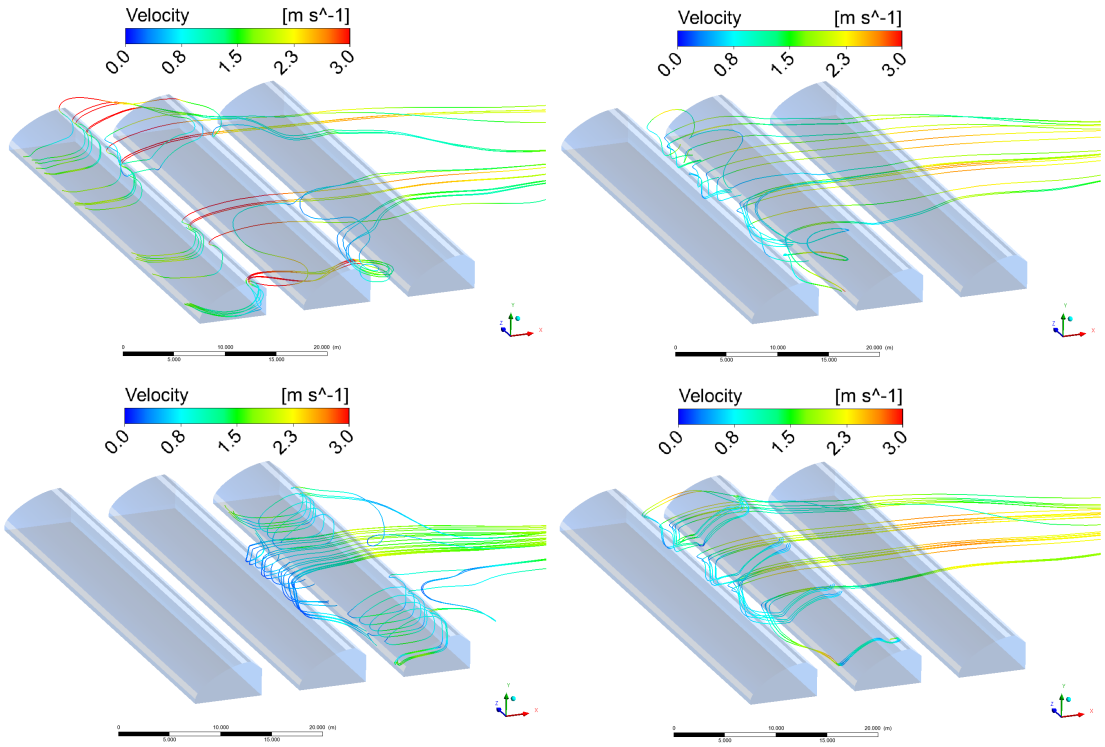

Fig. 1.36. Streamlines of windward flow when wind speed is 3 m s^{-1}.

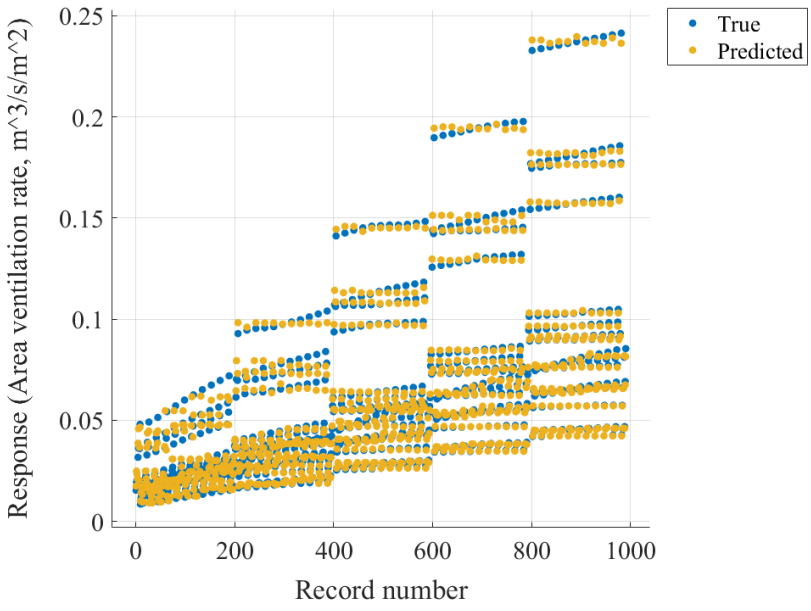

Fig. 1.37. Responses of regression trees ventilation model. The predicted vs actual plot.

The greenhouse climate spatial distribution maps are presented in Fig.1. 38 and 1. 39. The internal wall was simulated in each transient step and is higher than the air temperature. The air temperature was higher near the thick wall and lower near the semi-

transparent roof. However, the temperature distribution appears to be symmetrical in the east-west direction. The above distribution trend coincides with Wang et al. (2013). The leaf temperature distribution trend was consistent with that of air temperature, while the distribution trend of RH was the opposite that of air temperature. On the south side with a semi-transparent roof, the temperature is lower and the RH is higher, conditions that make it easier to form condensation that causes leaf damage. This conclusion coincides with Bournet's observations that cucumber leaves near the semi-transparent boundary have a greater risk of condensation than in other zones (Bournet et al., 2020).

Fig. 1.40 shows the heat flux on both sides of the wall. The positive wall heat flux in the right figure indicates that the wall dissipates heat to the indoor air. The negative wall heat flux in the left figure indicates that heat from the wall was lost to the outdoor zone. The greenhouse lost more heat from the semi-transparent roof and the heat flux distribution on the roof was not uniform.

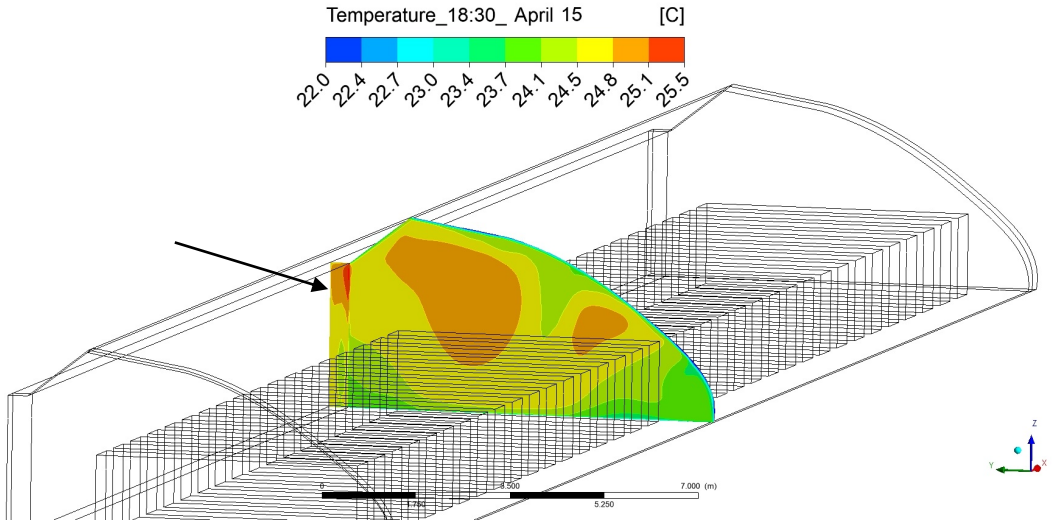

Fig. 1.38. Contour of simulated internal wall temperature and air temperature on the vertical plane. Y represents the north.

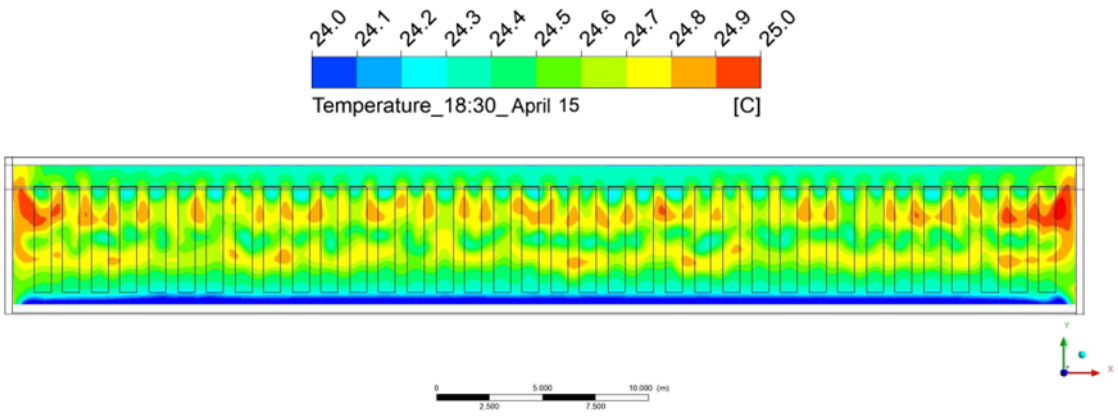

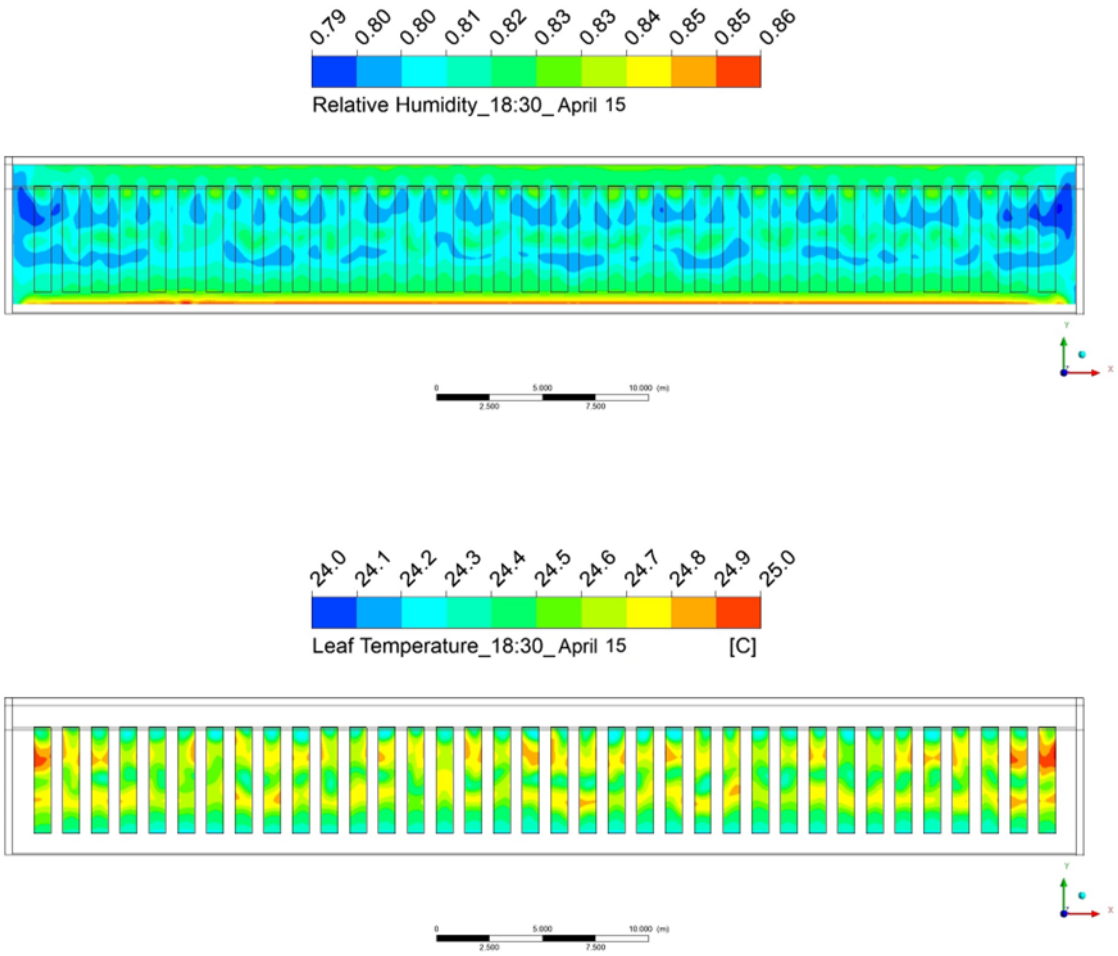

Fig. 1.39. Contour of simulated air temperature, relative humidity and leaf temperature on the horizontal plane.

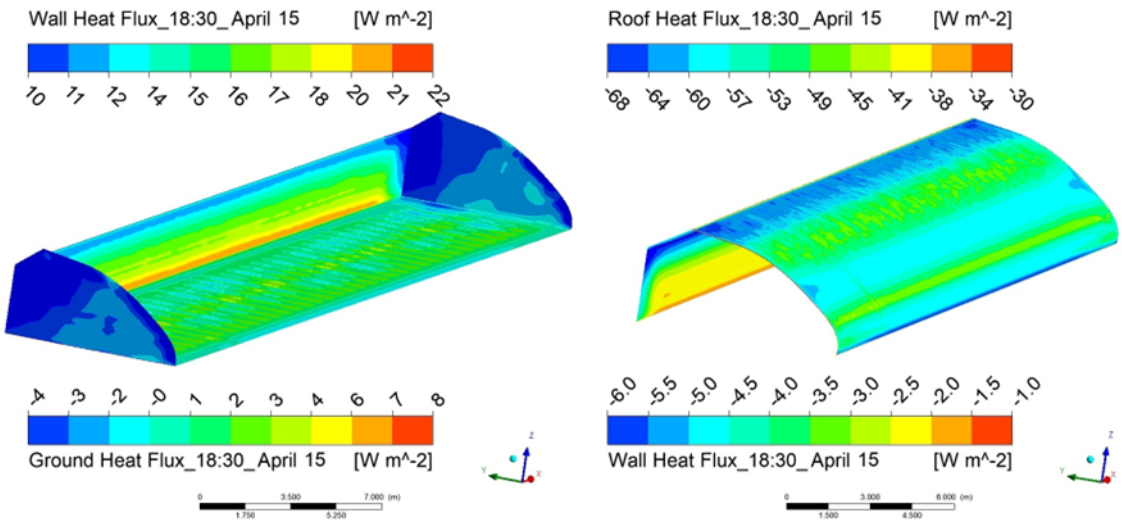

Fig. 1.40. Contour of simulated wall flux.

The simulations and measurements are compared in 15 different sample points along the vertical and horizontal directions, where wireless temperature and humidity sensors are placed (Fig. 1.41). The results show that the maximum error (MAE) of the T, RH, and leaf temperature during the two nights were 2.7 °C, 7.5%, and 2 °C (Fig. 1.42). Temperatures were underestimated by the model in the range of 12–17 °C, and then overestimated. The mean error (ME) of the RH was 2.7% and 2.8%, respectively, during the two nights. The root mean square error (RMSE) values of RH were 3.22% and 3.40%, respectively.

Fig. 1.41. A photo of air temperature and humidity sensors distributed in the greenhouse.

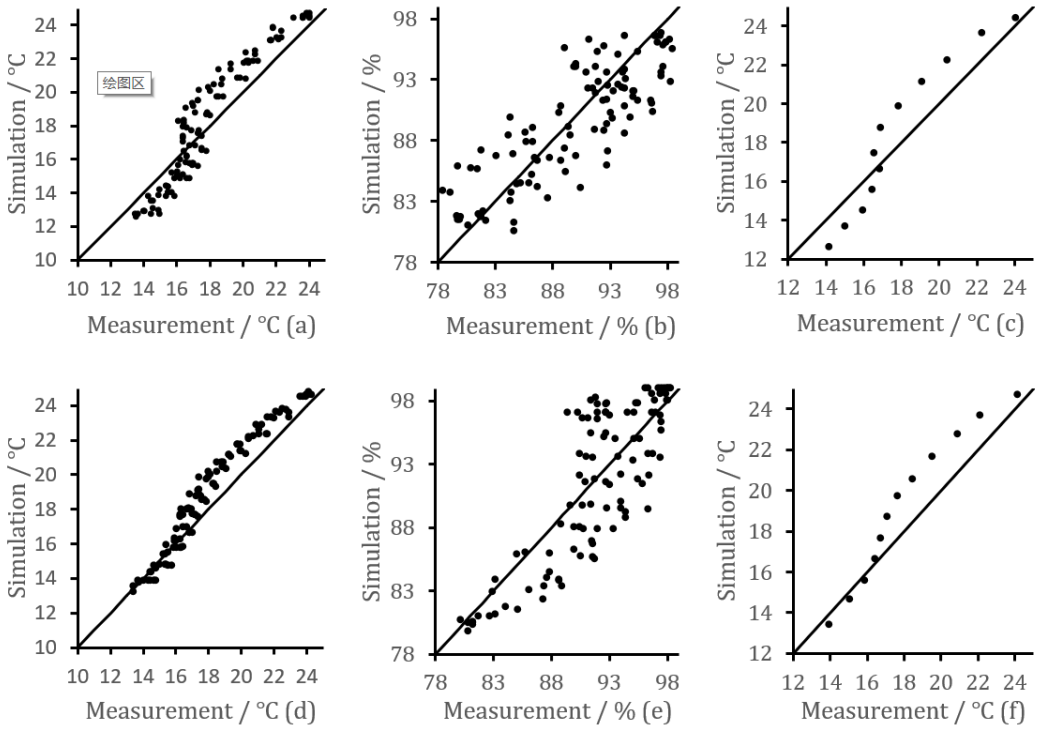

Fig. 1.42. Model evaluation of (a) T, (b) RH, and (c) leaf temperature on April 15–16; and (d) T, (e) RH, and (f) leaf temperature on April 16–17.

Based on the greenhouse climate simulation, the LWD distribution was simulated and validated. The simulated roof condensation first appeared from 19:30 on April 15 while the simulated leaf condensation first appeared from 01:30 on April 16 (Fig. 1.43). On the second night, the simulated roof condensation first appeared from 20:30 on April 16, while the simulated leaf condensation first appeared from 00:30 on April 17 (Fig. 1.44). Condensation always appeared first on the roof rather than on the leaves.

The observed condensation always occurred earlier than the simulated condensation. The average errors between the observed and simulated LWD were 1.2 h on April 15–16, and 1.3 h on April 16–17, respectively. The condensation results at each hour were marked as either Yes or No, according to the two-day evaluation. There are 216 pairs of data in the sample, the TNR is 1, TPR is 0.66, and the ACC is 0.89. The results show that the model is highly specific but lacks sensitivity.

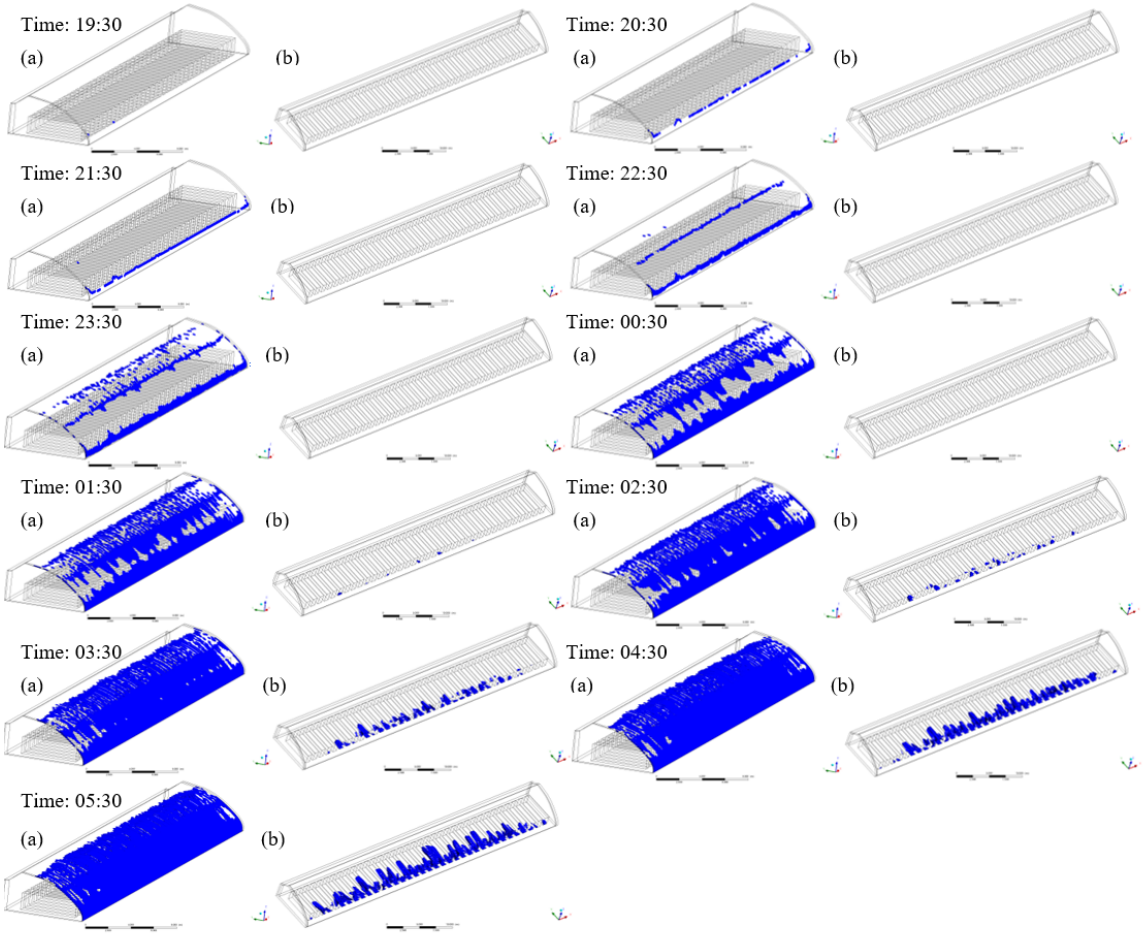

Fig. 1.43. Comparison of transient simulation of condensation on the (a) roof and (b) crop canopy on April 15–16. Y represents the north; X represents the east; and ■ represents the condensation that appeared based on simulation.

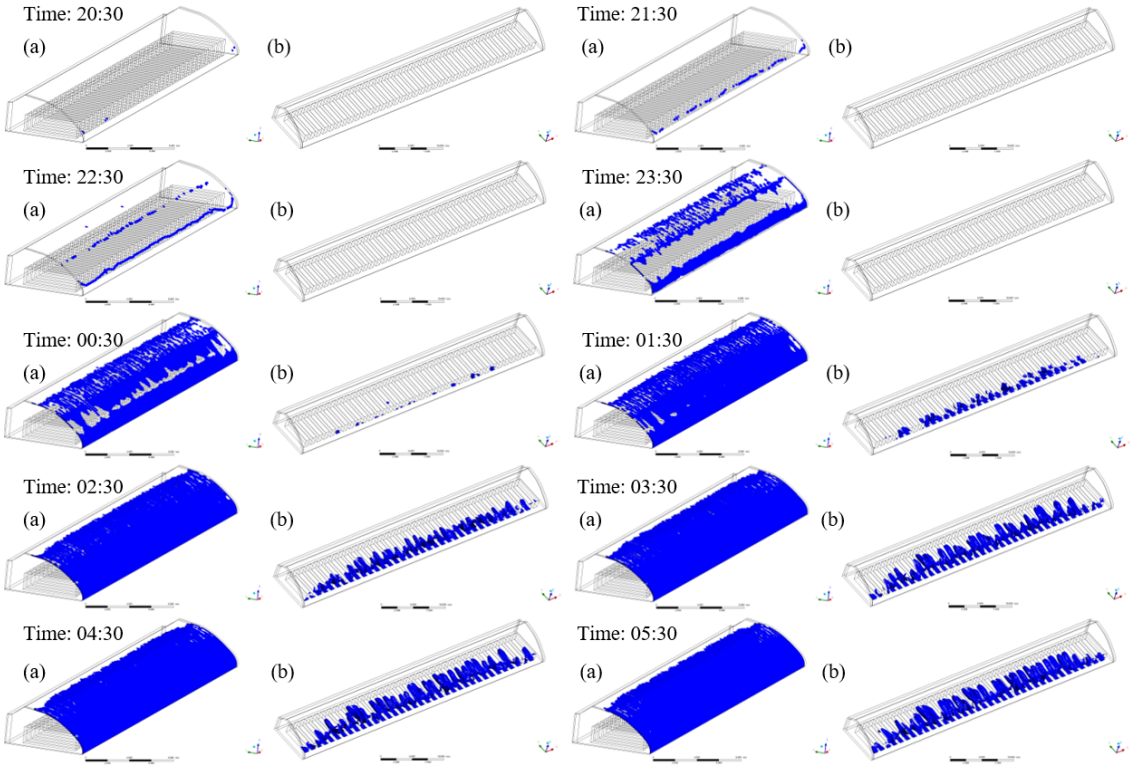

Fig. 1.44. Comparison of transient simulation of condensation on the (a) roof and (b) crop canopy on April 16–17. Y represents the north; X represents the east; and ■ represents the condensation that appeared based on simulation.

The leaf condensation distribution models were comprehensively evaluated using validation metrics such as accuracy, precision, and recall. To accurately verify the model simulation results of LWD, the three observation areas (F, M, and B, where area F was near the south roof and area B was near the north wall) were divided into nine areas, F1, F2, F3, M1, M2, M3, B1, B2, and B3, according to the crop canopy height (0.5, 1, and 1.5 m), and the simulation results of LWD in these nine areas were taken as the mean value (Fig. 1.45). The simulation and observation of the leaf surface condensation-level distribution trend revealed that the area near the south roof of the greenhouse (F) at night was more likely to cause leaf condensation than the area near the north wall (B). This was because of the relatively low temperature owing to higher convective heat transfer near the southern roof area, the saturated water vapor pressure decreases with temperature, and the rapid rise in relative humidity.

Then, the effect of ventilation on eliminating leaf wetting was simulated. After opening the vents (22:30–00:30), the surface of the leaves gradually changed from condensation to dryness owing to the combined effect of the difference between indoor and outdoor relative humidity (indoor was 88.62% and outdoor was 86.42%), and air flow (Fig. 1.46). In F3, M3, and other areas near the bottom of the vent and the ground, the leaves became dry first, which was related to the indoor transient air flow because the area near the ground and vent had higher air velocity (0.26 m s^{-1}, 0.34 m s^{-1}). As the

ventilation time increased, the indoor relative humidity stabilized (87.89%). After closing the vents (00:30–1:30), the indoor humidity rose rapidly to 90.83%, and leaf condensation occurred at 1:30.

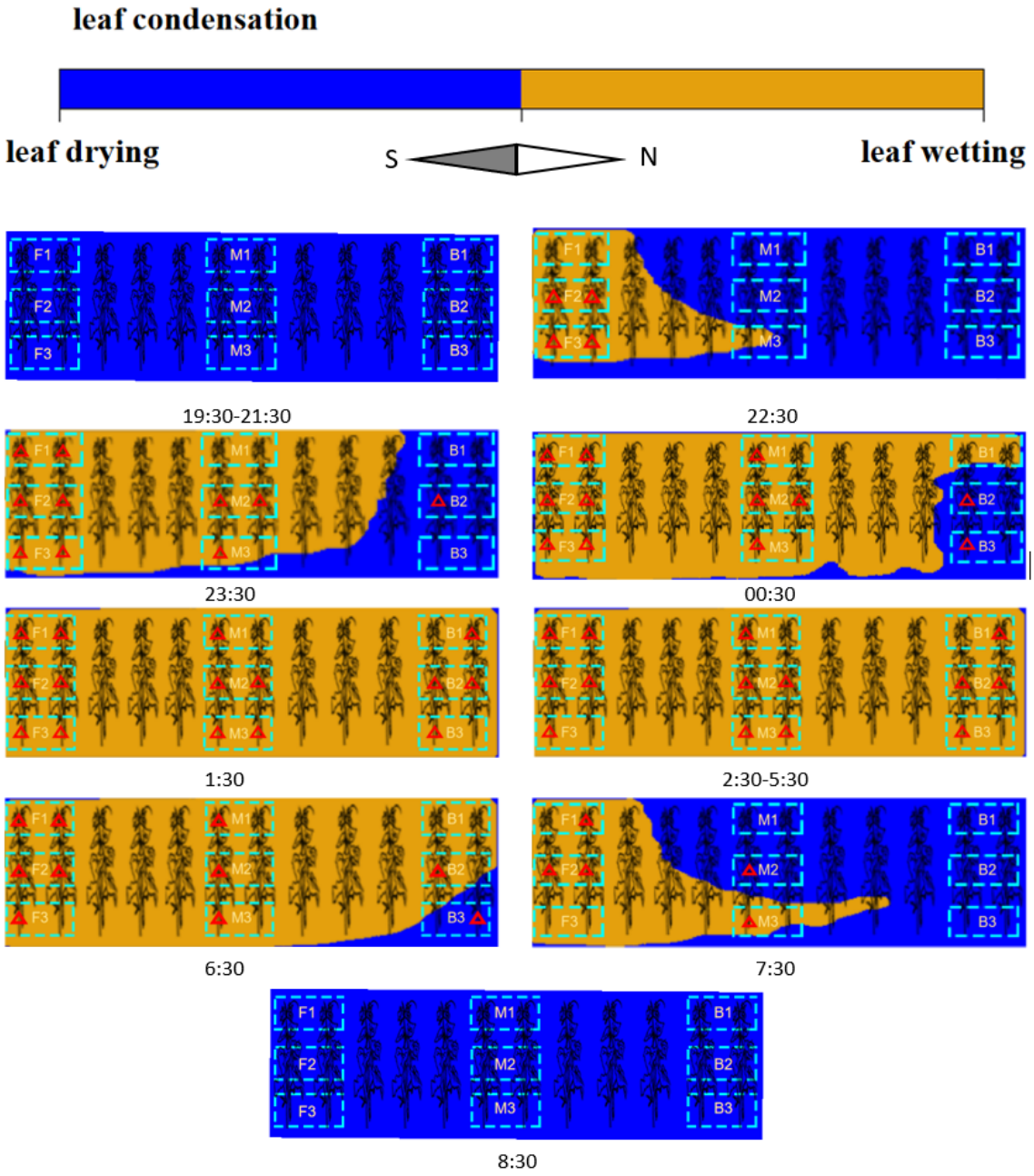

Fig. 1.45. Vertical cross section contour of simulated leaf condensation of distribution on the canopy on cloudy days: (▪▪) is the observation area. (△) indicates that the leaves are observed wet at this point.

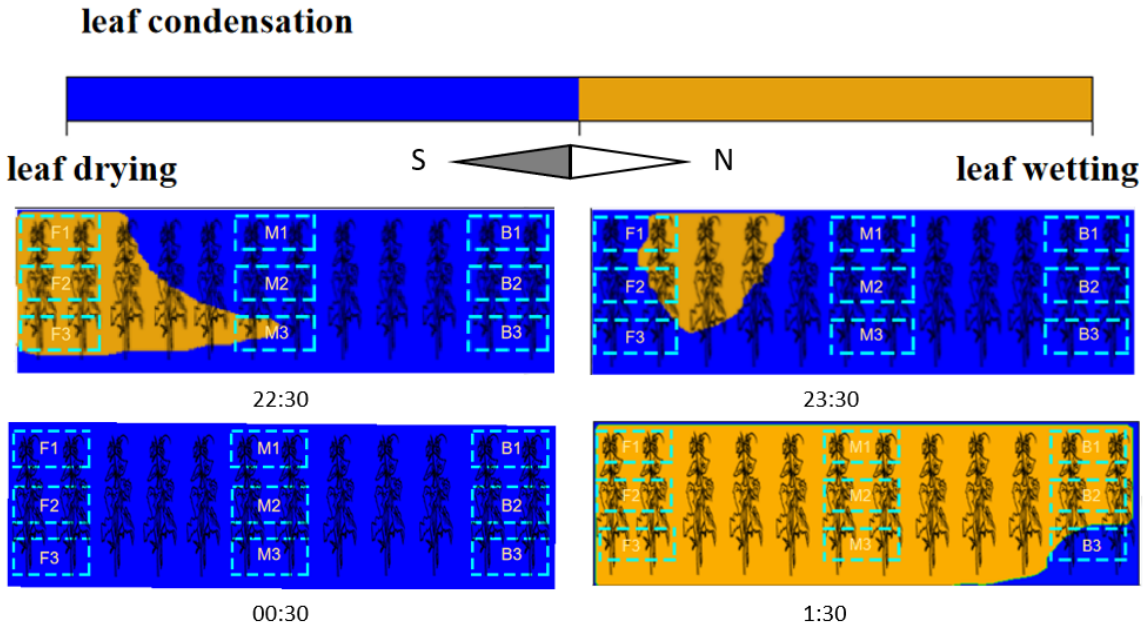

Fig. 1.46. Vertical cross section contour of simulated leaf wetness of distribution on the canopy under ventilation conditions: (▪▪) is the observation area.

2 SCIENTIFC CONTRIBUTIONS

2 Scientific Contributions

This Ph.D. thesis is presented as a compendium of publications according to modality A of the normative of the University of Almería (article 24). This normative establishes that any Ph.D. thesis can be presented in the compendium modality as long as it is supported by at least three scientific contributions. Two of them must be included in category A of the rating scale contained in the Research and Transfer Plan from the University of Almería approved in the corresponding year. The third contribution, different from the previous ones and that does not consist of a contribution to a congress, must be included in category B of the rating scale mentioned above. In this rating scale, category A is referred to the journals ranked in the highest position of their subject category, i.e., Q1 in the Journal Citation Report (JCR), and category B to those journals ranked in the second-highest place, i.e., Q2 or Q3 in the JCR.

This thesis project is supported by 4 published and 3 submitted scientific articles in journals ranked in the JCR, and 1 conference paper, which are classified as shown below:

- Q1 papers: 4 publications and 2 under review.
- Q4 papers: 1 (accepted for publication).
- International conference papers: 1 publication

The articles above have been included in this chapter according to the aforementioned normative.

2.1 Greenhouse climate modelling and evaluations

2.1.1 A fast and practical one-dimensional transient model for greenhouse temperature and humidity

Research in this field is supported by the following journal publication:

Title	A fast and practical one-dimensional transient model for greenhouse temperature and humidity
Authors	**R. Liu**, M. Li, J.L. Guzmán, F. Rodríguez
Journal	Computers and Electronics in Agriculture
Year	2021
Volume	186
Pages	106186
DOI	https://doi.org/10.1016/j.compag.2021.106186.
IF(JCR2022)	6.757
Categories	Horticulture (1/94) Q1 Computer Science Applications (38/747) Q1

Contribution of the Ph.D. Candidate

The Ph.D. candidate R. Liu is the main contributor and first author of this paper.

Computers and Electronics in Agriculture 186 (2021) 106186

Contents lists available at ScienceDirect

Computers and Electronics in Agriculture

journal homepage: www.elsevier.com/locate/compag

Original papers

A fast and practical one-dimensional transient model for greenhouse temperature and humidity

R. Liu [a], M. Li [b,c], J.L. Guzmán [a,*], F. Rodríguez [a]

[a] Department of Informatics, ceiA3, CIESOL, Ctra. Sacramento s/n, University of Almería, Almería, Spain
[b] Beijing Research Center for Information Technology in Agriculture, National Engineering Research Center for Information Technology in Agriculture, National Engineering Laboratory for Agri-product Quality Traceability, Meteorological Service Center for Urban Agriculture, China
[c] Meteorological Administration - Ministry of Agriculture and Rural Affairs, Key Laboratory of Agri-informatics, Ministry of Agriculture, Beijing, China

ARTICLE INFO

Keywords:
Controlled-environment simulation
Greenhouse climate
Transient model

ABSTRACT

This paper introduces a new transient greenhouse model which uses a mechanistic method to estimate the temperature and humidity in typical Chinese solar greenhouses. A novel and easy-to-use wall temperature estimation method based on the energy balance was adopted for the environment model rather than using boundary temperature measurements. In this way, the number of model inputs is considerably reduced, and the proposed model is able to predict future greenhouse climate conditions by utilizing only the weather forecast. The model validation was performed in two different greenhouses (each with different sizes and physical parameters, such as the greenhouse volume, the roof and wall areas, the wall materials and so on) on three typical days in 2019 and 2020, and over four consecutive weeks in different seasons during 2016 and 2019 . Promising results were obtained and the model performed well in different operating modes; these included having the vents completely closed, opening the vents, and completely closing the vents in the cold season with an additional thermal insulation blanket covering. The validation results demonstrate that the proposed model can be widely adapted to different sizes of typical Chinese solar greenhouses, as well as to different weather conditions. Thus, the developed model is a flexible and valuable tool that can be used for greenhouse climate simulation, temperature and humidity control, and as a decision-making support system to help manage solar greenhouses.

1. Introduction

Greenhouse modeling is a valuable method for understanding the effects of various parameters that influence cooling/heating demand and for obtaining optimal greenhouse operating conditions; this is of fundamental importance when selecting the greenhouse design parameters and when making management decisions in practical production (Choab et al., 2019).

Different aspects of greenhouse modeling can be evaluated including accuracy, functionality, portability and applicability. Designers choose which features to focus on or ignore depending on the model's purpose, thus an optimal model always matches its advantages with the reason it was developed. Zhang et al. developed an accurate model that involved high-resolution solar radiation equations for a Chinese solar greenhouse, considering the crop-environment interaction and including a detailed 3D tomato canopy model. However, a total running time of approximately 20 h was needed to simulate results for an 8-hour period using an Intel Core I7 CPU and 16 GB RAM (Zhang et al., 2020b). The other type of reliable high-resolution model was developed employing the CFD (Computational Fluid Dynamics) method, which also requires a high computational load (Boulard et al., 2017). Li et al. managed to reduce the computational cost by adopting a POD (Proper Orthogonal Decomposition)-based optimization scheme (Li et al., 2020). However, the performance of the model in transient simulations needs to be further studied. Nevertheless, the above models are excellent tools for understanding the temperature field, the solar radiation field and the other physical phenomena in greenhouses. Zhang et al. studied an unsteady-one-dimensional model for a glass greenhouse assuming that the indoor climate elements were uniform (Zhang et al., 2020a). The model considered the dynamic cover absorbance and transmittance caused by the variation in the sun's position as well as the combined effects of the cover, soil and air, thus making it a comprehensive model for temperature simulation. The developer chose to ignore the heterogeneity, ventilation, humidity, crop-environment interaction,

* Corresponding author.
E-mail addresses: lim@nercita.org.cn (M. Li), joseluis.guzman@ual.es (J.L. Guzmán).

https://doi.org/10.1016/j.compag.2021.106186
Received 12 December 2020; Received in revised form 6 April 2021; Accepted 27 April 2021
Available online 13 May 2021

condensation and so on, but the model is still a valuable tool that helps greenhouse designers determine the energy budget.

In this work, the objective has been to develop a model that can be computed rapidly and is widely applicable. The model can be used as a tool for temperature and humidity prediction and for control, two crucial processes for tackling plant disease in the cultivation taking place in typical Chinese single-slope solar greenhouses (Zhao et al., 2011). Currently, this is the main type of greenhouse used for cold-season vegetable production in northern China, with a total area of 1.96 million ha (Liu et al., 2021) being reported. However, these greenhouses lack standardization in terms of their size, structure and materials; two thirds of them are made of rammed soil walls with greenhouse lengths varying from 50 to 100 m and spans (widths) varying from 7 to 12 m (Guo et al., 2016). This makes it difficult to apply the model to a real greenhouse for the following reasons: the wall heat flux should be simulated on a case-by-case basis rather than by imposing an experimental value; the solar radiation gain varies depending on the structure, its size and the roof materials; and the tightness of the cover has been shown to directly influence the degree of air leakage (infiltration) (Jolliet et al., 1991; Ahamed et al., 2018).

In recent years, a variety of control devices have been applied to Chinese solar greenhouses, such as climate sensors, artificial light, CO_2 enrichment, and fan cooling systems. However, these are still at the small-scale demonstration stage. One of the devices most widely adopted by farmers is the thermal insulation blanket rolling machine; this has reached an application rate of more than 90% in Shandong province, the main protected vegetable production area in China, (Wen et al., 2019). Another common approach adopted by most farmers is to use natural ventilation to cool and dehumidify their crops (Li et al., 2018); this is because of the interaction between the energy cost and market prices, which will continue far into the future. Based on the above situations, the scenario in which this model is applied is a naturally ventilated greenhouse without an additional heat source, but where a thermal insulation blanket is included as a roof cover in the cold season.

Limited humidity simulation models have been developed for Chinese solar greenhouses using a mechanistic method. Quantifying the humidity source term seems to be even more difficult than quantifying the energy budget (due to a lack of standardization); this is because of ubiquitous soil evaporation and plant transpiration. The humidity source coming from plant transpiration has been quantified based on the stomatal resistance of several common cultivars grown in greenhouses (Villarreal-Guerrero et al., 2012). A few predictive humidity models have been designed over the last decade for Chinese solar greenhouses although these have neglected to include evapotranspiration and condensation (Zhang et al., 2019a). Under conditions in which the vents remain closed, the greenhouse humidity increases in the morning due to evapotranspiration from the crop canopy or the soil. With the decrease in temperature after midday, the humidity reduces by condensation or liquidation. In addition, air leakage occurs the entire time. The above mechanisms form the mass budget for greenhouse humidity under closed-vent conditions. Each of the modeling mechanisms is complex, which is why few mechanistic humidity models are applied to real situations.

Several predictive temperature and humidity models based on machine learning methods have been reported (Zou et al., 2017; He and Ma, 2010). Furthermore, various black box models have been developed to simulate temperature and humidity in glass greenhouses using machine learning methods such as neural networks and deep learning techniques (Jung et al., 2020). Black box models can be easily applied to real greenhouses and can predict future climate conditions. However, the data need to be collected and trained independently to make them applicable to different types of greenhouses. For mechanistic or white box models based on physical laws (Righini et al., 2020; Chen et al., 2020), boundary conditions limit the models' functioning. In many cases, real-time wall temperature or heat flux parameters are needed as model inputs (Boulard et al., 2017; Kichah et al., 2012), which makes it impossible to simulate the future indoor climate. In the single-slope solar greenhouses that are widely used in northern China, the thick wall on the north side of the greenhouse significantly affects heat storage performance during the winter. The greenhouse's heat budget cannot be calculated without knowing the temperature on both sides of the wall or without directly measuring the wall's heat flux. Although many of the mechanistic greenhouse models were designed using the traditional energy-balance-based modeling method, they generally performed well and were highly accurate (Sánchez-Molina et al., 2017; Rodriguez et al., 2015). However, the traditional modeling method usually requires multiple inputs such as the wall temperature, roof temperature and soil temperature, to simulate the resulting air temperature; this limits its applicability to real greenhouses where farmers need to predict the future greenhouse climate. In this paper, a new, simple model is introduced. Its simplicity derives from embedding a group of conservation equations relating to the boundary conditions. The steady-state equation series is solved in each transient simulation step to simplify the user's input conditions. To obtain the boundary conditions for each step, a feasible assumption is made to simulate the wall's future temperature distribution with the help of a weather forecast based on the finite difference method or finite volume method (Zhang et al., 2019b). However, for the greenhouse energy budget, only the temperature on both sides of the wall is needed, otherwise it would take up too much computational load. Therefore, a novel, easy-to-use wall temperature estimation method based on the energy balance was adopted for the environment model. It should be pointed out that few models have been developed to date that employ a mechanistic method combining temperature and humidity for use in Chinese solar greenhouses.

In this paper, several prior equations are integrated into the model to act as the mechanisms and middle links that exist in a real scenario. The final model was primarily chosen for its rigorous design and its similarity to the scenarios. Although some imperfections remain, it provides a method that serves as an example for the modelling. To summarize, the main contributions are as follows:

(i) A new greenhouse climate model is proposed that includes a novel and easy-to-use wall temperature estimation method based on the energy balance. With the help of the embedded group of conservation equations, the greenhouse boundary temperatures can be simulated rather than having to measure the boundary temperature at each time step. Therefore, the number of model inputs is reduced, and the model can estimate the future greenhouse climate using only the current or predicted weather variables.
(ii) Several typical management measurements were considered and then validated, such as: arbitrarily defining the vents' opening angle and the time they remain open, the time the greenhouse vents are completely closed, and whether to use the thermal insulation blanket as a roof covering. These aspects are not usually considered in climate models for Chinese solar greenhouses.
(iii) The model is computationally light and fast, and was calibrated and validated using data from different seasons and from different years.
(iv) The validation can be carried out in greenhouses of different sizes (and constructed from different materials) by switching the physical parameters; thus, the model is flexible and widely applicable. This was demonstrated by validating the proposed model in two greenhouses, each having a different size and located at different sites.
(v) The greenhouse temperature and humidity are simulated together using a mechanistic model – this is the first study to do so for Chinese solar greenhouses.

2. Materials and methods

This section summarizes the greenhouses where the experimental results were obtained for this work, the equipment used for the data

collection and the software tools employed for the model implementation.

2.1. Experiment description

2.1.1. Experimental greenhouse

The model validation was carried out using data from two different greenhouses. One is located in Xiaotangshan, at the National Precision Agriculture Demonstration Base (Greenhouse A, 40°18′ N, 116°47′ E), Changping District, Beijing, China, where the data from 2016 and 2019 were collected. The second greenhouse is located in Fangshan, on Hongke farm (Greenhouse B, 39°63′ N, 115°98′ E), Fangshan District, Beijing, where the data were gathered during 2019 and 2020 (Fig. 1).

Both greenhouses were the typical single-slope solar greenhouse-type with polyethylene (PE) film on the roof and a wall on the north side. The north wall of Greenhouse A is composed of bricks and gravelly soil whereas the north wall of Greenhouse B is made of hollow concrete blocks (Fig. 2). A cucumber crop was planted, and drip irrigation was installed, adopting a north–south cultivation line in Greenhouse A, and an east–west cultivation line in Greenhouse B. The 0.005 mm thick polyethylene film covers both greenhouses from the ground up to prevent soil evaporation. Greenhouse A is 50 m long, 7 m wide and 3.6 m high whereas Greenhouse B is 80 m long, 7.5 m wide and 4.2 m high.

2.1.2. Data collection

At each site, Davis Vantage Pro& Plus (Davis Instruments, Hayward, USA) outdoor weather stations were installed to measure the total solar radiation (range, 0–1800 W m^{-2}; accuracy, ±5%), wind speed (range, 0–67 m s^{-1}; accuracy, ±5%), air temperature (range, −40 - +65 ℃; accuracy, ±0.5℃), and relative humidity (range, 0–100%; accuracy, ±3%) (Fig. 3 (a)). Davis-6162 (Davis Instruments, Hayward, USA) weather stations were installed in the center of the greenhouses to measure the air temperature and relative humidity at a height of 1 m, solar radiation at a height of 1.5 m and soil temperature at a depth of 0.5 m (Fig. 3 (b)(c)). Considering the variables' rate of change, especially that for solar radiation, all the above data were measured and recorded at 15-minute intervals.

3. Model description

This section describes the proposed greenhouse climate model, where the new wall-temperature estimation method based on energy balance is introduced. Moreover, the opening and closing angles of the vents, and the thermal insulation blanket covering, are considered in the equations. The description of each model parameter and variable is given in the Appendix A nomenclature table. Furthermore, the tables in Appendix B summarize the values for the different model constants and variables.

3.1. Climate model

Under the assumption that air is transparent to solar radiation, the energy source terms for the air in the greenhouses belong to 5 sub-mechanisms: the ventilation energy source term, $q_v(t)$, W; the air leakage energy source term, $q_{lea}(t)$, W; the convective energy source term, $q_c(t)$, W; the water vapor liquidation energy source term, $q_{liq}(t)$, W; and the plant energy source term, $q_p(t)$, W (Fig. 4). The greenhouses' energy budget has a combined effect on the indoor temperature and humidity. The corresponding equation is given below:

$$\frac{dT(t)}{dt}*\rho*c_p*v + h(t)*\rho*c_{pw}*v*\frac{dT(t)}{dt} = q_v(t) + q_{lea}(t) + q_c(t) + q_{liq}(t) + q_p(t) \tag{1}$$

which can be simplified as,

$$\frac{dT(t)}{dt} = \frac{q_v(t) + q_{lea}(t) + q_c(t) + q_{liq}(t) + q_p(t)}{\rho*v*(c_p + c_{pw}*h(t))} \tag{2}$$

where, T is the indoor air temperature, K; h is the indoor absolute humidity, kg kg^{-1}; t is time, s; ρ is the air density, (1.293) kg m^{-3}; c_p is the specific heat capacity of the air, (1005) J kg^{-1} K^{-1}; c_{pw} is the specific heat capacity of the water vapor, (1850) J kg^{-1} K^{-1}; and v is the greenhouse volume, m^3.

The humidity equation was obtained by mass conservation. The greenhouses' humidity source terms come from the ventilation humidity source term, $s_v(t)$, kg kg^{-1} s^{-1}; the air leakage humidity source term, $s_{lea}(t)$, kg kg^{-1} s^{-1}; and the plant humidity source term, $s_p(t)$, kg kg^{-1} s^{-1}. The equation is given as follows,

$$\frac{dh(t)}{dt} = s_v(t) + s_{lea}(t) + s_p(t) \tag{3}$$

3.1.1. Ventilation source

This model includes the operations that affect the indoor climate, such as the vent opening angle and whether or not the thermal insulation cover is deployed. The natural ventilation adopted in this experiment relied on two rectangular vents at the top and bottom of the greenhouse. The opening angle, θ, is used to define the size of the vent opening. The driving force of the natural ventilation can be divided into thermal pressure ventilation and wind pressure ventilation (Roy et al., 2002), where the thermal pressure ventilation rate can be described in the following way:

In the case of both the upper and lower vents being open (Ma et al., 2008; NY/T 1451–2018, 2018),

$$L_T(t) = \mu_a(\theta_a(t))*A_{va}(t)*\sqrt{\frac{2*\left(\frac{T(t)}{T_o(t)} - 1\right)*g*H}{\left(\frac{T(t)}{T_o(t)}\right)^2*\left(\frac{\mu_a(\theta_a(t))*A_{va}(t)}{\mu_b(\theta_b(t))*A_{vb}(t)}\right)^2 + \frac{T(t)}{T_o(t)}}} \tag{4-1}$$

Fig. 1. Experimental greenhouses A (left) and B (right).

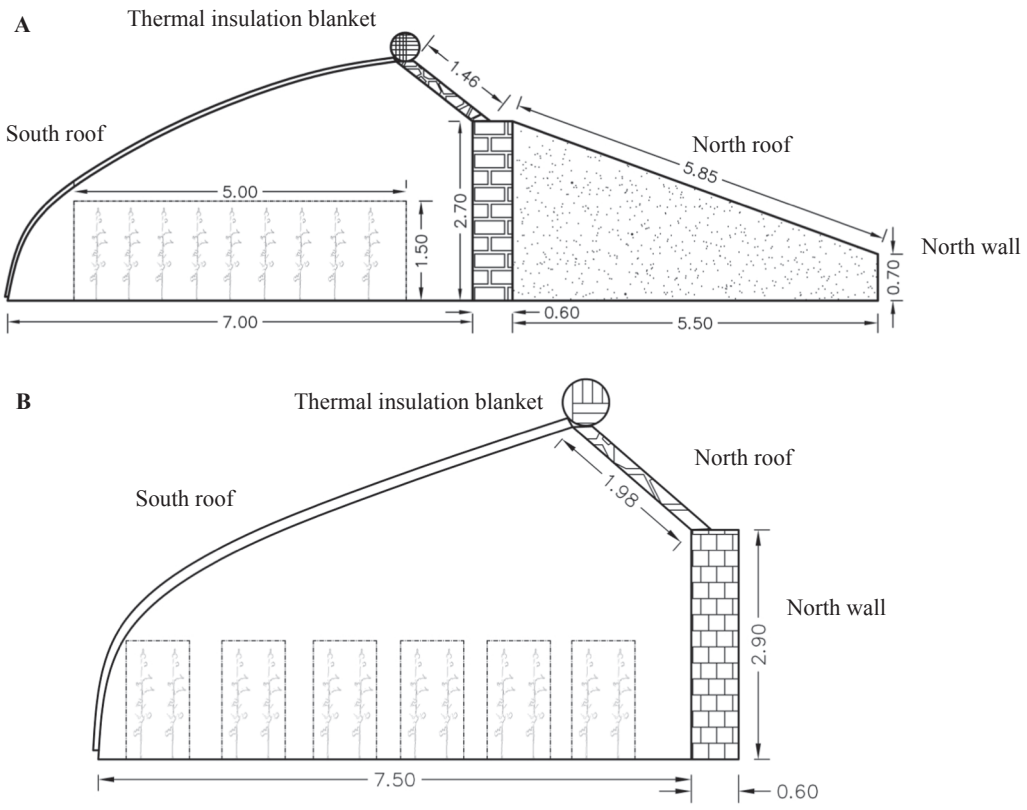

Fig. 2. Diagram of the structural dimensions (in meters) for greenhouses A and B.

Fig. 3. Sensors used for data collection.

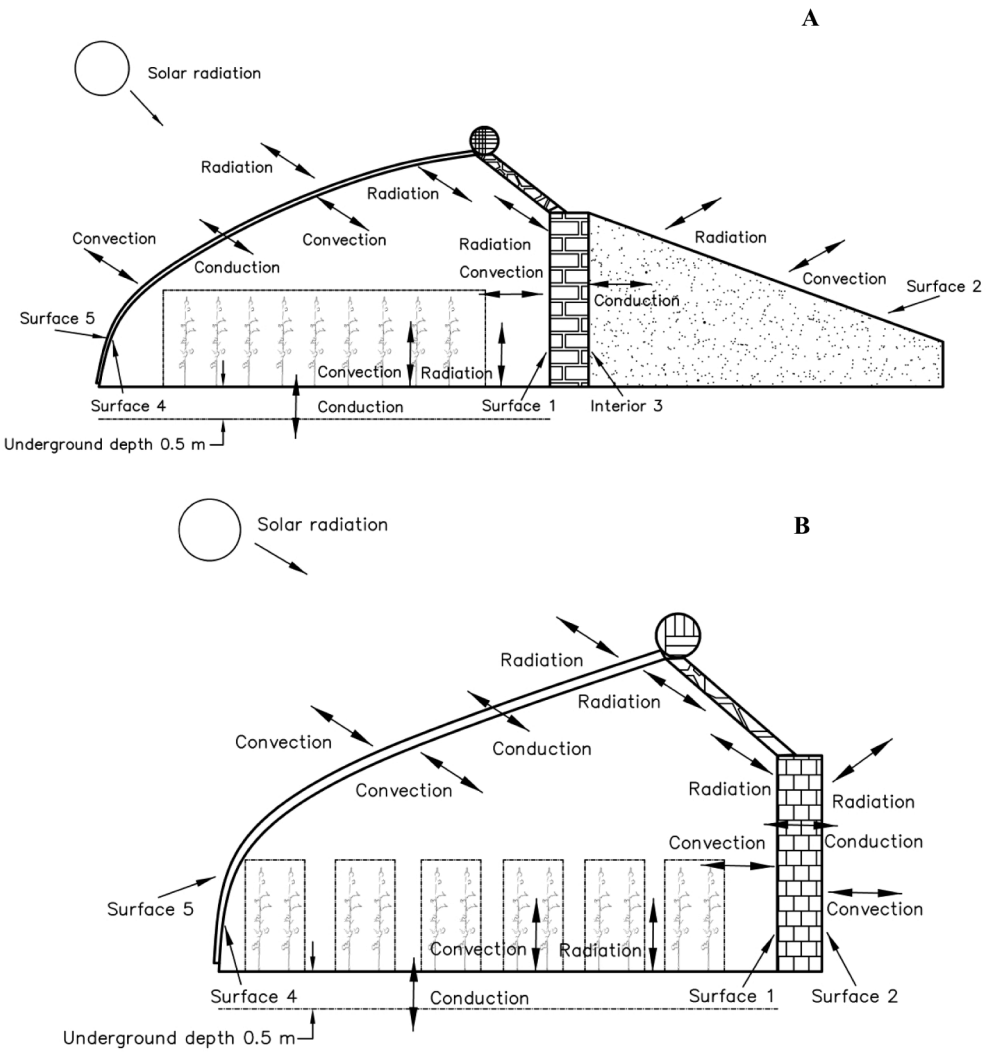

Fig. 4. Energy budget in greenhouses A and B.

$$A_{va}(t) = A_a * \left(sin \frac{\theta_a(t)}{2} \right) * 2 \tag{4-2}$$

$$A_{vb}(t) = A_b * \left(sin \frac{\theta_b(t)}{2} \right) * 2 \tag{4-3}$$

In the case of only the upper vent being open

$$L_T(t) = \mu_a(\theta_a(t)) * \frac{A_{va}(t)}{2} * \sqrt{\frac{\left(\frac{T(t)}{T_o(t)} - 1 \right) * g * H}{\left(\frac{T(t)}{T_o(t)} \right)^2 + \frac{T(t)}{T_o(t)}}} \tag{4-4}$$

where, L_T is the thermal pressure ventilation rate, $m^{-3}\ s^{-1}$; A_{va} is the open area of the upper vent, m^2; A_{vb} is the open area of the lower vent, m^2; A_a is the area of the upper vent plate (the movable part of the roof), m^2; A_b is the area of the lower vent plate, m^2; θ_a is the opening angle of the upper vent, °; θ_b is the opening angle of the lower vent, °; μ_a is the thermal pressure ventilation coefficient of the upper vent; μ_b is the thermal pressure ventilation coefficient of the lower vent ($\mu = 0.18$ when $\theta = 0$–15; $\mu = 0.33$ when $\theta = 15$–30; $\mu = 0.44$ when $\theta = 30$–45; $\mu = 0.53$ when $\theta = 45$–60; $\mu = 0.62$ when $\theta = 60$–90); If the greenhouse vents are opened (by rolling back the roof film), A_{va} and A_{vb} are input directly, with a corresponding μ of 0.62. g is the gravitational acceleration, 9.81 m s^{-2}; H is the height of the upper vent, m; and T_o is outdoor air temperature, K.

The wind pressure ventilation rate is expressed easily as an empirical equation (NY/T 1451–2018, 2018):

$$L_w(t) = \beta * A_{va}(t) * V_e(t) \tag{5}$$

where, L_w is the wind pressure ventilation rate, $m^{-3}\ s^{-1}$; β is the wind pressure coefficient (which is 0.5–0.6 when the wind direction is perpendicular to the vent and 0.25–0.35 when the wind direction is inclined), and V_e is the outdoor wind speed, m/s.

The ventilation energy source term, $q_v(t)$, is given by the following equation:

$$L(t) = \sqrt{L_T(t)^2 + L_w(t)^2} \tag{6}$$

$$q_v(t) = L(t) * \rho * c_p * (T_o(t) - T(t)) \tag{7}$$

$$s_v(t) = \frac{(h_o(t) - h(t)) * L(t)}{V} \tag{8}$$

where, L is the total ventilation rate, $m^{-3}\ s^{-1}$; and h_o is the outdoor absolute humidity, kg kg^{-1}.

3.1.2. Air leakage source

The air leakage rate has been studied for many years using the gas tracing method (Tong et al., 2008; Tong et al., 2009; Boulard et al.,

2017). In Chinese solar greenhouses, the air leakage rate varies widely from 0.13 to 2.31 h^{-1}, depending on the tightness of the cover, the wind speed, the solar radiation, and the temperature difference between the indoor and outdoor air (Tong et al., 2008; Tong et al., 2009; Zhang et al., 2019b). Using N_2O as the tracer gas, Boulard et al. (2017) found that the air leakage rate ranged from 0.075 to 0.09 h^{-1} at a wind speed of 0 ~ 0.9 m s^{-1} in a glass greenhouse. The empirical constant parameter seems to cause significant errors when applied to a real greenhouse, and even more so between new and old greenhouses. In this case, the following equation, which considers the tightness of the cover, the wind speed and the temperature difference, is the optimal estimation for the air leakage rate (Jolliet et al., 1991; Ahamed et al., 2018):

$$n_t = A_r * \eta_r * \sqrt{\beta^2 * V_e(t) + \eta_T^2 * (T(t) - T_o(t))} * \frac{3600}{V} \tag{9}$$

where, n_t is the air leakage rate, h^{-1}; A_r is the area of the transparent roof, m^2; η_T is the temperature difference factor (0.16, m s^{-1} $K^{-1/2}$); V_e is the wind speed, m s^{-1}; and η_r is the characterization of the tightness of the roof to air infiltration. Therefore, the air leakage energy source term, $q_{lea}(t)$, is described as follows:

$$q_{lea}(t) = \frac{n_t}{3600} * \rho * c_p * v * (T_o(t) - T(t)) \tag{10}$$

$$s_{lea}(t) = (h_o(t) - h(t)) * \frac{n_t}{3600} \tag{11}$$

3.1.3. Water vapor liquidation source

Water vapor liquidation is a phase-change mechanism that occurs when the air humidity is saturated; this has an impact on the greenhouse air temperature and humidity. The equations for these phenomena are described below (Snyder and Shaw, 1984):

$$P_s(T(t)) = 610.78 * e^{\left(\frac{T(t)-273.15}{T(t)-34.85} \times 17.2694\right)} \tag{12}$$

$$P_w(t) = \frac{h(t) * P}{0.622 + h(t)} \tag{13}$$

$$RH(t) = \frac{100 * P_w(t)}{610.78 * e^{\left(\frac{T(t)-273.15}{T(t)-34.85} * 17.2694\right)}} \tag{14}$$

$$h_s(T(t)) = 0.622 * \frac{P_s(T(t))}{P - P_s(T(t))} \tag{15}$$

where, $P_s(T(t))$ is the pressure of the saturated water vapor at T(t), pa; P is atmospheric pressure, pa; P_w is the water vapor pressure, pa; RH is the relative humidity, %; and $h_s(T(t))$ is the saturated humidity at T(t), kg kg^{-1}. So, when h(t) is higher than $h_s(T(t))$, the water vapor liquidation energy source term can be calculated in the following way:

$$q_{liq}(t) = \gamma * (h(t) - h_s(T(t))) * v * \rho \tag{16}$$

where, γ is the water evaporation constant, 2257600 J kg^{-1}. In this case, after liquidation, $h(t) = h_s(T(t))$ Alternately when h(t) is lower than $h_s(T(t))$:

$$q_{liq}(t) = 0 \tag{17}$$

3.1.4. Plant source

In general, the plant energy source term comes from the sensible heat exchange between the canopy and the surrounding environment, and from the heat released by condensation onto the canopy. The plant humidity source term derives from transpiration and condensation. In the above mechanisms, the canopy temperature is a necessary parameter. In this case, neglecting the sensitive heat exchange, the canopy temperature is assumed to be equal to the air temperature. Thus, the canopy's transpiration rate is described as follows (Boulard et al., 2017):

$$m_t(t) = \frac{LAD * \rho * C_p}{\zeta * \gamma} * \frac{P_s(T(t)) - P_w(t)}{r_a(t) + r_s(t)} \tag{18}$$

where, m_t is the transpiration rate, kg m^{-3} s^{-1}; LAD is the leaf area density, m^{-1}; r_a is the aerodynamic resistance, s m^{-1}; ζ is the psychrometric constant (value, 67.17 Pa K^{-1}); and r_s is stomatal resistance of the cucumber in relation to the irrigation conditions and the microclimate, s m^{-1}. r_a can be defined by the following formula (Boulard and Wang, 2002):

$$r_a(t) = 220 * \frac{l^{0.2}}{U^{0.8}} \tag{19}$$

where, l is the characteristic length (length of leaf), m; and U is the air speed in the crop zone, m s^{-1}. Solar radiation is the main meteorological factor affecting stomatal resistance in cucumber. The relationship between the solar radiation and the stomatal resistance in cucumber follows an exponential function, depending on the season of the year (Huang et al., 2020),

for the spring season, $r_s(t) = 144.3 + 1440.4 \cdot exp(-0.0124 * R_{sc}(t))$ (20)

$$r_s(t) = 224.4 + 1485.9 \cdot exp(-0.0185 * R_{sc}(t)) \tag{21}$$

$$R_{sc}(t) = (1 - exp(-K_c * LAI)) * R_s(t) * \tau \tag{22}$$

where, R_{sc} is the solar radiation absorbed by the crop canopy per second, W m^{-2}; R_s is the outdoor solar radiation intensity, W m^{-2}; τ is the short-wave transmissivity of the roof; K_c is the radiation attenuation coefficient, which was higher for the autumn cycle (0.86) than for the spring cycle (0.63) (Medrano et al., 2005); and LAI is the leaf area index.

The condensation rate on the canopy can be expressed using the following formula (Gerlein-Safdi et al., 2018):

$$m_c(t) = 0.622 * LAD * \rho * g_h(t) * \left(\frac{P_w(t) - P_s(T(t))}{p}\right) \tag{23}$$

where, m_c is the condensation rate on the canopy, kg m^{-3} s^{-1}, and g_h is the water vapor conductivity in the leaf boundary layer, m s^{-1}, which is a variable related to the Lewis number (N_{Le}) and the r_a,

$$g_h(t) = \left(r_a(t) * N_{Le}(t)^{2/3}\right)^{-1} \tag{24}$$

With

$$N_{Le}(t) = \frac{\alpha_a(t)}{D_w(t)} \tag{24-1}$$

$$\alpha_a(t) = T(t) * 1.32 \times 10^{-7} - 1.73 \times 10^{-5} \tag{24-2}$$

$$D_w(t) = T(t) * 1.49 \times 10^{-7} - 1.96 \times 10^{-5} \tag{24-3}$$

and where, N_{Le} is the Lewis number, dimensionless; α_a is the air thermal diffusivity, m^2 s^{-1}; and D_w is the water vapor diffusivity, m^2 s^{-1}.

Thus, the plant energy and humidity source terms, $q_p(t)$, $s_p(t)$, are expressed as follows:

$$q_p(t) = m_c(t) * \gamma * v_p * \tau \tag{25}$$

$$s_p(t) = \frac{(m_t(t) - m_c(t)) * v_p}{\rho * v} \tag{26}$$

where, v_p is plant canopy volume, m^3.

3.1.5. Convective source

This section describes the new method proposed for estimating the wall temperature. The convective energy source terms come from the walls (f_w, W), the roof (f_r, W) and the ground (f_g, W). Thus, the convective energy source, $q_c(t)$, can be expressed as,

$$q_c(t) = f_w(t) + f_r(t) + f_g(t) \tag{27}$$

It is assumed that convective heat transfer is the only direct energy exchange mechanism between the internal surfaces and the indoor air, whereas heat conduction only affects the temperature of the internal surfaces, thus affecting the indoor air temperature indirectly. Therefore:

$$f_w(t) = A_{s1}{*}c_{wi}(t){*}(T_1(t) - T(t)) \tag{28}$$

$$f_r(t) = A_r{*}c_{ri}(t){*}(T_4(t) - T(t)) \tag{29}$$

$$f_g(t) = A_g{*}c_g(t){*}\left(T_g(t) - T(t)\right) \tag{30}$$

where, A_{s1}, A_r, and A_g are the areas of the wall, roof and ground, m^2, respectively; c_{wi}, c_{ri} and c_g are the convective transfer coefficients on the internal surfaces of the opaque wall, the transparent roof and the ground, W m^{-2} K^{-1}, respectively; T_g is the ground temperature, K; and T_1 and T_4 are the wall surface temperatures, which are estimated as described below.

The wall temperature calculation is performed using the following energy balance through the easy wall temperature estimating (EWTE) method. For the wall composed of two different materials (Greenhouse A), the wall energy balance is calculated by dividing the wall into three surfaces – the internal wall surface (S.1), the external wall surface (S.2), and the interior space between the different wall materials (I.3) (Fig. 4 (A)). For Greenhouse B, the equations are calculated without I.3 (Fig. 4 (B)).

The surfaces on both sides of the transparent roof are calculated - the internal roof surface (S.4) and the external roof surface (S.5). The equations are shown below, and are divided into two cases: with and without the cover configuration of the thermal insulation blanket.

Cover configuration without the thermal insulation blanket (on the wall surfaces)

For S.1, the energy balance belongs to the convective term, the conduction term, and the long-wave and solar radiation term:

$$\begin{aligned} &A_{s1}{*}c_{wi}(t){*}(T(t) - T_1(t)) + \frac{(T_3(t) - T_1(t)){*}Cd_{w1}}{Th_{w1}}{*}A_{s1} + \sigma{*}e_{wr}{*}\left(T_4(t)^4\right. \\ &\left. - T_1(t)^4\right){*}A_{s1}{*}x_{wr} + \sigma{*}e_{ws}{*}\tau_l{*}\left(T_o(t)^4 - T_1(t)^4\right){*}A_{s1}{*}x_{wr} \\ &+ \tau{*}R_s(t){*}A_r{*}x_{rw}{*}a_{s1} = 0 \end{aligned} \tag{31-1}$$

For S.2, the equation terms are similar to Eq. (31 1), with the addition of the solar radiation term:

$$\begin{aligned} &A_{s2}{*}c_{wo}(t){*}(T_o(t) - T_2(t)) + \frac{(T_3(t) - T_2(t)){*}Cd_{w2}}{Th_{w2}}{*}A_{s3} \\ &+ \sigma{*}e_{ws}{*}\left(T_o(t)^4 - T_2(t)^4\right){*}A_{s2} = 0 \end{aligned} \tag{31-2}$$

For I.3:

$$\frac{(T_1(t) - T_3(t)){*}Cd_{w1}}{Th_{w1}}{*}A_{s1} + \frac{(T_2(t) - T_3(t)){*}Cd_{w2}}{Th_{w2}}{*}A_{s3} = 0 \tag{31-3}$$

(on the roof surfaces)

In the same way, for S.4:

$$\begin{aligned} &A_r{*}c_{ri}(t){*}(T(t) - T_4(t)) + \frac{(T_5(t) - T_4(t)){*}Cd_r}{Th_r}{*}A_r + \sigma{*}e_{rw}{*}\left(T_1(t)^4\right. \\ &\left. - T_4(t)^4\right){*}A_r{*}x_{rw} = 0 \end{aligned} \tag{31-4}$$

and for S.5:

$$\begin{aligned} &A_r{*}c_{ro}(t){*}(T_o(t) - T_5(t)) + \frac{(T_4(t) - T_5(t)){*}Cd_r}{Th_r}{*}A_r + \sigma{*}e_{rs}{*}\left(T_o(t)^4\right. \\ &\left. - T_5(t)^4\right){*}A_r = 0 \end{aligned} \tag{31-5}$$

T_1, T_2, T_3, T_4 and T_5, are the temperatures of S.1, S.2, I.3, S.4 and S.5 (in K), respectively; A_{s1}, A_{s2}, A_{s3} and A_r are the areas of S.1, S.2, I.3 and the south roof (in m^2), respectively; Cd_{w1} is the thermal conductivity of the wall material close to S.1,W m^{-1} K^{-1}; Th_{w1} is the wall thickness between S.1 and I.3, m; Cd_{w2} is the thermal conductivity of the wall material close to S.2, W m^{-1} K^{-1}; Th_{w2} is the wall thickness between S.2 and I.3, m; σ is the Boltzmann constant, (0.0000000567) W m^{-2} K^{-4}; e_{ws}, e_{wr}, e_{rw} and e_{rs} are the long-wave radiation exchange coefficients from the wall to the sky, from the wall to the south roof, from the south roof to the wall and from the south roof to the sky, respectively; x_{wr} is the view factor from the wall to the south roof; x_{rw} is the view factor from the south roof to the wall; τ is the short-wave transmissivity of the south roof; τ_l is the long-wave transmissivity of the south roof; a_{s1} is the absorbed solar radiation coefficient of surface 1; and c_{wo} and c_{ro} are the convective transfer coefficients of the external wall and roof surfaces, W m^{-2} K^{-1}. The thermal conductivities of the greenhouse materials are shown in Table 1.

Please see Appendix C for the simulation of the cover configuration using the thermal insulation blanket.

Under the assumption of a diffuse-grey surface, the view factor is used to calculate the radiative heat transfer between the surfaces that are separated by transparent media (Modest, 1993). The view factor between the south roof and the north wall depends on the spatial relationship and the shielding medium, i.e., the plant canopy between them. The crop canopy height is 0.5 m in early April and early September, and 1.5 m in May, October, and November. With the aid of auxiliary surfaces, the view factor can be calculated between two objects that have a complex spatial relationship. The corresponding view factor calculation is shown in Fig. 5 and the equations are shown below. It should be noted that the equations in each case are the same (Eq. (31 6)), but the sizes of the parameters are different.

$$\begin{cases} x_{rw} = \dfrac{A_1 + A_2 - A_3}{2A_1}{*}\dfrac{A_2 + A_5 - A_4}{2A_2}{*}\dfrac{A_5 + A_7 - A_6}{2A_5} \\ x_{wr} = \dfrac{A_1{*}X_{rw}}{A_7} \end{cases} \tag{31-6}$$

Convective transfer is the main form of energy gain (or loss) from (or to) the indoor air; this has been studied for many years (Roy et al., 2002). When using different convective transfer models, deviations of up to ± 30% are seen in the annual cooling energy demand (Mirsadeghi et al., 2013). It is important to choose an appropriate convection model according to the specific building and the parameters available. Regarding Chinese solar greenhouses, at least 4 different models are necessary for the convective transfer coefficients.

Convective transfer coefficients on the external and internal surface of the opaque wall

The Building Loads Analysis and System Thermodynamics (BLAST) model is comprehensive as it considers both the forced ($c_{wo,\ for}$, W m^{-2} K^{-1}) and the natural ($c_{wo,\ nat}$, W m^{-2} K^{-1}) convection components on the external wall surface (Walton, 1981; McClellan and Pedersen, 1997):

$$c_{wo}(t) = c_{wo,for}(t) + c_{wo,nat}(t) \tag{31-7}$$

$c_{wo,\ for}$ is estimated using the following equation, which is based on wind tunnel experiments using rectangular plates (Sparrow et al., 1979):

$$c_{wo,for}(t) = 2.537{*}W_f{*}R_f{*}\left(\frac{Pe{*}V_f(t)}{A}\right)^{1/2} \tag{31-8}$$

where, W_f is the wind direction modifier, with 1 for the windward surface and 0.5 for the leeward surface; Pe is the surface perimeter, m; A is the surface area, m^2; R_f is the surface roughness multiplier, 1.67 for brick and 1.52 for concrete (Walton, 1981); and V_f is the free-stream wind speed, m s^{-1}. In this case, the free-stream wind speed is

Table 1
Thermal conductivity of the materials (Zhang et al., 2019b; Carlini et al., 2020; Ahamed et al., 2018).

	Clay Brick	Gravelly soil	Polyethylene	Hollow block	Soil
Thermal conductivity(W m^{-1} K^{-1})	0.81	1.80	0.38	1.02	1.4

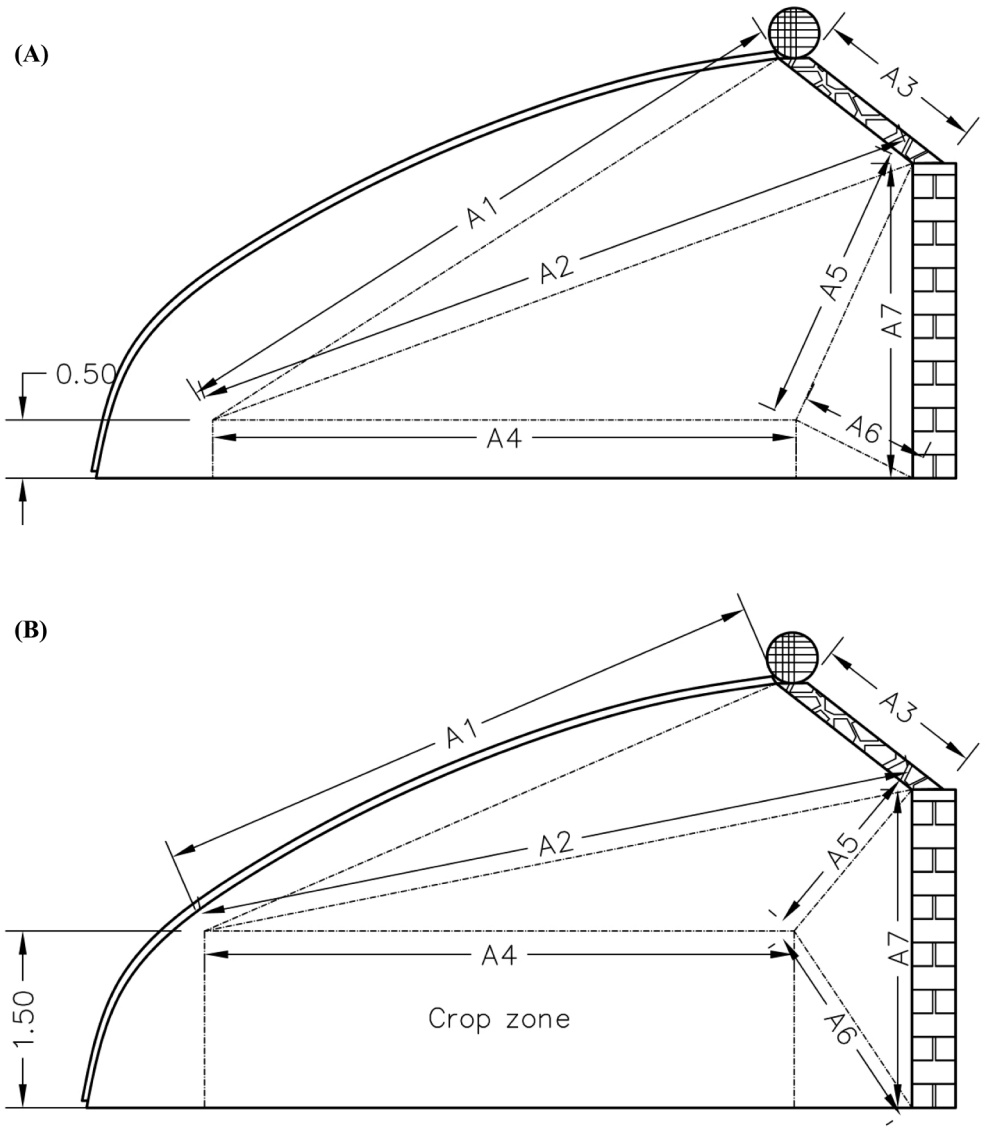

Fig. 5. Calculation of the view factor when the crop height is 0.5 m (A) and 1.5 m (B).

estimated using the wind profile model and the wind speed measured 2.5 m above the ground (Boulard et al., 2010). $c_{wo,\ nat}$ is the natural component of convection, which is calculated using the following equations (Walton, 1983; Mirsadeghi et al., 2013):

$$c_{wo,nat}(t) = 9.482*\frac{(|T_2(t) - T_o(t)|)^{\frac{1}{3}}}{7.238 - |cos\varphi|}, (T_2 > T_o) \quad (31\text{-}9)$$

$$c_{wo,nat}(t) = 1.810*\frac{(|T_2(t) - T_o(t)|)^{\frac{1}{3}}}{1.382 + |cos\varphi|}, (T_2 < T_o) \quad (31\text{-}10)$$

where, φ is the surface plane angle in relation to the ground plane, °.

The convective coefficient on the internal wall surface is estimated considering only the natural component:

$$c_{wi}(t) = 9.482*\frac{(|T_1(t) - T(t)|)^{\frac{1}{3}}}{7.238 - |cos\varphi|}, (T_1 > T) \quad (31\text{-}11)$$

$$c_{wi}(t) = 1.810*\frac{(|T_1(t) - T(t)|)^{\frac{1}{3}}}{1.382 + |cos\varphi|}, (T_1 > T) \quad (31\text{-}12)$$

Convective transfer coefficients on the external and internal surfaces of the transparent roof

A variety of roof convection models have been applied to different types of greenhouses, usually a wind speed-dependent model for the exterior and a temperature-difference model for the interior (Roy et al., 2002). In this case, the following equations were adopted to estimate the external and internal convection transfer coefficients, applied to conditions where there is a polyethylene-covered greenhouse, above which the wind speed is measured (5.6 m above the ground) at less than 6.3 m s^{-1} (Papadakis et al., 1992):

$$c_{ro}(t) = 0.95 + 6.76*Ve(t)^{0.49} \quad (31\text{-}13)$$

$$c_{ri}(t) = 2.21*(T(t) - T_4(t))^{\frac{1}{3}}, (0.3 < T - T_4 \leq 13.8^{\circ}C) \quad (31\text{-}14)$$

The long-wave radiation exchange coefficient between two grey-body surfaces can be described as follows (Liu and Zhang, 2011):

$$e_{ij} = \left(e_i^{-1} + e_j^{-2} - 1\right)^{-1} \quad (31\text{-}15)$$

where, e_{ij} is the long-wave radiation exchange coefficient, and e_i and e_j are the long-wave emissivity of two radiation objects, which are shown in Table 2.

The sky emissivity variable (e_s) is related to the outdoor air temperature (T_o, K) and the outdoor water vapor pressure (P_{wo}, Pa) (Kustas et al., 1994):

$$e_s(t) = 0.642(P_{wo}(t)/T_o(t))^{1/7} \quad (31\text{-}16)$$

The wall temperature is simulated using several outdoor climate variables, which can be provided by the weather forecast. In contrast to the wall temperature simulation, the ground temperature simulation requires the boundary temperature at a set depth beneath the ground. The ground temperature is simulated after taking the initial soil temperature at a depth of 0.5 m; this is measured using a temperature probe:

For the ground surface:

$$A_g{*}c_g(t){*}\big(T(t) - T_g(t)\big) + \frac{\big(T_d(t) - T_g(t)\big){*}Cd_g}{Th_g}{*}A_g + \sigma{*}e_{gr}{*}\big(T_4(t)^4 - T_g(t)^4\big){*}A_g{*}x_{gr} + \sigma{*}e_{gs}{*}\tau_l{*}\big(T_o(t)^4 - T_g(t)^4\big){*}A_g{*}x_{gr} + (R_s(t){*}\tau{*}x_{gr}{*}A_g - R_{sc}(t){*}A_p){*}a_g = 0 \quad (32\text{-}1)$$

For a depth of 0.5 m beneath the ground:

$$\frac{dT_d(t)}{dt}{*}\rho_g{*}c_{pg}{*}v_g = \frac{\big(T_g(t) - T_d(t)\big){*}Cd_g}{Th_g}{*}A_g \quad (32\text{-}2)$$

where, T_g is the ground surface temperature, K; T_d is the below-ground temperature at a depth of 0.5 m, K; ρ_g is the soil density, (1975) kg m^{-3}; c_{pg} is the specific heat capacity of the soil, (1480) J kg^{-1} K^{-1}; v_g is the soil volume, m^3; e_{gr} and e_{gs} are the long-wave radiation exchange coefficients from the ground to the roof and sky; x_{gr} is the view factor from the ground to the roof; A_g is the ground surface area, m^2; A_p is the plant area, m^2; a_g is the absorbed solar radiation coefficient of the ground (0.92); c_g is the convective transfer coefficient of the ground, W m^{-2} K^{-1}; Th_g is the thickness of the ground, 0.5 m; and Cd_g is the thermal conductivity of the soil, W m^{-1} K^{-1}. The convective transfer coefficient of the ground is estimated using the following equation, which was developed in a large-scale greenhouse (De Halleux, 1989),

$$c_g = 1.86{*}(|T_g(t) - T(t)|)^{\frac{1}{3}} \quad (32\text{-}3)$$

3.2. Model implementation and validation

The model system was implemented using Matlab and Simulink. The Root Mean Squared Error (RMSE) and Mean Error (ME) were used to evaluate the errors between the calculated and the measured data, as expressed in Eqs. (33,34):

$$RMSE = \sqrt{\frac{\sum_{i=1}^{N}(C_{ai} - M_{ei})^2}{N-1}} \quad (33)$$

$$ME = \frac{|C_{ai} - M_{ei}|}{N} \quad (34)$$

where, C_{ai} is the estimated value, M_{ei} is the measured value, and N is the sample size.

4. Results and discussion

This section presents the validation results for the proposed model. The temperature and humidity results are also given. The model was validated during different seasons with data from Greenhouse A and Greenhouse B. Note that the accuracy of the model is demonstrated not only by validating the model in different seasons and in different years, but also by calibrating it in one greenhouse and validating it in the other. The calibration process was performed in MATLAB implementing the Monte Carlo method to estimate the global model parameters, resulting in the table showing the calibrated model parameters in Appendix B.

4.1. Model performance on a single day

In this section, the thermal and mass (humidity) performance is validated on a single day when the vents are closed. Several middle links in this model are analyzed to show the energy and mass budget of the greenhouse. Subsequently, the ventilation is analyzed by simulating the greenhouse climate when the vents are open.

Fig. 6 shows the simulation and measurement when the vents are closed in Greenhouse A. The crop height is 1.5 m and the LAI is 2.55. The RMSE of the temperature is 2.6 K. The RMSE of the absolute humidity and the relative humidity are 3.1 g kg^{-1} and 14.6%, respectively. The simulation under closed-vent conditions is of great significance as it illustrates the model's performance. The curve fluctuation and peak value of the absolute humidity are consistent with the real situation, although the relative humidity error is striking due to the temperature difference. Fig. 7 shows that the thermal performance is also good when applied to Greenhouse B, with the temperature RMSE at 3.3 K. The RMSE of the absolute humidity and the relative humidity are 3.0 g kg^{-1} and 17.8%, respectively.

Compared to the dynamic models from other studies validated on typical days, the RMSE of T was 5.3 K with T increasing from 308 K to 343 K (Mohammadi et al., 2018). In Singh et al. (2006), the RMSE of T was 5.69 K with T increasing from 287 K to 301 K, and the RMSE of RH was 4.37% with the error ranging from 3.08% to 27.78% Notice that the error in the latter study was obtained with a temperature increase over 30 K, which demonstrates that the model is accurate in terms of the energy budget. This model also provides a leaf wetness risk that is based on simulating the crop canopy condensation (Fig. 6) which, when combined with temperature, can be a useful tool for a plant disease warning system (Zhao et al., 2011).

The indoor solar radiation intensity measured was higher at noon and lower at other times compared to the simulation (Fig. 8). A more precise method would be to adopt a variety of times to simulate τ. The transmittance is highest when the solar incidence angle is perpendicular to the roof, and gradually reduces as the angle increases (Soriano et al., 2004). However, the transmittance only changes slightly in the 0 to 60-degree incidence range, and decreases rapidly when the incident angle exceeds 60° (Zhang et al., 2020a). Thus, the roof transmittance value remains almost at the maximum during most of the daytime. Given the computational load needed to simulate it, and the consistency shown between the simulated and measured indoor solar radiation (Fig. 8), relying on the transmittance constant is feasible.

The air leakage rate varies from 0.2 h^{-1} to 0.6 h^{-1} and reaches its peak at noon. In a very tightly covered solar greenhouse with a span of 6.6 m and a ridge height of 3 m, the mean air leakage rate was 0.35 h^{-1} in the daytime and 0.15 h^{-1} at night (Tong et al., 2007). In another Chinese solar greenhouse, the air leakage rate measured using the carbon dioxide tracing method varied between 0.33 h^{-1} and 0.41 h^{-1} (Tong et al., 2007). Considering that the air leakage rate variable is positively related to wind speed, solar radiation, and the indoor/ outdoor temperature difference, the equation adopted in this model was able to simulate the air leakage rate accurately and proportionally.

The convective heat transfer coefficients used in this model have been proven to be applicable to other scenarios (De Halleux, 1989; Papadakis et al., 1992; Walton, 1983; Mirsadeghi et al., 2013). Of these,

Table 2
Long-wave emissivity of the objects and the long-wave radiation exchange coefficient estimated using Eq. (31–15).

Emissivity of objects	Wall (e_w)		Roof (e_r)		Thermal insulation blanket (e_b)	Sky (e_s)
Value	0.9		0.5		0.9	Eq. 31–16
Long-wave radiation exchange coefficient	e_{wr}	e_{rw}	e_{wb}	e_{bw}	e_{ws}	e_{rs}
Value	0.24	0.45	0.74	0.74	$(e_w{}^{-1} + e_s{}^{-2} - 1)^{-1}$	$(e_r{}^{-1} + e_s{}^{-2} - 1)^{-1}$

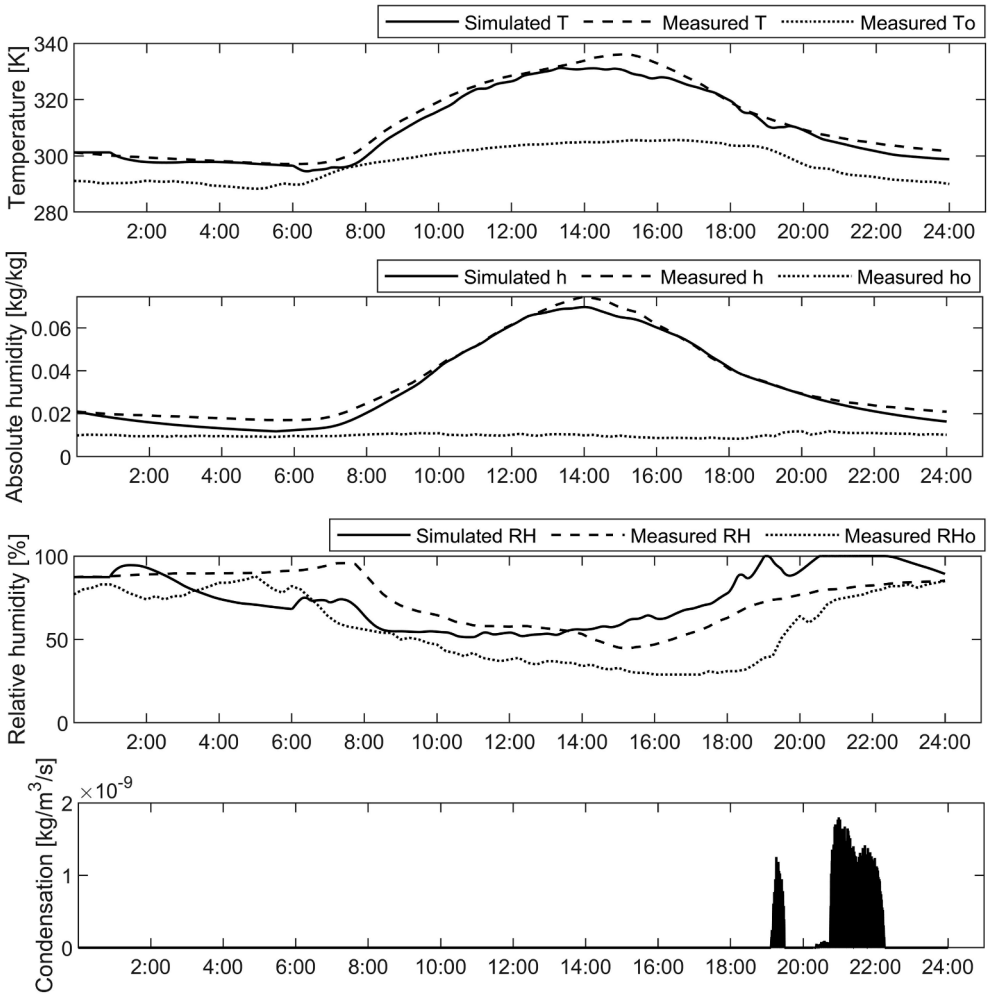

Fig. 6. Data set for the temperature, humidity, and crop canopy condensation under closed-vent conditions, recorded on 17 August 2019 in Greenhouse A.

the external roof coefficient was the highest while the internal wall coefficient was the lowest (Fig. 8). All the parameters peaked at noon, whereas the external wall, internal wall and external roof coefficients were close to 0 over night when the wind speed was low.

Transpiration in cucumber varies from 0 to 150 W m^{-2} in autumn with the LAI ranging from 2 to 3.5; this was measured using a sap-flow sensor in a Venlo greenhouse (Huang et al., 2020). The transpiration rate in Fig. 8 began to rise after 6:00 a.m. and reached its peak at noon; then, the transpiration rate gradually dropped to 0 after 18:00. This was similar to the transpiration rate measured by Huang et al. (2020) from 2 − 16 October 2018. Evapotranspiration is the main humidity source under closed-film conditions. Accurate transpiration rate simulation is an important middle link in humidity modeling.

Fig. 9 shows how the temperature increases and decreases in the energy budget. Based on the model assumption, the air is transparent to the solar radiation and is heated by convective heat transfer from the wall and soil surfaces; these absorb the solar radiation in the daytime, 34% of which is absorbed by the wall and 66% by the ground. Not all the solar radiation absorbed by the wall will be converted into air heating, and thus the process is simulated by solving the embedded conservative equation group for each second. The transparent roof is the main medium of greenhouse energy loss, accounting for 86% of losses in the daytime and 65% at night, followed by air leakage, which accounts for 14% of losses in the daytime and 23% at night. The ground is the main medium providing energy at night, but it is insufficient to offset the loss, and the net energy overnight is −19.5 MJ.

Fig. 10 shows the model's ventilation performance for different vent opening areas, in which the temperature curve and the absolute humidity curve indicate the energy and mass responses to the ventilation, respectively. The agreement between the measured and the simulated curves demonstrates the accuracy of the simulated ventilation rate. The RMSE of the temperature, absolute humidity, and relative humidity is 2.5 K, 1.1 g kg^{-1} and 8.6%, respectively. Fig. 10 also shows a significant positive correlation between the wind speed and the ventilation rate. The ventilation times are obtained from the hourly cumulative ventilation rate divided by the greenhouse volume - these are 2.23 h^{-1} when the opening area is 5 m^2 and 13.36 h^{-1} when the opening area is 10 m^2. Notice that this value is for the single-vent opening configuration, and would be higher if both the lower and upper vents were open.

4.2. Model performance on consecutive days

In this section, the model was validated on consecutive days in different seasons during 2016 and 2019. The number of consecutive days in each test amounted to 1 week, and the total days simulated amounted to four weeks. The outdoor weather station data was used as the model input and the validation data were taken from the indoor sensors. Different ventilation configurations were applied during the experiment along with the use of the thermal insulation blanket. The ME (Mean Error) and RMSE between the simulated and measured data are shown in Table 3.

4.2.1. Temperature performance

Figs. 11-14 show the input data set, which includes the outdoor

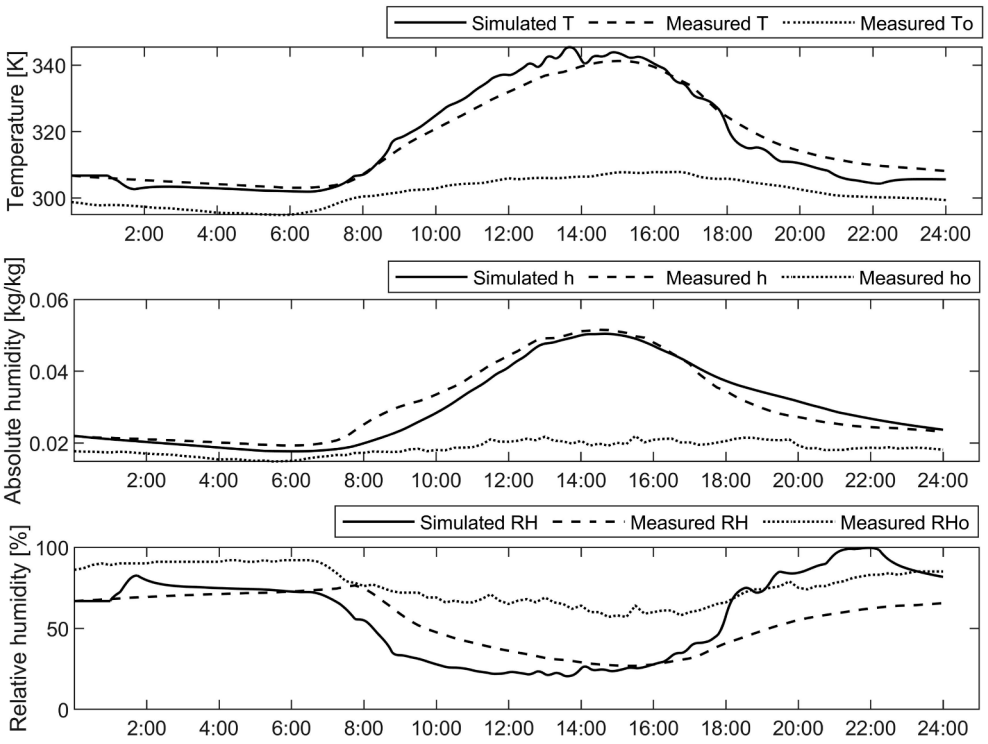

Fig. 7. Data set for the temperature and humidity under closed-vent conditions, recorded on 11 August 2020 in Greenhouse B.

temperature, outdoor humidity, outdoor solar radiation, wind speed, and the output. The simulated temperature fitted the real data measured in the spring, autumn and cold season (tests 1–4), with the ME and RMSE from 1.5 to 2.4 K, and from 2.0 to 2.9 K, respectively (Table 3). The temperature was underestimated in Fig. 14, which resulted in the RH exceeding the maximum saturation value. A similar phenomenon appeared in the semi-Quonset-type greenhouse simulation when the vents were closed in the cold season; here, the predicted RH value was higher than the measured value and the predicted T was lower than the measured value (Singh et al., 2006). Nonetheless, in Fig. 14, the model performed well under continuous low-temperature and low-illumination weather conditions from day 3 to day 6. The simulated temperature changed simultaneously and precisely in line with the solar radiation intensity, even under extremely low intensities (Figs. 11-14); this means that the model's simulated air temperature is sensitive to, and responds accurately to, changes in the outdoor solar radiation.

It should be pointed out that the validations were conducted in the same periods of the year for both Greenhouse A and Greenhouse B (Figs. 11-14), the data for which were not considered during the calibration process. As demonstrated by the figures and by the quantitative results in Table 3, the model provides very promising results when used in similar types of greenhouse (although of different sizes) as the one used for calibration purposes. It is worth remarking that this is the typical greenhouse structure found in China, and thus the model could be used to estimate the temperature and humidity of any of these greenhouses, simply by updating the greenhouse's structural parameters.

4.2.2. Humidity performance

The humidity performance values were good for weeks 1–4 with the ME and RMSE ranging from 6.9% to 13.1% and 8.8% to 16.6%, respectively, in the different seasons and the different greenhouses (Table 3). The simulation and measurement curves are perfectly consistent for the temperature, absolute humidity, and relative humidity (Figs. 11-14). The RH is sensitive to temperature, with the average variation in RH spatial distribution for a single-span greenhouse (with a floor area of 8 m × 20 m) being 13%, and where the maximum difference could be over 40% (Ahmed et al., 2019). Few mechanistic models for greenhouse humidity have been developed, with the exception of some CFD models (Boulard et al., 2017); this is due to the complexity of comprehensively considering the water vapor sources, which are estimated using a mass exchange model between the indoor and outdoor environments, as well as the liquidation model, condensation and leaf transpiration model. During the simulation, this study tried to consider all the middle links as far as possible, and the results are striking.

4.3. Schematic representation of the model: Inputs and outputs

This section describes how the model works with only 4 inputs and 3 initial-condition values. The model runs on the inputs shown in Fig. 15, which can be provided by the weather station or from weather forecast data. All the middle links are simulated by adopting proper equations developed under similar conditions in the first and second layers. In addition, prior to the simulation, the size of the construction and the properties of its physical materials should be given. Only 3 initial values were defined at the outset; these were the initial temperature T, the initial humidity h, and the initial soil T_d. The results show that the model is accurate for at least 7 days without recalibrating the initial conditions. Reducing the required number of sensor inputs not only lowers the cost, but also avoids any inconvenience caused by faulty sensors. Compared to the current models, it has been shown that the wall temperature or wall flux are necessary inputs (Li et al., 2020; Sánchez-Molina et al., 2017). Many models require sensors to be placed on the ground, the wall, and in the roof. When applied in practice, any sensor fault will lead to the model failing to run. The model in this paper not only effectively reduced the amount of inputs, but it could also be transplanted successfully to another greenhouse without affecting the model's performance from season to season or from year to year.

5. Conclusions

The model described in this paper allows one to estimate the

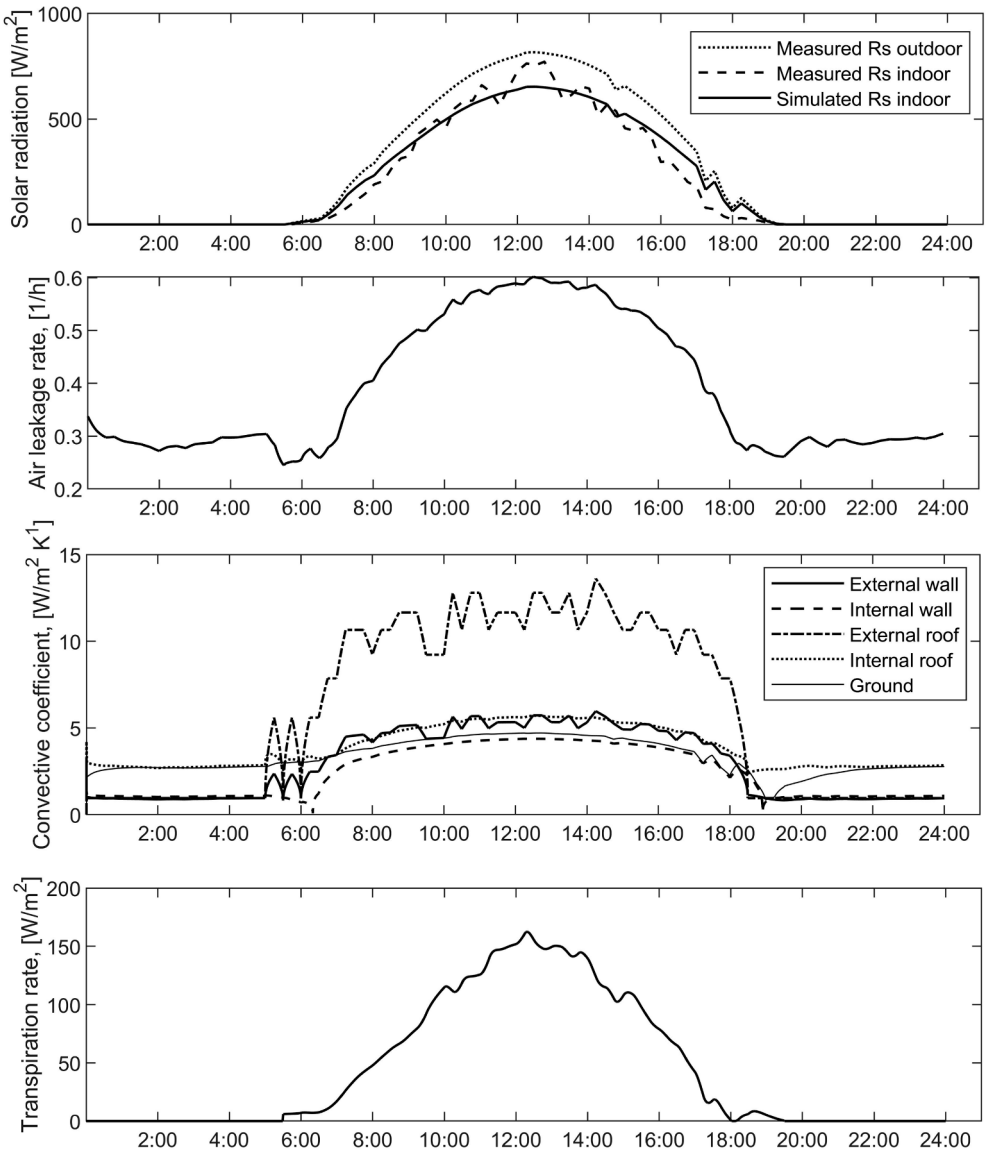

Fig. 8. Data set for the simulated solar radiation, air leakage rate, convective transfer coefficient and crop transpiration rate on 17 August 2019 in Greenhouse A.

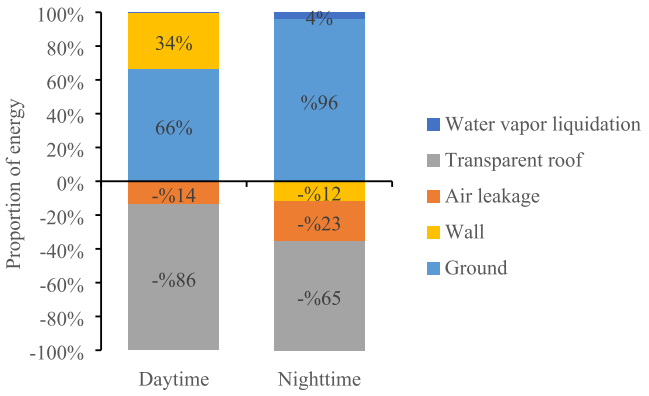

Fig. 9. The proportion of gain and loss to the greenhouse's energy for each link under closed-vent conditions on 17 August 2019 in Greenhouse A.

temperature and humidity of a typical Chinese solar greenhouse using only the solar radiation, outdoor temperature, outdoor humidity, and wind direction and speed, as the model inputs. The model also includes a variety of management modes, such as the vent opening angle, the time the vents are open or closed, and the time that the thermal insulation blanket covers the roof. The RMSEs for the predicted temperature on three separate days were 2.6 K, 3.3 K, 2.5 K, respectively, while the RMSEs for the predicted relative humidity were 14.6%, 17.8% and 8.6%, respectively. The RMSEs for the predicted temperature on four consecutive days (1 week for each test) remained in the 2.0 K to 2.8 K range while the RMSEs for the predicted relative humidity remained in the 8.8% to 16.6% range during different seasons in 2016 and 2019. Therefore, the simple model proposed has demonstrated its promising accuracy and ability to predict the future environmental behavior inside a greenhouse.

In addition, the model was validated in a second greenhouse, which was a different size to the one used for the calibration. Notice that only the physical model parameters were modified, such as the greenhouse volume, the roof and wall areas, the wall materials and so on; this is because the other parameters are common to both greenhouses. The validation for the transplanted modeling was good, which means that this model (or its methodology) can be widely adapted to typical Chinese solar greenhouse of different sizes.

In terms of ensuring the resolution and accuracy, the proposed model has the advantage of being fast. The most time-consuming part of the

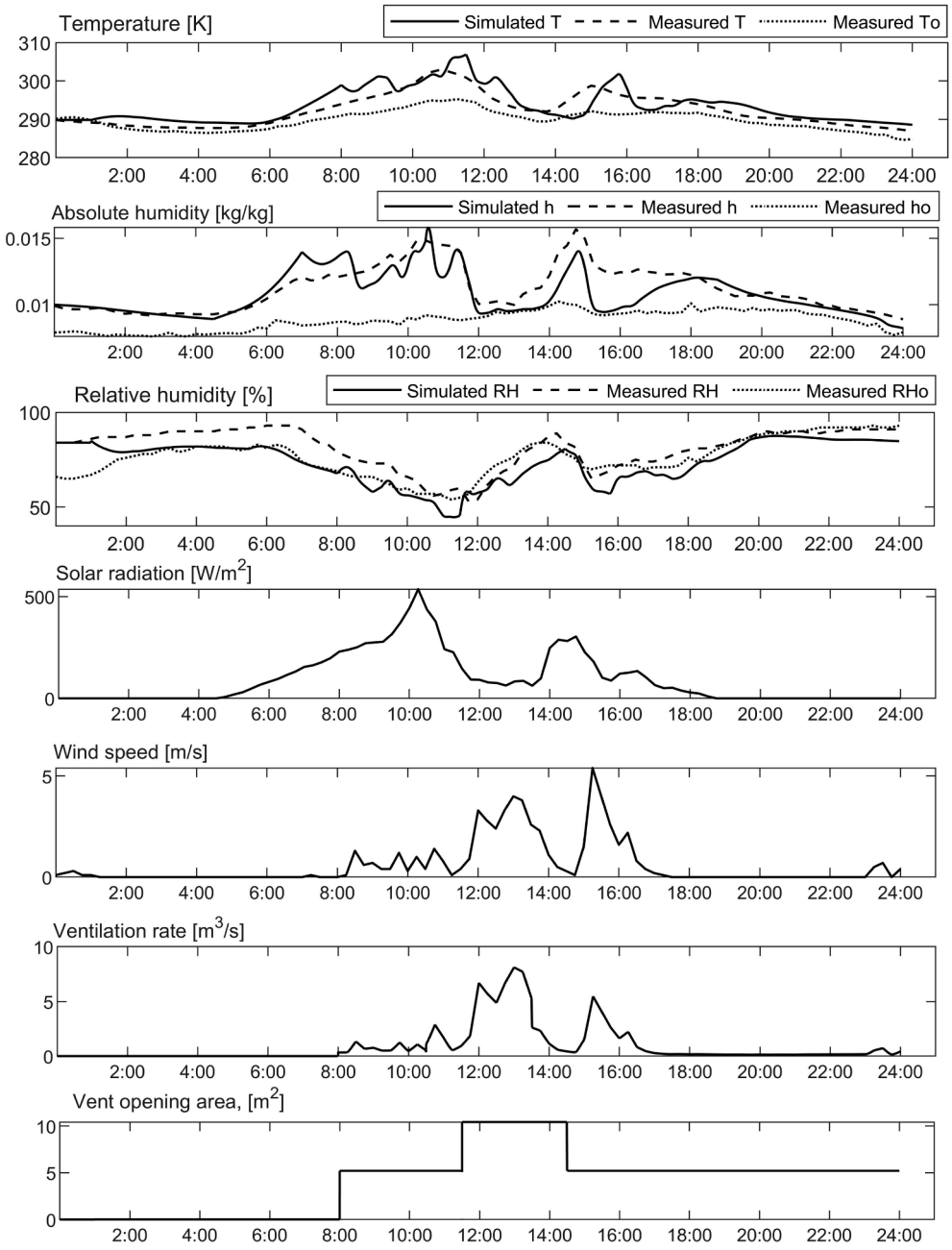

Fig. 10. Data set of the temperature, humidity, outdoor solar radiation, wind speed, simulated ventilation rate and the vent opening area under the single-vent opening configuration on 9 May 2019 in Greenhouse A.

Table 3
The Root Mean Squared Error (RMSE) and Mean Error (ME) of the simulated greenhouse temperature and humidity for each test.

Test	Week	RMSE / ME			Greenhouse
		T (K)	h (g kg^{-1})	RH (%)	
No. 1	20/09/2016–26/09/2016	2.3 / 1.5	1.3 /1.1	11.4 / 8.4	A
No. 2	10/05/2016–16/05/2016	2.8 / 2.0	1.5 / 2.1	16.6 / 13.1	A
No. 3	20/09/2019–26/09/2019	2.0 / 1.6	0.8 / 0.6	8.8 / 6.9	B
No. 4	18/11/2019–24/11/2019	2.8 / 1.9	1.8 / 1.2	11.7 / 9.5	B

model's system is solving the closed-equations group for the wall and roof temperature. Even so, the total running time for a 24 h simulation period is less than 15 mins (using an Intel Core I7 CPU and 16 GB RAM). The model's portability is especially significant, allowing it to be deployed in practical greenhouse cultivation to facilitate future decision-making management and real-time closed-loop automatic control.

Temperature and humidity interact with each other inside a greenhouse via the sensible and latent heat transitions; this makes it difficult to quantify the source term for the energy and water vapor. Therefore, in most of the current studies, black box techniques have been used to develop the greenhouse's temperature and humidity model. The model described in this paper quantified the water–vapor source term by incorporating the phase transition, leaf transpiration, leaf condensation, and the indoor/outdoor humidity exchange, to develop a mechanistic

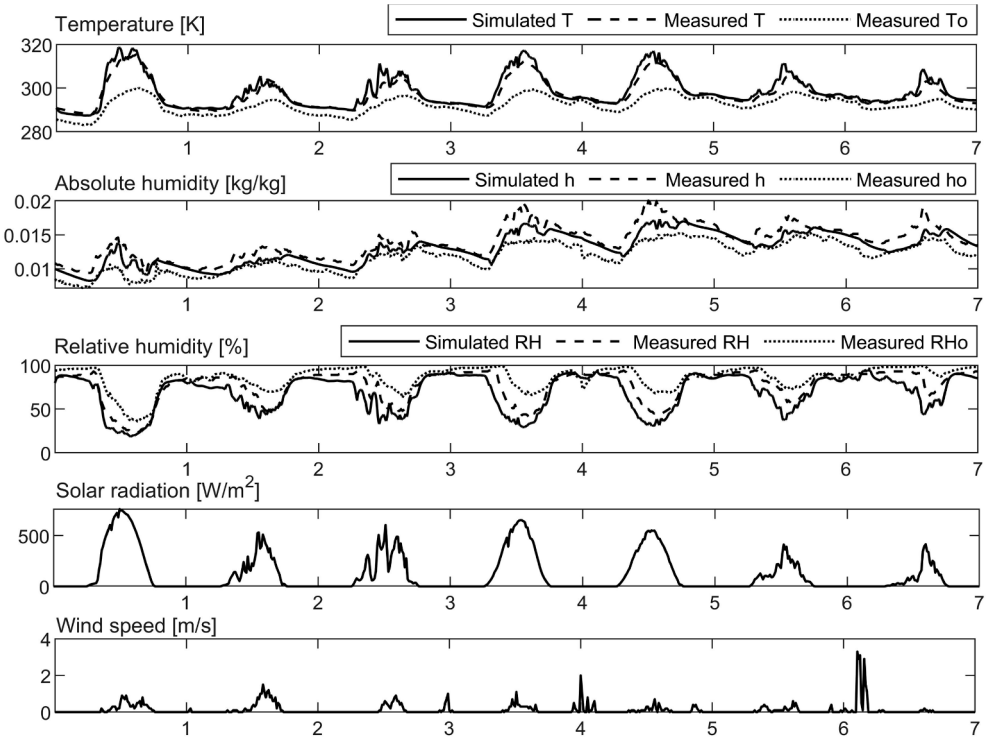

Fig. 11. Data set used for the model validation with the temperature and humidity, recorded on 20–26 September 2016 in Greenhouse A.

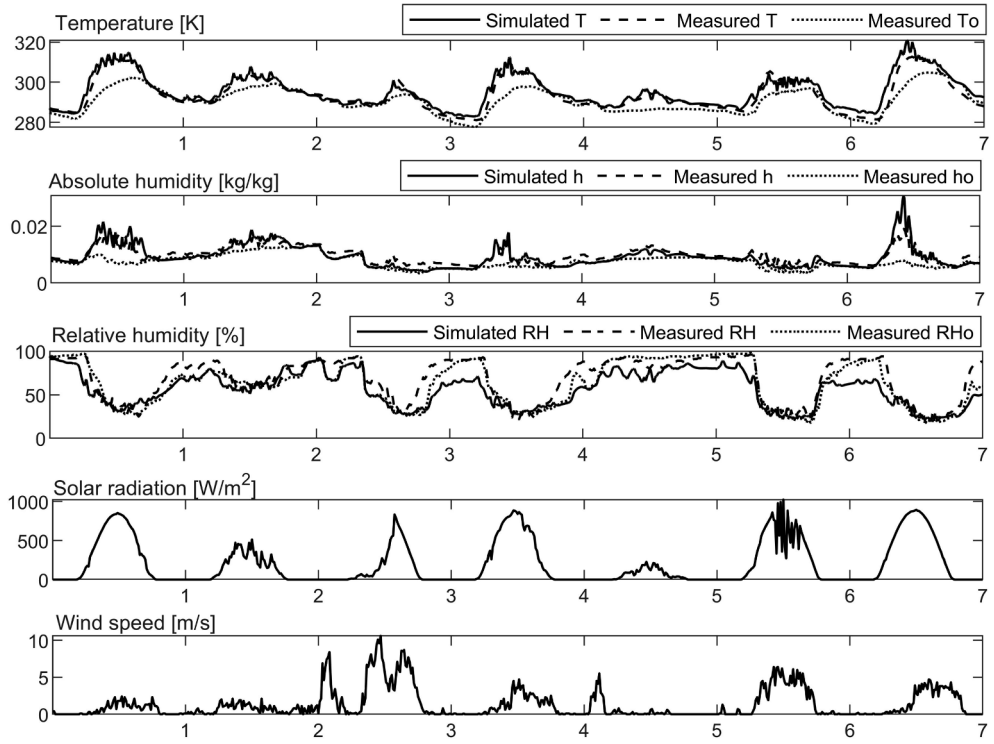

Fig. 12. Data set used for the model validation with the temperature and humidity on 10–16 May 2016 in Greenhouse A.

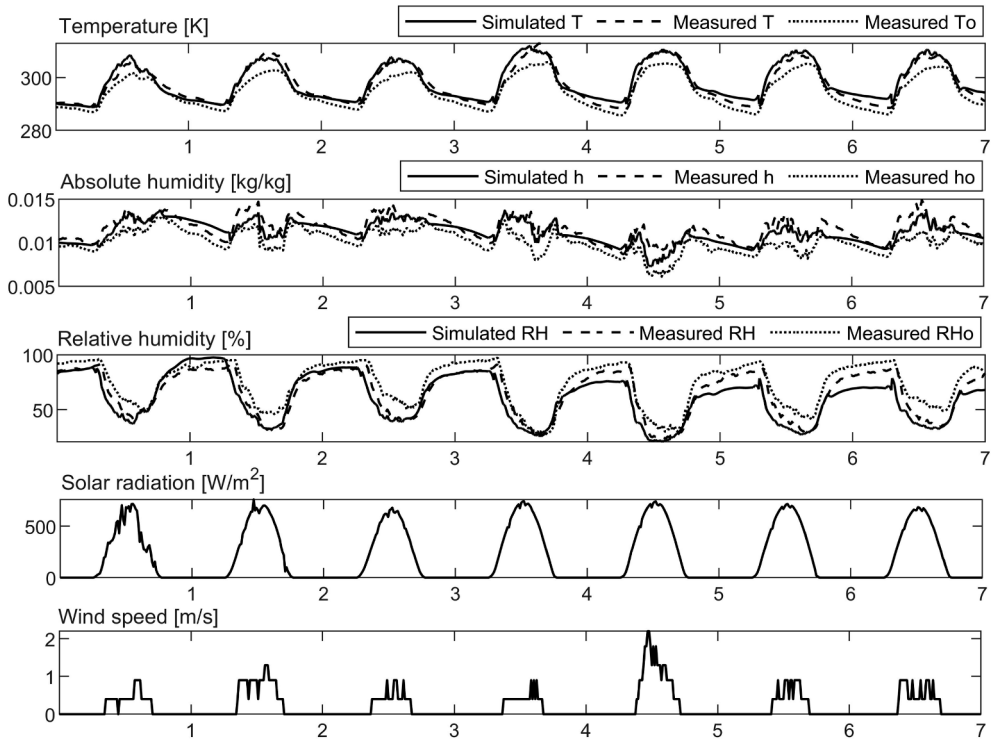

Fig. 13. Data set used for the model validation with the temperature and humidity on 20–26 September 2019 in Greenhouse B.

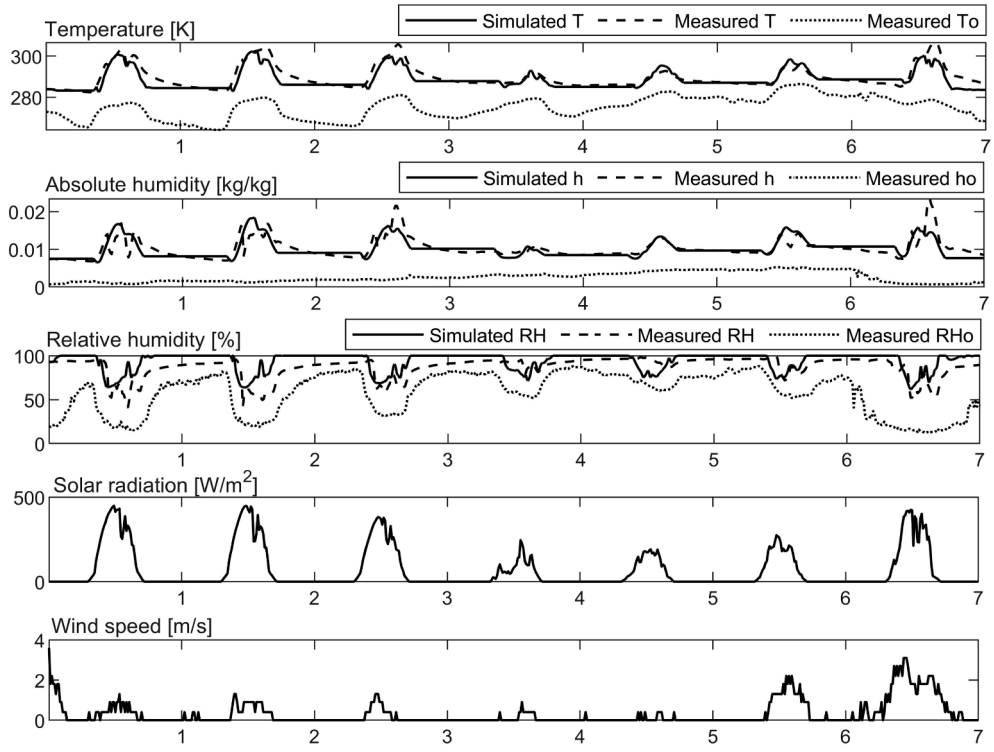

Fig. 14. Data set used for the model validation with the temperature and humidity on 18–24 November 2019 in Greenhouse B; the thermal insulation blanket covering was deployed from 17:00 to 08:00 every day.

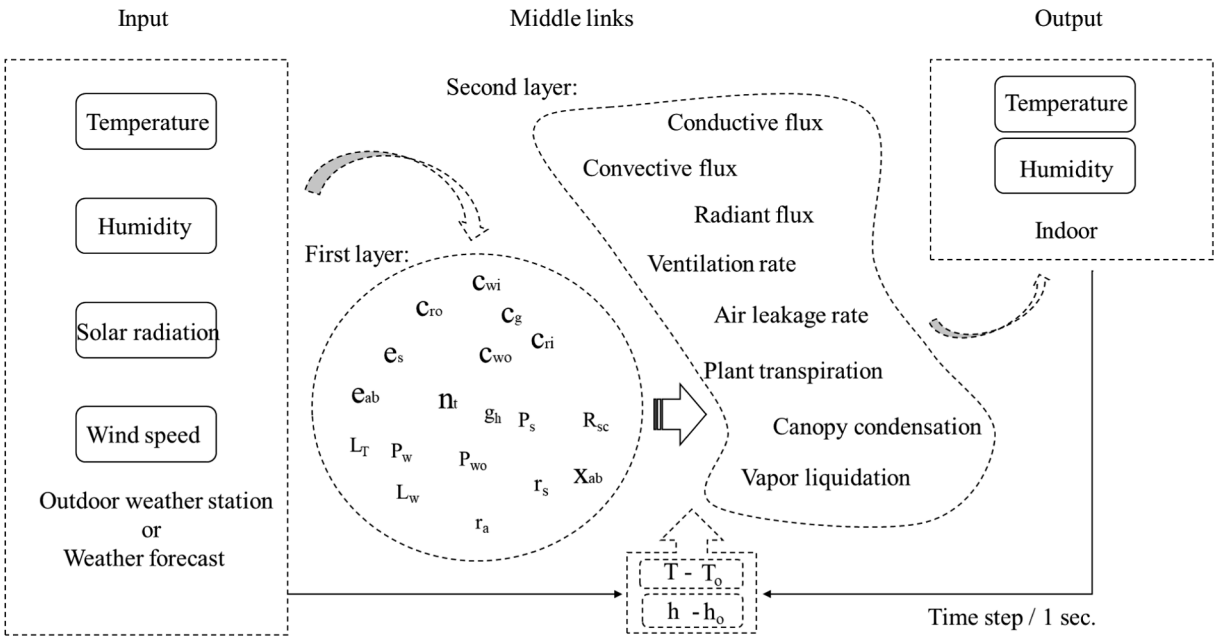

Fig. 15. Inputs, middle links, and outputs of the model. A description of the figure's characters is given in Appendix A.

greenhouse temperature and humidity model, which has been utilized to study Chinese single-slope greenhouses for the first time.

The model developed in this paper is a flexible and valuable tool that can be used for climate simulation, temperature and humidity control, and as decision support tool in Chinese solar greenhouses. Nevertheless, further research need to be undertaken, for example, developing crop models for particular cultivars, models that precisely simulate soil evaporation and ventilation, and optimization between one dimension and multi-dimension models.

Declaration of Competing Interest

The authors declare that they have no known competing financial interests or personal relationships that could have appeared to influence the work reported in this paper.

Acknowledgements

Liu Ran is most grateful for the financial support given by the China Scholarship Council for this research (no. 201909505002). This work has been funded by Project DPI2017-85007-R of the Spanish Ministry of Science, Innovation and Universities, and by ERDF funds.

Supplementary material

Supplementary data to this article can be found online at https://doi.org/10.1016/j.compag.2021.106186.

References

Ahamed, M.S., Guo, H.Q., Tanino, K., 2018. Development of a thermal model for simulation of supplemental heating requirements in Chinese-style solar greenhouses. Computers and Electronics in Agriculture. 150, 235–244. https://doi.org/10.1016/j.compag.2018.04.025.

Ahmed, H.A., TONG, Y.X., YANG, Q.C., Al-Faraj, A.A., Abdel-Ghany, A.M., 2019. Spatial distribution of air temperature and relative humidity in the greenhouse as affected by external shading in arid climates. Journal of Integrative Agriculture. 18 (12), 2869-2882. https://doi.org/10.1016/S2095-3119(19)62598-0.

Boulard, T., Roy, J.C., Fatnassi, H., Kichah, A., Lee, I.-B., 2010. Computer fluid dynamics prediction of climate and fungal spore transfer in a rose greenhouse. Computers and Electronics in Agriculture. 74 (2), 280–292. https://doi.org/10.1016/j.compag.2010.09.003.

Boulard, T., Roy, J.C., Pouillard, J.-B., Fatnassi, H., Grisey, A., 2017. Modelling of micrometeorology, canopy transpiration and photosynthesis in a closed greenhouse using computational fluid dynamics. Biosystems Engineering. 158, 110–133. https://doi.org/10.1016/j.biosystemseng.2017.04.001.

Boulard, T., Wang, S., 2002. Experimental and numerical studies on the heterogeneity of crop transpiration in a plastic tunnel. Computers and Electronics in Agriculture. 34, 173–190. https://doi.org/10.1016/S0168-1699(01)00186-7.

Carlini, M., Castellucci, S., Mennuni, A., Morelli, S., 2020. Numerical modeling and simulation of pitched and curved-roof solar greenhouses provided with internal heating systems for different ambient conditions. Energy Reports. 6 (3), 146–154. https://doi.org/10.1016/j.egyr.2019.10.033.

Chen, J.T., Ma, Y.W., Pang, Z.Z., 2020. A mathematical model of global solar radiation to select the optimal shape and orientation of the greenhouses in southern China. Solar Energy. 205, 380–389. https://doi.org/10.1016/j.solener.2020.05.055.

Choab, N., Allouhi, A., El Maakoul, A., Kousksou, T., Saadeddine, S., Jamil, A., 2019. Review on greenhouse microclimate and application: Design parameters, thermal modeling and simulation, climate controlling technologies. Solar Energy. 191, 109–137. https://doi.org/10.1016/j.solener.2019.08.042.

De Halleux, D., 1989. Dynamic model of heat and mass transfer in greenhouses: theoretical and experimental study. PhD Thesis, Gembloux, Belgium.

Gerlein-Safdi, C., Koohafkan, M.C., Chung, M., Rockwell, F.E., Thompson, S., Caylor, K. K., 2018. Dew deposition suppresses transpiration and carbon uptake in leaves. Agricultural and Forest Meteorology. 259, 305–316. https://doi.org/10.1016/j.agrformet.2018.05.015.

Guo, H.E., Liu, B., Wang, X., Zhang, C.K., 2016. Current situation and countermeasures for the development of the solar greenhouse in Shandong province. Bulletin of Agricultural Science and Technology. 10, 5–8. https://doi.org/10.3969/j.issn.1000-6400.2016.10.001.

He, F., Ma, C.W., 2010. Modeling greenhouse air humidity by means of artificial neural network and principal component analysis. Computers and Electronics in Agriculture. 71. Supplement 1, S19–S23. https://doi.org/10.1016/j.compag.2009.07.011.

Huang, S., Yan, H.F., Zhang, C., Wang, G.Q., Acquah, S.J., Yu, J.J., Li, L.L., Ma, J.M., Darko, R.O., 2020. Modeling evapotranspiration for cucumber plants based on the Shuttleworth-Wallace model in a Venlo-type greenhouse. Agricultural Water Management. 228, 105861 https://doi.org/10.1016/j.agwat.2019.105861.

Jolliet, O., Danloy, L., Gay, J.B., Munday, G.L., Reist, A., 1991. HORTICERN: an improved static model for predicting the energy consumption of a greenhouse. Agricultural and Forest Meteorology. 55 (3–4), 265–294. https://doi.org/10.1016/0168-1923(91)90066-Y.

Jung, D.H., Kim, H.S., Jhin, C., Kim, H.-J., Park, S.H., 2020. Time-serial analysis of deep neural network models for prediction of climatic conditions inside a greenhouse. Computers and Electronics in Agriculture. 173, 105402 https://doi.org/10.1016/j.compag.2020.105402.

Kichah, A., Bournet, P.-E., Migeon, C., Boulard, T., 2012. Measurement and CFD simulation of microclimate characteristics and transpiration of an Impatiens pot plant crop in a greenhouse. Biosystems Engineering. 112, 22–34. https://doi.org/10.1016/j.biosystemseng.2012.01.012.

Kustas, W., Rango, A., Uijlenhoet, R., 1994. A simple energy budget algorithm for the snowmelt runoff model. Water Resources Res. 30, 1515–1527. https://doi.org/10.1029/94WR00152.

Li, K.J., Sha, Z.D., Xue, W.P., Chen, X., Mao, H.P., Tan, G., 2020. A fast modeling and optimization scheme for greenhouse environmental system using proper orthogonal decomposition and multi-objective genetic algorithm. Computers and Electronics in Agriculture. 168, 105096 https://doi.org/10.1016/j.compag.2019.105096.

Li, T.H., Chang, J.M., Wei, M., Shi, G.Y., Zhang, Y.S., Chen, D.J., 2018. Application situation and problem analysis of ventilation facilities in solar greenhouse in Shandong province. Agricultural Engineering and Technology. 38 (16), 22-26. (In Chinese) https://doi.org/10.16815/j.cnki.11-5436/s.2018.16.003.

Liu C.X., Ma C.W., Wang P.Z., Zhao S.M., Cheng J.Y., Wang M.L., 2015. Analysis on affecting factors of heat preservation properties for thermal insulation covers. Transactions of the CSAE. 31 (20), 186-193. (In Chinese) https://doi.org/10.11975/j.issn.1002-6819.2015.20.026.

Liu, H.J., Yin, C.Y., Gao, Z.Z., Hou, L.Z., 2021. Evaluation of the cucumber yield, economic benefit, and water productivity under different soil matric potentials in solar greenhouses in North China. Agricultural Water Management. 243, 106442 https://doi.org/10.1016/j.agwat.2020.106442.

Liu X.Y., Zhang W., 2011. Establishment and analysis of forecasting model of temperature and humidity in PC board greenhouse. Agriculture Network Information. 7, 31-33. (In Chinese) https://kns.cnki.net/kcms/detail/detail.aspx?FileName=JSJN201107010&DbName=CJFQ2011.

Ma C., Wang Lin., Ding X., Hou C., Han J., 2008. Theories and methods for calculation of ventilation rate in design rule for greenhouse ventilation. Journal of Shanghai Jiaotong university (Agricultural Science). 26 (5), 416-423. (In Chinese) http://en.cnki.com.cn/Article_en/CJFDTotal-SHNX200805019.htm.

McClellan, T.M., Pedersen, C.O., 1997. Investigation of outside heat balance models for use in a heat balance cooling load calculation procedure. ASHRAE Transactions. 103 (2), 469–484.

Medrano, E., Lorenzo, P., Sánchez-Guerrero, M.C., Montero, J.I., 2005. Evaluation and modelling of greenhouse cucumber-crop transpiration under high and low radiation conditions. Scientia Horticulturae 105 (2), 163–175. https://doi.org/10.1016/j.scienta.2005.01.024.

Mirsadeghi, M., Cóstola, D., Blocken, B., Hensen, J.L.M., 2013. Review of external convective heat transfer coefficient models in building energy simulation programs: Implementation and uncertainty. Applied Thermal Engineering. 56 (1–2), 134–151. https://doi.org/10.1016/j.applthermaleng.2013.03.003.

Modest, M.F., 1993. Radiative Heat Transfer. McGraw-Hill, New York https://www.sciencedirect.com/book/9780123869449/radiative-heat-transfer.

Mohammadi, B., Ranjbar, S.F., Ajabshirchi, Y., 2018. Application of a dynamic model to predict some inside environment variables in a semi-solar greenhouse. Information Processing in Agriculture. 5 (2), 279–288. https://doi.org/10.1016/j.inpa.2018.01.001.

NY/T 1451-2018, 2018. Code for ventilation design of greenhouse. Ministry of Agriculture of the PRC. P:7-8. (In Chinese).

Papadakis, G., Frangoudakis, A., Kyritsis, S., 1992. Mixed, forced, and free convection heat transfer at the greenhouse cover. Journal of Agricultural Engineering Research. 51, 191–205. https://doi.org/10.1016/0021-8634(92)80037-S.

Righini, I., Vanthoor, B., Verheul, M.J., Naseer, M., Maessen, H., Persson, T., Stanghellini, C., 2020. A greenhouse climate-yield model focussing on additional light, heat harvesting and its validation. Biosystems Engineering. 194, 1–15. https://doi.org/10.1016/j.biosystemseng.2020.03.009.

Rodriguez, F., Berenguel, M., Guzman, J.L., Ramirez-Arias, A., 2015. Modeling and control of greenhouse crop growth. Advances in Industrial Control. https://doi.org/10.1007/978-3-319-11134-6.

Roy, J.C., Boulard, T., Kittas, C., Wang, S., 2002. PA—Precision Agriculture: Convective and Ventilation Transfers in Greenhouses, Part 1: The Greenhouse considered as a Perfectly Stirred Tank. Biosystems Engineering. 83 (1), 1–20. https://doi.org/10.1006/bioe.2002.0107.

Sánchez-Molina, J., Li, M., Rodriguez, F., Guzmán, J., Wang, H., Yang, X., 2017. Development and test verification of an air temperature model for Chinese solar and Spanish Almeria-type greenhouse. International Journal of Agricultural and Biological Engineering. 10, 66–76. https://doi.org/10.25165/j.ijabe.20171004.2398.

Singh, G., Singh, P.P., Singh Lubana, P.P., Singh, K.G., 2006. Formulation and validation of a mathematical model of the microclimate of a greenhouse. Renewable Energy. 31 (10), 1541–1560. https://doi.org/10.1016/j.renene.2005.07.011.

Snyder, R.L., Shaw, R.H., 1984. Converting humidity expressions with computers and calculators. University of California, Division of Agriculture and Natural Resources.

Soriano, T., Montero, J.I., Sánchez-Guerrero, M.C., Medrano, E., Antón, A., Hernández, J., Morales, M.I., Castilla, N., 2004. A Study of Direct Solar Radiation Transmission in Asymmetrical Multi-span Greenhouses using Scale Models and Simulation Models. Biosystems Engineering. 88 (2), 243–253. https://doi.org/10.1016/j.biosystemseng.2004.03.006.

Sparrow, E.M., Ramsey, J.W., Mass, E.A., 1979. Effect of Finite Width on Heat Transfer and Fluid Flow about an Inclined Rectangular Plate. Journal of Heat Transfer. 101, 199–204. https://doi.org/10.1115/1.3450946.

Tong, G.H, Che, Z.S., Bai, Y.K., Yamaguchi, T., 2008. Air exchange rate calculation for solar greenhouse using thermal balance method. Journal of Shenyang Agricultural University. 39 (4), 459-462. (In Chinese) https://doi.org/10.3969/j.issn.1000-1700.2008.04.017.

Tong, G.H., Christopher, D.M., Li, B., 2009. Numerical modelling of temperature variations in a Chinese solar greenhouse. Computers and Electronics in Agriculture. 68 (1), 129–139. https://doi.org/10.1016/j.compag.2009.05.004.

Tong G.H., Li B.M., Christopher D.M., Yamaguchi T., 2007. Preliminary study on temperature pattern in a Chinese solar greenhouse using computational fluid dynamic. Transactions of the CSAE. 23 (7), 178-185. (In Chinese) https://doi.org/10.3321/j.issn:1002-6819.2007.07.035.

Villarreal-Guerrero, F., Kacira, M., Fitz-Rodríguez, E., Kubota, C., Giacomelli, G.A., Linker, R., Arbel, A., 2012. Comparison of three evapotranspiration models for a greenhouse cooling strategy with natural ventilation and variable high-pressure fogging. Scientia Horticulturae. 134, 210–221. https://doi.org/10.1016/j.scienta.2011.10.016.

Walton, G.N., 1981. Passive Solar Extension of the Building Loads Analysis and System Thermodynamics (BLAST) Program. United States Army Construction Engineering Research Laboratory, Champaign, IL.

Walton, G.N., 1983. Thermal Analysis Research Program Reference Manual, NBSSIR 83–2655. National Bureau of Standards.

Wen, D., Wang, X., Sun, K.N., Wang, K.A., Yang, N., 2019. Development situation and prospects of mechanization for greenhouse vegetables in Shandong province. Agricultural Equipment & Vehicle Engineering. 57 (S1), 52-54. (In Chinese) https://doi.org/10.3969/j.issn.1673-3142.2019.S1.012.

Zhang, G.S., Ding, X.M., Li, T.H., Pu, W.Y., Lou, W., Hou, J.L., 2020a. Dynamic energy balance model of a glass greenhouse: An experimental validation and solar energy analysis. Energy. 198, 117281 https://doi.org/10.1016/j.energy.2020.117281.

Zhang, G.X., Fu, Z.T., Yang, M.S., Liu, X.X., Dong, Y.H., Li, X.X., 2019a. Nonlinear simulation for coupling modeling of air humidity and vent opening in Chinese solar greenhouse based on CFD. Computers and Electronics in Agriculture. 162, 337–347. https://doi.org/10.1016/j.compag.2019.04.024.

Zhang, X.D., Lv, J., Dawuda, M.M., Xie, J.M., Yu, J.H., Gan, Y.T., Zhang, J., Tang, Z.Q., Li, J., 2019b. Innovative passive heat-storage walls improve thermal performance and energy efficiency in Chinese solar greenhouses for non-arable lands. Solar Energy. 190, 561–575. https://doi.org/10.1016/j.solener.2019.08.056.

Zhang, Y., Henke, M., Li, Y.M., Yue, X., Xu, D.M., Liu, X.G., Li, T.L., 2020b. High resolution 3D simulation of light climate and thermal performance of a solar greenhouse model under tomato canopy structure. Renew. Energy 160, 730–745. https://doi.org/10.1016/j.renene.2020.06.144.

Zhao, C.J., Li, M., Yang, X.T., Sun, C.H., Qian, J.P., Ji, Z.T., 2011. A data-driven model simulating primary infection probabilities of cucumber downy mildew for use in early warning systems in solar greenhouses. Computers and Electronics in Agriculture. 76 (2), 306–315. https://doi.org/10.1016/j.compag.2011.02.009.

Zou, W.D., Yao, F.X., Zhang, B.H., He, C.X., Guan, Z.X., 2017. Verification and predicting temperature and humidity in a solar greenhouse based on convex bidirectional extreme learning machine algorithm. Neurocomputing. 249, 72–85. https://doi.org/10.1016/j.neucom.2017.03.023.

2.1.2 A 3-D simulation of leaf condensation on cucumber canopy in a solar greenhouse

Research in this field is supported by the following journal publication:

Title	A 3-D simulation of leaf condensation on cucumber canopy in a solar greenhouse
Authors	**R. Liu**, J. Liu, H. Liu, X. Yang, J.F. Bienvenido Bárcena, M. Li
Journal	Biosystems Engineering
Year	2021
Volume	210
Pages	310-329
DOI	https://doi.org/10.1016/j.biosystemseng.2021.08.008.
IF(JCR2022)	5.002
Categories	Agronomy and Crop Science (23/370) Q1 Control and Systems Engineering (32/270) Q1

Contribution of the Ph.D. Candidate

The Ph.D. candidate R. Liu is the main contributor and first author of this paper.

Available online at www.sciencedirect.com

ScienceDirect

journal homepage: www.elsevier.com/locate/issn/15375110

Research Paper

A 3-D simulation of leaf condensation on cucumber canopy in a solar greenhouse

Ran Liu [a,b,c], Jian Liu [a,c], Huiying Liu [c,**], Xinting Yang [a,c], José Fernando Bienvenido Bárcena [b], Ming Li [a,b,c,*]

[a] Information Technology Research Center, Beijing Academy of Agriculture and Forestry Sciences/ National Engineering Research Center for Information Technology in Agriculture/ National Engineering Laboratory for Agri-product Quality Traceability/ Meteorological Service Center for Urban Agriculture, China Meteorological Administration- Ministry of Agriculture and Rural Affairs/ Key Laboratory of Agri-informatics, Ministry of Agriculture, Beijing, China

[b] Department of Informatics, CeiA3, CIESOL, Ctra. Sacramento s/n, University of Almería, Almería, Spain

[c] College of Agriculture, Shihezi University/Key Laboratory of Special Fruits and Vegetables Cultivation Physiology and Germplasm Resources Utilization of Xinjiang Production and Construction Corps, Shihezi, Xinjiang, China

ARTICLE INFO

Article history:
Received 8 August 2020
Received in revised form
25 June 2021
Accepted 17 August 2021
Published online 15 September 2021

Keywords:
Computational fluid dynamics
Greenhouse
Cucumber
Canopy
Condensation

Leaf wetness duration (LWD) provides the necessary conditions for pathogen infection. Among them, dew condensation on the crop canopy due to high humidity in a greenhouse is a major cause of LWD formation. However, it would be costly to monitor the condensation of all the leaves in a greenhouse. A computational fluid dynamics model was studied for the spatial and temporal distribution of the indoor microclimate and leaf condensation in a single-slope Chinese solar greenhouse at night. Models were embedded to simplify the input parameters and enhance the practicality. Without compromising the performance of the model, the model inputs were reduced to five: outdoor solar radiation intensity, outdoor air temperature, outdoor relative humidity, outdoor average wind speed per hour, and soil temperature. The distributions of roof condensation and leaf condensation were simulated. Condensation always appeared first on the roof rather than on the leaves. The leaf condensation results were manually observed for comparison with the simulated results. Leaf condensation always occurred first in the area near the semi-transparent roof, both in the observations and the simulation. The LWD was simulated by considering the duration of the simulated leaf condensation at each point. The evaluation was conducted on 216 pairs of samples. The True Negative Rate (TNR), True Positive Rate (TPR), and Accuracy (ACC) were 1, 0.66, and 0.89, respectively. This paper can serve as a reference for an early warning model of disease based on the temporal and spatial distribution of leaf condensation.

* Corresponding author.
** Corresponding author.
E-mail addresses: hyliuok@aliyun.com (H. Liu), lim@nercita.org.cn, 349505082@qq.com (M. Li).
https://doi.org/10.1016/j.biosystemseng.2021.08.008

Nomenclature

A_j	area of canopy perpendicular to the incident radiation in the j-direction (m^2)
C_c	empirical constant of condensation (0.1 s^{-1})
C_d	drag coefficient (0.32)
C_P	specific heat capacity of air (J kg^{-1} K^{-1})
C_v	convection heat transfer coefficient (W m^{-2} K^{-1})
C_w	mass concentration of water vapour component (kg kg^{-1})
D_l	water vapour leakage rate (kg m^{-3} s^{-1})
D_w	diffusion coefficient of water vapour component (m^2 s^{-1})
e	net radiation exchange coefficient
e_{sky}	emissivity of the sky
G	total solar radiation intensity (W m^{-2})
G_o	solar radiation intensity on the horizontal plane outside the atmosphere (W m^{-2})
G_{sc}	solar constant (1353 W m^{-2})
gh	water vapour conductivity in leaf boundary layer (m s^{-1})
g_i	gravity acceleration component in the i-direction (m s^{-2})
H	crop height (m)
H_{loc}	local apparent solar time (h)
I_λ	radiation intensity at λ band (W m^{-3})
i, j, k	fixed directions in cartesian coordinate system
K_d	ratio of diffuse solar radiation intensity
K_t	clearness index
k	turbulent energy (m^2 s^{-2})
L	characteristic length of greenhouse (m)
LAD	leaf area density (m^{-1})
LAI	leaf area index
L_j	canopy length in the j-direction (m)
l	characteristic length of leaf (m)
m_a	condensation rate of water vapour in air (kg m^{-3} s^{-1})
m_c	condensation rate on crop canopy (kg m^{-3} s^{-1})
N_{Le}	Lewis number
n	day ordinal of a year
n_t	air exchange time (time h^{-1})
P	air pressure (pa)
P_j	optical path in the j-direction, m
$P_{vsat}(T_c)$	saturated water vapour pressure at crop canopy temperature (Pa)
P_{wi}	indoor water vapour pressure (Pa)
P_{wo}	outdoor water vapour pressure (Pa)
Q_l	heat leakage rate (W m^{-3})
R_n	net radiation per unit volume crop canopy (W m^{-3})
R_{so}	total solar radiation absorbed by the crop canopy zone (W m^{-3})
R_x	long wave net radiation from surface x (W m^{-3})
RH_i	indoor relative humidity (%)
RH_o	outdoor relative humidity (%)
$\hat{r}$	position vector
r_a	aerodynamic resistance (s m^{-1})
r_s	stomatal resistance (s m^{-1})
S_e	air leakage rate (kg m^{-3} s^{-1})
S_k	source term of k (kg m^{-1} s^{-3})
S_m	momentum source term (kg m^{-2} s^{-2})
S_r	radiation source term (W m^{-3})
$S_{r,\,c}$	effective radiate area from roof to crop canopy (m^2)
S_s	sensible heat exchange (W m^{-3})
S_t	energy source term (W m^{-3})
S_w	water vapour source term (kg m^{-3} s^{-1})
S_x	area of surface x (m^2)
$S_{x,\,c}$	effective radiation area from surface x to crop canopy (m^2)
S_ε	source term of ε (kg m^{-1} s^{-3})
S_ϕ	source term of ϕ
$\hat{s}$	direction vector
T	indoor air temperature (K)
T_b	temperature in leaf boundary layer (K)
T_c	crop canopy temperature (K)
T_{dew}	dew point temperature (K)
T_s	soil temperature (K)
T_o	outdoor air temperature (K)
T_x	average temperature of surface x (K)
t	flow time (s)
U	absolute air speed (m s^{-1})
UDFs	user-defined functions
u	velocity component (m s^{-1})
v	kinematic viscosity of air (m^2 s^{-1})
ws	wind speed (m s^{-1})
$X_{x,c}$	view factor from surface x to crop canopy
α_a	air thermal diffusivity (m^2 s^{-1})
γ	psychrometric constant (67.17 Pa K^{-1})
δ	declination angle (°)
ε	turbulent dissipation rate (m^2 s^{-3})
λ	wavelength (m)
ρ	air density (kg m^{-3})
σ	Stefan–Boltzmann constant (5.67×10^{-8} W m^{-2} K^{-4})
τ	short wave transmissivity of semi-transparent roof
ϕ	latitude (°)
Ω	solid angle
ω	hour angle (°)
ϕ	Variable in conservation equations
ϖ	heat of vaporisation (J kg^{-1})

1. Introduction

The simulation of the climate in a greenhouse is a necessary part of many models, including those for crop yield prediction, irrigation guidance, and disease management (Golzar, Heeren, Hellweg, & Roshandel, 2018; Bianchi, Masseroni, & Facchi, 2017; Fall, Van der Heyden, Beaulieu, & Carisse, 2015). Taking a greenhouse disease management model as an example, the leaf wetness duration (LWD) plays an important role in the disease warning system for crops (Zhao et al., 2011). However,

existing models use the environmental and LWD data of a single location in the greenhouse as the input to represent the conditions of the entire greenhouse (Frans et al., 2018; Wang, Sánchez-Molina, Li, & Rodriguez, 2019). On the one hand, there are remarkable non-uniformities in leaf microclimate within the canopy in a greenhouse, with implications for variable heat and mass exchange, and the heterogeneity distribution of greenhouse climate (Kimura, Yasutake, Yamanami, & Kitano, 2020). On the other hand, it may be costly to install many sensors in the greenhouse. A practical solution is to develop an LWD distribution model based on the greenhouse climate and computational fluid dynamics (CFD).

The continuous flow of air inside a greenhouse, despite the low speed, leads to the exchange of energy and mass. CFD is a method that can develop a model of the flow field. In recent years, CFD numerical methods have been widely used in greenhouse environment simulations (Tong, Christopher, & Zhang, 2017), most of which modelled ventilation and air temperature. Tong, Christopher, and Li (2009) developed a numerical model of temperature, which included the influence of roof condensation on the energy budget in a Chinese solar greenhouse. However, it was difficult to simulate the LWD, which plays an important role in disease prediction (Bassimba, Intrigliolo, Marta, Orlandini, & Vicent, 2017). Except for a few rainy days, leaf wetness always appeared at night and lasted until the early morning. This is a result of the leaf surface condensation process, which occurs when the canopy temperature falls below the dewpoint temperature of air (Mashonjowa, Ronsse, Mubvuma, Milford, & Pieters, 2013). Modelling canopy temperature and its surrounding microclimate is key to simulating canopy condensation (Tomaszkiewicz, Abou Najm, Zurayk, & El-Fadel, 2017). It is also essential to consider the interaction between crops and the environment.

Boulard and Wang (2002) modelled the effects of transpiration on the microclimate inside plastic tunnels used to grow lettuce. Subsequently, similar experiments were carried out in greenhouses with tomatoes, impatiens, roses, and begonia (Boulard, Roy, Fatnassi, Kichah, & Lee, 2010; Kichah, Bournet, Migeon, & Boulard, 2012; Chen et al., 2015; Boulard, Roy, Pouillard, Fatnassi, & Grisey, 2017). From these, simulations of the condensation process according to the local microclimate have been conducted by a few scholars. Bouhoun Ali, Bournet, Danjou, Morille, and Migeon (2014) developed a two-dimensional (2-D) transient model to assess condensation on roofs in a Venlo glasshouse. Piscia, Montero, Baeza, and Bailey (2012) studied the three dimensional (3-D) transient modelling of night-time condensation on a four-span greenhouse plastic cover, but the crop–environment interaction was neglected. The boundary conditions can limit the applicability of a model. For example, in previous studies, walls with fixed heat flux or fixed temperature were always adopted as the boundary conditions to simulate the greenhouse climate (Li et al., 2020; Zhang et al., 2019), which limits the simulation of the future climate. In contrast, a coupled wall was adopted in this study (Ansys-Fluent, 2010). Future conditions can be simulated based on weather forecasts. The parameters can be simplified using additional equations. The calculated results of the previous time step can be used as the input parameters of the next time step. There are few studies that combine crop and climate interactions with a canopy condensation model in CFD simulation. Few have also attempted to simplify the input parameters without compromising the accuracy of the model.

The goal of the modelling reported in this paper is to establish the precise temporal and spatial distributions of condensation around a cucumber canopy in a greenhouse at night to provide a decision-making basis for disease control.

2. Materials and methods

2.1. Experimental greenhouse and data collection

The experiment was conducted at the Xiaotangshan National Precision Agriculture Demonstration Base (40°18′ N, 116°47’ E, annual average temperature 11.8 °C, altitude 39 m, local pressure 101 kPa) in Changping District, Beijing. The greenhouse is a typical single-slope solar structure with semi-transparent polyethylene (PE) film on the south roof, an asbestos-cement board on the north roof (Fig. 1), and bricks and concrete walls on the north, east, and west sides.

The greenhouse is 50 m long, 7 m wide, and 3.6 m high. The cucumber cultivar ‘Jingyan Mini 2′ was used as the experimental material and was cultivated in an average of 36 rows. Drip irrigation under a plastic film was used. In this experiment, the model was developed under the condition that the vents were closed and without any heating devices.

The weather station Davis Vantage Pro 2 Plus (Davis Instruments, Hayward, USA) was located in an open space 5 m away from the south boundary of the greenhouse to measure the total solar radiation (range: 0–1800 W m^{-2}; accuracy: ±5%), wind speed (cup anemometer, range: 0–67 m s^{-1}; accuracy: ±5%), air temperature (range: −40 to +65 °C; accuracy: ±0.5 °C), and relative humidity (RH; range: 0–100%; accuracy: ±3%). The sensors were 2.5 m away from the ground (Fig. 2). The indoor weather station Davis-6162 (Davis Instruments, Hayward, USA) was placed at a height of 1 m at the centre of the greenhouse to measure air temperature, RH, and soil temperature at a depth of 0.5 m below the ground (range: −40 to +65 °C; accuracy: ±0.5 °C). The infrared thermometer SI-111 (Apogee Instrument Crop, USA) was placed at a height of 1 m at the centre of the greenhouse to measure the canopy temperature (range: −60 to +110 °C; accuracy: ±0.2 °C). The above data were measured and recorded every 15 min. At the same time, nine temperature-RH sensors distributed on the horizontal plane of the greenhouse at height of 1 m measured and recorded hourly data (range: −40 to +123.8 °C; accuracy: ±0.3 °C; range: 0–100%; accuracy: ±18%) to use as the test data (Fig. 1). All these sensors were manufactured by the China National Engineering Research Centre for Information Technology in Agriculture (NERCITA).

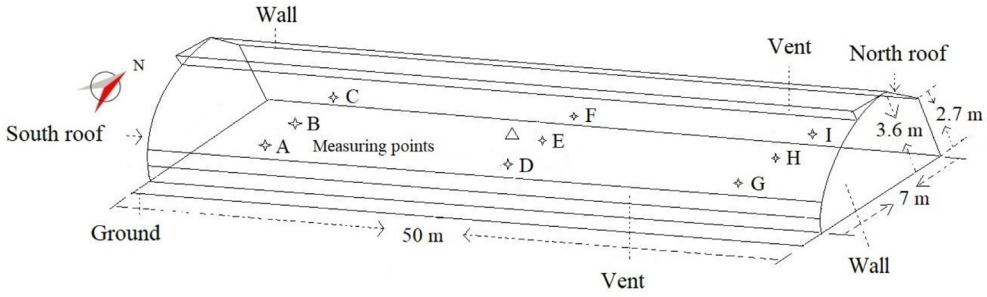

Fig. 1 – Drawing of the experimental greenhouse. A–I represent the T-RH measurement point positions on the horizontal plane at 1 m height. Three sensors were distributed in each row, which were 1 m, 3 m, and 5 m away from south boundary of the greenhouse, and 10 m, 25 m, and 40 m away from east boundary of the greenhouse, respectively. △ represents the Davis-6162 weather station and infrared thermometer.

Fig. 2 – Photos of sensors: ① is the SI-111 infrared thermometer; ② is the temperature-relative humidity sensors made by NERCITA; ③ is the Davis Vantage Pro & Plus outdoor weather station; and ④ is the Davis-6162 indoor weather station.

2.2. *Model structure*

Instead of inputting the initial conditions, the result file was generated by conducting a steady-state simulation of the internal wall temperature distribution as well as the surface temperature on both sides of the walls and roof. The transient simulation was conducted after loading the initial conditions file. All sub-models were integrated into the greenhouse system to formulate a crop canopy condensation model according to the energy balance, mass balance, and momentum balance (Fig. 3). The model system takes real-time data on temperature, RH, wind speed, solar position, and radiation intensity collected by outdoor sensors as input. Each time step for solving the model was 5 min with 20 iterations. The global model was solved by pressure–velocity coupling SIMPLEC method. In each iteration, the following are solved simultaneously: transpiration model reflecting crop–microclimate interaction (executed in the crop domain in the daytime); sensible heat exchange model; leaf net radiation model; leaf condensation model (executed in the crop domain); air leakage model; air condensation model (executed in the global domain).

2.3. *Simulation domain*

In this study, ANSYS ICEM 13.0 software was used to generate geometric and unstructured grids at a scale of 1:1 to the actual size of the greenhouse. A 3-D model was adopted. The simulation domain was limited to the interior of the greenhouse. Determining the reasonable range of simulation domains has been a concern of many authors. The key is to strike a balance between the computational load and the accuracy of the simulation. Considering that the vents were closed during the simulation, the influence of wind direction on the flow field inside the greenhouse was ignored. The external wind speed was input into the convective heat transfer model to calculate the energy exchange between both sides of the wall (Roy, Boulard, Kittas, & Wang, 2002). The imposed external climatic conditions, including the solar radiation intensity, sky temperature, and air temperature outside the enclosure — all

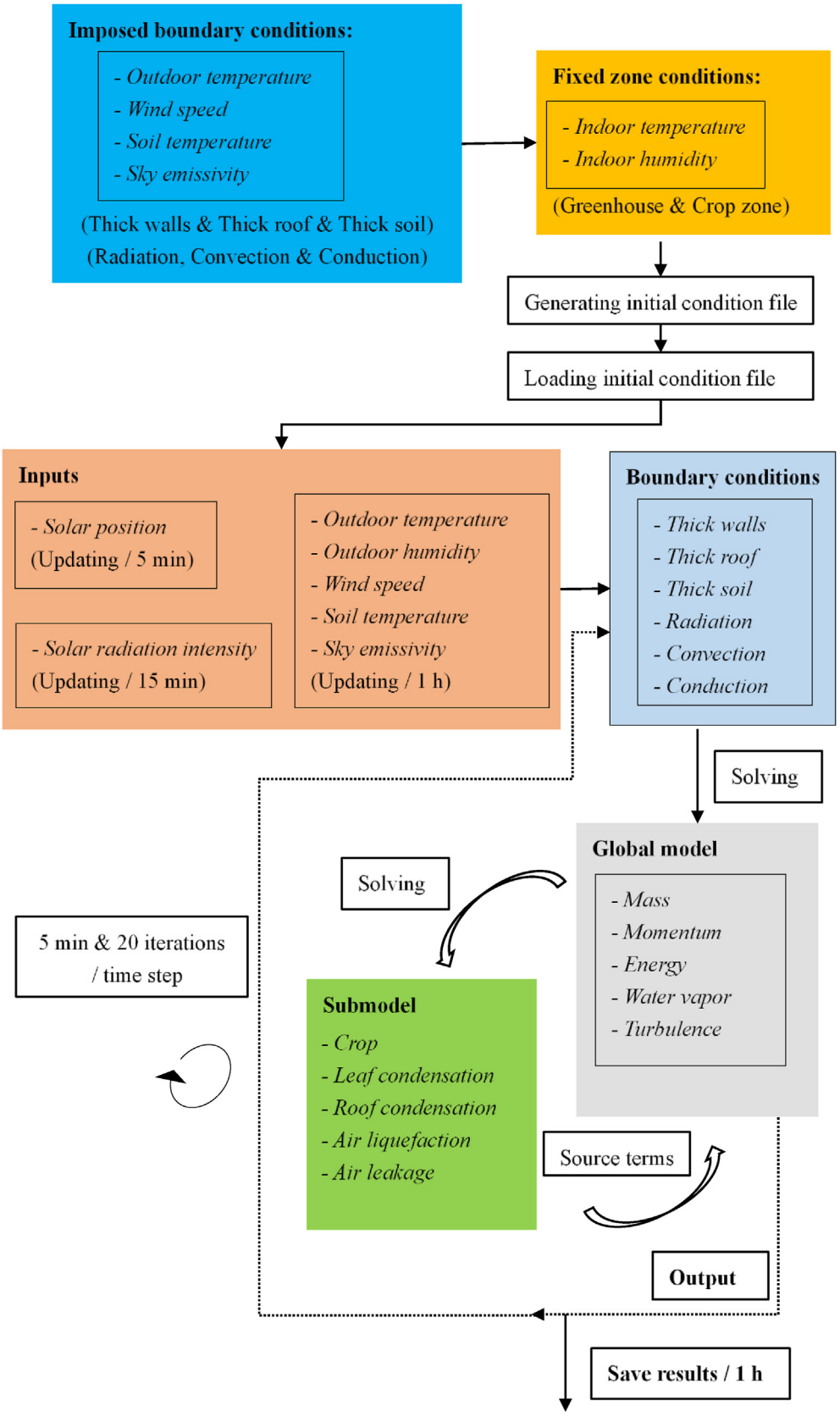

Fig. 3 – Flowchart of the simulation.

of which affect the convection, radiation, and conduction heat transfer into and out of the greenhouse — were defined as energy boundary conditions similar to that in Tong et al. (2009), and have been verified.

The zone near the south roof of the solar greenhouse facilitates the formation of condensation at night, which is accompanied by a reduction in water vapour and heat release. Considering that the grids must be densified in this zone, a large number of volume elements had to be adopted in the entire domain to balance the grid quality. The crop zone was simplified to 36 cuboids that were 5 m long, 0.8 m wide, and 1.5 m high (Fig. 4). Grids were densified near the crop zone. Instead of generating ground grids, one-dimensional heat conduction equations (along the thickness direction) were executed by defining the ground thickness and setting the soil temperature at a depth of 0.5 m to simulate the ground heat transfer. Several grid densities were tested according to file size until the residuals of the continuum equation, momentum equation, water vapour species equation, and k and ε equation was less than 10^{-3}, and the residual of the energy term was less than 10^{-6} by steady-state computation. The final number of elements was 257580 in the crop domain and 928476 in the rest of the fluid domain. Walls with actual thickness were added to the grid file, and the total number of elements in the solid domain was 221184.

2.4. Flow analysis

The air speed is extremely low when the vents are closed. The type of flow in this study can be judged using the Rayleigh number formula (Mistriotis, Arcidiacono, Picuno, Bot, & Scarascia-Mugnozza, 1997):

$$Ra = \frac{\beta * g * \Delta T * L^3}{v^2} * Pr \quad (1)$$

where Ra is the Rayleigh number (dimensionless); β is the volume expansion coefficient of air (K^{-1}); g is the local gravitational acceleration (m s^{-2}); ΔT is the temperature difference between the wall and air (K); L is the characteristic length; v is the kinematic viscosity of air (m^2 s^{-1}); and Pr is the Prandtl number (dimensionless, 0.85). The calculated value of R_a is approximately 5.2×10^8, which is greater than 2×10^7 (Mills, 1992). The flow in this study is considered to be a transient turbulent flow.

Three components were involved in the studied flow: air, water vapour, and dew, including gas and liquid phases. However, in general, dew on leaves is stagnant. To simplify the calculation, the flow was considered as the transport of water vapour by airflow. The condensation process on the crop canopy, roof, and air was quantified as the energy increment and mass reduction of water vapour caused by condensation. The positions and times of condensation on the crop canopy were marked by user-defined functions (UDFs).

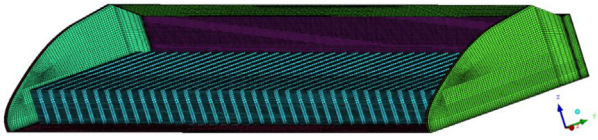

Fig. 4 – Grid model of the numerical domain considering only the interior of the greenhouse.

3. Equations and boundary condition

3.1. Governing equations

The governing equations of the 3-D transient flow field and crop porous zone in the greenhouse were established using an ideal gas model linking the density to the temperature, and by considering buoyancy effect of coupled energy and vertical momentum component equations (Ansys-Fluent, 2010):

$$\frac{\partial(\phi)}{\partial t} + \mathrm{div}(\vec{u}\phi) = \mathrm{div}(\Gamma\ \mathrm{grad}\phi) + S_\phi \quad (2)$$

where t is the flow time (s) and u is the velocity (m s^{-1}). The variables Φ and S_Φ, and the corresponding adopted conservation equations are shown in Table 1.

3.2. Radiative boundary conditions

A solar ray tracing model coupled with a Discrete Ordinates (DO) radiation model was used as the heat radiation source term (Ansys-Fluent, 2010). The position vector of the sun was updated every 5 min, and the intensity of direct and diffuse solar radiation was input every 15 min. The DO radiation model can simulate long-wave exchange between the internal walls of the greenhouse and the 0–120 um radiation band coming through the semi-transparent roof. The sky emissivity, which is a variable dependent on weather conditions (Eq. (8)), was updated every hour. The following fraction model was adopted to estimate the direct and diffuse solar radiation intensity from the data obtained by sensors (Erbs, Klein, & Duffie, 1982).

$$K_d = 1 - 0.09K_t \ (K_t \le 0.22)$$

$$K_d = 0.9511 - 0.1601K_t + 4.388K_t^2 - 16.638K_t^3 + 12.336K_t^4 \ (0.22 < K_t \le 0.8) \quad (5)$$

Table 1 – Φ and S_Φ and the corresponding conservation equations. ρ is the air density (kg m^{-3}); u is the velocity (m s^{-1}); g_i is the gravity acceleration component in the i-direction (m s^{-2}); C_P is the specific heat capacity of air (J kg^{-1} K^{-1}); T is the air temperature (K); C_w is the mass concentration of the water vapour component (kg kg^{-1}); k is the turbulent energy (m^2 s^{-2}); ε is the turbulent dissipation rate (m^2 s^{-3}); and S_m, S_r, S_t, S_w, S_k, and S_ε are the source terms of momentum, radiation, energy, water vapour, k, and ε, respectively, which are calculated by UDFs.

Conservation equation	Φ	S_Φ
Mass	ρ	0
Momentum	$\rho * \vec{u}$	$S_m + \rho * g_i$
Energy	$\rho * C_P * T$	$S_r + S_t$
Water vapour	C_w	S_w
k	ρ*k	S_k
ε	ρ*ε	S_ε

$K_d = 0.165K_t$ ($K_t > 0.8$)

where K_d is the ratio of the diffuse solar radiation intensity and the total solar radiation ivntensity in the horizontal plane, and K_t is the clearness index.

$$\begin{cases} K_t = \dfrac{G}{G_o} \\ G_o = G_{sc}*\left(1+0.033*\cos\left(\dfrac{360°*n}{365}\right)\right)\times(\sin\phi*\sin\delta+\cos\phi*\cos\delta*\cos\omega) \\ \delta = 23.45*sin\left(360°*\dfrac{284+n}{365}\right) \\ \omega = 15(H_{loc}-12) \end{cases} \quad (6)$$

where G is the total solar radiation intensity (W m^{-2}); G_o is the solar radiation intensity on the horizontal plane outside the atmosphere (W m^{-2}); G_{sc} is the solar constant, 1353 W m^{-2}; n is the day ordinal of a year; ϕ is latitude; δ is the declination angle; ω is the hour angle; and H_{loc} is the local apparent solar time. The boundary conditions of direct and diffuse solar radiation are listed in Table 2. All the measured solar radiations were 0 from 18:30 to 5:30 the next morning.

The DO radiation energy source term (W m^{-3}) of the energy conservation equation can be expressed as follows (Ansys-Fluent, 2010; Boulard et al., 2017):

$$S_r = -\mathrm{div}\left[\int_0^{\infty}\left(\int_0^{4\pi} I_\lambda*(\hat{r},\hat{s})*\hat{s}\,d\Omega\right)d\lambda\right] \quad (7)$$

where λ is the wavelength (m); I_λ is the radiation intensity at λ band (W m^{-3}); $\hat{r}$ is the position vector; $\hat{s}$ is the direction vector; and Ω is the solid angle. The thickness of the semi-transparent roof is 0.15 mm. The transmissivity of radiation was treated separately according to the band, i.e. 0.38–2.4 μm solar radiation band and 2.4–120 μm ground long-wave radiation band. The optical properties of the south roof are listed in Table 3.

The emissivity of each radiating medium follows Stefan–Boltzmann' s law. The emissivity of the walls is shown in Table 4. Absorption on the wall surface assumes that the absorptivity is equal to the emissivity.

The emissivity of the sky is related to the outdoor air temperature (T_o, K) and the pressure of the outdoor water vapour (P_{wo}, Pa). In this experiment, the sky emissivity was calculated using the hourly averaged T_o and P_{wo} (Kustas, Rango, & Uijlenhoet, 1994).

$$e_{sky} = 0.642*(P_{wo}/T_o)^{1/7} \quad (8)$$

Table 2 – Boundary conditions of direct and diffuse solar radiation.

Time		Direct radiation (W m^{-2})	Diffused radiation (W m^{-2})
April 15	17:30	38.7	112.3
	17:45	23.8	90.2
	18:00	0.9	43.1
	18:15	1.1	33.9
	18:30	1.7	20.3
April 16	17:30	9.7	104.3
	17:45	7.1	82.9
	18:00	2.4	55.6
	18:15	2.5	40.4
	18:30	2.4	22.6

3.3. *Thermal boundary conditions*

In most previous studies, the wall thermal boundary condition is defined as a fixed temperature wall, which means that the temperature of each wall in a greenhouse must be measured and input frequently. In this study, the actual thickness and material combination of greenhouse walls were considered (Table 5, Fig. 5).

The north, west, and east walls are composite walls. The material of the south roof is PE film, while the material of the north roof is asbestos cement board with a thickness of 15 cm. The measured indoor, outdoor, and soil temperatures at an initial depth of 0.5 m were taken as the boundary conditions. The measured indoor temperature and humidity were taken as the imposed zone conditions to conduct steady-state calculations. The result file of the steady-state calculation was loaded as the initial conditions of the subsequent transient simulation. Conductive, radiative, and convective boundary conditions were adopted on both sides of the walls and roof. The internal fluid-side heat transfer at the walls was computed using Fourier's law applied to walls in laminar flows and using the law-of-the wall for temperature in turbulent flows (Ansys-Fluent, 2010). The convection heat transfer coefficient of the external wall surface is defined by the following formula (Garzoli & Blackwell, 1987):

$$C_v = 7.2 + 3.84*ws \quad (9)$$

where C_v is the convection heat transfer coefficient of the external wall surface (W m^{-2} K^{-1}); and ws is the wind speed (m s^{-1}).

Both sides of the walls are adjacent to the air domain, while only one side of the soil can be regarded as the convection and radiation boundary conditions. It is necessary to input a fixed soil temperature parameter at a 0.5 m depth every hour in the subsequent transient calculations (Fig. 5).

Table 3 – Optical properties of south roof material.

Wavelength band (μm)	Absorptivity	Transmissivity	Reflectivity
0.38–2.4	0.2	0.76	0.04
2.40–120	0.4	0.56	0.04

Table 4 – Long wave emissivity of walls.

Material	Wall	North roof	South roof	Ground	Sky
Emissivity	0.9	0.8	0.4	0.9	Eq. 8

Table 5 – Physical properties of materials.

Material	Density (kg m^{-3})	Specific heat (J kg^{-1} K^{-1})	Thermal conductivity (W m^{-1} K^{-1})
Lime	1600	1050	0.814
Brick	1700	1080	0.810
Cement	1800	1050	0.930
Soil	1620	1480	1.300
PE Film	920	2550	0.330
Asbestos Board	500	1160	0.128

3.4. UDFs in the crop zone

In this experiment, it was assumed that the crop zone is a mixture of air and water vapour (Table 1), in which the drag coefficient was used to simulate the effects of crop canopy on momentum and turbulence. The energy equilibrium model (Eq. (13)) was used to simulate the effects of the canopy on energy and water vapour sources.

3.4.1. Effects of crop canopy on the flow (Boulard, Haxaire, Lamrani, Roy, & Jaffrin, 1999; Liu, Chen, Black, & Novak, 1996; Wilson, 1985)

$$S_m = -\rho * C_d * LAD * |\vec{u}| * \vec{u} \quad (10)$$

$$S_k = \rho * C_d * LAD * U^3 - 4 * \rho * C_d * LAD * U * k \quad (11)$$

$$S_\varepsilon = 1.5 * \rho * \frac{\varepsilon}{k} * C_d * LAD * U^3 - 2.4 * \rho * C_d * LAD * U * \varepsilon \quad (12)$$

where C_d is the drag coefficient (0.32); U is the absolute air speed (m s^{-1}); LAD is the leaf area density (m^{-1}), LAI is the leaf area index (2.55), and H is the crop height (m), LAD = LAI/H.

3.4.2. Source terms of energy and water vapour

The temporary steady-state equilibrium between crops and the environment is described as follows:

$$R_n - S_s - S_{tr} = 0 \quad (13)$$

where R_n is the net radiation per unit volume canopy (W m^{-3}); S_s is the sensible heat exchange between the canopy and environment per unit volume (W m^{-3}); and S_{tr} is the latent heat exchange between the canopy and environment per unit volume (i.e. transpiration, which exists only in the daytime, W m^{-3}). R_n is estimated as follows:

$$R_n(i,j,k) = R_{so}(i,j,k) + \sum_{x=1}^{n} R_x(i,j,k) \quad (14)$$

where R_{so} is the total solar radiation absorbed by the crop canopy zone per second (W m^{-3}); R_x is the long-wave net radiation from surface x (north wall, east wall, west wall, ground, south roof, north roof, and sky, respectively, W m^{-3}). i, j, and k are fixed directions in the Cartesian coordinate system. The net radiation exchange coefficient between two grey body surfaces can be described as follows (Liu & Zhang, 2011):

$$e_{x,\,y} = \left(e_x^{-1} + e_y^{-2} - 1\right)^{-1} \quad (15)$$

where $e_{x,\,y}$ is the net radiation exchange coefficient from surface x to surface y. The radiation that reaches a certain depth inside the crop canopy is a variable based on the optical path due to the radiation attenuation coefficient (Fig. 6). The

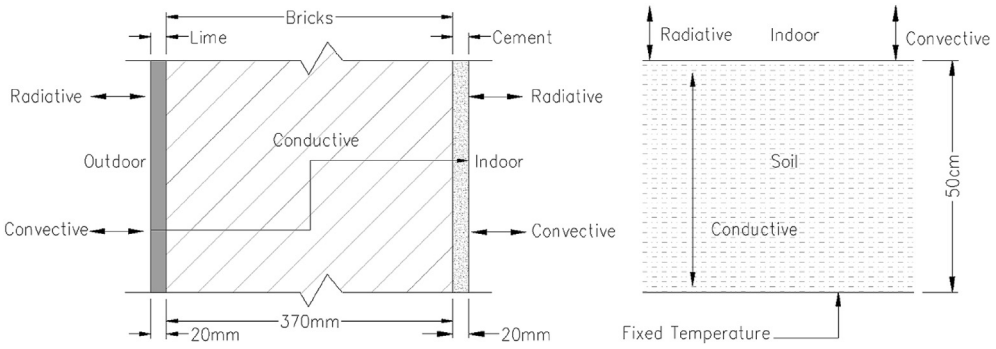

Fig. 5 – Thermal boundary condition of the wall and ground.

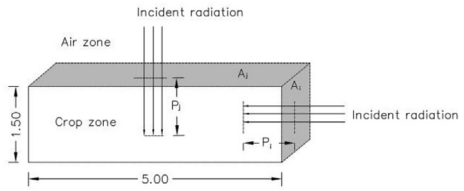

Fig. 6 – Diagram of optical path in the j- and i-direction.

radiation intensity decays as the optical path increases following the Beer–Lambert law. R_{SO} and R_x in a fixed j-direction in Eq. (14) can be described by the following:

$$\begin{cases} R_{so}(j) = \dfrac{G*\tau*S_{r,c}*\exp(-K_c*LAD*P_j)}{P_j*A_j} \\ R_x(j) = \dfrac{e_{x,c}*\sigma(T_x^4 - T_c^4)*S_{x,c}*\exp(-K_c*LAD*P_j)}{P_j*A_j} \end{cases} \quad (16)$$

where τ is the short-wave transmissivity of the semi-transparent roof. $S_{r,c}$ is the effective radiate area from the roof to the crop canopy (m^2). T_x is the average temperature of the surface x (north wall, east wall, west wall, ground, south roof, and north roof calculated at every 30 s step, respectively, K). $e_{x,c}$ is the net radiation exchange coefficient from surface x to the crop canopy. σ is the Stefan–Boltzmann constant (W m^{-2} K^{-4}) and T_c is the crop canopy temperature (K). The net radiation between the sky and canopy was calculated by the hourly averaged sky temperature measured by the weather station. $S_{x,c}$ is the effective radiate area from surface x and the crop canopy (m^2). The effective radiate area was estimated as the product of the area of surface x and the corresponding view factor. The view factors are shown in Appendix A, which were estimated under the assumption of an isothermal homogeneous diffuse-grey surface (Modest, 1993). K_c is the radiation attenuation coefficient (0.75) (Guyot, 1999); P_j is the optical path in the j-direction (m); and A_j is the area of the crop canopy perpendicular to the incident radiation in the j-direction (m^2).

The sensible heat exchange between the crop canopy and environment is defined by the following formula (Boulard et al., 2010):

$$S_s = \frac{2*LAD*\rho*C_p}{r_a}(T_c - T) \quad (17)$$

where r_a is the aerodynamic resistance (s m^{-1}). r_a at low velocity can be defined by the following formula (Stanghellini & Jong, 1995):

$$r_a = \frac{1174*l^{0.5}}{(l|T_c - T| + 207*U^2)^{0.25}} \quad (18)$$

where l is the characteristic leaf length (m). The latent heat exchange between the crop canopy and environment is the heat of water vapour released by the crop canopy during the day through transpiration, which can be described by the following formula:

$$S_{tr} = \frac{LAD*\rho*C_p}{\gamma} * \frac{P_{vsat}(T_c) - P_{wi}}{r_a + r_s} \quad (19)$$

where γ is the psychrometric constant (67.17 Pa K^{-1}); $P_{vsat}(T_c)$ is the saturated water vapour pressure at crop canopy temperature (Pa), P_{wi} is the indoor water vapour pressure (Pa), and r_s is the stomatal resistance of cucumber (s m^{-1}). Solar radiation is the main meteorological factor affecting the stomatal resistance of cucumber. The relationship between the solar radiation and stomatal resistance of cucumber follows an exponential function (Yan et al., 2019).

$$r_s = (104.8 + 497.8*\exp(-0.037*R_{so}(i,j,k))) \quad (20)$$

The condensation rate on the leaf can be calculated using the following formula (Gerlein-Safdi et al., 2018):

$$m_c = 0.622*LAD*\rho*g_h\left(\frac{P_{wi} - P_{vsat}(T_c)}{P}\right) \quad (21)$$

where m_c is the condensation rate on the crop canopy (kg m^{-3} s^{-1}); g_h is the water vapour conductivity in the leaf boundary layer (m s^{-1}); P is the air pressure (pa); and g_h is a variable related to the Lewis number (N_{Le}) and r_a.

$$\begin{cases} g_h = (r_a*N_{Le}^{2/3})^{-1} \\ N_{Le} = \dfrac{\alpha_a}{D_w} \\ \alpha_a = T_b*1.32*10^{-7} - 1.73*10^{-5} \\ D_w = T_b*1.49*10^{-7} - 1.96*10^{-5} \\ T_b = (T + T_c)/2 \end{cases} \quad (22)$$

where N_{Le} is the Lewis number (dimensionless); α_a is the air thermal diffusivity (m^2 s^{-1}); D_w is the diffusion coefficient of the water vapour component (m^2 s^{-1}); and T_b is the temperature in the leaf boundary layer (K).

3.5. *UDFs in the global domain*

Equation (23) shows the air leakage between the indoor and outdoor air. The air leakage rate varies with the management modes and wind speed, which has been studied by many researchers. Using N_2O as the tracer gas, Boulard et al. (2017) found that the air exchange time (n_t, times h^{-1}) ranged from 0.0754 to 0.0897 at a wind speed of 0–0.9 m s^{-1} in a glasshouse. In this study, the n_t was calibrated by tracing the water vapour concentration in the greenhouse using data from March to June 2018. The experimental conditions include no irrigation, a ground covered with plastic film, and data collection at night; therefore, soil evaporation and crop transpiration were ignored. During this period, the wind speed was mainly in the range of 0–2 m s^{-1}. The averaged wind speed was 0.34 m s^{-1}, because it's windless in most of the nights. The n_t was estimated as 0.076 times h^{-1} under the simulated conditions in this experiment.

$$\begin{cases} S_e = \dfrac{n_t*\rho}{3600} \\ Q_l = S_e*C_P*(T - T_o) \\ D_l = S_e*(C_w - d_o) \end{cases} \quad (23)$$

where S_e is the air leakage rate (kg m^{-3} s^{-1}); n_t is the air exchange time (0.0759 times h^{-1}); Q_l is the heat leakage rate (W m^{-3}); T is the indoor air temperature (K); T_o is the outdoor air temperature (K); d_o is the outdoor absolute humidity (kg kg^{-1}); and D_l is the water vapour leakage rate (kg m^{-3} s^{-1}).

For the air near the roof, the temperature is lower and condensation first appears near the roof. Roof condensation was simulated using Eq. (24). It is noted that Eq. (24) was executed in the global domain, but a separate zone that belongs to the boundary layer of the roof was divided when generating the grid file, which will be considered as roof condensation. The phase transition of water vapour in air is quantified by the following formula (Phan, Won, & Park, 2018):

$$m_a = C_c * \rho * C_w * \max\left(1 - \frac{T}{T_{dew}}, 0\right) \quad (24)$$

where m_a is the condensation rate of water vapour in air (kg m^{-3} s^{-1}); C_c is the empirical constant (0.1, s^{-1}); and T_{dew} is the dewpoint temperature (K) (Bu & Wang, 2001).

$$T_{dew} = \frac{238.3 * \ln\left(\frac{P_{wi}}{610.78}\right)}{17.2694 - \ln\left(\frac{P_{wi}}{610.78}\right)} \quad (25)$$

3.6. Summary of energy source term and water vapour source term

The energy source term of air (W m^{-3}) is

$$S_t = S_s + (m_c + m_a) * \varpi - Q_l \quad (26)$$

where ϖ is the heat of vaporisation (J kg^{-1}). The water vapour source term of air (kg m^{-3} s^{-1}) is

$$S_w = \frac{S_{tr}}{\varpi} - m_c - m_a - D_l \quad (27)$$

for the grids except for the crop domain; S_s, S_{tr}, and m_c are 0.

3.7. Initial and hourly boundary conditions

The data collected by outdoor and indoor sensors (Davis Instruments, Hayward, USA) were used as boundary and fixed zone conditions to conduct steady-state simulations to generate initial data files (Table 6). Note: the units of temperature in data collection and evaluation were consistent with the sensors (in °C), and the corresponding thermodynamic temperature (in K) was used in the process of energy budget.

Transient simulations were conducted by loading initial data files and by inputting the following hourly boundary conditions (Tables 7 and 8).

4. Numerical method

ANSYS FLUENT 13.0 software was used as a platform to solve the equations using the finite volume method. UDFs were used to embed energy, momentum, and species source term equations to describe the interaction between the crops and the environment. Indoor and outdoor sensor data were updated hourly as boundary conditions to conduct transient calculations, which started an hour before sunset and ended at sunrise.

Table 7 – Hourly boundary conditions on April 15–16. T_o is the outdoor temperature; RH_o is the outdoor relative humidity; C_w is the mass concentration of the water vapour component; T_s is the soil temperature at 0.5 m depth.

Time	T_o (°C)	RH_o (%)	C_w (g kg^{-1})	T_s (°C)	Wind speed (m s^{-1})
17:30–18:30	24.3	21	3.87	21.7	1.22
18:30–19:30	22.4	23	3.83	21.4	0.22
19:30–20:30	20.6	25.8	3.85	21.2	0.24
20:30–21:30	19.4	27.8	3.85	21	0.22
21:30–22:30	17.7	30.8	3.85	20.8	0.24
22:30–23:30	15.9	31.6	3.50	20.6	0.43
23:30–00:30	14	36.2	3.56	20.5	0.22
00:30–01:30	13	43.8	4.05	20.2	0
01:30–02:30	11.7	52	4.41	20	0
02:30–03:30	10.2	55	4.22	19.8	0
03:30–04:30	8.5	58.6	4.00	19.6	0
04:30–05:30	7	63.2	3.90	19.3	0

Table 8 – Hourly boundary conditions on April 16–17. T_o is the outdoor temperature; RH_o is the outdoor relative humidity; C_w is the mass concentration of the water vapour component; T_s is the soil temperature at 0.5 m depth.

Time	T_o (°C)	RH_o (%)	C_w (kg kg^{-1})	T_s (°C)	Wind speed (m s^{-1})
17:30–18:30	23.8	41.8	7.63	21.9	2.2
18:30–19:30	22	46.2	7.56	21.8	0.72
19:30–20:30	20	50.6	7.31	21.7	0.48
20:30–21:30	19.1	53.4	7.27	21.5	1.74
21:30–22:30	18	55.8	7.11	21.3	2.62
22:30–23:30	16.5	58.2	6.74	21.1	0.98
23:30–00:30	15	62.2	6.54	20.9	0.18
00:30–01:30	14	65.2	6.44	20.7	0.22
01:30–02:30	11.8	73.6	6.26	20.5	0.18
02:30–03:30	10.5	77.4	6.07	20.3	0
03:30–04:30	9.3	78.2	5.63	20.1	0
04:30–05:30	7.8	85	5.61	20	0

Table 6 – Boundary and fixed zone conditions of steady-state simulation. T_o is the outdoor temperature; T is the indoor temperature; T_s is the soil temperature at 0.5 m depth; and RH_i is the indoor relative humidity; C_w is the mass concentration of the water vapour component.

Time	Boundary conditions				Fixed zone conditions		
	T_o (°C)	Sky emissivity	Wind speed (m s^{-1})	T_s (°C)	T (°C)	RH_i (%)	C_w (g kg^{-1})
17:30 (April 15)	25.2	0.71	1.8	22.0	25.5	82	16.48
17:30 (April 16)	24.6	0.87	2.1	22.5	25.2	81	16.31

5. Model evaluation

The evaluation time was from 17:30 to 5:30 the next day, every day for two days from April 15 to 17, 2019. The total simulation time each day was 12 h, which crossed the periods of evening, night, and dawn. During this period, the management mode was no irrigation, closed vents, and no additional cover on the roof. The wind direction was mainly southwest in the first 12 h, and mainly southeast in the next 12 h. The condensation on the leaves at the A–I measurement points (Fig. 1) was observed manually for comparison with the simulation results each hour. The root-mean-squared error (RMSE) was used to evaluate the errors between the calculated and measured data.

$$\mathrm{RMSE} = \sqrt{\frac{\sum_{i=1}^{N}(C_{ai} - M_{ei})^2}{N-1}} \tag{28}$$

where C_{ai} is the calculated value, M_{ei} is the measured value, and N is the sample size. The condensation distribution model was tested using five statistical indicators: true positive rate (TPR), true negative rate (TNR), false positive rate, false negative rate, and accuracy (ACC).

6. Results and discussion

6.1. Temperature and humidity

Figure 7 compares the simulations and measurements at nine locations A–I from 18:30 to 5:30. The results show that the maximum error (MAE) of the T, RH, and T_c during the two nights were 2.7 °C, 7.5%, and 2 °C, respectively (Table 9). Bouhoun Ali et al. (2014) conducted 2-D transient CFD simulations considering the condensation on the roof at night and crop–air interaction. The MAE of T and T_c were both 1 °C in 6 h. This is accurate, but the boundary conditions adopted between the two cases were different. The boundary conditions of the fixed wall temperature and fixed wall flux resulted in a more accurate simulation. However, less inputs must be considered to find a balance between practicality and accuracy.

Table 9 – Error between simulated and measured T, RH, and T_c. MAE is the maximum error; MIE is the minimum error; ME is the mean error, and RMSE is the root-mean-squared error.

		MAE	MIE	ME	RMSE
April 15–16	T (°C)	2.7	0.1	1.2	1.38
	RH (%)	6.9	0	2.7	3.22
	T_C (°C)	2	0.3	1.3	1.36
April 16–17	T (°C)	2.3	0	0.9	1.10
	RH (%)	7.5	0	2.8	3.40
	T_C (°C)	2	0.1	1.1	1.27

Temperatures were underestimated by the model in the range of 12–17 °C, and then overestimated (Fig. 7). The simulated temperatures decreased linearly at night (Fig. 8). The rate of decrease of the measured temperatures tends to slow down, which is related to the decrease in wind speed in the second half of the night (Tables 7 and 8). There is no other heat source in the greenhouse other than solar radiation. The

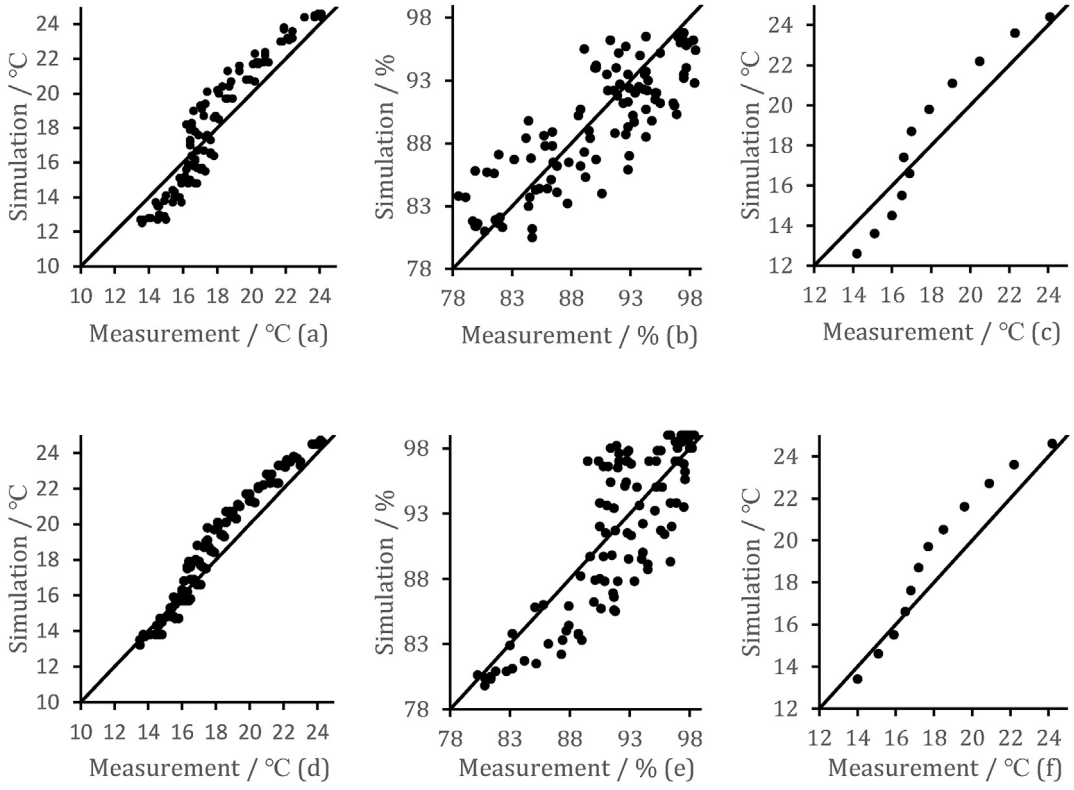

Fig. 7 – Model evaluation of (a) T, (b) RH, and (c) T_c on April 15–16; and (d) T, (e) RH, and (f) T_c on April 16–17.

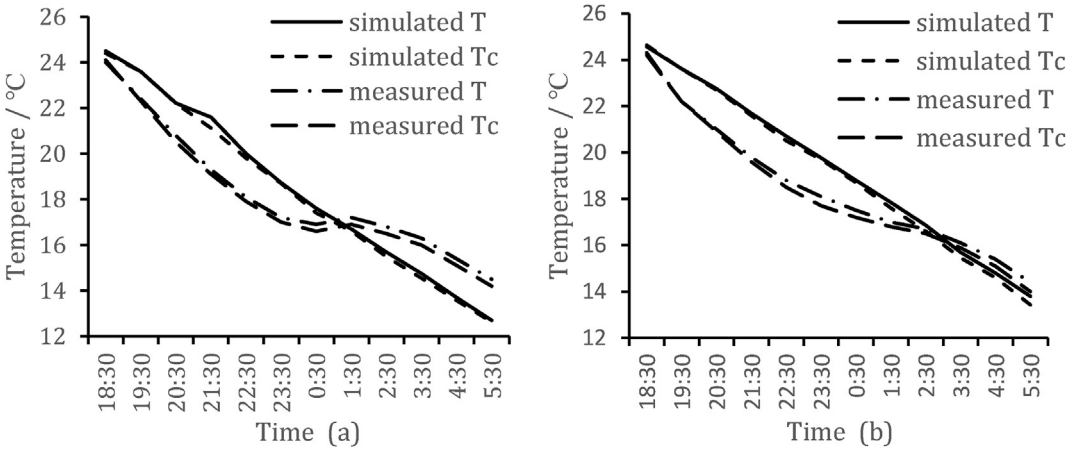

Fig. 8 – T and T_c in the greenhouse on (a) April 15–16 and (b) April 16–17.

air leakage rate of the greenhouse was proven to be positively correlated with wind speed when the vents were closed, which may explain the trend of the measured temperature at night (Boulard et al., 2017). Although the heat transfer coefficient of the external walls and roof was positively correlated with wind speed (Eq. (9)), the results show that this is insufficient to affect the trend of the simulated temperature (Fig. 8). The reason may be the constant air leakage rate

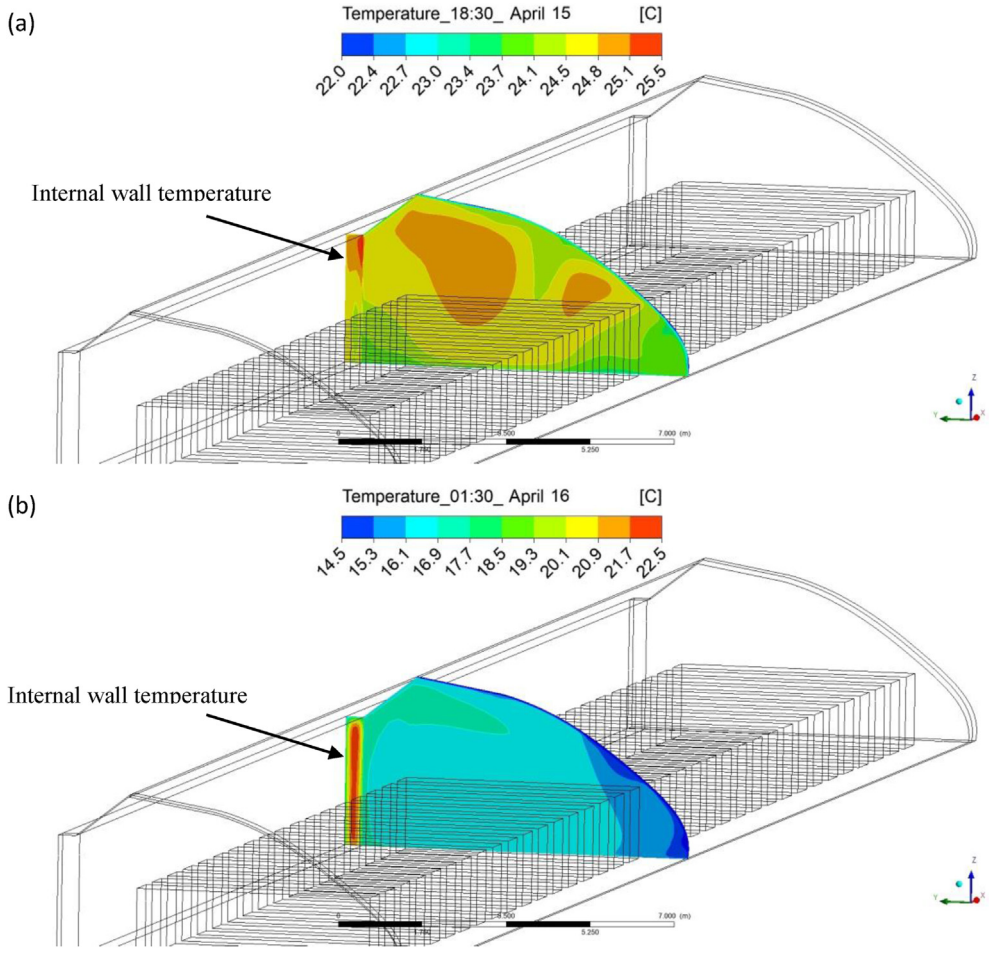

Fig. 9 – Contour of simulated internal wall temperature and air temperature on the vertical plane. Y represents the north; X represents the east. (a) April 15, 18:30 and (b) April 16, 01:30.

adopted in this study. The modelling of the heat performance when the vents are closed in the greenhouse must be studied precisely.

In the actual production process, the RH is often a reference parameter with guiding significance, and is closely related to condensation and frost damage. The ME of the RH was 2.7% and 2.8%, respectively, during the two nights. The RMSE values of RH were 3.22% and 3.40%, respectively. Considering the crop–air interaction, the RMSE of the RH simulated by another CFD model was 6.4% in 6 h (Bouhoun Ali et al., 2014). Compared with this experiment, the ventilation boundary condition was considered, which increased the difficulty of quantifying the water vapour concentration. Both models simulated roof condensation, while the leaf condensation model was embedded in this experiment.

The spatial distribution maps are presented in Figs. 9 and 10. The first hour of the transient simulation was 18:30, while the simulated leaf condensation occurred for the first time at 1:30. The internal wall temperatures were higher than the air temperature, and this difference increased over time (Fig. 9). As the temperature difference became evident, the wall heat flux increased (Fig. 11 (a) and (c)). The air temperature at the top of the greenhouse was higher than that at the bottom, and changed suddenly near the roof, similar to Tong et al. (2009).

On the horizontal plane, the air temperature was higher near the thick wall and lower near the semi-transparent roof (Fig. 10). However, the temperature distribution appears to be symmetrical in the east-west direction. The above distribution trend coincides with Wang, Luo, and Li (2013). The temperature difference on the horizontal plane at 1:30 was greater than that at 18:30. The leaf temperature distribution trend was consistent with that of air temperature, while the distribution trend of RH was the opposite that of air temperature.

In the absence of heating at night, the brick walls of the greenhouse can store and prevent heat loss. On the south side with a semi-transparent roof, the temperature is lower and the RH is higher, conditions that make it easier to form condensation that causes leaf damage. This conclusion coincides with Bournet's observations that cucumber leaves near the semi-transparent boundary have a greater risk of condensation than in other zones (Bournet, Brajeul, Truffault, Chantoiseau, & Naccour, 2020).

Figure 11 shows the heat flux on both sides of the wall. Wall heat flux in (a) and (c) represent that on the internal wall surface, while (b) and (d) represent that on the external wall surface. The positive wall heat flux of (a) and (c) indicates that the wall dissipates heat to the indoor air. The negative wall heat flux of (b) and (d) indicates that heat from the wall was lost to the outdoor zone. The greenhouse lost more heat from the semi-transparent roof at 1:30 than at 18:30. The heat flux distribution on the roof was not uniform, which explains the distribution of condensation on the roof (Figs. 13 and 14). The ground heat flux heated the indoor air at 1:30, but was approximately 0 at 18:30.

Tables 10 and 11 show the maximum differences in temperature and RH at points A–I. With the same distribution, the maximum difference in temperature at other times ranged from 0.6 °C to 1.9 °C by measurement, and 0.2 °C–1.2 °C by simulation. The heterogeneity of the

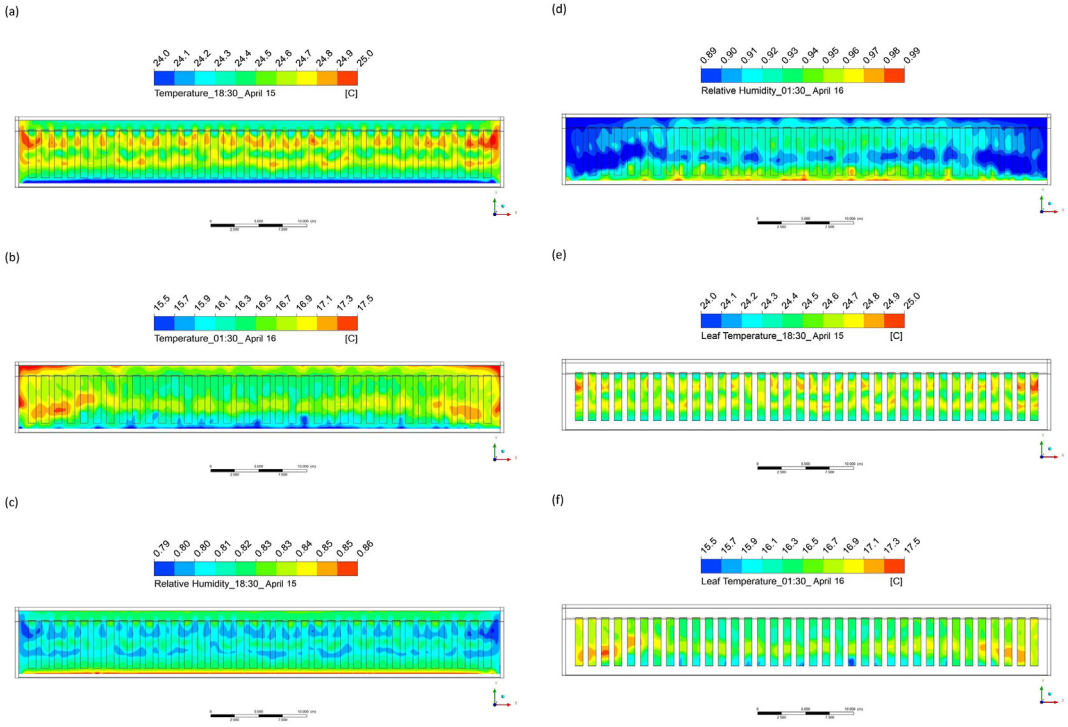

Fig. 10 – Contour of simulated T, RH, and T_c on the horizontal plane at 1 m height. Y represents the north; X represents the east. The rectangles represent crop rows. (a) (c) (e) April 15, 18:30 and (b) (d) (f) April 16, 01:30.

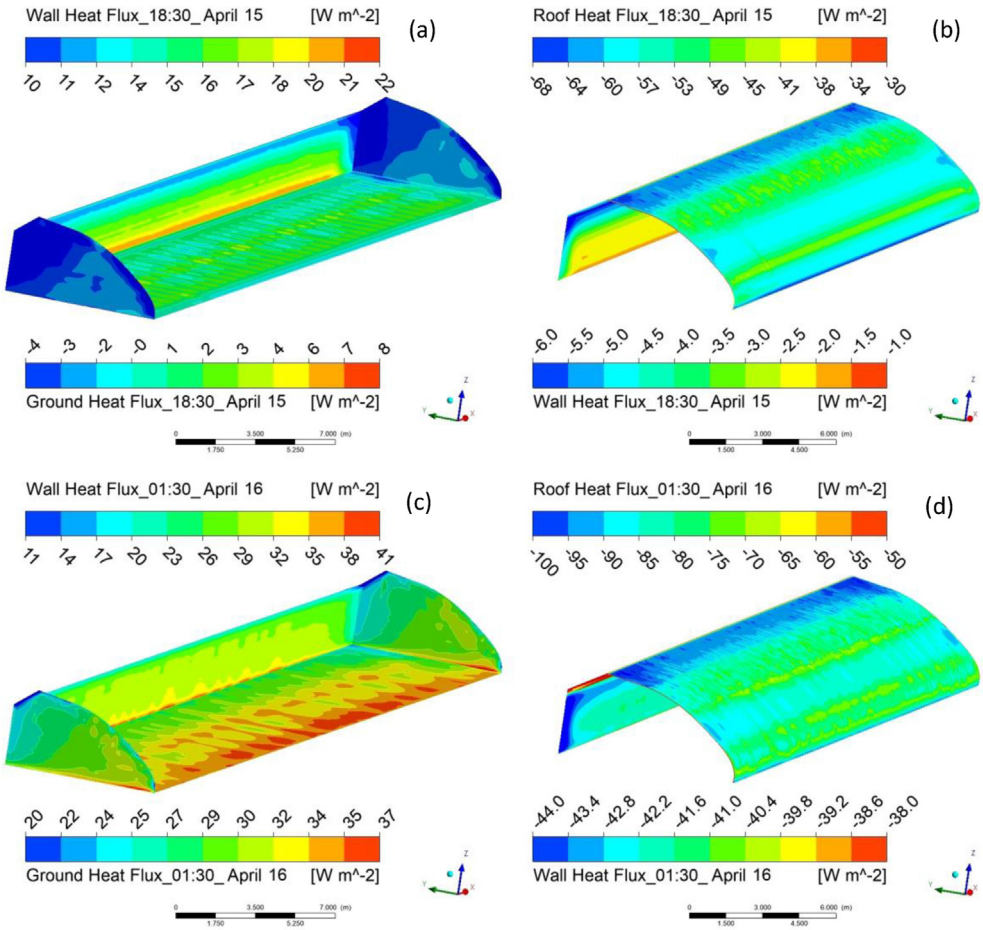

Fig. 11 – Contour of simulated heat flux of the walls, ground, and roof. Y represents the north; X represents the east. (a) (b) April 15, 18:30 and (c) (d) April 16, 01:30.

temperature distribution in a real greenhouse was greater than that in the simulation. One possible reason is that the model overestimated the thermal insulation of the semi-transparent roof in the south or underestimated the heat storage performance of the thick wall in the north. Owing to the deterioration of the wall and roof, there are differences between thermal insulation performance of the actual and ideal greenhouse. Another reason is that the turbulence model parameters require further correction to reduce the air convection between the north and south sides of the greenhouse when the vents are closed. The maximum difference of RH ranged from 2.3% to 10.7% and 1.1%–5.7% by measurement and simulation (Tables 10 and 11), respectively. The results show that simulations mitigated the differences, which explains why leaf condensation was always observed first near the semi-transparent roof rather than in the simulation (Table 12).

6.2. *Condensation*

The simulated roof condensation first appeared from 19:30 on April 15 while the simulated leaf condensation first

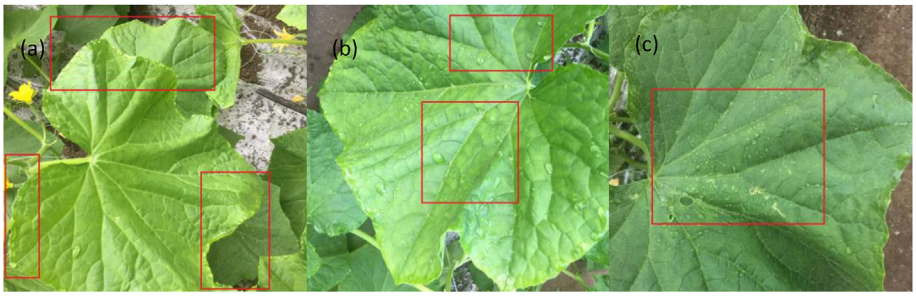

Fig. 12 – Photos of (a) guttation, (b) drops of water from the above leaves, and (c) condensation on leaves.

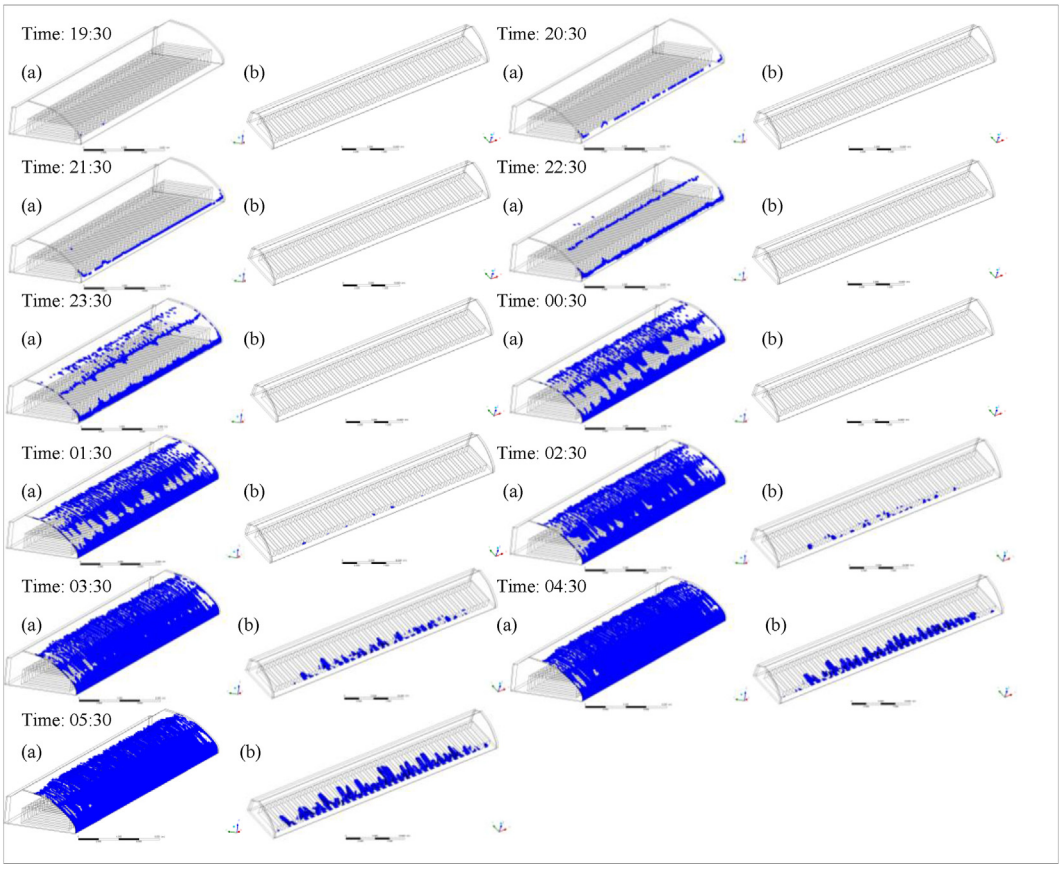

Fig. 13 – Comparison of simulated condensation on the (a) roof and (b) crop canopy on April 15–16. Y represents the north; X represents the east; and ■ represents the condensation that appeared based on simulation.

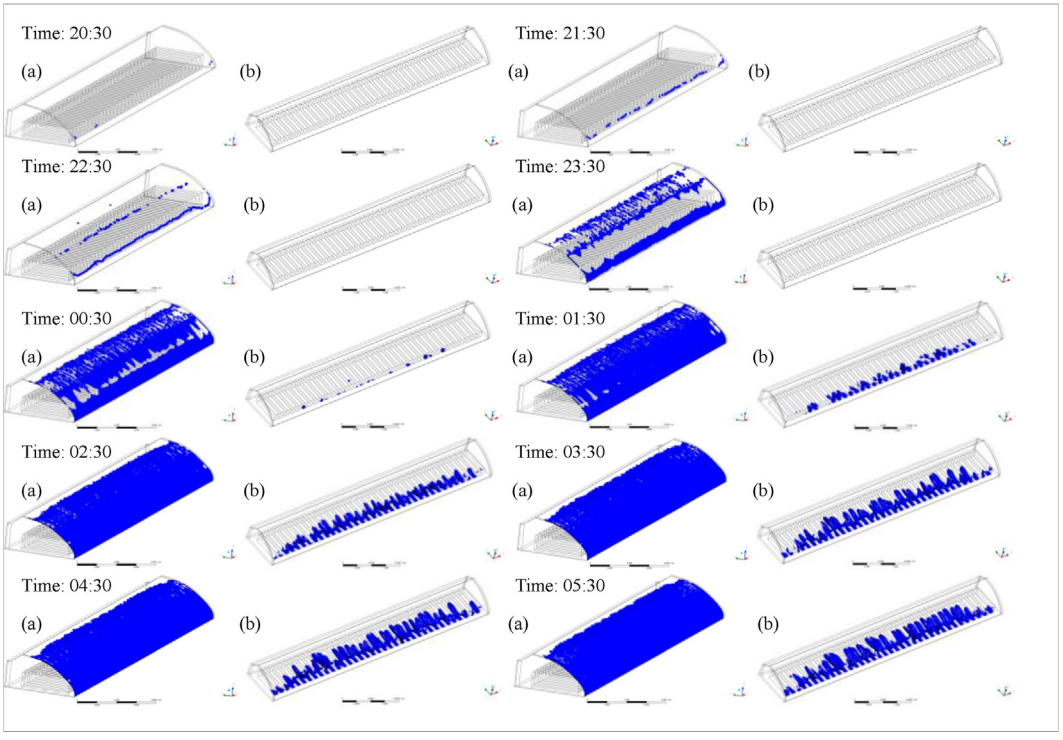

Fig. 14 – Comparison of simulated condensation on the (a) roof and (b) crop canopy on April 16–17. Y represents the north; X represents the east; and ■ represents the condensation that appeared based on simulation.

Table 10 – Maximum difference of temperature (T) and relative humidity (RH) at points A–I on April 15–16.

Time	Measurement		Simulation	
	Difference T (°C)	Difference RH (%)	Difference T (°C)	Difference RH (%)
17:30–18:30	1	2.3	0.2	1.1
18:30–19:30	0.7	8.9	0.8	3.9
19:30–20:30	0.9	7.9	0.7	3.5
20:30–21:30	1.9	9.8	1.2	5
21:30–22:30	1.9	10.6	0.9	4.5
22:30–23:30	1.9	10.7	1	5.3
23:30–00:30	1.2	8.3	0.9	5.2
00:30–01:30	1.3	7.3	1.1	3.3
01:30–02:30	1.2	7.3	0.9	5.2
02:30–03:30	1.4	7.6	0.8	4.5
03:30–04:30	1.5	9.4	0.6	3.8
04:30–05:30	1.5	8.6	0.5	2.3
Max	1.9	10.7	1.2	5.3
Min	0.7	2.3	0.2	1.1
Average	1.4	8.2	0.8	4

Table 11 – Maximum difference in temperature (T) and relative humidity (RH) at points A–I on April 16–17.

Time	Measurement		Simulation	
	Difference T (°C)	Difference RH (%)	Difference T (°C)	Difference RH (%)
17:30–18:30	0.6	2.9	0.2	1.3
18:30–19:30	1.3	5.7	0.6	2.5
19:30–20:30	1.2	6.6	0.8	3.6
20:30–21:30	1	5.6	0.7	4
21:30–22:30	1.1	6.2	0.7	3.9
22:30–23:30	1.1	6.4	1.1	5.7
23:30–00:30	1.2	7	1.1	5.5
00:30–01:30	1.1	6.8	0.5	5.3
01:30–02:30	1.1	7	0.8	4
02:30–03:30	1.2	7.5	0.6	2.8
03:30–04:30	1.3	8.1	0.5	2.5
04:30–05:30	1.3	9	0.6	2
Max	1.3	9	1.1	5.7
Min	0.6	2.9	0.2	1.3
Average	1.1	6.6	0.7	3.6

appeared from 01:30 on April 16 (Fig. 13). On the second night, the simulated roof condensation first appeared from 20:30 on April 16, while the simulated leaf condensation first appeared from 00:30 on April 17 (Fig. 14). Condensation always appeared first on the roof rather than on the leaves.

The leaf condensation results were observed manually for comparison with the simulated results. It is important to note that more than one phenomenon can wet the leaves. Aside from condensation, guttation is another common phenomenon that makes leaves wet. Drops of water from above the leaves sometimes cause leaf wetness. Guttation is easy to distinguish, as it always appears at the edge of the leaves (Fig. 12(a)). Water that drops from elsewhere usually takes different forms. However, regardless of the shape, they are always unevenly distributed on the leaves (Fig. 12 (b)). The water droplets on the leaf surface from condensation are very small and evenly distributed (Fig. 12 (c)). All of the above phenomena can result in leaf wetness. However, (a) is a complex physiological process that requires further study to establish a model; (b) can be simulated by two-phase flow modelling, but it is time-consuming, especially considering that the phenomenon accounts for a small percentage of leaf wetness. In this study, only condensation on leaves was modelled and observation (c) was recorded for comparison with the simulated result.

The condensation on leaves appeared earlier on April 17 than on April 16 because the outdoor and indoor humidity on the night of April 17 were higher than on April 16 (Tables 7 and 8, Fig. 7). Leaf condensation always occurred first in the area near the semi-transparent roof (at points A, D, G), both in the observation and simulation (Table 12, Fig. 15). Because the leaves near the roof are exposed to lower air temperatures, leaf temperatures are lower and the RH is higher in these areas, which leads to leaf condensation.

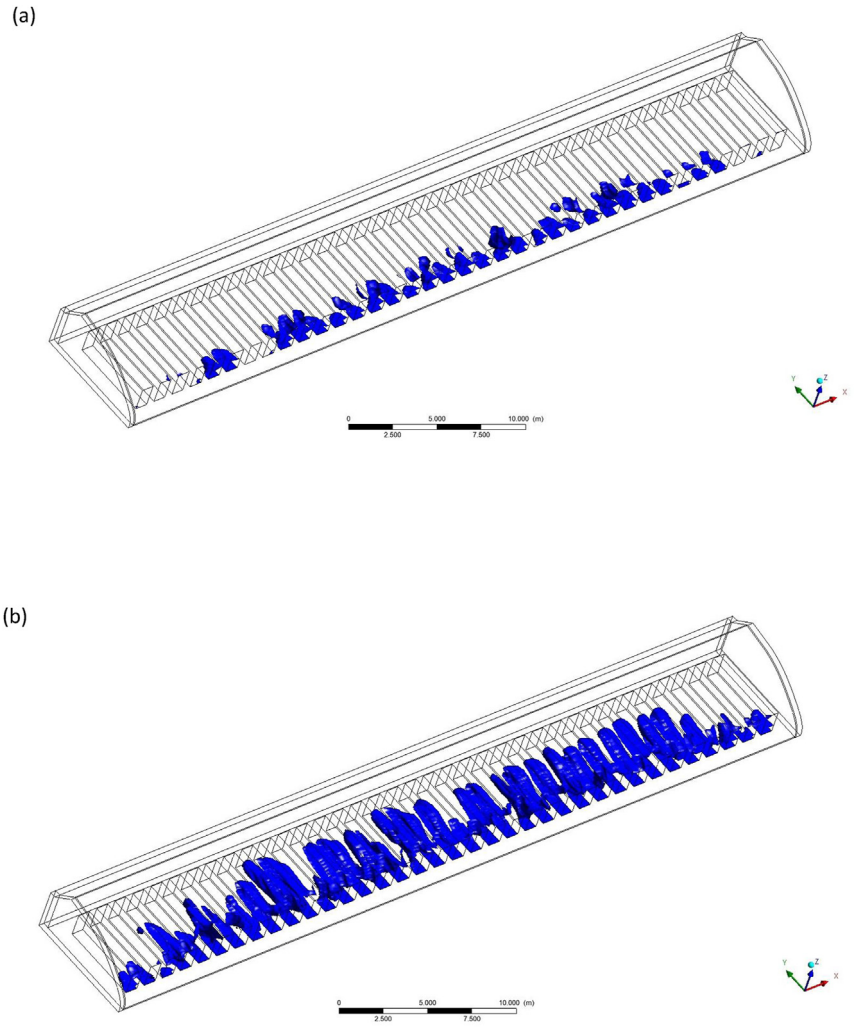

Fig. 15 – Simulated leaf condensation on April 17 at (a) 01:30 and (b) 05:30. Y represents the north; X represents the east; and ■ represents the condensation that appeared based on simulation.

6.3. LWD

The simulated LWD was considered as the duration of the simulated condensation at each point. The observed condensation always occurred earlier than the simulated condensation (Table 12). The average errors between the observed and simulated LWD were 1.2 h on April 15–16, and 1.3 h on April 16–17, respectively. The error in this model was compared with that of the Gembloux dynamic greenhouse climate model used by Mashonjowa et al. (2013). Their idea is similar to that in this

Table 12 – Results of simulated and observed condensation. The symbol (–) means no condensation. LWD is the leaf wetness duration (h).

	Position	A	B	C	D	E	F	G	H	I
April, 15–16, 2019	First Simulated	1:30	5:30	–	1:30	5:30	–	2:30	5:30	–
	First Observed	0:30	5:30	–	0:30	4:30	–	23:30	0:30	–
	Simulated LWD (h)	4	0	0	4	0	0	3	0	0
	Observed LWD (h)	5	0	0	5	1	0	6	5	0
	Error of LWD (h)	1	0	0	1	1	0	3	5	0
	Averaged Error (h)	1.2								
April, 16–17, 2019	First Simulated	0:30	2:30	–	0:30	3:30	–	0:30	3:30	–
	First Observed	23:30	0:30	–	23:30	0:30	–	23:30	23:30	–
	Simulated LWD (h)	5	3	0	5	2	0	5	2	0
	Observed LWD (h)	6	5	0	6	5	0	6	6	0
	Error of LWD (h)	1	2	0	1	3	0	1	4	0
	Average Error (h)	1.3								

paper, which is to model the greenhouse environment and determine the environmental conditions. Then, the environmental parameters are taken as the inputs of the condensation model to simulate the LWD. The average errors using the dewpoint depression of canopy temperature (DPD_c), dewpoint depression of air temperature (DPD_a), constant RH, and extended RH were 1.77 h, 0.93 h, 1.27 h, and 1.47 h, respectively. The average errors of the model in this study were similar, especially as it is a transient distribution model in which external disturbances exist in the actual situation.

The condensation results at each hour were marked as either Yes or No, according to the two-day evaluation. There are 216 pairs of data in the sample, the TNR is 1, TPR is 0.66, and the ACC is 0.89. The results show that the model is highly specific but lacks sensitivity. For example, the observed LWD was significantly greater than the simulated one in the east of the greenhouse (Table 12). One reason is that simulations mitigated the differences in temperature and humidity between the south and north of the greenhouse. The large difference in temperature and humidity distribution in an actual greenhouse leads to local condensation. Another reason is that there are many accidental and unquantifiable sources of humidity; for example, the junction of drip irrigation systems in the east of the greenhouse or human activities that interfere with water sources.

In the presence of the spores, infection depends primarily on interactive effects of temperature and leaf wetness (Elad, Malathrakis, & Dik, 1996; Arauz, Neufeld, Lloyd, & Ojiambo, 2010). For cucumber downy mildew (caused by *Pseudoperonospora cubensis*), the optimal infection condition was considered to be around 20 °C for air temperature and no less than 2 h for LWD (Aegerter, Nuñez, & Davis, 2003; Zhao et al., 2011). More than 2 h of LWD were simulated in specific zone of the greenhouse (Table 12). However, the corresponding simulated air temperature was lower than 17 °C (Fig. 10 (b)). Taking the infection conditions of cucumber downy mildew as an example, no risk warning was issued during the simulation.

7. Conclusion

In contrast to current research, this paper proposes a model for simulating the distribution of leaf condensation. The main contributions of this study are summarised as follows:

(i) The air temperature, RH, and leaf temperature in 24 h were evaluated by 3-D CFD modelling.
(ii) The distributions of roof condensation and leaf condensation were simulated. Condensation always appeared first on the roof rather than on the leaves. The leaf condensation results were observed for comparison with the simulated results. Leaf condensation always appeared first in the area near the semi-transparent roof, as shown by both the observations and simulation.
(iii) The LWD was simulated by considering the duration of the simulated leaf condensation at each point. The evaluation was conducted on 216 pairs of samples. The TNR, TPR, and ACC were 1, 0.66, and 0.89, respectively.
(iv) Models were embedded to simplify the input parameters and enhance practicality. Without compromising performance, the model inputs were reduced to five: outdoor solar radiation intensity, outdoor air temperature, outdoor RH, outdoor average wind speed per hour, and soil temperature.

Further study is to adjust the management of the greenhouse by taking the simulated temperature and LWD as references. Greenhouse vents are usually closed at night in the Northern China except on summer. Farmers have to choose a vents configuration between keeping the greenhouse warm and preventing dewing leaves. With the help of this model, there will be an optimal decision, which is to open the vents intermittently when the simulation showed that leaf wetness will occur. The simulations of leaf wetness disappearing and greenhouse temperature decreasing when the vents are opened at night by using CFD method are expected to be studied. It is of great significance for providing optimum control strategy to reduce the plant disease infection in the greenhouse.

Declaration of competing interest

The authors declare that they have no known competing financial interests or personal relationships that could have appeared to influence the work reported in this paper.

Acknowledgement

This work was funded by the Science and Technology Innovation Capacity Building Project of Beijing Academy of Agriculture and Forestry Sciences (No. KJCX20211002); Youth Program of National Natural Science Foundation of China (31401683); and the FP7 Framework Program (PIRSES-GA-2013-612659); We thank the China Scholarship Council for its financial support for this research (NO. 201909505002).

Appendix A. Supplementary data

Supplementary data to this article can be found online at https://doi.org/10.1016/j.biosystemseng.2021.08.008.

REFERENCES

Aegerter, B. J., Nuñez, J. J., & Davis, R. M. (2003). Environmental factors affecting rose downy mildew and development of a forecasting model for a nursery production system. *Plant Disease*, *87*, 732–738. https://doi.org/10.1094/PDIS.2003.87.6.732

Ansys. (2010). *Ansys fluent 13.0 user's guide*. Canonsburg, PA, USA: Ansys, Inc.

Arauz, L. F., Neufeld, K. N., Lloyd, A. L., & Ojiambo, P. S. (2010). Quantitative models for germination and infection of pseudoperonospora cubensis in response to temperature and duration of leaf wetness. *Phytopathology*, *100*(9), 959–967. https://doi.org/10.1094/PHYTO-100-9-0959

Bassimba, D. D. M., Intrigliolo, D., Marta, A., Orlandini, S., & Vicent, A. (2017). Leaf wetness duration in irrigated citrus

orchards in the Mediterranean climate conditions. *Agricultural and Forest Meteorology, 234–235*, 182–195. https://doi.org/10.1016/j.agrformet.2016.12.025

Bianchi, A., Masseroni, D., & Facchi, A. (2017). Modelling water requirements of greenhouse spinach for irrigation management purposes. *Hydrology Research, 48*(3), 776–788. https://doi.org/10.2166/nh.2016.079

Bouhoun Ali, H., Bournet, P.-E., Danjou, V., Morille, B., & Migeon, C. (2014). CFD simulations of the night-time condensation inside a closed glasshouse: Sensitivity analysis to outside external conditions, heating and glass properties. *Biosystems Engineering, 127*, 159–175. https://doi.org/10.1016/j.biosystemseng.2014.08.017

Boulard, T., Haxaire, R., Lamrani, M. A., Roy, J. C., & Jaffrin, A. (1999). Characterization and modelling of the air fluxes induced by natural ventilation in a greenhouse. *Journal of Agricultural Engineering Research, 74*(2), 135–144. https://doi.org/10.1006/jaer.1999.0442

Boulard, T., Roy, J. C., Fatnassi, H., Kichah, A., & Lee, I.-B. (2010). Computer fluid dynamics prediction of climate and fungal spore transfer in a rose greenhouse. *Computers and Electronics in Agriculture, 74*(2), 280–292. https://doi.org/10.1016/j.compag.2010.09.003

Boulard, T., Roy, J. C., Pouillard, J. B., Fatnassi, H., & Grisey, A. (2017). Modelling of micrometeorology, canopy transpiration and photosynthesis in a closed greenhouse using computational fluid dynamics. *Biosystems Engineering, 158*, 110–133. https://doi.org/10.1016/j.biosystemseng.2017.04.001

Boulard, T., & Wang, S. (2002). Experimental and numerical studies on the heterogeneity of crop transpiration in a plastic tunnel. *Computers and Electronics in Agriculture, 34*(1–3), 173–190. https://doi.org/10.1016/S0168-1699(01)00186-7

Bournet, P.-E., Brajeul, E., Truffault, V., Chantoiseau, E., & Naccour, R. (2020). Impact of heating location, forced ventilation and screens on the energy efficiency and condensation risks inside a cucumber greenhouse. *Acta Horticulturae, 1271*, 25–32. https://doi.org/10.17660/ActaHortic.2020.1271.4

Bu, W. F., & Wang, S. H. (2001). Correction of an empirical calculation formula of dew point temperature. *Journal of Beijing Polytechnic university, 3*, 369–370 (In Chinese) https://kns.cnki.net/kcms/detail/detail.aspx?FileName=BJGD200103023&DbName=CJFQ2001.

Chen, J., Xu, F., Tan, D., Shen, Z., Zhang, L., & Ai, Q. (2015). A control method for agricultural greenhouses heating based on computational fluid dynamics and energy prediction model. *Applied Energy, 141*, 106–118. https://doi.org/10.1016/j.apenergy.2014.12.026

Elad, Y., Malathrakis, N., & Dik, A. (1996). Biological control of Botrytis-incited diseases and powdery mildews in greenhouse crops. *Crop Protection, 15*(3), 229–240. https://doi.org/10.1016/0261-2194(95)00129-8

Erbs, D. G., Klein, S. A., & Duffie, J. A. (1982). Estimation of the diffuse radiation fraction for hourly, daily and monthly-average global radiation. *Solar Energy, 28*(4), 293–302. https://doi.org/10.1016/0038-092X(82)90302-4

Fall, M. L., Van der Heyden, H., Beaulieu, C., & Carisse, O. (2015). Bremia lactucae infection efficiency in lettuce is modulated by temperature and leaf wetness duration under Quebec field conditions. *Plant Disease, 99*, 1010–1019. https://doi.org/10.1094/PDIS-05-14-0548-RE

Frans, M., Moerkens, R., Van, Gool, S., Sauviller, C., Van, Laethem, S., Luca, S., et al. (2018). Modelling greenhouse climate factors to constrain internal fruit rot (fusarium spp.) in bell pepper. *Journal of Plant Diseases and Protection, 125*, 425–432. https://doi.org/10.1007/s41348-018-0159-3

Garzoli, K. V., & Blackwell, J. (1987). An analysis of the nocturnal heat loss from a double skin plastic greenhouse. *Journal of Agricultural Engineering Research, 36*(2), 75–86. https://doi.org/10.1016/0021-8634(87)90114-4

Gerlein-Safdi, C., Koohafkan, M. C., Chung, M., Rockwell, F. E., Thompson, S., & Caylor, K. K. (2018). Dew deposition suppresses transpiration and carbon uptake in leaves. *Agricultural and Forest Meteorology, 259*, 305–316. https://doi.org/10.1016/j.agrformet.2018.05.015

Golzar, F., Heeren, N., Hellweg, S., & Roshandel, R. (2018). A novel integrated framework to evaluate greenhouse energy demand and crop yield production. *Renewable and Sustainable Energy Reviews, 96*, 487–501. https://doi.org/10.1016/j.rser.2018.06.046

Guyot, G. (1999). In Dunod (Ed.), *Climatologie de l'environnement: Cours et exercices corrigés, P. 525*.

Kichah, A., Bournet, P.-E., Migeon, C., & Boulard, T. (2012). Measurement and CFD simulation of microclimate characteristics and transpiration of an Impatiens pot plant crop in a greenhouse. *Biosystems Engineering, 112*(1), 22–34. https://doi.org/10.1016/j.biosystemseng.2012.01.012

Kimura, K., Yasutake, D., Yamanami, A., & Kitano, M. (2020). Spatial examination of leaf-boundary-layer conductance using artificial leaves for assessment of light airflow within a plant canopy under different controlled greenhouse conditions. *Agricultural and Forest Meteorology, 280*, 107773. https://doi.org/10.1016/j.agrformet.2019.107773

Kustas, W. P., Rango, A., & Uijlenhoet, R. (1994). A simple energy budget algorithm for the snowmelt runoff model. *Water Resources Research, 30*(5), 1515–1527. https://doi.org/10.1029/94WR00152

Li, K. J., Sha, Z. D., Xue, W. P., Chen, X., Mao, H. P., & Tan, G. (2020). A fast modeling and optimization scheme for greenhouse environmental system using proper orthogonal decomposition and multi-objective genetic algorithm. *Computers and Electronics in Agriculture, 168*, 105096. https://doi.org/10.1016/j.compag.2019.105096

Liu, J., Chen, J. M., Black, T. A., & Novak, M. D. (1996). E-ε modelling of turbulent air flow downwind of a model forest edge. *Boundary-Layer Meteorology, 77*, 21–44. https://doi.org/10.1007/BF00121857

Liu, X. Y., & Zhang, W. (2011). Establishment and analysis of forecasting model of temperature and humidity in PC board greenhouse. *Agriculture Network Information, 7*, 31–33. https://kns.cnki.net/kcms/detail/detail.aspx?FileName=JSJN201107010&DbName=CJFQ2011.

Mashonjowa, E., Ronsse, F., Mubvuma, M., Milford, J. R., & Pieters, J. G. (2013). Estimation of leaf wetness duration for greenhouse roses using a dynamic greenhouse climate model in Zimbabwe. *Computers and Electronics in Agriculture, 95*, 70–81. https://doi.org/10.1016/j.compag.2013.04.007

Mills, A. F. (1992). *Heat transfer*. Boston, USA: Irwin.

Mistriotis, A., Arcidiacono, C., Picuno, P., Bot, G. P. A., & Scarascia-Mugnozza, G. (1997). Computational analysis of ventilation in greenhouses at zero- and low-wind-speeds. *Agricultural and Forest Meteorology, 88*(1–4), 121–135. https://doi.org/10.1016/S0168-1923(97)00045-2

Modest, M. F. (1993). *Radiative heat transfer*. New York: McGraw-Hill.

Phan, T. H., Won, S. S., & Park, W. G. (2018). Numerical simulation of air–steam mixture condensation flows in a vertical tube. *International Journal of Heat and Mass Transfer, 127*(C), 568–578. https://doi.org/10.1016/j.ijheatmasstransfer.2018.08.043

Piscia, D., Montero, J. I., Baeza, E., & Bailey, B. J. (2012). A CFD greenhouse night-time condensation model. *Biosystems Engineering, 111*(2), 141–154. https://doi.org/10.1016/j.biosystemseng.2011.11.006

Roy, J. C., Boulard, T., Kittas, C., & Wang, S. (2002). PA—Precision agriculture: Convective and ventilation transfers in

greenhouses, Part 1: The greenhouse considered as a perfectly stirred tank. *Biosystems Engineering, 83*(1), 1–20. https://doi.org/10.1006/bioe.2002.0107

Stanghellini, C., & Jong, T. (1995). A model of humidity and its applications in a greenhouse. *Agricultural and Forest Meteorology, 76*(2), 129–148. https://doi.org/10.1016/0168-1923(95)02220-R

Tomaszkiewicz, M., Abou Najm, M., Zurayk, R., & El-Fadel, M. (2017). Dew as an adaptation measure to meet water demand in agriculture and reforestation. *Agricultural and Forest Meteorology, 232*, 411–421. https://doi.org/10.1016/j.agrformet.2016.09.009

Tong, G., Christopher, D. M., & Li, B. (2009). Numerical modelling of temperature variations in a Chinese solar greenhouse. *Computers and Electronics in Agriculture, 68*(1), 129–139. https://doi.org/10.1016/j.compag.2009.05.004

Tong, G., Christopher, D. M., & Zhang, G. Q. (2017). New insights on span selection for Chinese solar greenhouses using CFD analyses. *Computers and Electronics in Agriculture, 149*, 3–15. https://doi.org/10.1016/j.compag.2017.09.031

Wang, X. W., Luo, W. Y., & Li, X. P. (2013). CFD based study of heterogeneous microclimate in a typical Chinese greenhouse in central China. *Journal of Integrative Agriculture, 12*(5), 914–923. https://doi.org/10.1016/S2095-3119(13)60309-3

Wang, H., Sánchez-Molina, J., Li, M., & Rodriguez, F. (2019). Improving the performance of vegetable leaf wetness duration models in greenhouses using decision tree learning. *Water, 11*(1), 158. https://doi.org/10.3390/w11010158

Wilson, J. D. (1985). Numerical studies of flow through a windbreak. *Journal of Wind Engineering and Industrial Aerodynamics, 21*(2), 119–154. https://doi.org/10.1016/0167-6105(85)90001-7

Yan, H. F., Zhao, B. S., Zhang, C., Huang, S., Fu, H. W., Yu, J. J., et al. (2019). Estimating cucumber plants transpiration by Penman-Monteith model in Venlo-type greenhouse. *Transactions of the Chinese Society of Agricultural Engineering*, 35(8), 149–157 (In Chinese) https://kns.cnki.net/kcms/detail/detail.aspx?FileName=NYGU201908018&DbName=CJFQ2019.

Zhang, G. X., Fu, Z. T., Yang, M. S., Liu, X. X., Dong, Y. H., & Li, X. X. (2019). Nonlinear simulation for coupling modeling of air humidity and vent opening in Chinese solar greenhouse based on CFD. *Computers and Electronics in Agriculture, 162*, 337–347. https://doi.org/10.1016/j.compag.2019.04.024

Zhao, C. J., Li, M., Yang, X. T., Sun, C. H., Qian, J. P., & Ji, Z. T. (2011). A data-driven model simulating primary infection probabilities of cucumber downy mildew for use in early warning systems in solar greenhouses. *Computers and Electronics in Agriculture, 76*(2), 306–315. https://doi.org/10.1016/j.compag.2011.02.009

2.1.3 A CFD transient model of leaf wetness duration on greenhouse cucumber leaves

Research in this field is supported by the following journal publication:

Title	A CFD transient model of leaf wetness duration on greenhouse cucumber leaves
Authors	C. Zhang, **R. Liu** (Double first authors), K. Liu, X. Yang, H. Liu, M. Diao, M. Li
Journal	Computers and Electronics in Agriculture
Year	2022
Volume	200
Pages	107257
DOI	https://doi.org/10.1016/j.compag.2022.107257.
IF(JCR2022)	6.757
Categories	Horticulture (1/94) Q1 Computer Science Applications (38/747) Q1

Contribution of the Ph.D. Candidate
The Ph.D. candidate R. Liu is the main contributor and one of the double first authors of this paper.

Computers and Electronics in Agriculture 200 (2022) 107257

Contents lists available at ScienceDirect

Computers and Electronics in Agriculture

journal homepage: www.elsevier.com/locate/compag

A CFD transient model of leaf wetness duration on greenhouse cucumber leaves

Chunhao Zhang [a,b,1], Ran Liu [a,b,c,1], Kaige Liu [a,b], Xinting Yang [a,b], Huiying Liu [a], Ming Diao [a,*], Ming Li [a,b,c,*]

[a] Department of Horticulture, Agricultural College of Shihezi University/Key Laboratory of Special Fruits and Vegetables Cultivation Physiology and Germplasm Resources Utilization of Xinjiang Production and Construction Corps, Shihezi, Xinjiang, China
[b] Information Technology Research Center, Beijing Academy of Agriculture and Forestry Sciences/ National Engineering Research Center for Information Technology in Agriculture/ National Engineering Laboratory for Agri-product Quality Traceability/ Meteorological Service Center for Urban Agriculture, China Meteorological Administration- Ministry of Agriculture and Rural Affairs, Beijing, China
[c] Department of Informatics, ceiA3, CIESOL, Ctra. Sacramento s/n, University of Almería, Almería, Spain

ARTICLE INFO

Keywords:
Solar greenhouse
Computational fluid dynamics
Leaf condensation
Dehumidification

ABSTRACT

The estimation of leaf wetness duration (LWD) is important for crop disease monitoring and early warning, because LWD provides the necessary conditions for pathogen infection. Crop canopy condensation caused by high humidity in greenhouses is one of the main causes of LWD formation, and measuring LWD in greenhouses is difficult. A simulation model based on agricultural meteorological parameters is typically used to replace field measurements. This study was conducted in a Chinese solar greenhouse. A 2D transient model based on computational fluid dynamics (CFD) was used to estimate the distribution of cucumber leaf condensation in a solar greenhouse during early summer nights in Beijing. The LWD was estimated by considering the duration of the simulated leaf condensation at each point and simulating the dehumidification effect under ventilation conditions. The visual observations of leaf condensation were compared with the simulation results from May 31 to June 1 and from June 3 to June 4, 2021 (cloudy and clear days, respectively). The horizontal leaf condensation was observed first near the south roof, whereas the vertical canopy had a longer LWD at 1 m from the ground (average value of 8 h). LWD was estimated using relative humidity thresholds (RMSE of 1.944 h on cloudy days and RMSE of 0.5 h on clear days), and the good agreement between measurements and estimation indicated that the 2D CFD model combined with the relative humidity threshold method could be used to estimate the temporal and spatial distribution of canopy LWD.

1. Introduction

The high humidity prevailing in greenhouses at night promotes leaf condensation (Mashonjowa et al., 2013), and leaf wetness duration (LWD),as a quantitative parameter for its description, plays an important role in crop disease early warning systems. Therefore, LWD can be monitored to determine the beginning of high-risk periods of infection (Mashonjowa et al., 2013) and facilitate regular interventions. However, using sensor measurements in greenhouses to obtain data has the disadvantage of requiring high economic inputs and instability, and simulation models based on agro-meteorological parameters are often used as an alternative to field measurements (Magarey et al., 2005; Wang et al., 2019). The existing LWD estimation models mostly use environmental data from a single location as input and assume that the spatial distribution of the greenhouse microclimate is homogeneous. For example, Parisa et al. (2019) evaluated the potential of four machine learning models and two climate reanalysis datasets for site-specific LWD estimation using nine weather stations in Alabama and six weather stations in California. Zito et al. (2020) installed leaf humidity sensors at four locations in a vineyard in Burgundy, France, and obtained daily data to develop a sinusoidal index model for estimating grape canopy LWD. However, this approach of considering temperature and humidity at a single point as unique values for the entire canopy does not apply to greenhouses with widely varying north–south structures. Furthermore, there is a continuous distribution of air flow in the

* Corresponding authors.
E-mail addresses: diaoming@shzu.edu.cn (M. Diao), lim@nercita.org.cn (M. Li).
[1] Chunhao Zhang and Ran Liu contributed equally to this work.

https://doi.org/10.1016/j.compag.2022.107257
Received 7 February 2022; Received in revised form 19 July 2022; Accepted 23 July 2022
Available online 31 July 2022

Nomenclature

C_p	specific heat, J kg^{-1} K^{-1}
r_a	canopy aerodynamic resistance, s/m
L_{ai}	leaf area index, 2.32 m^2 m^{-2}
T_L	leaf temperature, ℃
T_a	indoor air temperature, ℃
ρ	air density, kg m^{-3}
R_n	net radiation, W/m^{-2}
d	characteristic length of leaves, m
u	simulation velocity vector, m/s
Γ_φ	diffusion coefficient, m^2s^{-1}
S_φ	source term of φ, W/m^{-3}
φ	universal variable
Q_v	cold air permeability, kg m^{-3} s^{-1}
n_t	number of cold air exchanges, h^{-1}
v	greenhouse volume, 1077.3 m^3
RH	outdoor relative humidity, %
$RH_{2.5m}$	relative humidity in 2.5 m
Φ_x	ground heat flux, W/m^{-2}
P	atmospheric pressure, pa
$T_{2.5m}$	temperature in 2.5 m, ℃
k	turbulent kinetic energy, m2/s^{-2}
u_*	friction velocity, m/s
z_0	friction length, 0.02 m
T	outdoor air temperature, ℃
D_v	water vapor exchange rate, kg m^{-3} s^{-1}
H	absolute humidity of the outdoor air, kg m^{-3}
H_a	absolute humidity of the indoor air, kg m^{-3}
A_r	area of the south roof, 329.4 m^2
η_T	temperature difference coefficient, 0.16
V_e	outdoor wind speed, m/s
β	wind pressure coefficient, 0.22
η_r	seal of the roof to air permeability, 0.0005
S_k	source term of k, kg m^{-1} s^{-3}
S_t	source term of energy, W/m^{-3}
S_m	source term of momentum, kg m^{-2} s^{-2}
S_ε	source term of ε, kg m^{-1} s^{-3}
S_w	source term of water vapor, kg m^{-3} s^{-1}
RH_a	indoor relative humidity, %
RH_c	relative humidity in canopy
T_t	south roof surface temperature, ℃
T_n	north wall surface temperature, ℃
T_c	canopy temperature, ℃
U	wind speed at vertical entrance, m/s
ε	turbulent dissipation rate, m2/s^{-3}
K	von Karman constant, 0.42
z	vertical height, m

greenhouse environment with air and water vapor as the medium, causing variable heat and mass exchange; however, there is unevenness in the leaf microclimate in the greenhouse canopy, which is related to the heterogeneous distribution of the greenhouse climate (Liu et al., 2021).

Leaf condensation is caused by the exchange of energy and mass between crop environmental conditions, particularly at night when the canopy exchanges radiant heat with colder cover material or air, resulting in a canopy that is usually colder than the surrounding air (Mashonjowa et al., 2013). LWD estimation models based on this energy balance approach have been studied for several crops. Mashonjowa et al. (2013) used four methods to estimate rose canopy LWD and develop a greenhouse dynamic climate model (GDGCM) that calibrates leaf condensation thresholds. Leca et al. (2011) used the Penman-Monteith (PM) approximation equation to solve for steady-state evaporation and heat transfer from the leaf surface, combined with a fixed evaporation rate, to calculate the LWD in the apple canopy, and their overall LWD estimation results were more satisfactory. In this context, the heterogeneity distribution of canopy LWD can be obtained using a calculation method based on the entire canopy. Tong et al. (2007) simulated the dynamic change of temperature in a solar greenhouse by using a Computational Fluid Dynamics (CFD) unsteady method to solve the control equation. Boulard et al. (2017, 2010, 2002) developed a series of greenhouse microclimate simulation models considering the sensible and latent heat exchange between crops and the environment. Their models are typical methods for describing the distribution of temperature, pressure, and other environmental factors in a greenhouse, considering the mechanical interaction between the greenhouse, plant canopy, and flowing air. Using the aforementioned methods, Liu et al. (2021) developed a 3D model to simulate the microclimate distribution of solar greenhouses and used it as an input parameter for LWD. However, 3D simulation often requires a significant computational load. The 2D CFD model proved to be useful for studying the distribution of greenhouse microclimate (Boulard et al., 2010). Boulard et al. (2010) used the Euler equation in a 2D CFD greenhouse climate simulation model to simulate the diffusion of *Botrytis cinerea*. Bartzanas et al. (2004) used a 2D CFD model to study the effects of different vent configurations on greenhouse ventilation. 2D models are often used to determine the heterogeneity of greenhouse microclimates affected by cover materials (Zhang et al., 2016). However, few studies have considered the effect of greenhouse clusters on the environment inside the greenhouse, particularly during ventilation exchange, when the wind speed and direction at the vents can change, affecting the indoor temperature and humidity distribution (Chen et al., 2020; Stanciu et al., 2016). The CFD method developed by Boulard et al. (2010), which uses a post-greenhouse nursery in the calculation domain, is considered an applicable calculation method for a four-span compartmented plastic greenhouse but has not yet been applied to single-span solar greenhouse clusters.

In this study, we used the CFD method to account for the influence of greenhouse clusters, and two greenhouses in the front and back (3 m apart) were used as an indoor calculation domain to develop a 2D solar greenhouse microclimate distribution model at night. We performed transient distribution simulations of environmental factors such as air temperature and relative humidity, used the output of the microclimate distribution model as the input parameters of the LWD, and developed the LWD distribution model using the relative humidity threshold estimation method to accurately simulate the leaf wetness time. The purpose of the crop canopy spatial distribution was to simulate the effect of natural ventilation on cucumber leaf condensation in a solar greenhouse based on the wind direction and speed in summer in Beijing to provide a reference for the dehumidification control of the solar greenhouse.

2. Materials and methods

2.1. Experimental greenhouse

The experimental greenhouse was located in the Xiaotangshan National Precision Agriculture Experimental Base in the Changping District of Beijing, China (l40.18°N, 116.44°E). The greenhouse was a second-generation solar greenhouse with an east–west alignment and a front greenhouse 3 m away from the experimental greenhouse. The experimental greenhouse used solar energy and a building structure to maintain the proper temperature without a wet curtain on the side gable, fans, and heating equipment, and the upper and lower vents on the transparent roof were used for ventilation. The north wall was a 0.5-m-wide composite wall composed of bricks, lime mortar, and cement

mortar. A 0.005 mm thick polyethylene film was used as the front roof covering material, and the rear roof material was made of asbestos cement board. Table 1 lists the specific greenhouse structure parameters.

Cucumber cultivars, Lyujingling No.2, were transplanted from north to south in early March 2021, with a row spacing of 0.8 m, plant spacing of 0.4 cm, and ridge width of 0.8 m. To avoid differences in environmental monitoring owing to manual operations, environmental regulations were managed uniformly, following local summer solar greenhouse production practices, with vents fully opened at 6:30 for ventilation and closed at 18:30 for 12 h. On cloudy days, vents were opened at 8:30 and closed at 18:30 for 14 h.

2.2. Experimental device and method

Beijing is located in the northern part of the North China Plain, surrounded by mountains to the west and north and plains to the southeast, and is influenced by polar marine air masses in the summer, with warm and rainy weather (Liu et al., 2006). To verify the accuracy of the model under different weather conditions, experiments were conducted on 31 May to 1 June and 3–4 June 2021, with 1 June being a cloudy day and 4 June being a clear day.

This experiment aims to develop a model for the distribution of LWD in a typical solar greenhouse at night, considering the installation of sensor equipment, the collection of initial conditions with data validation, and the initial conditions in the front greenhouses. The vertical section in the middle of the east–west direction of the greenhouse (19 m from both walls) was the data measurement plane. Indoor ground heat flux measured using the HFP01SC heat flux sensor (Hukseflux Thermal Sensors, The Netherlands) was placed in the soil at a depth of 0.3 m. An SI-111 (Apogee Instrument Crop, USA) infrared thermometer was used to measure the temperatures of the south roof and north wall. The indoor air temperature and humidity were monitored using Davis Temp/Hum sensors (Davis Instruments, Hayward, USA), which were set at different heights (0.5, 1.5, and 2.5 m) at 1, 3.5, and 6 m from the north wall to measure air temperature and humidity at different locations in the room. The time interval for recording data at all measurement points was 15 min, and the input data were averaged hourly. The specific installation plan is shown in Fig. 1.

Cucumber LWD was visually determined at different canopy heights (0.5, 1, and 1.5 m) at 1, 3.5, and 6 m from the north wall for each vertical profile of temperature and humidity monitoring in the greenhouse crop area (F1, F2, F3, M1, M2, M3, B1, B2, and B3). Two cucumbers with the same plant height and leaf area were selected as the sampling plants, and cucumber leaves were observed and recorded from 19:30 to 8:30 the next morning. Observations were made once hourly to record the time when more than 10 % of the leaves of each cucumber plant were wet (LW) and the time when more than 90 % of the leaves became dry (LD). Then, the difference between LW and LD was computed as the wetness duration of the entire leaf (Li et al., 2010), taking the average of the wetness duration of two cucumber leaves at the same observation point.

2.3. LWD distribution model of solar greenhouse

The CFD method was used to simulate the transient and spatial distribution of environmental factors in the greenhouse, such as night air temperature and relative humidity, and the relative humidity threshold method was used to develop the LWD distribution model.

Table 1
Structural parameters of the experiment greenhouse.

Length	Span	Ridge	North wall	Sink	North roof angel	Vent size
38 m	7 m	3.5 m	2.7 m	0.8 m	30°	0.4 m

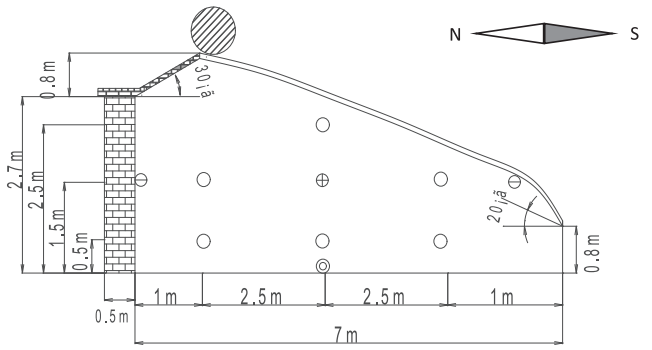

Fig. 1. Drawing of experimental greenhouse: T_a and RH_a sensors (○), T_a, RH_a, solar radiation sensors (⊕), infrared thermometer (⊖), and heat flux plates (◎).

2.3.1. Govern equations

The govern equations include the continuum, momentum, and energy conservation equations (Ren et al., 2015), as well as the k-ε supplementary-two-equation and the component transport equation for water vapor (Boulard et al., 2017).

$$\frac{\partial(\rho\phi)}{\partial t} + div(\partial\phi\vec{u}) = div(\Gamma_\phi grad\phi) + S_\phi \quad (1)$$

where ρ is the air density (kg m^{-3}), t is the time (s), $\vec{u}$ is the velocity vector (m s^{-1}), Γ_φ is the diffusion coefficient (m^{2}s^{-1}), S_φ is the general source term (Wm^{-3}), and φ is a universal variable representing the independent variable in the equations of conservation of mass, momentum, and energy.

2.3.2. Net radiation model

The absorption of radiation by the leaves is accompanied by the exchange of sensible and latent heat between the crop canopy and air, neglecting the latent heat loss caused by nighttime transpiration (Liu et al., 2021). Based on the interaction between crop and air, the net radiation model (Boulard et al., 2002) is given by the following equation:

$$R_n - \frac{\rho C_p L_{ai}(T_L - T_a)}{r_a} \quad (2)$$

where C_p is the specific heat of air under constant pressure (J kg^{-1} K^{-1}), r_a is the canopy aerodynamic resistance (s m^{-1}), L_{ai} is the leaf area index, T_L and T_a are the leaf and indoor air temperatures, respectively (K), and ρ is the air density (kg m^{-3}). The first term represents the net radiation (R_n W m^{-2}). The aerodynamic resistance of the leaf (Stanghellini et al., 1995) r_a is expressed as follows:

$$r_a = \frac{1174d^{0.5}}{(d|T_L - T_a| + 207u^2)^{0.25}} \quad (3)$$

where d is the characteristic length of cucumber leaves (m).

2.3.3. Air infiltration model

The airtightness of the enclosure structure, indoor and outdoor temperature differences, wind speed, and other environmental factors contribute to air infiltration. Therefore, to accurately calculate air infiltration of the greenhouse, the air infiltration model (Liu et al., 2021) was selected for calculation and solution. The specific equation is as follows:

$$Q_v = \frac{n_t}{3600}\rho C_p v(T - T_a) \quad (4)$$

where Q_v is the air infiltration rate (kg m^{-3} s^{-1}), n_t is the number of air exchanges (h^{-1}), v is the greenhouse volume (m^3), and T is the outdoor air temperature (K). The water vapor exchange rate (Liu et al., 2021)

was calculated using the following equation:

$$D_v = \frac{n_t}{3600}(H - H_a) \quad (5)$$

where D_v is the water vapor exchange rate (kg m^{-3} s^{-1}), H is the absolute humidity of the outdoor air (kg m^{-3}), and H_a is the absolute humidity of the indoor air (kg m^{-3}). Tong et al. (2007) determined the number of air changes in the solar greenhouse as 0.5 times/hour based on the degree of loss and space size of the greenhouse. The number of air exchanges in this experiment is affected by the transient changes in environmental factors such as indoor and outdoor temperature differences and air flow speed. A transient model is used to estimate the number of cold air exchanges (Liu et al., 2021) as follows:

$$n_t = A_r \eta_r \sqrt{\beta^2 V_e(t) + \eta_T^2 (T - T_a)}\ \frac{3600}{V} \quad (6)$$

where A_r is the area of the south roof (m^2), η_T is the temperature difference coefficient (dimensionless, 0.16), V_e is the outdoor wind speed (m s^{-1}), β is the wind pressure coefficient (dimensionless, 0.22), and η_r is the seal of the roof to air infiltration (dimensionless, 0.0005).

2.3.4. Source term

2.3.4.1. Momentum source term of crop area (S_m). The hypothetical crop area is a mixture of air and water vapor, similar to other domains. The momentum reduction caused by the drag effect of the crop (Boulard et al., 2002), that is, S_m, is expressed using the following equation:

$$S_{m(x,y)} = -LADC_d \overrightarrow{u}^2 \quad (8)$$

where $S_{m(x,y)}$ is the source term of the momentum drop of the fluid in each direction (x and y) of the crop area (kg m^{-2} s^{-2}), C_d is the drag coefficient (0.32), and LAD is the leaf area density (m^{-1}).

2.3.4.2. Turbulence source terms (S_k and S_ε). The turbulence kinetic energy equation and turbulence dissipation rate equation source terms (Boulard et al., 2017) are expressed as follows:

$$S_k = \rho C_d LAD \overrightarrow{u}^3 - 4\rho C_d LAD \overrightarrow{u} k \quad (9)$$

$$S_\varepsilon = \frac{3}{2}\rho \frac{\varepsilon}{k} C_d LAD \overrightarrow{u}^3 - 2.4\rho C_d LAD \overrightarrow{u} \varepsilon \quad (10)$$

where S_k is the source term of the turbulence kinetic equation (kg m^{-1} s^{-3}) and S_ε is the source term of the turbulence dissipation rate equation (kg m^{-1} s^{-3}).

2.3.4.3. Energy source term (S_t) and water vapor source term (S_w). The energy source terms (Boulard et al., 2017) include sensible heat exchange and air infiltration heat exchange. The specific equation is as follows:

$$S_t = \frac{\rho C_p L_{ai}(T_L - T_a)}{r_a} - Q_v \quad (11)$$

The water vapor source term per cubic meter (Boulard et al., 2017) is calculated as follows:

$$S_w = -D_v \quad (12)$$

where D_v is the water vapor exchange rate (kg m^{-3} s^{-1}).

2.3.5. LWD model

Empirical models, such as the constant relative humidity threshold estimation method, are highly site-specific and require site-specific calibration. Li et al. (2010) conducted an experiment and obtained a threshold value of 89 % for an estimation model of LWD. When the relative humidity of the air in the greenhouse was greater than or equal to 89 %, the time of condensation was recorded. When the relative humidity of the air was <89 %, the drying time was recorded. LWD was defined as the number of hours greater than or equal to a constant threshold.

2.3.6. Boundary and initial conditions

The simulation starts after sunset when the windows was closed and continues until sunrise when the windows was opened. Because the outdoor wind direction during the test time was mostly southerly, perpendicular to the span axis and the south roof surface, the south-facing boundary was set as the velocity inlet and the north-facing boundary as the pressure outlet. No solar radiation was required at night, the north wall and south roof were used as constant temperature boundaries, the ground served as a constant heat flux boundary, the hourly mean wall temperature and heat flux were measured using sensors and used as boundary input, and the south roof served as a fluid–solid coupling surface. The sample time was 60 s, and the specific initial and boundary conditions (real-time input based on sensor data) are listed in Table 2.

The near-surface air flow is continuously influenced by surface constituents and obstacles, the inlet velocity profile at the left-hand boundary of the region (Fig. 2) has been adjusted according to the following equation (Boulard et al., 2010):

$$U = \frac{u_*}{K} ln(\frac{z}{z_0}) \quad (13)$$

where U is the wind speed at vertical entrancen (m/s); u_* is the friction velocity (m/s); K is the von Karman constant (0.42); z_0 is the friction length (0.02 m); and z is the vertical height (m). The turbulent kinetic energy (k) and the turbulent dissipation rate (ε) are described by the following expressions (Boulard et al., 2010):

$$k = \frac{u_*^2}{\sqrt{C_\mu}} \quad (14)$$

$$\varepsilon = \frac{u_*^3}{K(z + z_0)} \quad (15)$$

where C_μ is the standard k-ε model constant, 0.09.

2.3.7. Computational domain and convergence index

The ANSYS ICEM 13.0 software was used to develop a geometric model (2D) based on the actual greenhouse size. The calculation domain consists of three parts: the front greenhouse, the experimental greenhouse, and the outdoor calculation domain (Fig. 2). Taking into account the effect of gravity (g = −9.8 m s^2, multiplied by air density in the momentum govern equation for buoyancy effects), a transient atmospheric airflow field was simulated using the wind speed and direction measured by the weather station in the outdoor area. Additionally, the radiative heat exchange between the canopy and structure was calculated using the DO radiation model. Based on the above geometric model construction method, a calculation domain of 70 m long and 30 m high, including the greenhouse, was used, with the indoor crop rows were simplified to a rectangle of 5 m long and 1.5 m high. After the grid independence test, the final grid overview was 61,711 grids, of which 49,637 and 12,074 were in outdoor and indoor areas, respectively. The convergence criterion for the mass, momentum, and turbulence complementary equations was 10^{-3}, whereas for the energy and species transport equations was 10^{-6}, and convergence was reached after approximately 20 iterations in each time.

3. Results

The indoor night simulation results from May 3 to June 1, 2021, and from June 3 to June 4, 2021, were verified. The vents were closed at night. Between June 3 and June 4, 2021, the weather was fair. Because

Table 2
Boundary and initial conditions. T_t is the south roof surface temperature; Φ_x is the ground heat flux; T_n is the north wall surface temperature; T_a, RH_a, and V_e is the outdoor temperature, relative humidity and wind speed; T and RH is the indoor temperature and relative humidity; P is the atmospheric pressure.

Time	Boundary conditions						Initial conditions		
	South roof	Ground	Wall	Inlet and outlet Boundary			Indoor		Whole
	T_t	Φ_x	T_n	T_a	RH_a	V_e	T	RH	P
18:30 (5.31)	20.3℃	−0.539 W m^{-2}	25.8℃	15.4℃	88 %	0.11 m s^{-1}	21.5℃	88.8 %	101750pa
18:30 (6.3)	23.1℃	−7.554 W m^{-2}	31.4℃	33℃	24 %	0.4 m s^{-1}	25.4℃	50.8 %	101210pa

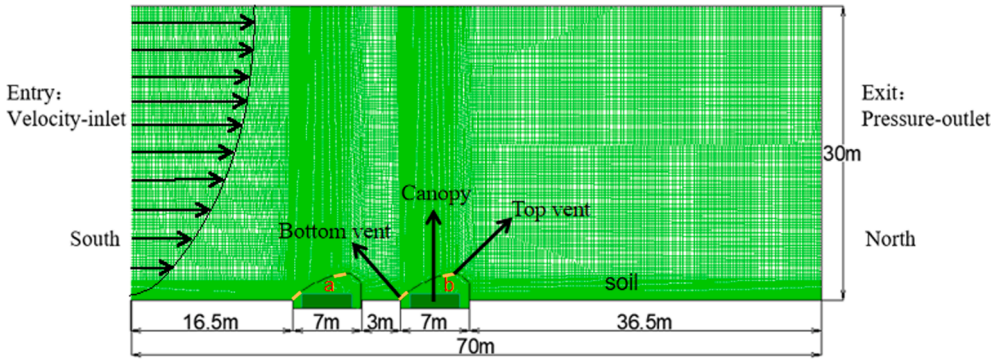

Fig. 2. Computational domain: (a) front greenhouse and (b) experimental greenhouse.

there were fewer cumulus clouds during the day, it is considered more suitable for transient simulation studies on clear nights. May 31 to June 1, 2021, were typical cloudy days, with an average outdoor relative humidity of 92.08 %.

3.1. Simulation and verification of air temperature and relative humidity

To simulate the indoor environmental distribution more realistically, a leaf-wall net radiation model and a sensible heat exchange model were added to the source term, and the equilibrium relationship between leaf temperature and air temperature was calculated. The results of the cloudy day calculations are shown in Fig. 3. The area near the south roof had a lower temperature and higher humidity, and the horizontal temperature and humidity distribution pattern was as expected. However, the vertical simulation model reduced the difference in humidity between the canopy and the upper 2.5 m of the canopy, as shown by the mean-simulated value of RH_c-$RH_{2.5\ m}$ = 0.22 % compared with the measured value of RH_c-$RH_{2.5\ m}$ = 4.3 %. Based on the results of this temperature and humidity distribution simulation, the indoor area was divided into two: the crop canopy (0–1.5 m) and above the canopy (2.5 m), and the average values of the measured points in the area were used for verification. Fig. 4 compares the simulated and measured results in the two areas from 19:30 to 8:30. The temperature at night decreased significantly (approximately 5.7 °C) because of the weak radiation, showing the same trend as the simulation results (approximately 4.7 ℃). Owing to the small difference between indoor and outdoor relative humidity (4.2 %), the humidity with time curve tends to be flat (Fig. 4). As shown in Table 3, the model had higher accuracy for calculating canopy temperature and humidity, and the root mean square error (RMSE) was 0.55 ℃ and 2.58 %, respectively.

Similar to cloudy conditions, the model reduced the difference in humidity between the top and bottom of the canopy under fair weather conditions (Figs. 5 and 6), as shown by the mean-simulated value of RH_c-$RH_{2.5\ m}$ = 0.7 % compared to the measured value of RH_c-$RH_{2.5\ m}$ = 2.4 %. The humidity simulation showed a large error before 21:30, with a maximum absolute error of 17.88 % in humidity on clear days. The saturated water vapor pressure and atmospheric pressure in this test were defined and kept constant in the User Defined Function (UDF) by hourly sensor data assignment rather than transient calculations using the relevant model values, and the lack of model specificity was caused by the large variability in environmental parameters from evening to night, resulting in large model errors in the evening. Shorter time steps

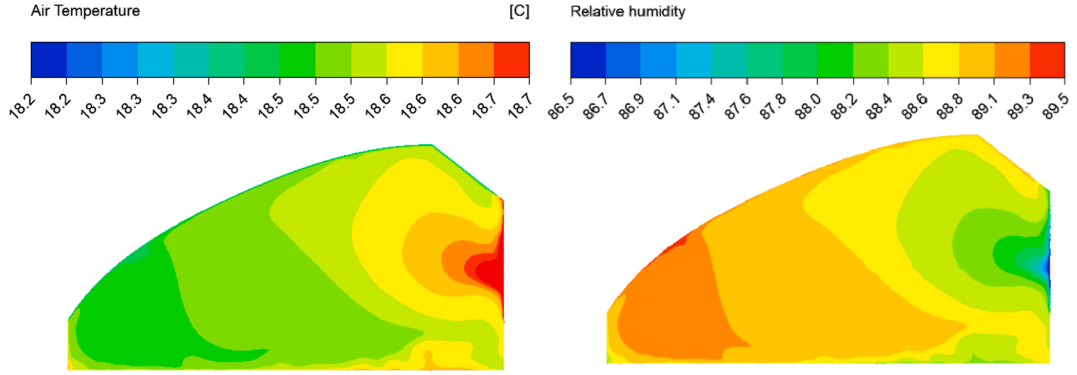

Fig. 3. Contour of simulated in greenhouse at 5.31–6.1–21.30.

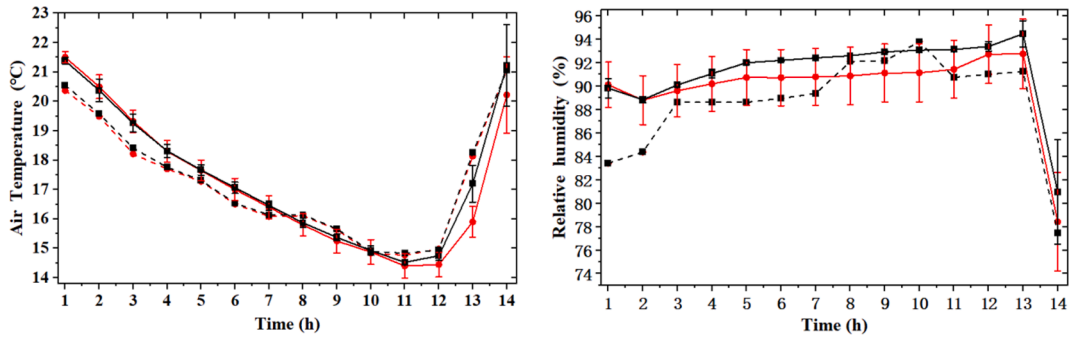

Fig. 4. Air temperature and humidity at indoor and canopy at 5.31–6.1: (—●—) simulated temperature and humidity at canopy, (—●—) measured at canopy, (—■—) simulated temperature and humidity at 2.5 m, (—■—) measured at 2.5 m. The measured values are averaged use four acquisitions per hour, so error lines have been added to the graph.

Table 3
Calculation error index. T_c and RH_c is the temperature and relative humidity in canopy; $T_{2.5\ m}$ and $RH_{\ 2.5\ m}$ is the temperature and relative humidity in 2.5 m.

Index	5.31–6.1				6.3–6.4			
	Air inside the canopy		Air above the canopy		Air inside the canopy			Air above the canopy
	T_c	RH_c	$T_{2.5\ m}$	$RH_{\ 2.5m}$	T_c	RH_c	$T_{2.5m}$	$RH_{2.5m}$
MIE	0.03℃	0.68 %	0.04℃	0.50 %	0.25℃	1.01 %	0.3℃	0.09 %
MAE	1.06℃	6.69 %	2.23℃	6.39 %	1.93℃	7.91 %	3.06℃	17.88 %
ME	0.47℃	2.05 %	1.13℃	2.71 %	0.97℃	3.32 %	1.15℃	5.2 %
RMSE	0.55	2.58	0.88	3.11	1.1	3.97	1.36	7.30

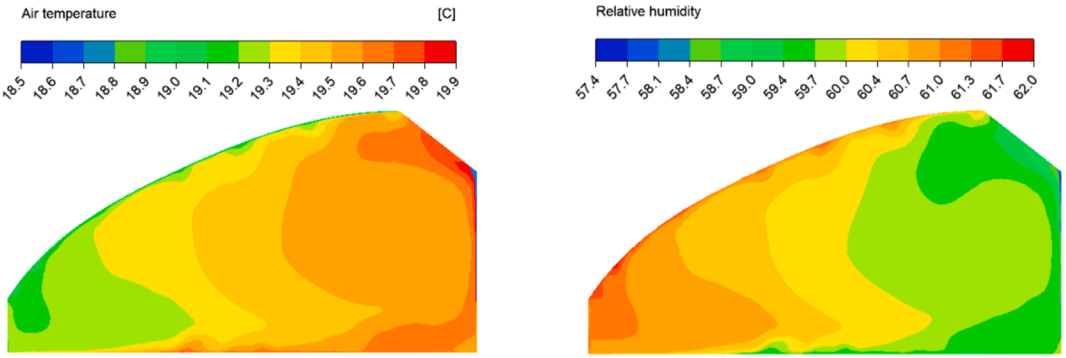

Fig. 5. Contour of simulated in greenhouse at 6.3–6.4–21.30.

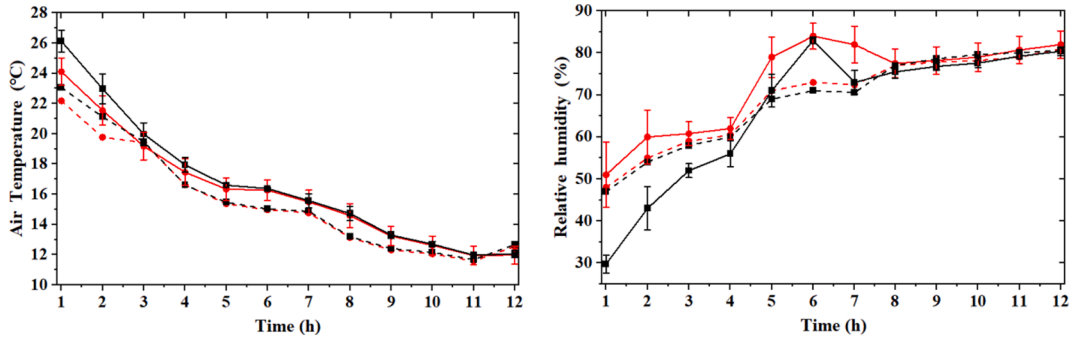

Fig. 6. Air temperature and humidity at indoor and canopy at 6.3–6.4: (—●—) simulated temperature and humidity at canopy, (—●—) measured at canopy, (—■—) simulated temperature and humidity at 2.5 m. (—■—) measured at 2.5 m. The measured values are averaged use four acquisitions per hour, so error lines have been added to the graph.

appeared to improve the computational accuracy of the model throughout the simulation, but they were not conducive to farmers applying the model to actual production.

3.2. Simulation and verification of LWD

The use of canopy relative humidity as a criterion for judging leaf condensation in this experiment has a direct effect on the overall assessment of the LWD distribution model. As shown in Table 3, the model provided greater accuracy in calculating canopy relative

humidity. Even though the evening had a large error (6.69 %, 17.88 %), by comparing the extensive literature with actual measurements (Mashonjowa et al., 2013; Wang et al., 2019; Liu et al., 2021), most of the leaves showed that they were not moistened or dried at that time. Additionally, based on the relationship between the measured and simulated RH values for most of the time (simulated <= measured < 89 %), the simulated results were similar to the measured results and were therefore considered to have a low impact on the LWD distribution model. The indoor nighttime simulation results were validated for 31 May – 1 June 2021 (cloudy) and 3 June – 4 June 2021 (clear day), respectively. The leaf condensation distribution models (0.5, 1, and 1.5 m) were comprehensively evaluated using validation metrics such as accuracy, precision, and recall. To accurately verify the model simulation results of LWD, the three observation areas (F, M, and B, where area F was near the south roof and area B was near the north wall) were divided into nine areas, F1, F2, F3, M1, M2, M3, B1, B2, and B3 (Fig. 7), according to the crop canopy height (0.5, 1, and 1.5 m), and the simulation results of LWD in these nine areas were taken as the mean value. The validation results are shown in Figs. 8 and 9.

The simulation results of the dew condensation distribution on the leaf surface for 12 h at night and 2 h after sunrise were verified, as shown in Fig. 8. The simulation and observation of the leaf surface condensation-level distribution trend revealed that the area near the south roof of the greenhouse (F) at night was more likely to cause leaf condensation than the area near the north wall (B). This was because of the relatively low temperature owing to higher convective heat transfer near the southern roof area, the saturated water vapor pressure decreases with temperature, and the rapid rise in relative humidity. The temperature decrease at the north wall and ground lagged behind the indoor air at night, causing leaf condensation to appear first in areas F1, F2, F3, and M3 near the south roof and ground, as shown in Fig. 9.

In the measured LWD data, it was found that F2(10 h) > F1(8.5 h), F3 (6.5 h), and similar situations also appeared in the M and B regions; however, this distribution was not present in the model. One reason for this was that the simulation model reduced temperature and humidity differences between the top and bottom of the canopy. The large temperature and humidity distribution differences in the actual canopy resulted in local condensation (Liu et al., 2021). Another reason was that in the cloudy night ($TL < Ta$), the energy exchange source term was negatively correlated with the leaf area index, as shown in Equation (11). The relatively large leaf area at 1 m in the canopy facilitated the interception of roof condensation droplets, while resulting in a higher heat loss. The leaf area data of each point on June 2nd was measured (1.5-m leaf area: 0.0221 m^2, 1-m leaf area: 0.0766 m^2, 0.5-m leaf area: 0.0828 m^2), and the model used the overall leaf area average value to calculate the L_{ai} (2.32 m^2/m^2). This further complicates and reduces the accuracy of the vegetation LWD simulation. For example, it may underestimate the heat loss of 0.5 m and 1 m and consequently transfer this part of the heat loss to 1.5 m. The simulation results for 12 h on a clear day and night are shown in Fig. 9. Leaf condensation did not occur in the simulated results because of the low relative humidity (simulated values, measured values < 89 %). A higher LWD was observed in zone F2 (1.5 h) than in zones F1 and F3 (0 h), most likely because of the condensation dripping from the southern roof, as the southern crop canopy was closer to the southern roof skeleton structure.

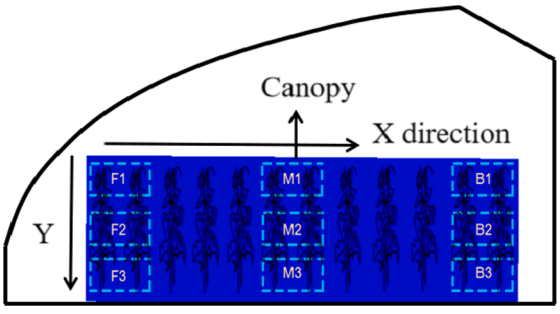

Fig. 7. Vertical distribution of the cucumber canopy: F1, F2, F3, M1, M2, M3, B1, B2, and B3 are the observation areas.

Table 4 and Fig. 10 show the validation results where the LWD estimation models based on relative humidity thresholds for LWD are higher than the measured values, cloudy days reached 1.944 h. Although the mean clear day LWD error was only 0.166 h, this was caused by individual and sample variation (LWD error in the F2 region was averaged over nine regions) and did not represent a more accurate estimate of clear day LWD. In the calculation for cloudy days, the average error in the F2, M2, and B2 regions was the smallest (0, 0, and 0.5 h), while the average error in the F1, M1, and B1 was the largest (1.5, 4.5, and 4.5 h). As mentioned above, this was related to the parameter input of the model in the crop area, where the measured leaf area in the F2, M2, and B2 areas (0.0766 m^2) was closer to the mean canopy leaf area (0.0764 m^2), while the measured leaf area in the F1, M1, and B1 areas was only 0.0221 m^2; therefore, the method for representing the mean canopy leaf area for the entire canopy was considered the main reason for this difference. In the actual process (Mashonjowa et al., 2013), LWD depends on leaf orientation, leaf age, individual physiological factors, and environmental factors. Because these conditions were different for each leaf, the LWD measured visually was inevitably scattered, and the model did not consider the effect of feature differences and lacked some specificity. The results showed that even if there were errors in the calculation data of the model, the overall accuracy was acceptable (cloudy was 83.2 % and clear was 98.6 %). Therefore, the 2D CFD model was found to be useful for simulating and estimating the distribution of leaf condensation and LWD in a greenhouse.

3.3. Effect of ventilation on leaf condensation

Based on the verification of the leaf condensation model, to analyze the influence of ventilation on the leaf condensation, the model used the same boundary and initial conditions, as shown in Table 2; only the boundary type at the vent was changed.

The external wind speed has a strong influence on the formation mechanism and distribution characteristics of the microclimate in a greenhouse (Xue et al., 2019). Ventilation at different wind speeds would result in variable humidity distributions, which might affect leaf condensation. Therefore, the flow field distribution in the greenhouse must first be determined. In contrast, finite element methods have proven to be more appropriate for modeling greenhouse airflows (Molina-Aiz et al., 2010). As shown in Fig. 11, the airflow patterns observed in the two greenhouse (a and b) simulations are very different. The air entered greenhouse (a) through the bottom vent and exited through the top vent, the internal air circuit rotated counterclockwise, and the average wind speed in the room was 0.31 m s^{-1}, with the maximum wind speed occurring at the bottom vent (0.47 m s^{-1}). Air entered the greenhouse through the upper vents, moved horizontally along the floor, and exited through the bottom vents. The internal air circuit rotated counter-clockwise, and the average wind speed in the room was 0.24 m s^{-1}, with the top vents experiencing the highest wind speed of 0.39 m s^{-1}. Air was circulated between the vents, the internal walls, and the soil surface in both greenhouses, and a clockwise rotated air circuit was formed at 3 m intervals between the two greenhouses. The disturbed effect on the airflow between adjacent greenhouses or walls (caused by pressure changes) was the direct cause of the vortex field of gases, causing this part of the airflow to move around the vortex center (Qi et al., 2012), creating a return flow at the top vent of the greenhouse (b), resulting in different airflow patterns in the two greenhouses. This was similar to the simulated results of Azi et al. (2010) for two separate compartments in a continuous greenhouse under windward conditions. In the simulation results, when the leaves started to condense (22:30 at night), the upper and lower vents were opened to ventilate and dehumidify under the influence of this greenhouse cluster

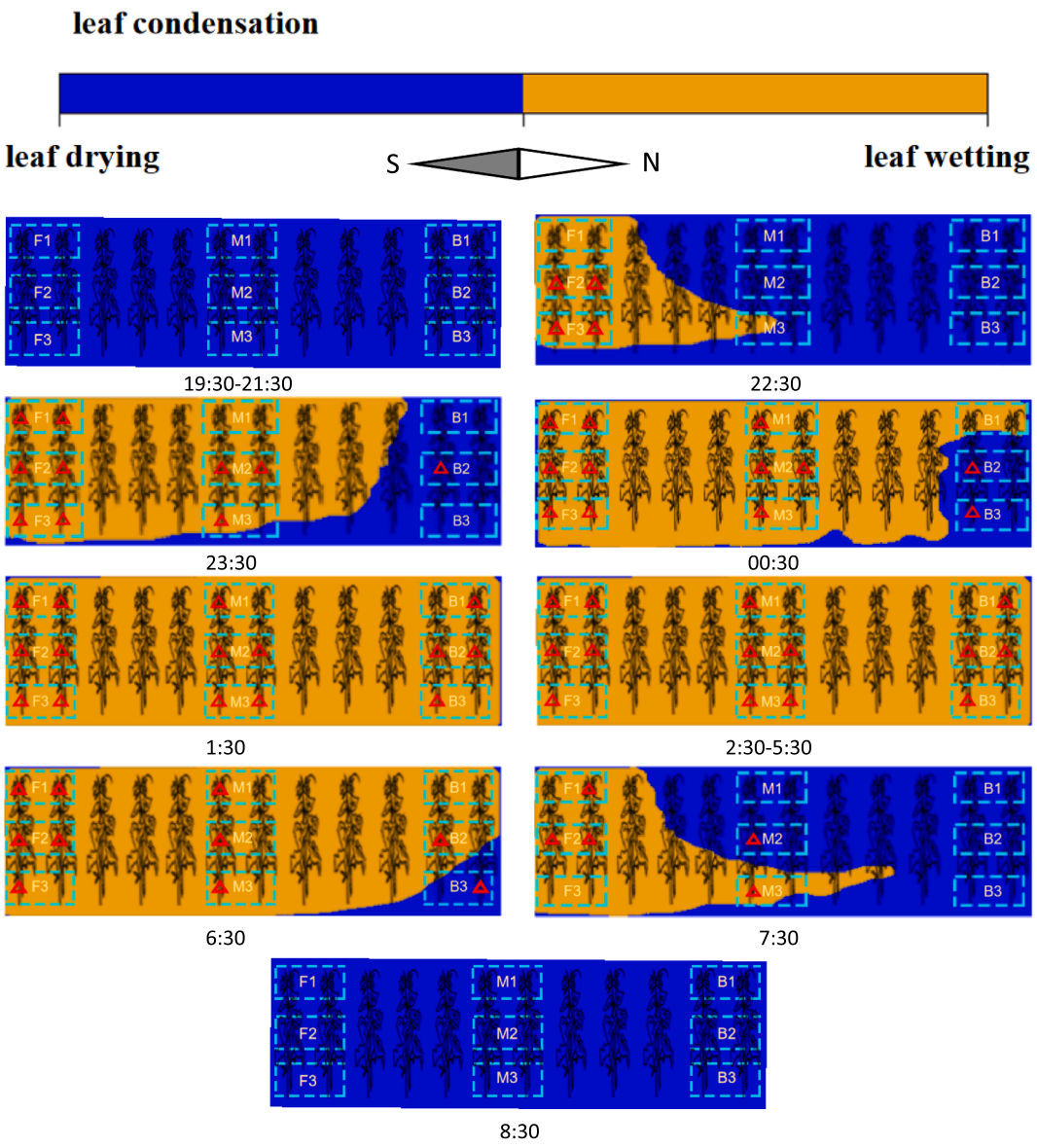

Fig. 8. Contour of simulated leaf condensation of distribution on the canopy on cloudy days: (■ ■) is the observation area. (△) indicates that the leaf is wet at this point.

to analyze the effect of ventilation on the leaf condensation. After the leaves were dry (00:30 at night), the vents were closed to reduce heat loss. The simulation results of leaf condensation are shown in Fig. 12.

After opening the vents (22:30–00:30), the surface of the leaves gradually changed from condensation to dryness owing to the combined effect of the difference between indoor and outdoor relative humidity (indoor was 88.62 % and outdoor was 86.42 %) and air flow (Fig. 12). In F3, M3, and other areas near the bottom of the vent and the ground, the leaf became dry first, which was related to the indoor transient air flow because the area near the ground and vent had higher air velocity (0.26 m s^{-1}, 0.34 m s^{-1}). As the ventilation time increased, the indoor relative humidity stabilized (87.89 %). After closing the vents (00:30–1:30), the indoor humidity rose rapidly to 90.83 %, and leaf condensation occurred at 1:30. Although ventilation effectively reduced the humidity of the indoor air to achieve dehumidification, it was inevitably accompanied by heat loss. During the ventilation period, the indoor temperature dropped from 17.15 ℃ to 15.3 ℃, a decrease of 1.85 ℃. Even with the vent closed, the indoor temperature continued to drop (decreased by 0.36 ℃) at this time owing to the temperature difference between indoor and outdoor (2.1 ℃). The results showed that ventilation could be used as a night dehumidification method for solar greenhouses, but the temperature drop caused by it needs to be addressed.

4. Discussion

This study supported the hypothesis that accounting for greenhouse clustering effects, combined with an energy balance approach and site-specific calibrated empirical model thresholds, could simulate canopy leaf wetting distributions more accurately. Similar to the research results of Marta et al. (2005), the estimated error of the model constructed in this study was approximately 1–2 h. Most of the time (cloudy), the model overestimated the LWD (the average absolute error was 1.944 h). This might be related to the identification of physiological characteristics such as leaf orientation, leaf age, and individual physiological differences (Mashonjowa et al., 2013). Sentelhas et al. (2004) used sensor location, internal design, and surface material composition to approximate the true leaf inclination and physical characteristics to accurately measure leaf condensation. Wang et al. (2011) analyzed the correlation between root pressure, xylem osmotic pressure, and leaf exudate of different bamboo varieties in Asia. It appeared to be more conducive to

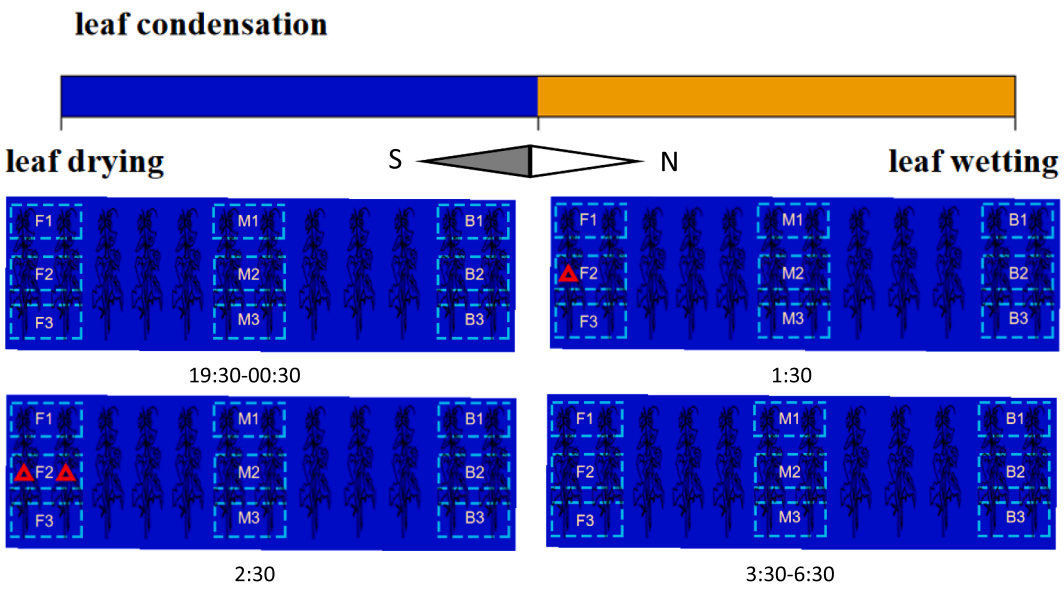

Fig. 9. Contour of simulated leaf condensation of distribution on the canopy on clear days: (■ ■) is the observation area; (△) indicates that the leaf is wet at this point.

Table 4
Leaf condensation.

Time	Leaf condensation Validation		
	Accuracy (%)	Precision (%)	Recall (%)
5.31–6.1	81.79	72.4	94.3
6.3–6.4	98.58	—	—

leaf exudates when xylem osmotic pressure was greater than the root pressure. External factors such as soil water potential and inorganic salt content would affect root pressure (Meychik et al., 2021). Because of this individual difference, the simulation of canopy LWD became more complicated, reducing the accuracy and robustness of the empirical model. Li et al. (2010) developed a solar greenhouse LWD estimation model based on canopy relative humidity. The estimation error is approximately 2 h. Based on this error, even if the simulated value of canopy relative humidity was classified correctly in the empirical threshold most of the time (analog value <= measured value < 89 % or 89 % < analog value <= measured value), it might still cause errors in the LWD simulation. Owing to the lack of specificity of the model, a few times (clear days) the model underestimated the LWD (0.5 h). In addition to the above reasons, the leaf is not the only source of moisture (Liu et al., 2021). Other potential water sources exist, such as the greenhouse skeleton structure. This situation can also occur if the condensation water on the cladding material fell on crop leaves (Mashonjowa et al., 2013). Ali et al. (2014) simulated roof condensation in a glass greenhouse. Hernandez et al. (2017) evaluated fixed anti-leakage nets and mobile devices. The interception effect of the greenhouse microclimate reduced condensation drips while effectively reducing canopy air humidity (up to 5 %).

In this study, the LWD estimation model was based on 2D CFD and transient analysis to obtain temperature, humidity, and LWD distribution, as opposed to empirical methods that require a large amount of data input, with a certain degree of portability, but still requires calibration of the site-specific leaf condensation threshold. The LWD estimation results were considered to meet the requirements for early warning of most high-humidity diseases in solar greenhouses because the infection of cucumber downy mildew required at least 2 h of LWD

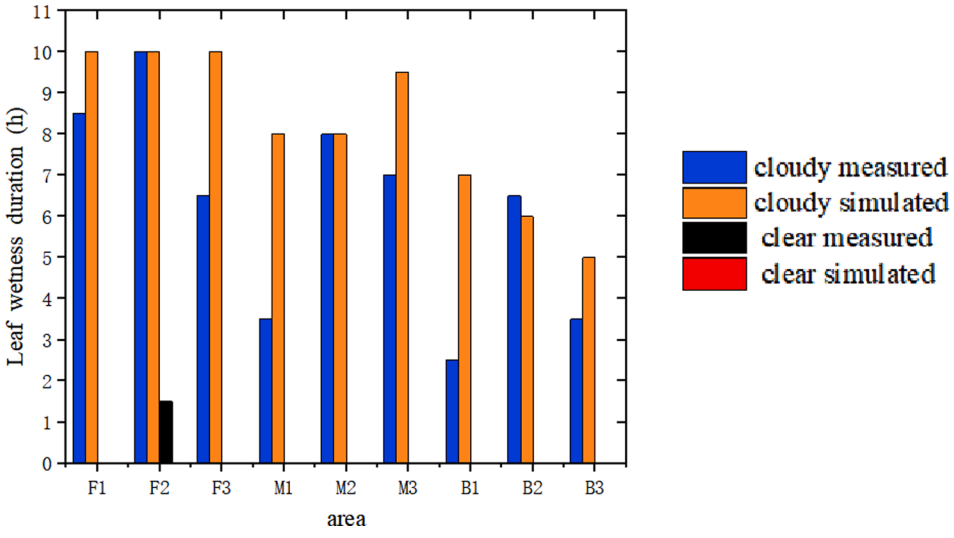

Fig. 10. LWD validation.

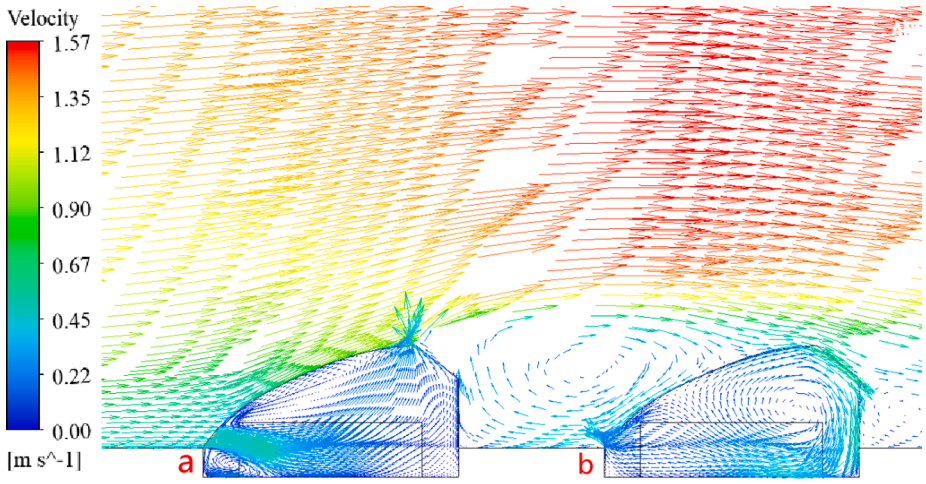

Fig. 11. Simulation of indoor and outdoor flow field under ventilation conditions: (a) front greenhouse, (b) experimental greenhouse.

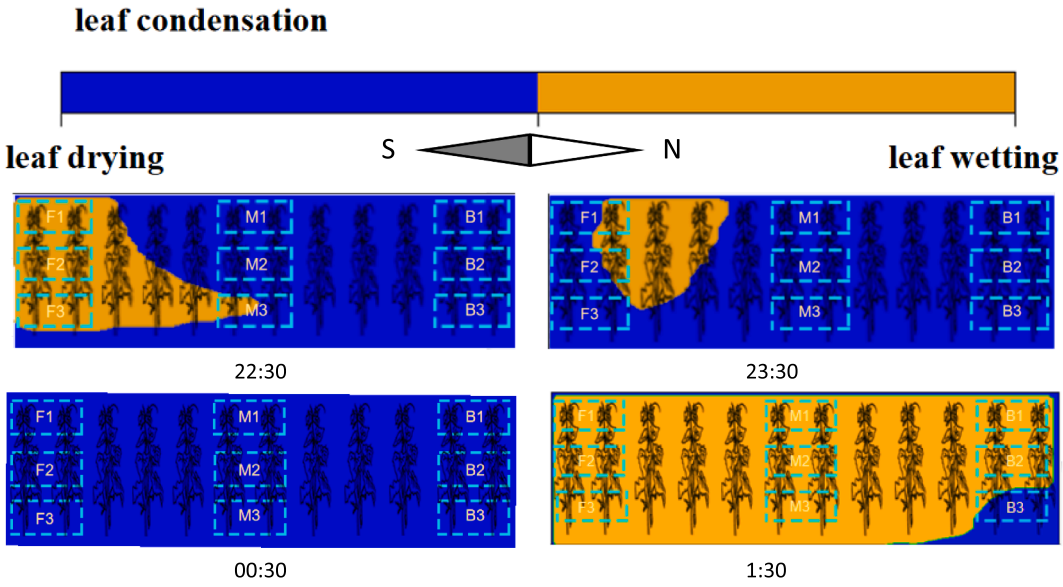

Fig. 12. Contour of simulated leaf wetness of distribution on the canopy under ventilation conditions: (■ ■) is the observation area.

(Shi et al., 2005), whereas the occurrence of cucumber gray mold required 7 h of LWD (Yunis et al., 1994). The errors in the model were compared with the 3D CFD model (Liu et al., 2021) via a similar modeling approach, using environmental parameters as inputs to the LWD estimation model; the average error in the calculation was 1.25 h, which was close to the error calculated in this study (1.944 h), and although the 2D model reduced the accuracy, it applied less grid and was able to perform the overall LWD of the canopy estimation. Based on the validation of the LWD estimation model, it was used to investigate the effect of ventilation exchange on leaf dehumidification, with immediately adjacent greenhouses 3 m apart significantly affecting the wind direction at the test greenhouse vents (Fig. 11). The results showed that short-term ventilation could be used as a method for nighttime dehumidification in heliotrope greenhouses, but it reduced the room temperature (1.85 ℃), which significantly reduced the chlorophyll content of cucumber (Li et al., 2021), and negatively affected the net photosynthesis of cucumber the next day (Miao et al., 2009). Therefore, the next experiments need to find a balance between the required room temperature and ventilation and dehumidification of the crop and apply this to the simulation of greenhouse clusters.

5. Conclusion

Combined with the current domestic and foreign related research, this study has made some contributions as the following:

(1) Evaluated the air temperature and relative humidity inside the solar greenhouse at night using a 2D CFD model.

(2) Using the simulated value of environmental parameters as input, combined with the empirical model threshold to simulate the distribution of leaf condensation, a visual observation method was used to observe the leaf condensation, and the results were compared with the simulation results.

(3) Using the results of leaf condensation at each point, we calculated the LWD at this point and divided it into nine areas for verification. The average error of cloudy days was 1.944 h, while the average error of clear days was 0.166 h.

(4) Based on the verification of the LWD estimation model, the dew condensation distribution of cucumber crop leaves under natural ventilation conditions was simulated. The two-hour ventilation could help dehumidify the greenhouse at night.

The simulation results showed that the development of a 2-D CFD greenhouse climate model could help calculate the LWD distribution of

the cucumber canopy as a component of the LWD estimation model, which agrees well with the measured data. Farmers could use the measured climate data inside and outside the greenhouse to estimate the indoor microclimate distribution canopy LWD, which could then be combined with disease prediction models to predict and prevent the occurrence of certain climate-related diseases, such as downy mildew and powdery mildew. Furthermore, the 2D CFD model was considered relatively simple in terms of numerical complexity, allowing it to be integrated into the greenhouse climate control system as an auxiliary means of suppressing the development and spread of plant diseases.

CRediT authorship contribution statement

Chunhao Zhang: Methodology, Software, Validation, Investigation, Writing – original draft. **Ran Liu:** Methodology, Software, Investigation. **Kaige Liu:** Methodology, Investigation. **Xinting Yang:** Supervision, Project administration, Funding acquisition. **Huiying Liu:** Supervision, Project administration, Funding acquisition. **Ming Diao:** Supervision, Funding acquisition. **Ming Li:** Conceptualization, Investigation, Supervision, Project administration, Funding acquisition, Writing – original draft, Writing – review & editing.

Declaration of Competing Interest

The authors declare that they have no known competing financial interests or personal relationships that could have appeared to influence the work reported in this paper.

Data availability

The data that has been used is confidential.

Acknowledgement

This work was funded by the Science and Technology Innovation Capacity Building Project of Beijing Academy of Agriculture and Forestry Sciences (No. KJCX20211002); Youth Program of National Natural Science Foundation of China (31401683); and the FP7 Framework Program (PIRSES-GA-2013-612659).

References

Ali, H.B., Bournet, P.E., Danjou, V., Morille, B., Migeon, C., 2014. CFD simulations of the night-time condensation inside a closed glasshouse: sensitivity analysis to outside external conditions, heating and glass properties. Biosyst. Eng. 127, 159–175. https://doi.org/10.1016/j.biosystemseng.2014.08.017.

Bartzanas, T., Boulard, T., Kittas, C., 2004. Effect of vent Arrangement on windward ventilation of a tunnel greenhouse. Biosyst. Eng. 88 (4), 479–490. https://doi.org/10.1016/j.biosystemseng.2003.10.006.

Boulard, T., Roy, J.C., Fatnassi, H., Kichah, A., Lee, I.B., 2010. Computer fluid dynamics prediction of climate and fungal spore transfer in a rose greenhouse. Comput. Electron. Agric. 74 (2), 280–292. https://doi.org/10.1016/j.compag.2010.09.003.

Boulard, T., Roy, J.C., Pouillard, J.B., Fatnassi, H., Grisey, A., 2017. Modelling of micrometeorology, canopy transpiration and photosynthesis in a closed greenhouse using computational fluid dynamics. Biosyst. Eng. 158, 110–113. https://doi.org/10.1016/j.biosystemseng.2017.04.001.

Boulard, T., Wang, S., 2002. Experimental and numerical studies on the heterogeneity of crop transpiration in a plastic tunnel. Comput. Electron. Agric. 34 (1–3), 173–190. https://doi.org/10.1016/S0168-1699(01)00186-7.

Chen, J.T., Ma, Y.W., Pang, Z.Z., 2020. A mathematical model of global solar radiation to select the optimal shape and orientation of the greenhouses in southern China. Sol. Energy 205, 380–389. https://doi.org/10.1016/j.solener.2020.05.055.

Hernández, J., Bonachela, S., Granados, M., López, J.C., Magán, J.J., Montero, J.I., 2017. Microclimate and agronomical effects of internal impermeable screens in an unheated mediterranean greenhouse. Biosyst. Eng. 163, 66–77. https://doi.org/10.1016/j.biosystemseng.2017.08.012.

Leca, A., Parisi, L., Lacointe, A., Saudreau, M., 2011. Marc Saudreau, Comparison of Penman-Monteith and non-linear energy balance approaches for estimating leaf wetness duration and apple scab infection. Agric. For. Meteorol. 151 (8), 1158–1162. https://doi.org/10.1016/j.agrformet.2011.04.010.

Li, M., Zhao, C.J., Qiao, S., 2010. Estimation model of leaf wetness duration based on canopy relative humidity for cucumbers in solar greenhouse. Transactions of the CSAE, 26(9), 286-291. https://t.cnki.net/kcms/detail?v=3uoqIhG8C44YLTlOAiTRKgchrJ08w1e7_IFawAif0my&uniplatform=NZKPT.(In Chinese).

Li, Y.L., 2021. Effects of low temperature and poor light on photosynthesis of cucumber seedlings. South China Agriculture, 15(21), 6-7+10. https://t.cnki.net/kcms/detail?v=3uoqIhG8C44YLTlOAiTRKibYlV5Vjs&uniplatform=NZKPT.(In Chinese).

Liu, X.M., Hu, F., Li, L. Wang, Y., 2006. Summer urban climate trends and environmental effect in the Beijing area. Chin. J. Geophys., (03), 689-697. https://t.cnki.net/kcms/detail?v=3uoqIhG8C44YLTlOAiTRKgchrJ0&uniplatform=NZKPT.(In Chinese).

Liu, R., Liu, J., Liu, H.Y., Yang, X.T., Bárcena, J.F.B., Li, M., 2021a. A 3-D simulation of leaf condensation on cucumber canopy in a solar greenhouse. Biosyst. Eng. 210, 310–329. https://doi.org/10.1016/j.biosystemseng.2021.08.008.

Liu, R., Li, M., Guzmán, J.L., Rodríguez, F., 2021b. A fast and practical one-dimensional transient model for greenhouse temperature and humidity. Comput. Electron. Agric. 186, 106186. https://doi.org/10.1016/j.compag.2021.106186.

Magarey, R.D., Sutton, T.B., Thayer, C.L., 2005. A simple generic infection model for foliar fungal plant pathogens. Phytopathology 95 (1), 92–100. https://doi.org/10.1094/PHYTO-95-0092.

Marta, A.D., Magarey, R.D., Orlandini, S., 2005. Modelling leaf wetness duration and downy mildew simulation on grapevine in Italy. Agric. For. Meteorol. 132 (1–2), 84–95. https://doi.org/10.1016/j.agrformet.2005.07.003.

Mashonjowa, E., Ronsse, F., Mubvuma, M., Milford, J.R., Pieters, J.G., 2013. Estimation of leaf wetness duration for greenhouse roses using a dynamic greenhouse climate model in Zimbabwe. Comput. Electron. Agric. 95, 70–81. https://doi.org/10.1016/j.compag.2013.04.007.

Meychik, N., Nikolaeva, Y.L., Kushunina, M., 2021. The significance of ion-exchange properties of plant root cell walls for nutrient and water uptake by plants. Plant Physiol. Biochem. 166, 140–147. https://doi.org/10.1016/j.plaphy.2021.05.048.

Miao, M., Zhang, Z., Xu, X., Wang, K., Cheng, H., Cao, B., 2009. Different mechanisms to obtain higher fruit growth rate in two cold-tolerant cucumber (Cucumis sativus L.) lines under low night temperature. Sci. Hortic. 119 (4), 357–361. https://doi.org/10.1016/j.scienta.2008.08.028.

Molina-Aiz, F.D., Fatnassi, H., Boulard, T., Roy, J.C., Valera, D.L., 2010. Comparison of finite element and finite volume methods for simulation of natural ventilation in greenhouses. Comput. Electron. Agric. 72 (2), 69–86. https://doi.org/10.1016/j.compag.2010.03.002.

Parisa, A., Di, T., 2021. Estimating leaf wetness duration with machine learning and climate reanalysis data. Agric. For. Meteorol 307, 108548. https://doi.org/10.1016/j.agrformet.2021.108548.

Qi, W.D., Song, J.C., 2012. Simulation study of gas flow field in bell-type annealing furnace. Metall. Equip., (03): 12-16. https://t.cnki.net/kcms/detail&uniplatform=NZKPT.(In Chinese).

Ren, S.G., Yang, W., Wang, H.Y., 2015. Prediction model on temporal and spatial variation of air temperature in greenhouse and ventilation control measures based on CFD. Trans. CSAE, 31(13), 207-214. https://t.cnki.net/kcms/detail?v=3uoqIhG8C44YLTlOAiTRKibYlV&uniplatform=NZKPT.(In Chinese).

Sentelhas, P.C., Monteiro, J.E.B.A., Gillespie, T.J., 2004. Electronic leaf wetness duration sensor: why it should be painted. Int. J. Biometeorol. 48 (4), 202–205. https://doi.org/10.1007/s00484-004-0200-z.

Shi, Y.X., Li, B.J., Liu, X.M., 2005. Several infection factors of *Pseudoperonospora cubensis*. Chin. J. Appl. Ecol., 16(2), 257-261. https://t.cnki.net/kcms/detail?v=3uoqIhG8C44YLKgchrJ08w1e7F1I&uniplatform=NZKPT.(In Chinese).

Stanciu, C.L., Stanciu, D., Dobrovicescu, A., 2016. Effect of greenhouse orientation with respect to E-W axis on its required heating and cooling loads. Energy Procedia 85, 498–504. https://doi.org/10.1016/j.egypro.2015.12.234.

Stanghellini, C., Jong, T.D., 1995. A model of humidity and its applications in a greenhouse. Agric. For. Meteorol. 76 (95), 129–148. https://doi.org/10.1016/0168-1923(95)02220-R.

Tong, G.H., Li, B.M., David, M.C., Shan, K.Z.Z., 2007. Preliminary study on temperature pattern in China solar greenhouse using computational fluid dynamics. Trans. CSAE, 23(7), 178-185.https://t.cnki.net/kcms/detail?v=3uoqIhG8C44YLTlOAiTRKgchrJ08w1&uniplatform=NZKPT.(In Chinese).

Wang, H., Sanchez-Molina, J.A., Li, M.R., Díaz, F., 2019. Improving the performance of vegetable leaf wetness duration models in greenhouses using decision tree learning. Water 11, 158. https://doi.org/10.3390/w11010158.

Wang, F., Tian, X., Ding, Y., Wan, X., Tyree, M.T., 2011. A survey of root pressure in 53 asian species of bamboo. Ann. Forest Sci. 68 (4), 783–791. https://doi.org/10.1007/s13595-011-0075-1.

Xue, X.P., Su, W., 2019. CFD simulation of humidity distribution in solar greenhouse under natural ventilation. J. Mar. Meteorol., 39(4), 90-96. https://t.cnki.net/kcms/detail?v=3uoqIhG8C44YLTlOAiTRKibYl&uniplatform=NZKPT.(In Chinese).

Yunis, H., Shtienberg, D., Elad, Y., 1994. Qualitative approach for modeling out breaks of grey mould epidemics in non-heated cucumber greenhouses. Crop Prot. 13 (2), 99–104. https://doi.org/10.1016/0261-2194(94)90158-9.

Zhang, X., Wang, H.L., Zou, Z.R., Wang, S.J., 2016. CFD and weighted entropy based simulation and optimisation of chinese solar greenhouse temperature distribution. Biosyst. Eng. 142, 12–26. https://doi.org/10.1016/j.biosystemseng.2015.11.006.

Zito, S., Castel, T., Richard, Y., Rega, M., Bois, B., 2020. Optimization of a leaf wetness duration model. Agric. For. Meteorol. 291, 108087. https://doi.org/10.1016/j.agrformet.2020.108087.

2.1.4 Simulation of night-time condensation on cucumber leaves in single slope solar greenhouse

Research in this field is supported by the following journal publication:

Title	Simulation of night-time condensation on cucumber leaves in single slope solar greenhouse
Authors	**R. Liu**, J. Liu, A.X. Ren, H.Y. Liu, J.L. Guzmán, J.F. Bienvenido, X.T. Yang, M. Li
Journal	Acta Horticulturae
Year	2020
Volume	1296
Pages	133-140
DOI	https://doi.org/10.17660/ActaHortic.2020.1296.18.
Conference	Greensys
Categories	Agronomy and Crop Science

Contribution of the Ph.D. Candidate

The Ph.D. candidate R. Liu is the main contributor and first author of this paper.

Simulation of night-time condensation on cucumber leaves in single slope solar greenhouse

R. Liu[1,2], J. Liu[1,2], A.X. Ren[1], H.Y. Liu[2], J.L. Guzmán[3], J.F. Bienvenido[3], X.T. Yang[1,2] and M. Li[1,2,a]

[1]Beijing Research Center for Information Technology in Agriculture, National Engineering Research Center for Information Technology in Agriculture, National Engineering Laboratory for Agri-product Quality Traceability, Key Laboratory of Agri-informatics, Ministry of Agriculture, Beijing, China; [2]College of Agriculture, Shihezi University, Shihezi, Xinjiang, China; [3]Department of Informatics, University of Almeria, Almeria, Spain.

Abstract

Condensation on cucumber leaves provides a necessary condition for pathogen infection. However, it could be costly to monitor the condensation of all leaves in a greenhouse. Therefore, the CFD model for the spatial and temporal distribution of leaf microclimate, condensation on leaf surface and the indoor microclimate of single-slope solar greenhouse under closed-film condition at night was studied. In order to simplify the input parameters, the boundary condition variables of the model were reduced to 5 h^{-1}, which were outdoor solar radiation intensity, outdoor air temperature (T_a), outdoor relative humidity (RH), outdoor average wind speed per hour and soil temperature at 0.5 m depth, without affecting the simulation performance of the model. According to the verification of the measured and simulated values of each microclimate parameter inside greenhouse, the results show that the mean absolute error (MAE) of T_a in 12 h was 1.47°C. The MAE of RH in 12 h was 1.95%. The absolute error (AE) of leaf wetness duration (LWD) between simulated and measured value was less than 1 h. In the study of spatial distribution simulation, the MAE of T_a was 0.31°C and the MAE of RH was 1.05%. The simulation result of condensation distribution on leaves within 12 h at night were tested. The true positive rate (TPR), true negative rate (TNR), false positive rate (FPR), false negative rate (FNR) and accuracy (ACC) of the model were 0.89, 0.99, 0.01, 0.28 and 0.9, respectively. This paper provided a reference for early warning model of disease based on the temporal and spatial distribution characteristics of microclimate in solar greenhouse.

Keywords: CFD, cucumber leaves, greenhouse, temperature, relative humidity, condensation

INTRODUCTION

Leaf wetness duration (LWD) played an important role in the disease warning system for crops (Zhao et al., 2011). Leaf surface condensation, guttation, fog and drops of dew from the roof are four factors of influencing LWD in solar greenhouses. The structure of single slope solar greenhouse differs greatly from that of large multi-span greenhouse. It is more like a tunnel greenhouse, but there is a wall on the north side. Therefore, the microclimate of single slope solar greenhouse is heterogeneous. It is difficult and costly to monitor LWD distribution in solar greenhouses. At present, one weather station was deployed in almost each greenhouse. It is practicable to improve the spatial and temporal resolution of disease infection prediction by making clear leaf condensation distribution using weather forecast and deployed an environmental monitoring network inside and outside the solar greenhouse.

In recent years, CFD (computational fluid dynamics) numerical method has been widely used in greenhouse environment simulation (Tong et al., 2018). Most of them were modeling of ventilation and air temperature. However, accurate simulation of microclimate such as humidity, leaf surface temperature, ventilation and so on is the precondition of simulating condensation. In addition, it is necessary to take into account the interaction between crops and the environment. Boulard and Wang (2002) modeled the effects of transpiration on microclimate in a lettuce greenhouse for the first time. Subsequently, similar experiments

[a]E-mail: lim@nercita.org.cn

Acta Hortic. 1296. ISHS 2020. DOI 10.17660/ActaHortic.2020.1296.18
Proc. Int. Symp. on Advanced Technologies and Management for Innovative Greenhouses – GreenSys2019
Eds.: P.E. Bournet et al.

were carried out in greenhouses with tomatoes, impatiens, roses or crabapples inside (Boulard et al., 2010, 2017; Kichah et al., 2012; Chen et al., 2015). On this basis, further study of the condensation process simulation based on local microclimate has been done by a few authors. Ali et al. (2014) developed a 2D transient model to assess condensation on roofs in a closed Venlo glasshouse. Piscia et al. (2012) studied the 3D transient modeling of the night-time condensation on a four-span greenhouse plastic cover, but crop environment interaction was neglected. However, because of the special asymmetric structure of single slope solar greenhouse, it is necessary to develop a 3D transient model to find out when and where the condensation will occur.

MATERIALS AND METHODS

Experimental greenhouse and data collection

The experiment was conducted in Xiaotangshan National Precision Agriculture Demonstration Base (40°18'N; 116°47'E, annual average temperature 11.8°C, altitude 39 m, local pressure 101 kPa), Changping District, Beijing from 2017 to 2018. The type of greenhouse was typical single slope solar greenhouse with polyethylene (PE) film on the south roof and asbestos-cement board on the north roof (Figure 1).

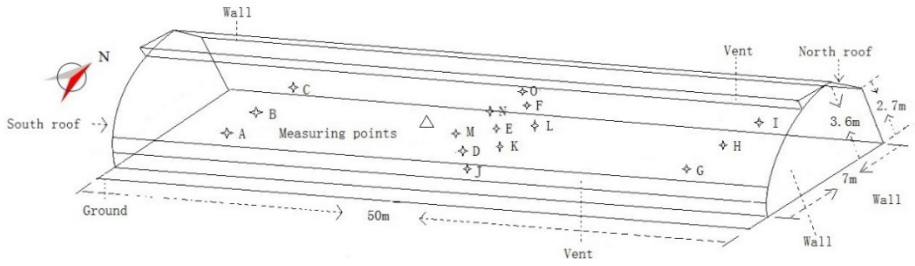

Figure 1. Drawing of experimental greenhouse. A-I represent the T_a-RH measured point positions in the horizontal plane of 1 m high. Three sensors of each row were distributed, which was 1, 3, 5 m away from south boundary of greenhouse, respectively, and 10, 25, 40 m away from east boundary of greenhouse respectively. D-F and J-O represent the T_a-RH measured point positions in the vertical plane. The height of each row was 0.5, 1 and 1.5 m, respectively. △ represents Davis-6162 weather station and infrared thermometer.

The greenhouse, with bricks and concrete wall on the north, east and west sides, was 50 m long and 7 m wide. The cucumber cultivar 'Jingyan Mini 2' was used as the experimental material that was cultivated in an average of 36 rows. Drip irrigation under plastic film was used. In this experiment, the model was developed under the condition that the vents were closed during night.

An outdoor weather station Davis Vantage Pro&Plus (Davis Instruments, Hayward, USA) (Figure 2) was arranged to measure the total solar radiation (range, 0-1800 W m^{-2}; accuracy, ±5%), wind speed (range, 0-67 m s^{-1}; accuracy, ±5%), air temperature (T_a, range, -40 to +65°C; accuracy, ±0.5°C), relative humidity (RH, range, 0-100%; accuracy, ±3%). A weather station Davis-6162 (Davis Instruments, Hayward, USA) (Figure 2) was arranged at the height of 1 m in the center of the greenhouse to measure T_a, RH, soil water potential and soil temperature at 0.5 m depth. In addition, an infrared thermometer SI-111 (Apogee Instrument Crop, USA) (Figure 2)was arranged at the same position to measure the leaf temperature. The above data were measured and recorded every 15 min. At the same time, 15 T_a-RH sensors (Figure 2) that measured and recorded data (T_a, range, -40 to +123.8°C; accuracy, ±0.3°C. RH, range, 0-100%; accuracy, ±1.8%) every hour was distributed on the horizontal plane at 1 m height and central north-south vertical plane of the greenhouse to be test data (Figure 1). All these sensors were made by the China National Engineering Research Center for Information Technology in Agriculture (NERCITA).

Figure 2. Sensors. (1) SI-111 infrared thermometer; (2) T_a-RH sensors made by NERCITA; (3) Davis Vantage Pro& Plus outdoor weather station; (4) Davis-6162 indoor weather station.

Model structure

All sub-models were integrated into the greenhouse system to form a leaf surface condensation model based on energy balance, mass balance and momentum balance (Figure 3). The model system takes real-time data of T_a, RH, wind speed, solar position and radiation intensity collected by outdoor sensors as input. Each time step of solving the model was 30 s with 20 iterations. In each iteration, energy, momentum, mass conservation equation, supplementary equation of turbulence model, transpiration model reflecting crop-microclimate interaction (executed in daytime), sensible heat exchange model, leaf net radiation model and condensation model are solved simultaneously. The data collected by outdoor and indoor T_a and RH sensors were used as initial conditions 1 h before sunset. Thereafter, the thermal boundary conditions of walls, roofs and soil will be calculated in real time by convection, conduction and radiation process between indoor and outdoor air.

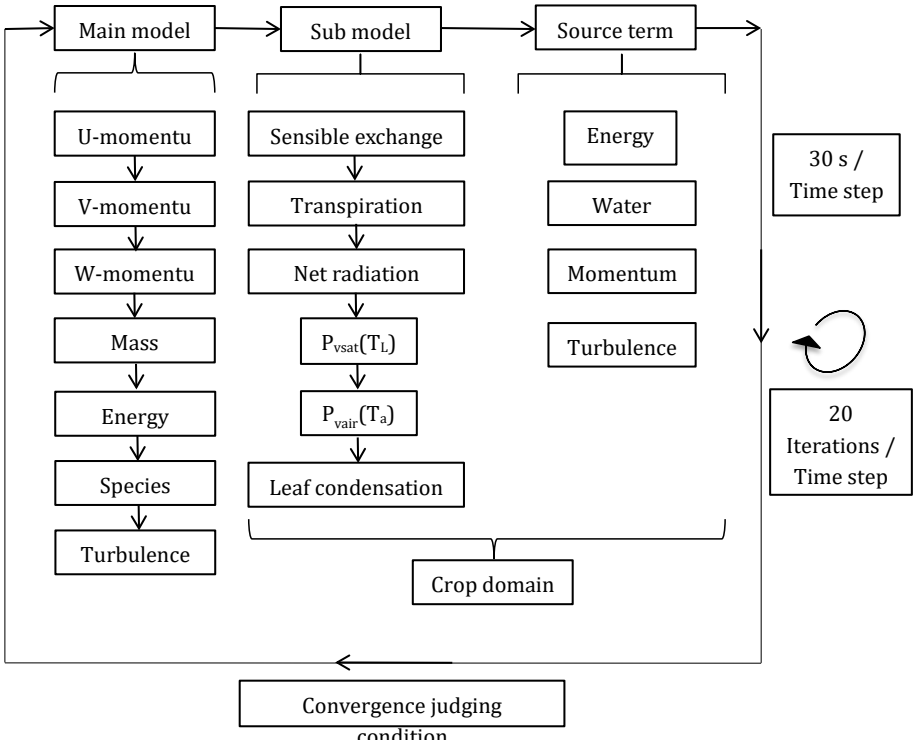

Figure 3. Model structural graph based on energy, mass, and momentum balance.

Simulation domain

In this study, ANSYS ICEM 15.0 software was used to generate geometry and unstructured grids according to the ratio of 1:1 to the actual size of greenhouse. A 3D model was adopted. The simulation domain was limited to the interior of the greenhouse. Determining a reasonable range of simulation domain has been addressed by many authors. The key is to find a balance between computation load and accuracy of simulation. Considering that vents were closed during the simulation, the influence of wind direction on the flow field inside greenhouse was ignored. The external wind speed was input into the convective heat transfer model and air leakage model to calculate the energy and mass exchange between indoor and outdoor (Roy et al., 2002; Baille et al., 2006). The crop zone was simplified to 36 cuboids of 5 m long, 0.8 m wide and 1.5 m high (Figure 4). Grids were densified near crop zone. Considering the computational capacity and simulation accuracy, we tried under several different grid files, and the final number of volume elements was 31080 in crop domain part and 433649 in the rest of domain part.

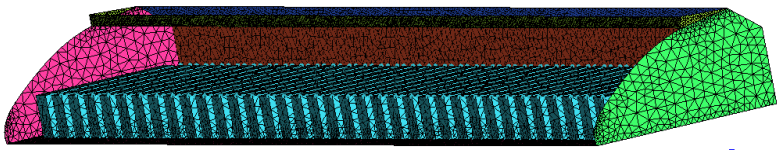

Figure 4. Grid model of the numerical domain considering only the interior of the greenhouse.

Flow analysis

Air velocity is extremely low under closed film condition. The kind of flow in this study can be judged using Rayleigh number formula (Mistriotis et al., 1997). The calculated value of R_a was about 1.4×10^{12}, which was larger than 2×10^{7} (Mills, 1992). Therefore, the flow in this study was transient turbulence flow.

Three components were involved in the studied flow, which were air, water vapor, and dew, including gas and liquid phases. However, in general, dew on leaves is stagnant. In order to simplify the calculation, the flow was considered as a species transport flow of air and water vapor, but not a two-phase flow. The condensation process on leaves and in the air was quantified as the energy increment and mass reduction of water vapor caused by liquefaction, but there was not real water produced. In addition, the position and time of condensation occurrence on leaves were marked to simulate the condensation. The condensation rate on the leaf can be calculated by the following formula (Gerlein-Safdi et al., 2018):

$$m_{cds} = 0.622LAD \cdot \rho \cdot g_h \left(\frac{P_{vair}(T_a) - P_{vsat}(T_L)}{p}\right) \quad (1)$$

where, m_{cds} is condensation rate on leaves, kg m^{-3} s^{-1}; LAD is leaf area density, m^{-1}; LAD = LAI/H, where, LAI is leaf area index and H is crop height, m; ρ is air density, kg m^{-3}; g_h is water vapor conductivity in leaf boundary layer, m s^{-1}; $P_{vair}(T_a)$ is air water vapor pressure, Pa; $P_{vsat}(T_L)$ is saturated water vapor pressure at leaf temperature, Pa; p is pressure, Pa; g_h is a variable related to Lewis number (N_{Le}) and r_a,

$$\begin{cases} g_h = \left(r_a N_{Le}^{2/3}\right)^{-1} \\ N_{Le} = \frac{\alpha_a}{D_w} \\ \alpha_a = T_b \cdot 1.32 \times 10^{-7} - 1.73 \times 10^{-5} \\ D_w = T_b \cdot 1.49 \times 10^{-7} - 1.96 \times 10^{-5} \\ T_b = (T + T_c)/2 \end{cases} \quad (2)$$

where, r_a is aerodynamic resistance, s m^{-1}. N_{Le} is Lewis number, dimensionless; α_a is air thermal diffusivity, m^2 s^{-1}; D_w is water vapor diffusivity, m^2 s^{-1}; T_b is temperature in leaf boundary layer, K.

But the above equations are not enough to close the group. The detail of equations cannot be included in this paper due to page limitation. Please see reference for equations for T_a, T_L, e, r_a, etc. (Ansys-Fluent, 2013; Boulard et al., 2010; Stanghellini and de Jong, 1995).

Data validation

The validation time was from 17:30 on April 19 to 5:30 on April 20, 2018, and the total time was 12 h, which crossed the periods of evening, night and dawn. During the period, the management mode was no irrigation, the vents were closed and there is no heat preservation covering on the polyethylene roof. The weather condition was cloudy, southeast wind in 5-6 grades. The condensation on leaves at A-I measuring point (Figure 1) was observed manually. In the temporal study, the simulation results within 12 h at night were tested. In the study of spatial distribution simulation, the simulated values of the first hour (18:30) were chosen to compare with the 15 measured points distributed in greenhouse. Root mean squared error (RMSE) was used to evaluate the errors between calculated and measured data.

$$\mathrm{RMSE} = \sqrt{\frac{\sum_{i=1}^{N}(C_{ai}-M_{ei})^2}{N-1}} \quad (3)$$

where, C_{ai} is calculated value, M_{ei} is measured values, N is sample size. The condensation distribution model was tested by five statistical indicators: true positive rate (TPR), true negative rate (TNR), false positive rate (FPR), false negative rate (FNR) and accuracy (ACC).

RESULTS AND DISCUSSION

Microclimate distribution

It is necessary to test T_a, T_L and RH before condensation validation because they are important input parameters for condensation model. The errors of simulated T_a, T_L and RH are shown in Table 1. Considering that the model was initialized only once at the beginning of 12 h, boundary conditions input per hour such as wall temperature were calculated rather than measured, the Max AE of T_L (2.34 K) is acceptable. It is necessary to validate relative humidity rather than absolute humidity because RH is important to both condensation and disease. And considering that the response of RH to temperature is sensitive, the Max AE of RH (6.08%) which appeared at 12 h of the simulation is acceptable.

Table 1. The errors of simulated T_a, T_L and RH. HP represents horizontal plane; VP represents vertical plane.

	Variables		Min AE	Max AE	Aver AE	RMSE
Time scale Validation (12 h)	T_a (K)		0.23	2.16	1.47	1.59
	T_L (K)		0.25	2.34	1.76	2.87
	RH (%)		0.08	6.08	1.95	2.75
Spatial distribution validation	HP	T_a (K)	0.20	0.83	0.43	0.53
		RH (%)	0.30	2.63	1.16	1.46
	VP	T_a (K)	0.06	0.37	0.31	0.34
		RH (%)	0.30	1.47	0.88	1.00

Condensation distribution

The true positive rate, true negative rate, false negative rate, false positive rate and accuracy of the model were 0.89, 0.99, 0.01, 0.28 and 0.9, respectively, which shows that accuracy of the model was good, and there would not be false alarm in high probability, but the sensitivity was not enough, so it was easy to miss the alarm. Detailed information is shown

in Figure 5 and Table 2. The results show that there were 3 missed reports at 1:30 and 2:30, respectively, in 81 observations during 17:30 to 2:30. There were the 27 observations during 3:30-5:30, 9 of which were simulated as condensation, but only 8 were actually observed. In additin, 7 of 27 were observed as cndensation, but were not be simulated. It shows that the model was conservative and lacked sensitivity, but the overall accuracy was acceptable.

Table 2. Observation of leaf wetness on horizontal plane at 1 m height in greenhouse during 12 h. Y represents leaf wetness was observed; - represents leaf wetness was not observed.

Time	Position								
	A	B	C	D	E	F	G	H	I
17:30-0:30	-	-	-	-	-	-	-	-	-
1:30	-	-	-	-	-	-	Y	-	-
2:30	-	-	-	Y	-	-	Y	-	-
3:30	-	-	-	Y	-	-	Y	Y	-
4:30	Y	Y	-	Y	Y	-	Y	Y	-
5:30	Y	Y	-	Y	Y	-	Y	Y	-

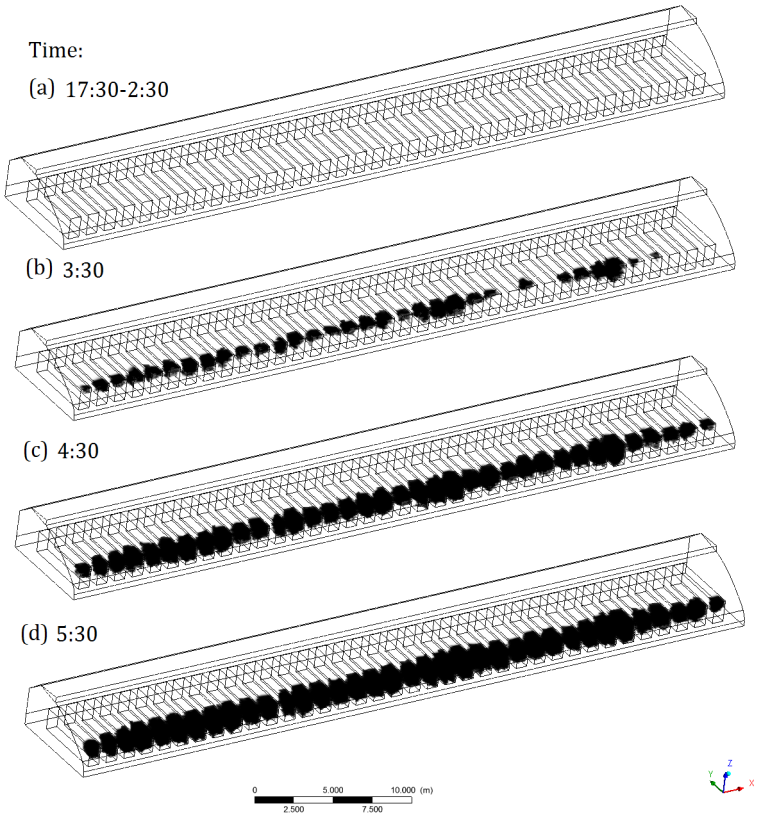

Figure 5. Contour of simulated condensation on canopy during 12 h. Y represents north; X represents east. ■ represents condensation appeared based on simulation.

The results of simulation and observation show that the zone near the southern boundary of greenhouse at night was easier to dew than that near the north wall. This conclusion coincides with Bournet's observations that cucumber leaves near the semi-transparent boundary have a greater risk of condensation than other zones (Bournet et al., 2018).

CONCLUSIONS

The following conclusions can be drawn from the study:

- The innovation of this study was to simulate the condensation on cucumber leaves. The simulation result of condensation distribution on leaves within 12 h at night were tested. The true positive rate, true negative rate, false negative rate, false positive rate and accuracy of the model were 0.89, 0.99, 0.01, 0.28 and 0.9, respectively;
- The boundary condition variables of the model were reduced to 5 h^{-1}, which was outdoor solar radiation intensity, outdoor air temperature, outdoor air relative humidity, outdoor average wind speed per hour and soil temperature at 0.5 m depth, without affecting the simulation performance of the model.

ACKNOWLEDGEMENTS

This study is funded by Shandong Provincial Key Research and Development Project (2017CXGC0216) and National Natural Science Fund of China (31401683). The authors want to thank all their colleagues and students for their assistance in the research for this paper.

Literature cited

Ali, H.B., Bournet, P.-E., Danjou, V., Morille, B., and Migeon, C. (2014). CFD simulations of the night-time condensation inside a closed glasshouse: sensitivity analysis to outside external conditions, heating and glass properties. Biosyst. Eng. *127*, 159–175 https://doi.org/10.1016/j.biosystemseng.2014.08.017.

Ansys-Fluent. (2013). User's Guide, Vol. 15 (Fluent), p.0.

Baille, A., López, J.C., Bonachela, S., González-Real, M.M., and Montero, J.I. (2006). Night energy balance in a heated low-cost plastic greenhouse. Agric. For. Meteorol. *137* (*1-2*), 107–118 https://doi.org/10.1016/j.agrformet.2006.03.008.

Boulard, T., and Wang, S. (2002). Experimental and numerical studies on the heterogeneity of crop transpiration in a plastic tunnel. Comput. Electron. Agric. *34* (*1-3*), 173–190 https://doi.org/10.1016/S0168-1699(01)00186-7.

Boulard, T., Roy, J.C., Fatnassi, H., Kichah, A., and Lee, I.-B. (2010). Computer fluid dynamics prediction of climate and fungal spore transfer in a rose greenhouse. Comput. Electron. Agric. *74* (*2*), 280–292 https://doi.org/10.1016/j.compag.2010.09.003.

Boulard, T., Roy, J.C., Pouillard, J.-B., Fatnassi, H., and Grisey, A. (2017). Modelling of micrometeorology, canopy transpiration and photosynthesis in a closed greenhouse using computational fluid dynamics. Biosyst. Eng. *158*, 110–133 https://doi.org/10.1016/j.biosystemseng.2017.04.001.

Bournet, P.-E., Brajeul, E., Truffault, V., Chantoiseau, E., and Pinoit, C. (2018). Impact of heating location and mechanical ventilation on climate distribution inside a greenhouse cucumber crop. Acta Hortic. *1227*, 339–346 https://doi.org/10.17660/ActaHortic.2018.1227.42.

Chen, J., Xu, F., Tan, D., Shen, Z., Zhang, L., and Ai, Q. (2015). A control method for agricultural greenhouses heating based on computational fluid dynamics and energy prediction model. Appl. Energy *141*, 106–118 https://doi.org/10.1016/j.apenergy.2014.12.026.

Gerlein-Safdi, C., Koohafkan, M.C., Chung, M., Rockwell, F.E., Thompson, S., and Caylor, K.K. (2018). Dew deposition suppresses transpiration and carbon uptake in leaves. Agric. For. Meteorol. *259*, 305–316 https://doi.org/10.1016/j.agrformet.2018.05.015.

Kichah, A., Bournet, P.-E., Migeon, C., and Boulard, T. (2012). Measurement and CFD simulation of microclimate characteristics and transpiration of an *Impatiens* pot plant crop in a greenhouse. Biosyst. Eng. *112* (*1*), 22–34 https://doi.org/10.1016/j.biosystemseng.2012.01.012.

Mills, A.F. (1992). Heat Transfer (Boston, USA: Irwin).

Mistriotis, A., Arcidiacono, C., Picuno, P., Bot, G.P.A., and Scarascia-Mugnozza, G. (1997). Computational analysis of ventilation in greenhouses at zero- and low-wind-speeds. Agric. For. Meteorol. *88* (*1-4*), 121–135 https://doi.org/10.1016/S0168-1923(97)00045-2.

Piscia, D., Montero, J.I., Baeza, E., and Bailey, B.J. (2012). A CFD greenhouse night-time condensation model. Biosyst. Eng. *111* (*2*), 141–154 https://doi.org/10.1016/j.biosystemseng.2011.11.006.

Roy, J.C., Boulard, T., Kittas, C., and Wang, S. (2002). PA – precision agriculture: convective and ventilation transfers in greenhouses, Part 1: the greenhouse considered as a perfectly stirred tank. Biosyst. Eng. *83* (*1*), 1–20 https://doi.org/10.1006/bioe.2002.0107.

Stanghellini, C., and de Jong, T. (1995). A model of humidity and its applications in a greenhouse. Agric. For.

Meteorol. *76* (*2*), 129–148 https://doi.org/10.1016/0168-1923(95)02220-R.

Tong, G., Christopher, D., and Zhang, G. (2018). New insights on span selection for Chinese solar greenhouses using CFD analyses. Comput. Electron. Agric. *149*, 3–15 https://doi.org/10.1016/j.compag.2017.09.031.

Zhao, C.-J., Li, M., Yang, X.-T., Sun, C.-H., Qian, J.-P., and Ji, Z.-T. (2011). A data-driven model simulating primary infection probabilities of cucumber downy mildew for use in early warning systems in solar greenhouses. Comput. Electron. Agric. *76* (*2*), 306–315 https://doi.org/10.1016/j.compag.2011.02.009.

2.1.5 Numerical analysis of the wind field around greenhouse clusters and natural ventilation rate for the Chinese solar greenhouse

Research in this field is supported by the following journal publication:

Title	Numerical analysis of the wind field around greenhouse clusters and natural ventilation rate for the Chinese solar greenhouse	
Authors	**R. Liu**, P.-E. Bournet, J. L. Guzmán1, Ming Li	
Journal	Computers and Electronics in Agriculture	
Year	2022	
Volume	Under review	
Pages	--	
DOI	--	
IF(JCR2022)	6.757	
Categories	Horticulture Q1	(1/94)
	Computer Science Applications Q1	(38/747)

Contribution of the Ph.D. Candidate
The Ph.D. candidate R. Liu is the main contributor and first author of this paper.

Numerical analysis of the wind field around greenhouse clusters and natural ventilation rate for the Chinese solar greenhouse

Ran Liu[1], Pierre-Emmanuel Bournet[3], José Luis Guzmán[1,*], Ming Li[2,*]

[1]Department of Informatics, ceiA3, CIESOL, Ctra. Sacramento s/n, University of Almería, Almería, Spain

[2]Information Technology Research Center, Beijing Academy of Agriculture and Forestry Sciences/ National Engineering Research Center for Information Technology in Agriculture/ National Engineering Laboratory for Agri-product Quality Traceability/ Meteorological Service Center for Urban Agriculture, China Meteorological Administration- Ministry of Agriculture and Rural Affairs/ Key Laboratory of Agri-informatics, Ministry of Agriculture, Beijing, China

[3]EPHor, Institut Agro Rennes Angers, SFR 4207 QuaSaV, 49045 Angers, France

*Corresponding author: José Luis Guzmán (joguzman@ual.es); Ming Li (lim@nercita.org.cn)

Abstract:

Nowadays, the agriculture production facilities progressively evolved towards greenhouse clusters which impact the natural ventilation of each greenhouse. The main contribution of this paper is proposed constraints for the current two-dimensional CFD (Computational Fluid Dynamics) studies regarding its validity, especially when buildings are clustered. In this study, the wind flow patterns around and inside multiple

greenhouses are compared using 20 two-dimensional (2D) and three-dimensional (3D) CFD models. The results show that the error on the ventilation rate prediction could exceed 50%, if 2D models are not properly used. Besides, estimation of ventilation rate is a professional approach that requires multiple complex parameters. This study looks forward to creating an easily used model for estimating natural ventilation rate, using one thousand CFD samples. This model is efficient to deal with the combined effect of wind pressure and thermal gradients under various vent configurations, with only four necessary inputs.

Keywords: CFD; multiple Chinese solar greenhouses; airflow pattern; regression trees; natural ventilation model

Introduction

The horticultural greenhouse facility area in China is now 3.7 million hectares. Solar greenhouses are the major type in northern provinces due to their heat preservation and low energy cost (Wu et al., 2020). In recent years, the agriculture production facilities progressively evolved towards greenhouse clusters which impact the ventilation of each greenhouse (Fig. 1). The spacing between each other is usually small, which makes it necessary to study the validity of most current two-dimensional CFD (Computational Fluid Dynamics) studies in this ubiquitous scenario. Up to now, most of the current CFD studies focus on a single greenhouse, especially for the typical Chinese solar greenhouse (CSG), the wind field and ventilation rate around and inside multiple

42 greenhouses has not been fully studied. However, the real situation is that the model is
43 usually used in greenhouse clusters, which causes errors with ideal experiments.

44

45 Fig. 1. Chinese solar greenhouse clusters.

46 Estimation of ventilation rate is an indispensable part in modelling the greenhouse
47 climate, as well as for controlling the climate inside the greenhouse, which is essential
48 for cooling and dehumidification. Ventilation is achieved either by natural ventilation
49 or by forced ventilation facilities (e.g. exhaust fan and fan-pad cooling system) (Cheng
50 et al., 2021). Natural ventilation is currently widely preferred by farmers in practical
51 production, given its low energy cost (Li et al., 2018; Zhang et al., 2019; Liu et al.,
52 2021). Natural ventilation is driven by two forces induced by wind and thermal
53 gradients (Mistriotis et al., 1997; Ould Khaoua et al., 2006). On contrary to
54 mechanically forced ventilation, natural ventilation is characterized by varied input
55 conditions and hence it makes it difficult to quantify the flow rate.
56 Gas tracing and energy balance are two common methods to obtain the ventilation rate
57 before the CFD technique was adopted in the last two decades to simulate the
58 greenhouse flow field (Katsoulas et al., 2006). The gas tracing method requires that the
59 tracer gas distribution be uniform and its concentration over a given operation point
60 (Nederhoff et al., 1985). The energy balance method relies greatly on the accuracy of
61 the flux sensors or the greenhouse model (Tong et al., 2008). In addition to the

inconvenient practice, both methods have an error of up to 30% (Van Buggenhout et al., 2007). Compared with the above methods, the cost of the CFD method is lower, and in addition, this approach guarantees a high level of accuracy, provided that the quality of the mesh, the optimal design of the model in the flow field, and the convergence of the solution are correctly checked.

CFD technique has been widely applied in the optimal design and the simulation of ventilation since the 1990s (Mistriotis et al., 1997; Boulard et al., 1997). In the 21st century, more comprehensive models were developed including the interaction between the microclimate and the crop (Boulard and Wang, 2002; Majdoubi et al., 2009; Boulard et al., 2010; Kichah et al., 2012; Chen et al.,2015; Boulard et al., 2017; Liu et al., 2021). By using the CFD method, the impact of wind speed, vent opening configuration, and greenhouse structures on the airflow pattern have been investigated by many researchers (Ould Khaoua et al., 2006; Molina-Aiz et al., 2010; Rocha et al., 2021). Bournet and Boulard (2010) reviewed optimum solutions for designers and analyzed the effect of ventilator configurations on the distributed climate inside greenhouses from CFD simulations published over 25 years.

Up until now, a vast majority of current research is reviewed to be two-dimensional (Bournet and Boulard, 2010; Villagrán et al., 2019; Benni et al., 2016). As well as many previous 2D models about the CSG. (Wang et al., 2013; He et al., 2018; Zhang et al., 2016). Improving the mesh quality of 3D mesh requires proficient skills of designers. For the CSG, the fan-shaped geometry of the south roof makes it a challenge to creat boundary layer grids. In addition, the calculation load of three-dimensional CFD model

is heavy. These are why two-dimensional models are more widely used. However, such as the fact that the asymmetric structure of the CSG, and the wind impact from surrounding buildings, few previous studies proposed constraints for the two-dimensional CFD models regarding its validity. The ventilation rate of a greenhouse with restricted vents opening areas is proved to be greatly reduced when neighbouring objects are high enough (Villagrán and Bojacá, 2019). In the present study, the impact of building obstacles in front and behind the greenhouse on the ventilation rate is studied separately using 2D and 3D modelling. 20 cases were selected (10 cases for 2D and 10 cases for 3D) to compare the corresponding predicted natural ventilation rate and the wind field.

Using CFD model to obtain ventilation rate requires complex steps such as geometric modeling, meshing, coding functions, and defining boundary conditions. It also relies on the modeler's skill in mesh design, and problem understanding and formalizing. It usually requires mesh reconstruction and boundary condition redefining when vent configuration or building structures are different, which necessitate relatively heavy workloads and hence makes it primarily implemented for research purposes rather than for practical use (Kim et al., 2020). From enough CFD samples, it could be possible to develop a black box model for natural ventilation. Indeed, conducting virtual wind tunnel simulations to obtain comprehensive and orderly samples is feasible, whereas it would be difficult to obtain a sufficient number of samples in field experiments, due to unstable and unpredictable weather conditions (Kim et al., 2021). In this study, from a high number of CFD simulations (990 cases), a natural ventilation rate model was

106 developed using a nonlinear regression trees model (Fehér, 2006). As a result, by
107 combining CFD simulations and trees models, it is possible to assess the ventilation
108 characteristics, making it possible to avoid several parameters that are difficult to
109 measure (e.g. wind pressure, thermal pressure), which is a significant step forward for
110 optimal design or real-time greenhouse climate simulation.

111

Nomenclature		q_c	Convective energy, W
A_g	Area of the greenhouse, m^2	q_{liq}	Water vapor liquidation energy, W
c_p	Specific heat capacity of the air, J kg^{-1} K^{-1}	q_p	Plant energy, W
c_{pw}	Specific heat capacity of the water vapor, J kg^{-1} K^{-1}	R	Universal gas constant, m^3 Pa K^{-1} mol^{-1}
e	Ratio error	s_v	Ventilation humidity, kg kg^{-1} s^{-1}
F_j	Effective area of the air inlet, m^2	s_{lea}	Air leakage humidity, kg kg^{-1} s^{-1}
F_p	Effective area of the air outlet, m^2	s_p	Plant humidity, kg kg^{-1} s^{-1}
f_m	Simulated mass flow rate through the vents, kg m^{-1} s^{-1}	T	Indoor air temperature, K
f_u	Coefficient of the thermal pressure ventilation rate	T_o	Outdoor air temperature, K
g	Gravitational acceleration, m s^{-2}	t	Time, s
H	Reference height, m	u	Wind speed, m s^{-1}
H_0	Aerodynamic roughness length, m	u_j	Flow coefficient of the air inlet
Hv	Height between upper and lower vents, m	u_p	Flow coefficient of the air outlet
h	Indoor absolute humidity, kg kg^{-1}	u_{ref}	Reference wind speed, m s^{-1}
L	Area ventilation rate, m^3 s^{-1} m^{-2}	$u_{2.5}$	Wind speed at 2.5 m height, m s^{-1}
L_2	Ventilation rate simulated	u_*	Friction velocity, m s^{-1}

	by 2D case $m^3 s^{-1}$		
L_3	Ventilation rate simulated by 3D case $m^3 s^{-1}$	v	Greenhouse volume, m^3
L_w	Wind pressure ventilation rate, $m^{-3} s^{-1}$	y_c	Estimated height of the first cell in the boundary layer, m.
L_T	Thermal gradients ventilation rate, $m^{-3} s^{-1}$	y^+	A non-dimensional distance
l_g	Length of the greenhouse, m	β	Wind pressure coefficient
M_w	Molecular weight of the gas, kg mol^{-1}	μ	Dynamic viscosity, Pa s^{-1}
P_{op}	Operating pressure, Pa	ρ	Air density, kg m^{-3}
$q_v(t)$	Ventilation energy, W	κ	von Karman constant, 0.42
$q_{lea}(t)$	Air leakage energy, W		

112

113

1. Materials and methods

1.1 Experimental greenhouses and vent configurations

The object considered for the present study is the typical single slope solar greenhouse in China (Fig. 2). The roof vent (upper vent) and side vent (lower vent) are both equipped with a rolling film. The width of the full vent opening for both the upper and the lower vent is 0.6 m. The ventilation rates for different vent configurations were assessed in the experiment (Table 1). Crops are not considered in this experiment, because the aim of this study is to obtain a general ventilation rate model that is applied to most of the CSGs. However, the specific crop height or leaf area index could affect the ventilation rate and thus limit the application scope.

Table 1. Simulated greenhouse size and vent opening configurations.

Width	Ridge	Length	Depth	Vent type	Vent opening area

(m)	height (m)	(m)	(m)		(m^2) Lower vent	Upper vent
7	3.6	50	0.5	Rolling Film	10	10 20 30
					20	10 20 30
					30	10 20 30

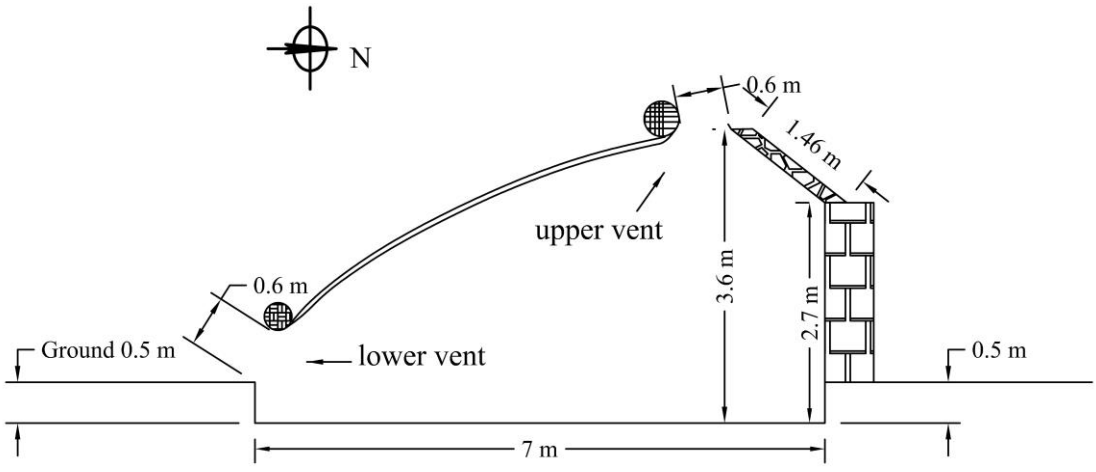

Fig. 2. Structure of the experimental greenhouse.

1.2 Calculation domain

The CFD mesh was generated based on a 1:1 scale greenhouse i.e. considering the actual size of the greenhouse. For the study, 3 greenhouses were meshed in the flow field, with an interval of 4 m, and in addition, 9 different vent combinations of the upper vent and the lower vent were designed as described in Table 1, considering the same combination for all three greenhouses. The height of the calculation domain is 14 m and the length of the upstream portion is determined as 3 times the ridge height (10.8 m), while the downstream portion is 10 times the ridge height (36 m, Fig. 3). Indeed, it was established that the backflow cannot form inside the computational domain within

10 times of the ridge height (Kim et al., 2017). Based on the same size as the above 2D domain, the 3D domain includes three greenhouses with a width of 50 m and an extension of 86 m on both sides of the greenhouses.

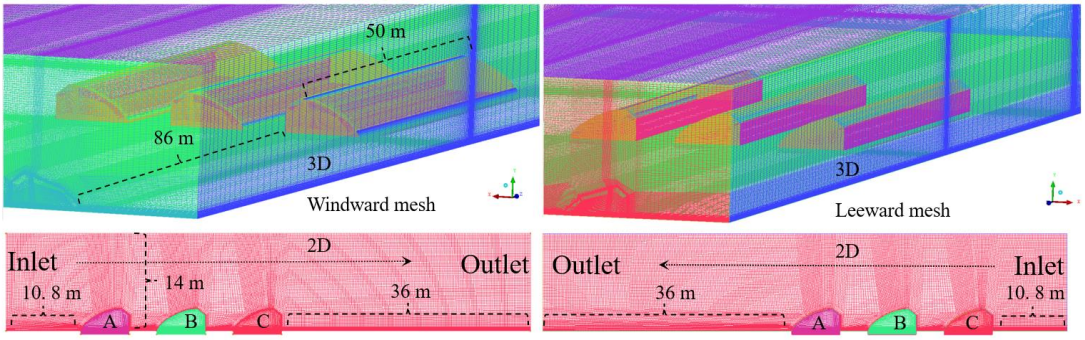

Fig. 3. Mesh of windward and leeward flow field and greenhouses A, B, C.

1.3 Models, solver, and material

The conservation equations for mass, momentum, energy, and standard k-ε viscous model combined with buoyancy effect (g= -9.81 m s^{-2}) were solved by the SIMPLEC (Semi-Implicit for Pressure Linked Equations Consistent) method using Fluent™ software (Ansys Inc., PA, USA). The flow in the near-wall region was solved using the Standard Wall Function. The incompressible-ideal-gas was used as state law to link the temperature and pressure. The corresponding physical properties of air specified in the model are gathered in Table 2.

Table 2. Physical properties of the air

Material	Density (kg m^{-3})	Specific heat (J kg^{-1} K^{-1})	Thermal conductivity (W m^{-1} K^{-1})	Viscosity (kg m^{-1} s^{-1})

Air	Incompressible-ideal-gas	1006	0.024	1.7894×10^{-5}

155
156

157 1.4 Generation of the mesh file

158 The mesh file was generated by ICEM software (Ansys Inc., PA, USA). The blocks
159 were associated with a set of grids, which were then converted to unstructured grids
160 when generating the mesh file. The height of the cell in the first boundary layer was
161 estimated from the y^+ value, which is given by the following equation (Piscia et al.,
162 2012),

163 $$y_c = \frac{y^+ \mu}{\rho u_*} \quad (1)$$

164 where, y_c is the estimated height of the first cell in the boundary layer and y^+ is a non-
165 dimensional distance, which must satisfy $30<y^+<300$ for the Standard Wall Function
166 (Ansys-Fluent, 2010). μ is the dynamic viscosity, Pa s^{-1}; ρ is the density of the fluid, kg
167 m^{-3}; u_* is the friction velocity, m s^{-1}. The friction velocity is defined as $\sqrt{\frac{shear\ stress}{fluid\ density}}$,
168 which is a variable related to the flow speed and roughness of the surface. The shear
169 stress is difficult to measure or estimate, so u_* was calculated by the following empirical
170 equation (van Druenen et al., 2019),

171 $$u_* = \kappa \frac{u_{ref}}{ln(\frac{H+H_0}{H_0})} \quad (2)$$

172 where, κ is von Karman constant, 0.42; u_{ref} is the reference wind speed, m s^{-1}; H is the
173 reference height, m; H_0 is the aerodynamic roughness length: classical value is 0.005
174 for the featureless land surface without any noticeable obstacles and with negligible
175 vegetation, and 0.03 for a level country with low vegetation (e.g. grass) (Toparlar et al.,
176 2019). The roughness length was also determined as 0.0193 for the simulation of

177 greenhouse ventilation and its surrounding flow field (Boulard et al., 2010). In the
178 present study, a value of 0.02 was retained for H_0.
179 The first step in creating a mesh file is to build a geometric model. Then the geometric
180 model is associated with created blocks, including associating Points with Vertex,
181 associating Curves with Edges, associating Surfaces with Faces (Fig. 4 (a)). The former
182 is the name corresponding to the geometric model, and the latter is the name
183 corresponding to the block. The next key step is to split the blocks. Note that it is not
184 easy in meshing high-quality boundary layer around the semi fan-shaped south roof.
185 The solution in this case is to use 'Ogrid Block' splitting method along the side wall of
186 the greenhouse (Fig. 4 (b)). Finally, it is beneficial to move the vertex in order to find
187 the optimal quality and check the global association (Fig. 4 (c)).

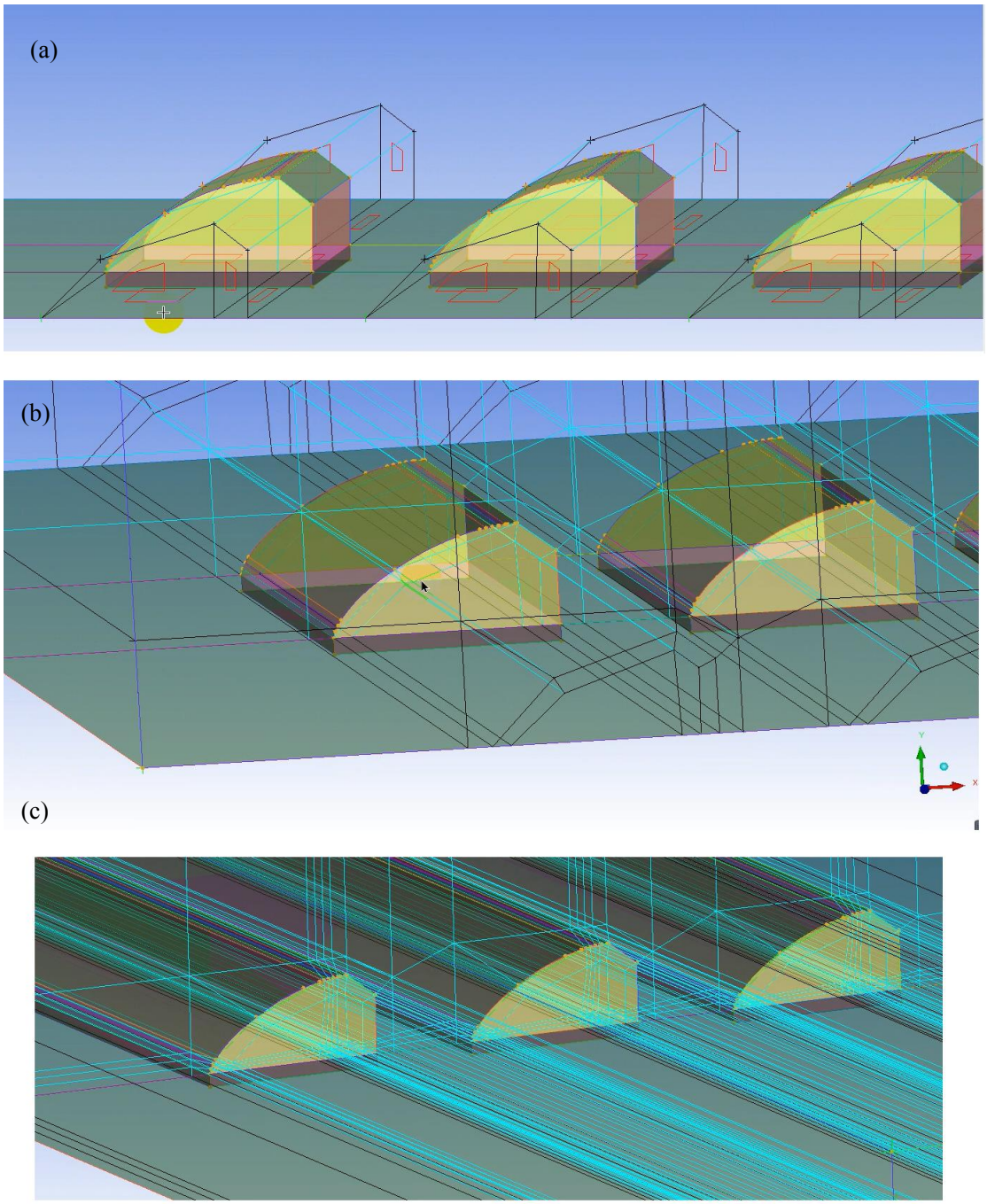

Fig. 4. Process of creating a mesh file.

1.4.1 Tests of grid independence

The height of the first cell from the wall in the boundary layer was determined by conducting iteration tests of independence of the results regarding the grid density. The

tested case corresponded to a windward flow for which a wind profile was imposed at the entrance of the calculation domain as follows (Haxaire, 1999),

$$u = \frac{u_*}{\kappa} ln(\frac{H+H_0}{H_0}) \quad (3)$$

where u is wind speed, m s^{-1}.

The turbulent kinetic energy k and dissipation rate ε distributions at the entrance are defined by the following equations (Hoxey and Richardson, 1983),

$$k = \frac{u_*^2}{\sqrt{C_\mu}} \quad (4)$$

$$\varepsilon = \frac{{u_*}^3}{\kappa(H+H_0)} \quad (5)$$

The wind speed at 2.5 m height ($u_{2.5}$) was 5 m s^{-1} for the tested case. The criterion for the convergence residual was 1×10^{-3} for the continuity, k, and ε equations, and it was 1×10^{-6} for the energy equation.

The steady-state solution was generally reached within 500 steps for the 2D case and within 900 steps for the 3D case. The first cell height giving the optimum y+ solution was 0.025 m based on the iteration independence tests. Fig. 5 shows that the wall y+ satisfies $30<y^+<300$ for the Standard Wall Function. The total elements number is shown in Table 3 and the mesh files are shown in Fig. 3 both for the windward and leeward cases.

Table 3. Elements number of 2D and 3D Mesh.

Mesh	Windward mesh	Leeward mesh
2D	36722	36726
3D	16807531	16776673

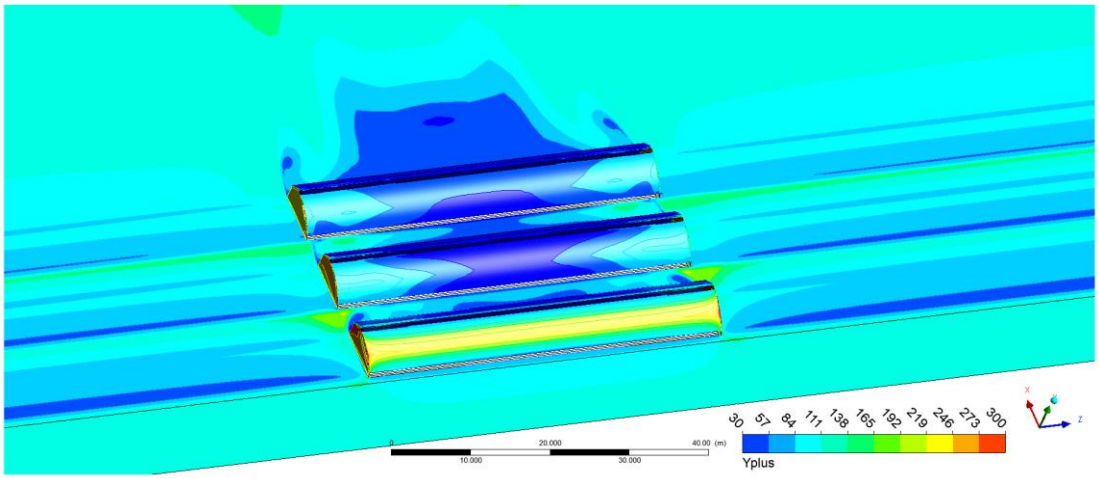

Fig. 5. Wall y^+ value for the case where the first cell height is 0.025 m.

1.5 Sample data

In the first step, 2D and 3D modelling were conducted in parallel. 20 cases were selected (10 cases for 2D and 10 cases for 3D) to compare their natural ventilation rate and the wind field. For these cases, the vents of the 3 greenhouses were fully open. Windward and leeward wind directions were applied, with a log law wind profile at the inlet (see Table 4). Also, five values of the reference velocity $u_{2.5}$ from 1 to 5 m s^{-1} were chosen for the simulations. The temperature difference between indoor and outdoor was 0 K (300 K for the indoor and outdoor domain). The ventilation rate through the vents of each greenhouse was monitored. The criterion of quality estimation of the fit between the 2D and the 3D models was defined as follows (Eq. 6),

$$e = \left|\frac{L_2 - L_3}{L_3}\right| \quad (6)$$

where e is the ratio error; L_2 is the ventilation rate simulated by 2D case m^3 s^{-1} and L_3 is the ventilation rate simulated by 3D case m^3 s^{-1}.

In the second step, 990 samples were collected using 2D simulations. A natural ventilation rate model was then developed using a nonlinear regression trees model (see

232 section 1.7). For these cases, there was only one greenhouse in the calculation domain.
233 Eleven temperature differences between a fixed temperature of 300 K at the inlet and
234 the average temperature inside the greenhouse from 0 to 10 K were tested. The steady
235 indoor temperature was simulated by defining fixed wall temperature. The indoor
236 average temperature was monitored by conducting iteration tests until it reached the
237 targeted value. Combined with the 9 vent opening configurations described in Table 1,
238 windward and leeward directions were tested, with a log law wind profile at the inlet,
239 and five values of $u_{2.5}$ from 1 to 5 m s^{-1}. This means in total 11*9*2*5=990 cases. The
240 area ventilation rate was monitored and calculated by the following equations,

241 $$L = \frac{f_m}{\rho}\frac{l_g}{A_g} \quad (7)$$

242 where L is the area ventilation rate, m^3 s^{-1} m^{-2}; f_m is the simulated mass flow rate through
243 the vents, kg m^{-1} s^{-1}; l_g is the length of the greenhouse, m; A_g is the area of the
244 greenhouse, m^2 and ρ is the density of the fluid (incompressible-ideal-gas), kg m^{-3},
245 which is calculated by the following equation (Ansys-Fluent, 2010),

246 $$\rho = \frac{P_{op}}{\frac{R}{M_w}T} \quad (8)$$

247 where R is the universal gas constant, 8.31 m^3 Pa K^{-1} mol^{-1}; M_w is the molecular weight
248 of the gas, kg mol^{-1}; P_{op} is the operating pressure, Pa.

249 Table 4. Boundary conditions

250

Boundary	Boundary condition	
	Momentum	Thermal
Wall	No-slip wall	Fixed temperature
South roof	No-slip wall	Fixed temperature

North roof	No-slip wall	Fixed temperature
Ground	No-slip wall	Fixed temperature
External top, both sides	Symmetry	
Inlet of the external domain	Velocity-inlet: Wind profile Eq. 3, 4, 5; Temperature 300 K	
Outlet of the external domain	Pressure-outlet; Temperature 300 K	

1.6 Monitoring of wind speed at 2.5 m height

Wind speed is a required parameter of the natural ventilation model. Although, the appropriate distance of anemometers from objects is common knowledge in wind engineering. However, in most practice experiments, due to the variable structure of greenhouses and different experimental scenes, it is necessary to specify a standard to provide a brief guidance for researchers who study the CSG climate prediction but have little knowledge in wind engineering. The method is to monitor the change of wind speed with position, thus help to determine a limited area ensuring that the wind speed is in the free stream. The red lines in Fig. 6 show the monitoring locations at 2.5 m height, which cross the external domain and the whole greenhouse in two orthogonal directions. 10 groups of samples were monitored, which were respectively $u_{2.5}$ = 1~5 m s^{-1} as the inlet inputs under windward and leeward flow.

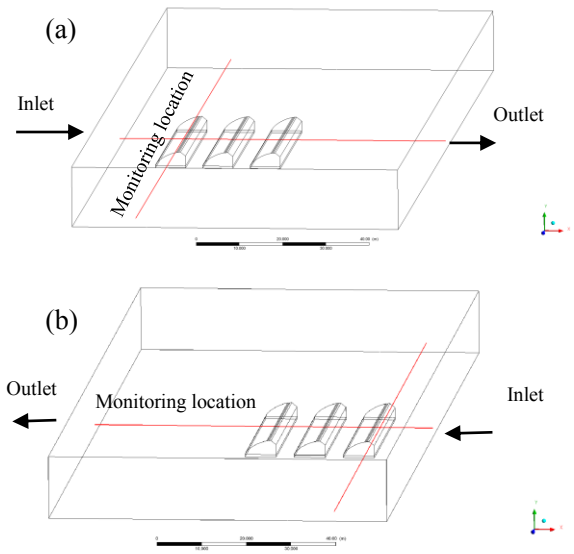

Fig. 6. Monitoring location (red lines) of wind speed, (a) for windward flow, and (b) for leeward flow.

1.7 Ventilation model establishment using regression trees

Regression trees and classification trees belong to a particular kind of nonlinear predictive model, namely prediction trees. Regression trees are a way of making quantitative predictions, which use the trees to represent the recursive partition. Each of the leaves represents a cell of the partition and has attached to it a simple model which applies in that cell only (Shalizi, 2006). The inputs are respectively wind speed and directions, the upper and lower vent opening ratio areas (vent area/greenhouse area), and the temperature difference between indoor and outdoor. The output is the area ventilation rate, $m^3\ s^{-1}\ m^{-2}$. In this work, this technique has been used to obtain the natural ventilation rate model.

1.8 Statistics and Machin Learning Toolbox

MATLAB´s "Statistics and Machin Learning Toolbox" provides functions and applications to describe, analyze, and model data. It contains a Regression Trees Predict

281 block that calculates responses to given input data. The regression trees model was
282 trained and predicted by following the tree from the root node down to a leaf node. At
283 each node, the model decides which branch to follow using the rule associated with that
284 node and it continues until it arrives at a leaf node. Each step in a prediction involves
285 checking the value of one predictor variable (MATLAB, 2021).

286 1.9 Evaluation of the regression trees ventilation model

287 The evaluation of regression trees model was conducted to compare its output with an
288 existing validated theoretical model used to simulate the ventilation rate of the CSG.
289 The equations are shown below (Zhang et al., 2019),
290 assume that the indoor and outdoor air temperatures distribution is uniform:

291 $$L_T = f_u\sqrt{\frac{2g\Delta H_v(T-T_o)}{T}} \quad (9)$$

292 where

293 $$f_u = \frac{1}{\sqrt{\frac{1}{u_j^2F_j^2}+\frac{1}{u_p^2F_p^2}}} \quad (10)$$

294 where, L_T is the thermal gradients ventilation rate, m^{-3} s^{-1}; f_u is the coefficient of the
295 thermal pressure ventilation rate; g is the gravitational acceleration, m s^{-2}; ΔH_v is the
296 height difference between the upper vent and the lower vent, m; T is the indoor air
297 temperature, K; T_o is the outdoor air temperature, K; u_j is the flow coefficient of the air
298 inlet; F_j is the effective area of the air inlet, m^2; u_p is the flow coefficient of the air outlet;
299 F_p is the effective area of the air outlet, m^2.
300 The wind pressure ventilation rate is estimated by an empirical value given by NY/T
301 1451-2018 (2018),

302 $$L_w = \beta F_j u \quad (11)$$

where, L_w is the wind pressure ventilation rate, m^{-3} s^{-1}; β is the wind pressure coefficient. The area ventilation rate was the square root of the quadratic sum divides area of the greenhouse,

$$L = \frac{\sqrt{{L_T}^2 + {L_w}^2}}{A_g} \quad (12)$$

The evaluation was to calculate the averaged absolute error (AE) of predicted ventilation rate by entering the same inputs to the regression trees and the theoretical model, including gradient wind speeds, vent opening areas and temperature differences between indoor and outdoor, under leeward and windward conditions (Fig. 7).

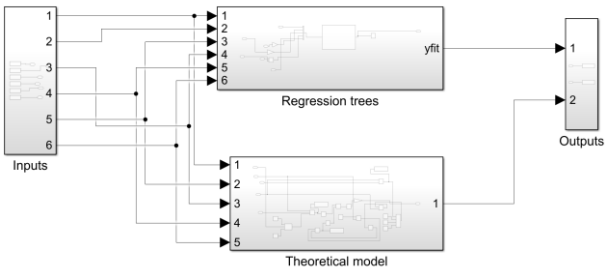

Fig. 7. Comparison of predicted ventilation rate between the regression trees and theoretical models.

2. Results and discussion

This section describes the main results for the numerical analysis of the wind field in rows of the CSG, and the development of a natural ventilation model. First, the wind flow pattern around and inside multiple greenhouses and the ventilation rate are compared using 2D and 3D cases. Afterward, the limited area ensuring that the wind speed is in the free stream is demonstrated. Finally, a regression trees natural ventilation rate model is developed and evaluated.

322

323 2.1 Ventilation rate and airflow pattern under the windward condition

324 The airflow pattern is analyzed under windward conditions. Fig. 8 shows the
325 comparative analysis between 2D and 3D cases. The vents openings are 100% in this
326 comparative analysis section. The first row in Fig. 8 is for the windward condition. The
327 ventilation rate of 2D and 3D are very close for the greenhouse A, for which the ratio
328 errors are below 0.1 (Fig. 8) for 1-5 m s^{-1} $u_{2.5}$ wind speeds. However, for greenhouses
329 B and C (different positions in building clusters), the ratio errors are above 0.5. Besides,
330 the errors for the greenhouse B are greater than the greenhouse C and it is positively
331 correlated with wind speed. Notice that the negative value of the ventilation rate for the
332 greenhouse B means that the upper vent is the inlet and the lower vent is the outlet,
333 which is described in detail in the next paragraph. This result demonstrates that 2D
334 cases are sufficient when there is no obstacle in front and behind the greenhouse in
335 windward conditions. However, if there are other greenhouses in front and behind, 3D
336 cases must be adopted.

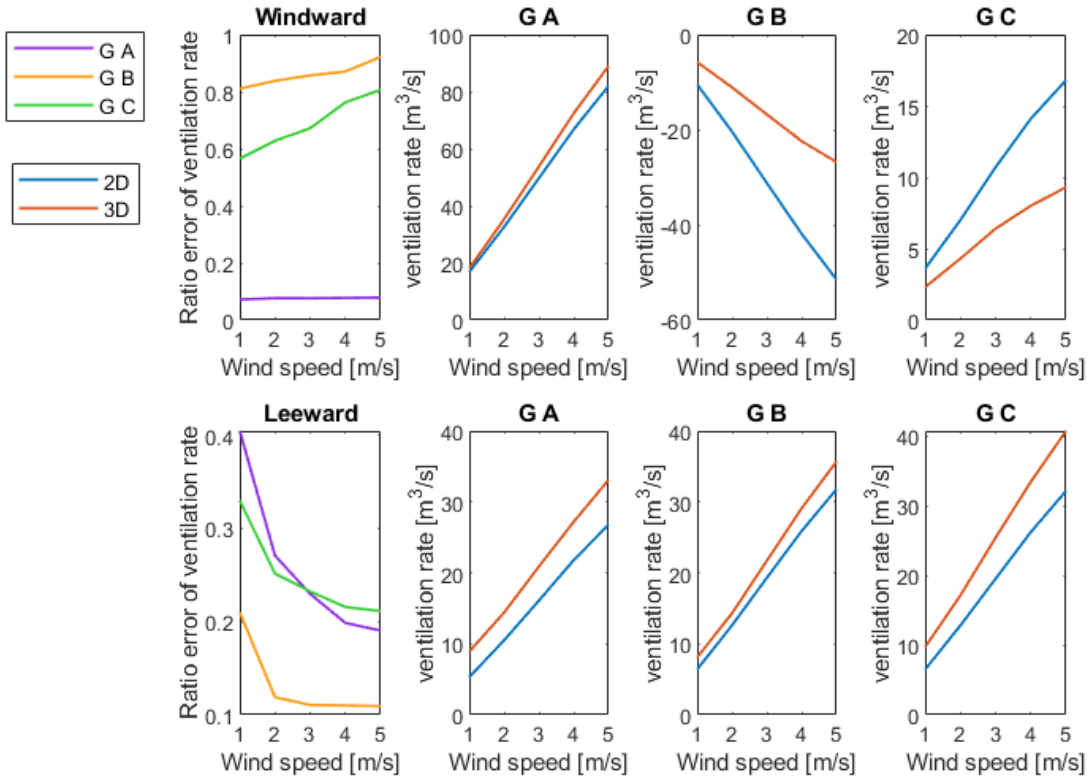

Fig. 8. Ratio error of ventilation rate between 2D and 3D cases under windward and leeward conditions. Ventilation rate from 2D and 3D cases for each greenhouse. G A, G B, G C are respectively greenhouse A, B and C. See Fig. 3 for positions of greenhouses A, B, C.

Fig. 9 shows the velocity vectors obtained from 2D and 3D cases and depicts larger differences for the greenhouses B and C than for the A. The airflow patterns calculated from 2D and 3D simulations are indeed similar in the central vertical section of the front greenhouse of (Fig. 9 (a), (b)). Without considering the influence of the thermal gradients, it can also be seen that the lower vents of greenhouses A and C act as an inlet, while it is an outlet for the greenhouse B for both 2D and 3D cases, considering the same central location in the 3D case (Fig. 9 (a), (b)). When adopting 2D case, for the middle and the back row greenhouses, the airflow pattern of the central section of the

greenhouse thus cannot be regarded as that of the whole greenhouse. This fact explains why the middle and back row greenhouse has the great error in Fig. 9 regarding the ventilation rate prediction. This means also that if the 2D model is used for windward flow, there shall be no obstacles in front of and behind the greenhouse. Otherwise, the error could reach more than 50%.

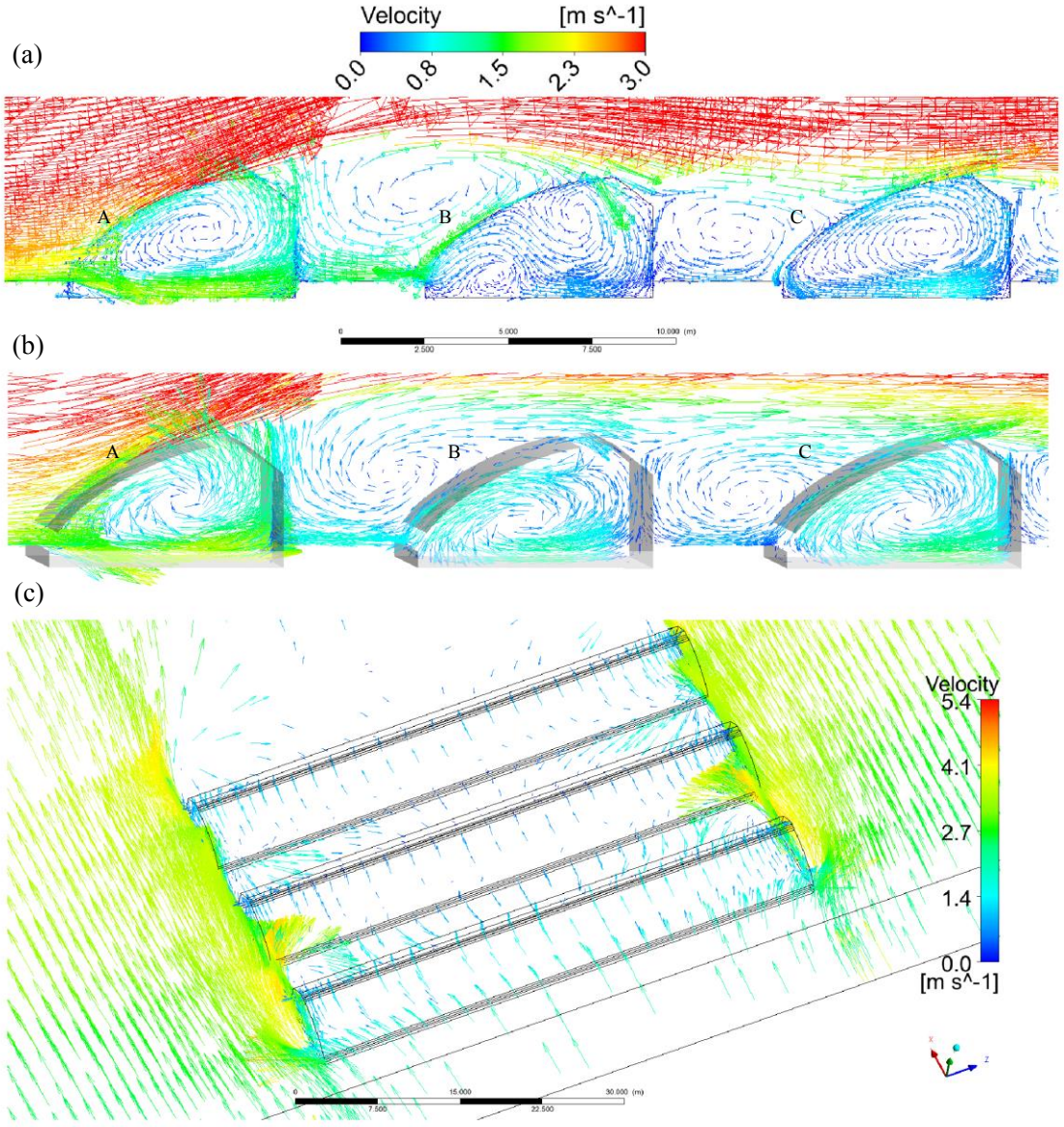

Fig. 9. Velocity vectors of windward flow when $u_{2.5}$ is 3 m s^{-1}. (a) from 2D simulation and (b) at the same location from 3D simulation. (c) overhead view at lower vents height from 3D simulation.

From Fig. 10 it can be seen more clearly. It shows that for greenhouse A, all air enters through the lower vent (Fig. 10 (a)). For greenhouse C, most of the air enters from the lower vent (Fig. 10 (c)). In the center of the greenhouse C, there is flow in the opposite direction. Nevertheless, the inflow of the lower vent is significantly greater than the outflow. For greenhouse B, most of the air enters the room from the upper vent and left from the lower vent (Fig. 10 (b), (d).

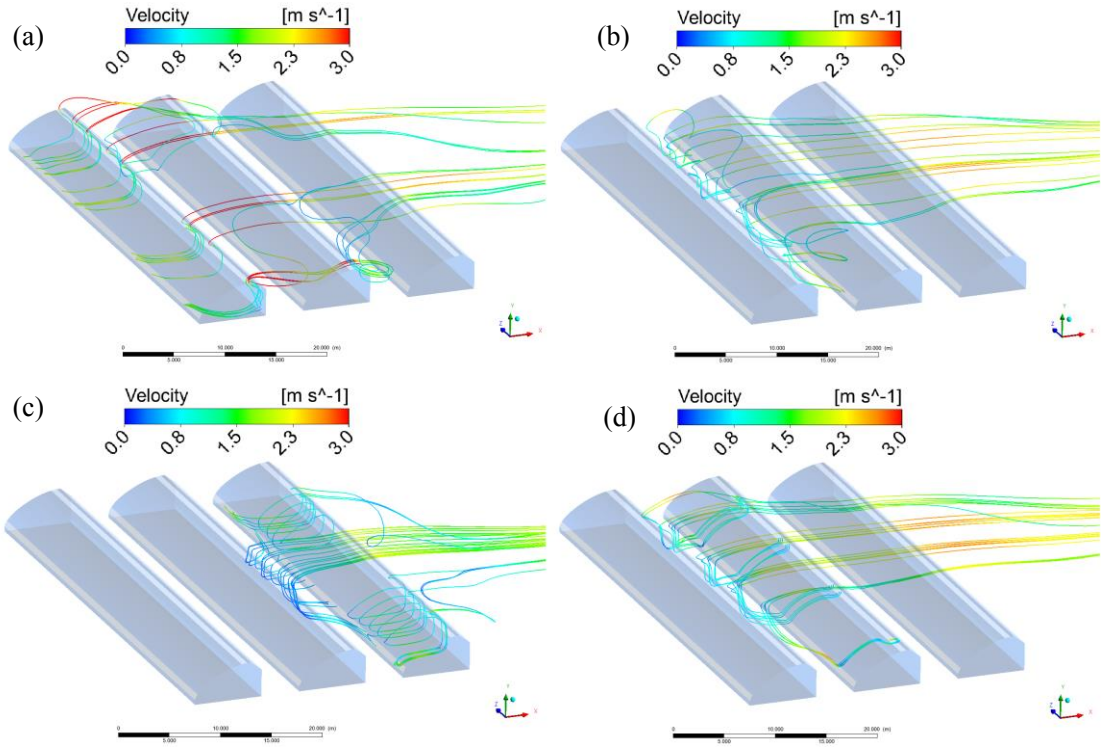

Fig. 10. Streamlines of windward flow when $u_{2.5}$ is 3 m s^{-1}. (a), (b) and (c) are for greenhouse A, B and C, where streamlines start from the lower vents. (d) is for the greenhouse B, where streamlines start from the upper vents.

The above description is when the temperature difference inside and outside the greenhouse is 0 K, which means that wind pressure is dominant, the ventilation rate of

greenhouse B is negative (Fig. 8). A negative value means that most of the air enters from the upper vent and flows out from the lower vent. Let's see how the flow pattern changes of greenhouse B when thermal pressure is dominant. When thermal pressure is dominant, it's the exact opposite. Fig. 11 shows that when there is a temperature difference of about 5 K inside and outside the greenhouse, the upper vent is the outlet, and the ventilation rate is positive. The wind speed is 1 m s^{-1} and the ventilation rate is 6.5 m^3 s^{-1}. Note that the ventilation rate is -5.8 m^3 s^{-1} when the temperature difference inside and outside the greenhouse is 0 K (Fig. 8).

It also significantly increased the ventilation rate of greenhouse C. It increased from 2.3 m^3 s^{-1} to 8.9 m^3 s^{-1} under windward flow when $u_{2.5}$ is 1 m s^{-1}. This illustrates that in the greenhouse clusters, wind pressure and thermal pressure may form an antagonistic force, so that the natural ventilation rate is weakened. Appropriately increasing the spacing between greenhouses is essential for maintain ventilation.

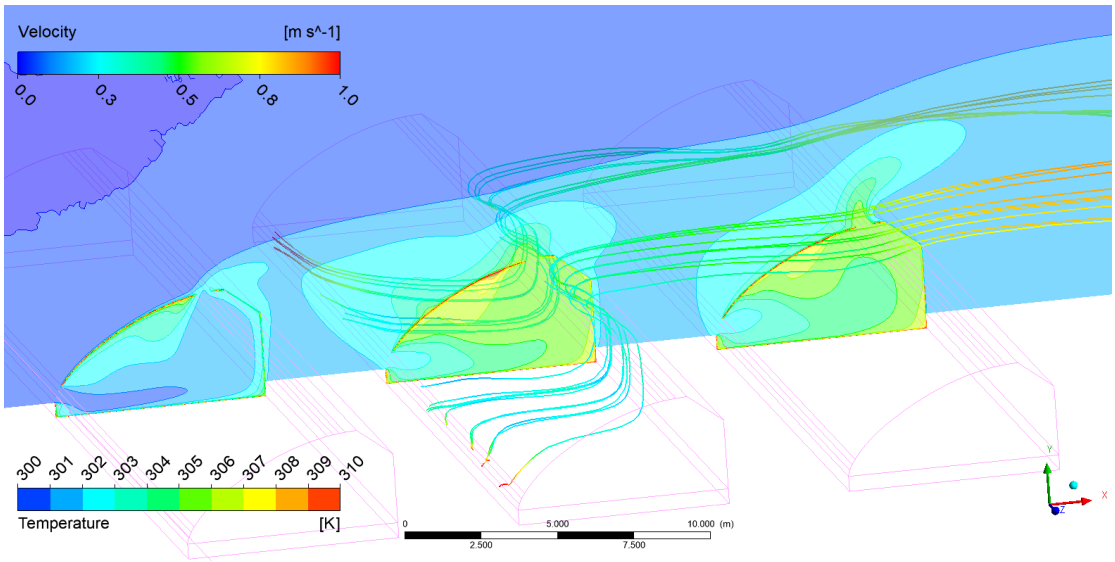

Fig. 11. Streamlines of windward flow when u2.5 is 1 m s^{-1}, and temperature contour for greenhouse B.

2.2 Ventilation rate and airflow pattern under the leeward condition

Under leeward flows, the lower vents are the inlet (Fig. 12 (a), (b)), and the ventilation rates from 3D simulations are greater than 2D in all the samples. This is probably because in 3D cases the inflow through lower vents comes from both the roof and lateral sides, whereas it comes only from the roof in 2D cases (Fig. 12 (c)). When adopting 2D simulation, this difference in the flow field is more enhanced inside the greenhouses A and C, than inside the greenhouse B. Besides, this impact is negatively correlated with wind speed.

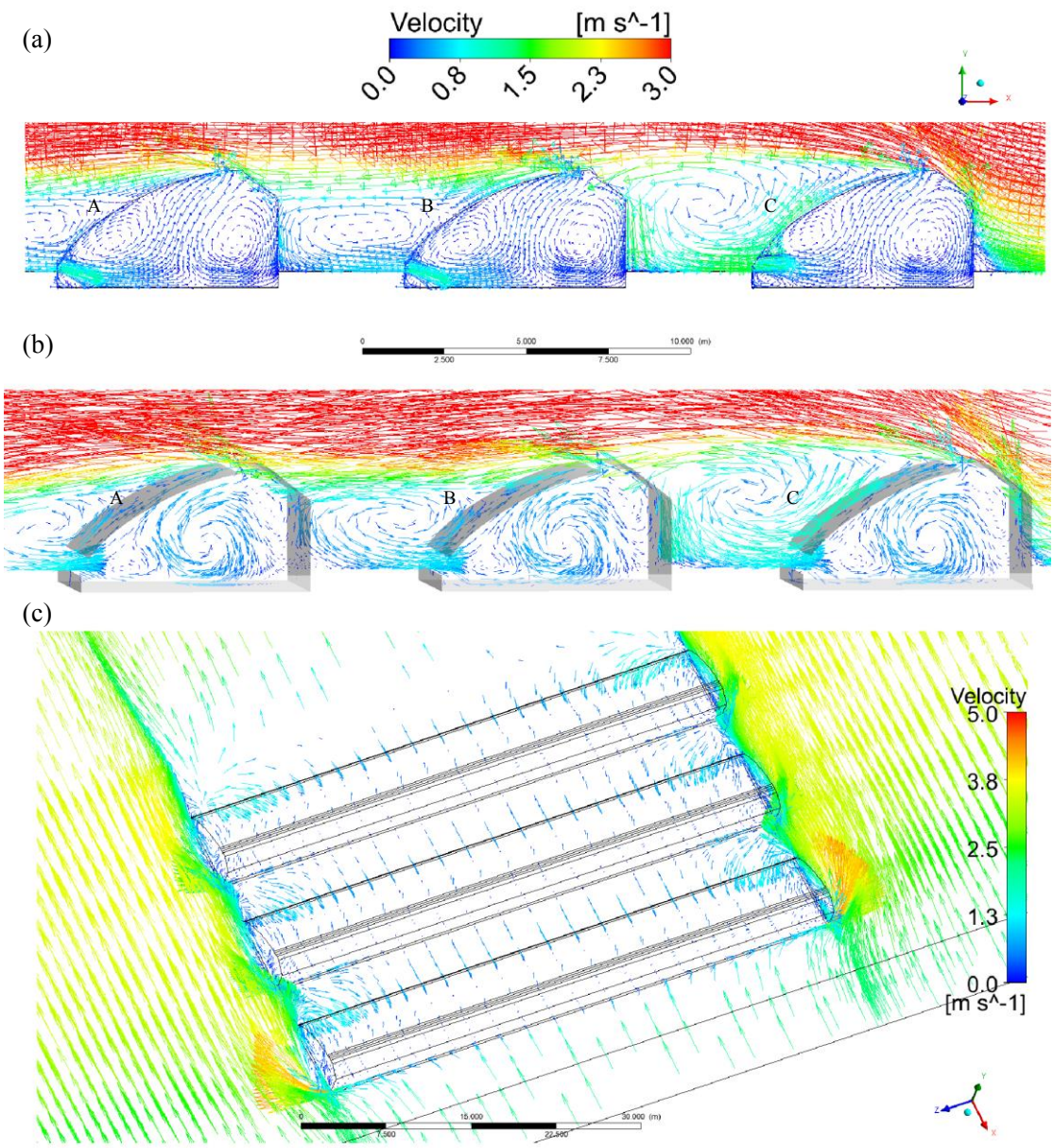

Fig. 12. Velocity vectors of leeward flow when $u_{2.5}$ is 3 m s^{-1}. (a) is from 2D simulation and (b) is the same location from 3D simulation. (c) is the overhead view at lower vents height from 3D simulation.

Up until now, a vast majority of current research is reviewed to be two-dimensional (Bournet and Boulard, 2010; Villagrán et al., 2019; Benni et al., 2016). As well as many previous 2D models about the CSG (He et al., 2018; Zhang et al., 2016). Current studies

405 are aimed at a single greenhouse, ignoring the influence of surrounding buildings, and
406 the wind direction is relatively simple. However, the modelling of flow fields in
407 greenhouse clusters is of great relevance for both production and research in the future.
408 Another reason for which most researchers choose 2D model is that their calculation is
409 transient, and it is known that with three dimensional transient CFD simulation, it is
410 difficult to achieve convergence at each time step, which affects the accuracy (He et al.,
411 2018; Tong et al., 2018). Although, with the progress of hardware, these problems are
412 expected to be solved in the next few years, the methodology in this study looks forward
413 to bringing time-consuming numerical computations into the fast transient simulation
414 by training their results in the black box model.
415
416 2.3 Analysis of wind speed at the monitoring location
417 In the direction perpendicular to the wind, the impact of the building on the wind speed
418 is positively correlated with wind speed (Fig. 13). The gray area in Fig. 13 (a), (b) shows
419 the recommended area to place wind speed sensors ensuring that the measured wind is
420 in free stream (the greenhouse wall is at 86 m from the western side) i.e. the area where
421 the building does not impact the flow field anymore. Under the windward condition,
422 the ranges where the wind speed changes sharply on both sides outside the greenhouse
423 are below 8, 10, 16, 20, and 23 m away from the greenhouse under 1~5 m s^{-1} wind
424 speed respectively. Under the leeward condition, the distances are respectively below
425 7, 9, 13, 17, 20 m under 1~5 m s^{-1} wind speed. Beyond these distances, the measured
426 wind speed is considered in the free stream. The impact of buildings on air flow on
427 lateral sides is clearly seen from Fig. 14. This disturbance is more obvious for the

greenhouse in the rear row. It is recommended to measure the free stream wind speed in the windward upstream of the building clusters.

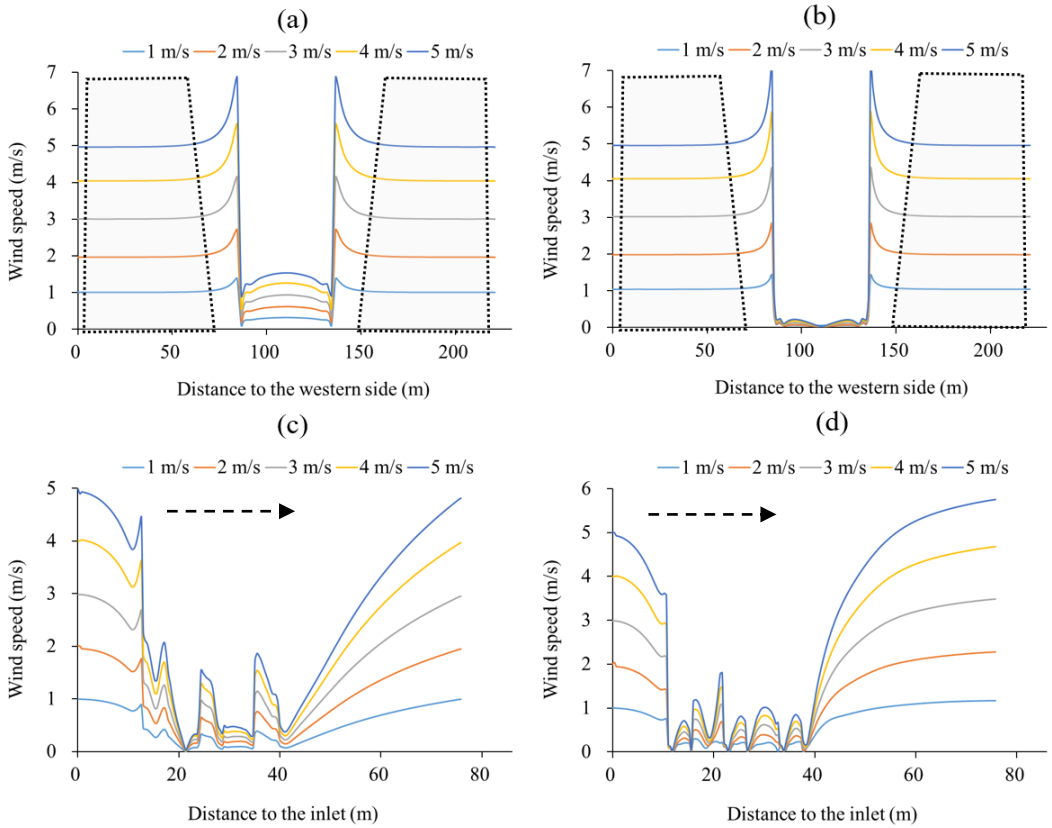

Fig. 13. Wind speed at the monitoring location. (a) (c) are under windward flow, (b) (d) are under leeward flow. (a) (b) are located perpendicular to the wind direction. (c) (d) are located parallel to the wind direction. The gray area is the recommended area to place wind speed sensors. ------▶ is the wind direction.

In the direction parallel to the wind (the inlet is 10.8 m from the greenhouse), whether windward or leeward, the optimal distance to the greenhouse would be beyond 10.8 m (3 times the ridge height) in the upstream direction and above 36 m (10 times of the ridge height) in the downstream portion is 10 times, ensuring the wind speed is free

(Fig. 13 (c), (d)). This conclusion was confirmed by Kim et al. (Kim et al., 2017). Measurements of the wind speed is a necessary step for simulating the greenhouse climate. Anemometers have to be placed in an open area outside of the greenhouse, this study gives the reference value of this distance in various cases.

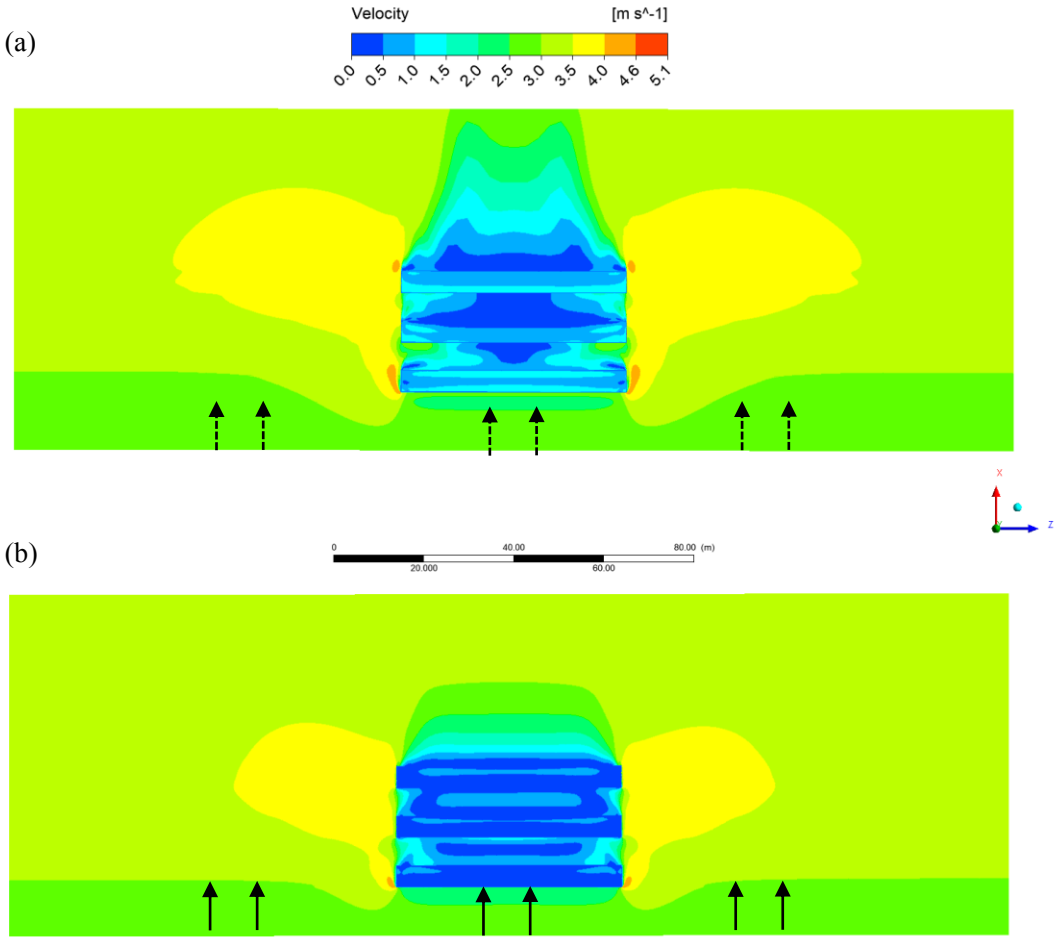

Fig. 14. Contour of wind speed on the 2.5 m height horizontal plane. (a) is windward flow and (b) is leeward flow.

2.4 Ventilation model establishment using regression trees

Estimation of ventilation rate is a laborious work and usually requires multiple complex parameters. In this section, a regression trees ventilation model was developed from

990 CFD samples. This model applies to a greenhouse in an open area. Its inputs are the wind speed at a height of 2.5 m, the ratio area of the upper and lower vents, the area of the greenhouse, and the temperature difference between inside and outside of the greenhouse. The output is the area ventilation rate in $m^3\ s^{-1}\ m^{-2}$. The temperature difference was achieved by the imposed fixed wall temperature. The greenhouse temperature decreases from top to bottom, and an air temperature near the opaque walls higher than in other areas (He et al., 2018). By embedding the buoyancy equation, the contribution of thermal gradients to the ventilation rate is calculated by steady-state simulation.

990 samples are used to train the model. In Fig. 15, the so-called "true" response is provided by CFD results while the predicted response is provided by the regression trees ventilation model. From left to right in Fig. 15, the velocity speed is increased, and from bottom to top, the vent opening area is increased. The points on each short line correspond to the tested temperature differences which increase from left to right. There are therefore 11 points in each short line, representing the temperature difference between 0 to 10 K. It shows that at low wind speed, the temperature difference makes the lines tilt greatly. But at high wind speeds, all the lines are almost horizontal, which demonstrates that under low wind speed, thermal pressure ventilation becomes predominant, and vice versa. From bottom to top, the vents opening areas are increased. There are 18 rows (9 vents combination * 2, windward and leeward) at each wind speed. Fig. 15 shows that choosing a larger vent area at high wind speed is more positive for

increasing the ventilation rate than at low wind speed. The RMSE of the regression trees model is 0.002. This model can perfectly deal with the combined effect of wind pressure and thermal gradients.

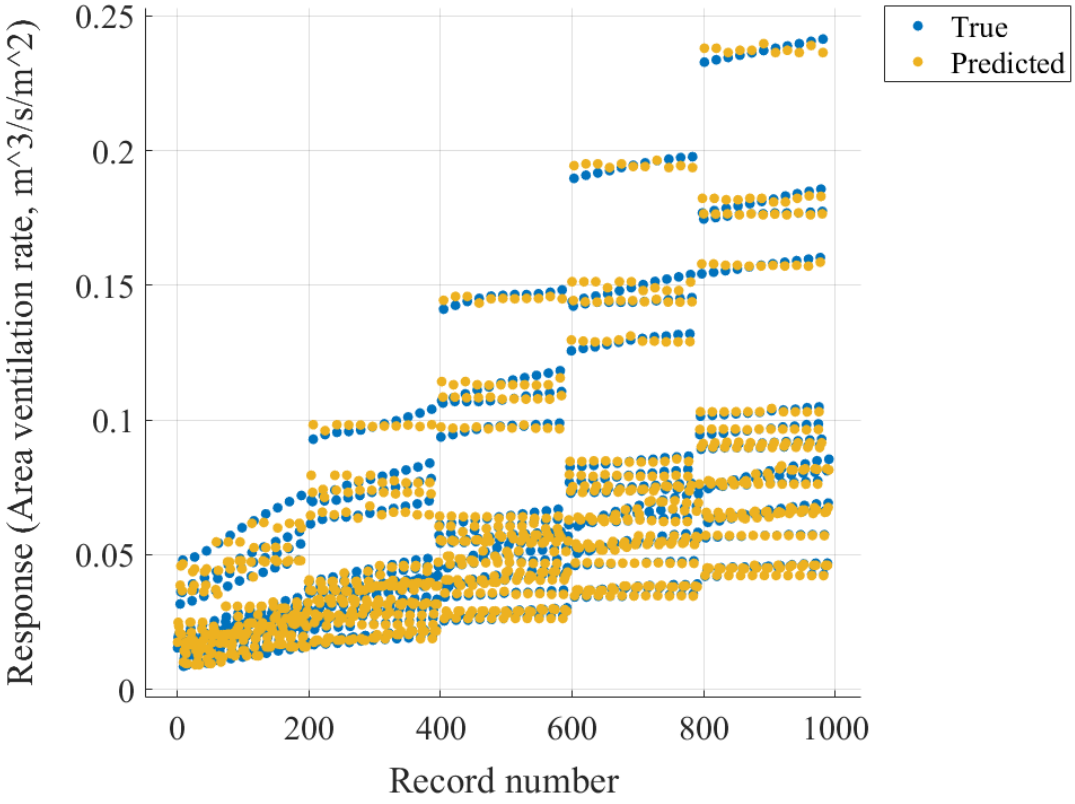

Fig. 15. Responses of regression trees ventilation model. The predicted vs actual plot.

2.5 Comparison between the regression trees and theoretical models

Fig. 16 shows 330 pairs of samples. Each pair of samples is a comparison of the two models under the same input. The result shows that the curves of the regression trees and theoretical models are very close, with an AE between two models are 0.0077 $m^3/m^2/s$ (Fig. 16 (a)). From samples No.0-30, it is known that ventilation models are linear when the wind pressure is the only driving force. From samples No.31-330, the

results show that the regression trees model can totally take over accurate predictions when the wind pressure and thermal pressure act simultaneously, without any theoretical parameters and laborious equation modeling.

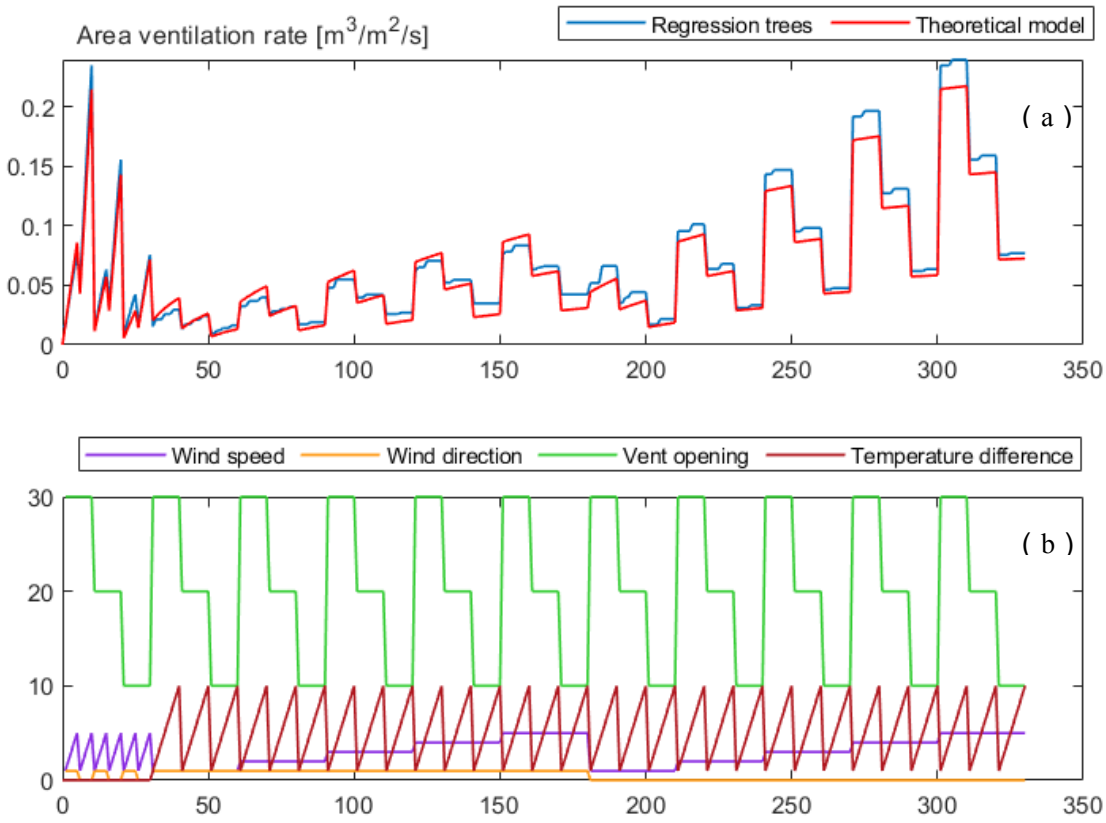

Fig. 16. Comparison of predicted ventilation rate between the regression trees and theoretical models. (a) is outputs and (b) is inputs. Wind speeds range 1-5 m s^{-1} (purple line); temperature differences range 0-10 K (red line); equally vent opening area for the upper and lower vents, respectively 10, 20, 30 m^2 (green line); 0 represents windward and 1 represents leeward (orange line). The β value of the theoretical model is 0.5 under windward flow and 0.2 under leeward flow.

2.6 Application of the regression trees ventilation model in simulating

greenhouse climate

Currently, the application of natural ventilation models relies on multiple complex parameters. Because those researches are from wind engineering background so that the parameters could be professional and difficult to measure. This is unfriendly to those researchers from agriculture who use natural ventilation to study the greenhouse climate. In this section, a brief introduce of the application about the regression trees ventilation model is shown in Fig. 17. The greenhouse temperature system has 5 source terms, such as convection, conduction and radiation (Liu et al., 2021), as they are described in Appendix A. One of the source terms requires real-time ventilation rate parameters. The connection of the regression trees ventilation model helps to quantify the energy and water vapor transfer between inside and outside of the greenhouse. The current ventilation rate is easily estimated by only four inputs and requires very little running time. Meanwhile, the reliability of ventilation rate calculation comes from the huge amount of computation and simulation time behind each training data.

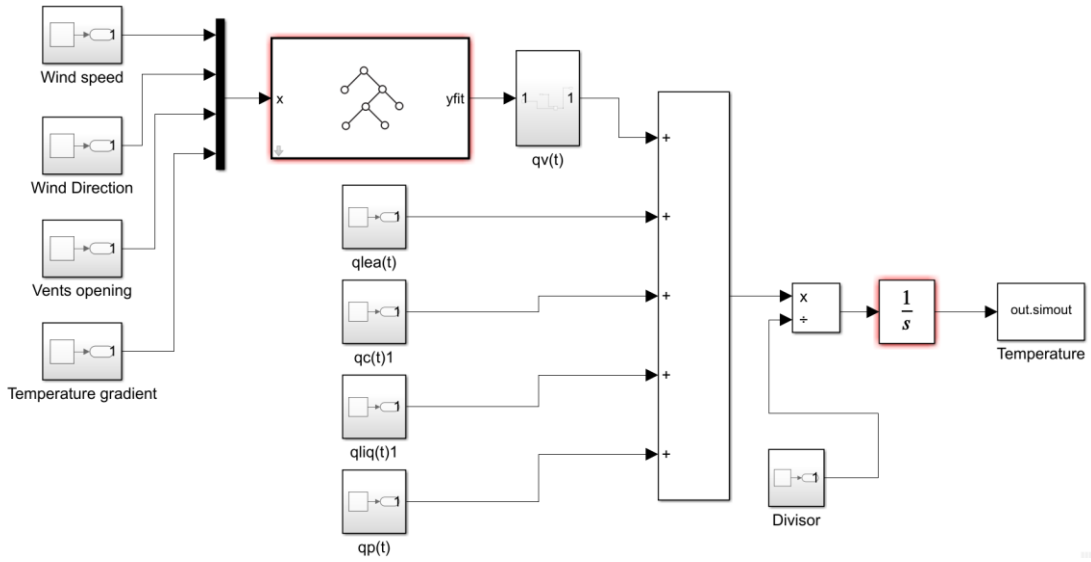

Fig. 17. The application of the regression trees natural ventilation model in a

518 greenhouse system.

519

520 ## 3. Conclusion

521 This paper provides a numerical analysis of the airflow field in greenhouse rows.
522 Several important issues for the numerical analysis of greenhouse natural ventilation
523 are illustrated and proved. Its main contributions may be summarized as follows:

524 (i) Three-dimensional simulations require a huge amount of computation load. It
525 costs more than 30 hours to complete 900 iterations to achieve convergence in
526 each 3D case, using an Intel Core I7 CPU and 16 GB RAM. For that reason,
527 two-dimensional CFD simulations are still often adopted to study the wind flow
528 pattern around the greenhouse. The present study compares 2D and 3D
529 simulations, the results show that 2D model are sufficient when there is no
530 obstacle in front and behind the greenhouse, especially in windward flows. But
531 if there are other greenhouses nearby, 3D model should be adopted, Otherwise,
532 the error could reach 50% on the ventilation rate prediction.

533 (ii) Turbulence around buildings makes it difficult to measure wind speed, this
534 paper demonstrated limited area around rows of CSGs ensuring that the wind is
535 in the free stream and gives the recommended distance to the greenhouse to
536 place anemometers.

537 (iii) A regression trees natural ventilation model is developed using results from 990
538 two-dimensional CFD samples. This model perfectly deals with the combined
539 effect of wind pressure and thermal gradients. This regression trees natural

ventilation model is embedded in a published greenhouse model. The application shows this trees model performs ideal for a 7-day simulation (Appendix A).

CFD method provides a theoretical basis for virtual wind tunnel experiments. A huge number of reliable samples can be obtained through virtual wind tunnel experiments. In the future, with the update of computer hardware, a refined ventilation model is looked forward to being trained through a large number of three-dimensional simulation results, including arbitrary wind direction and better accuracy.

Acknowledgments

Liu Ran is most grateful for the financial support given by the China Scholarship Council for this research (no. 201909505002).

References

Ansys. 2010. Ansys Fluent User's guide. Ansys, Inc., Canonsburg, PA, USA ed.

Benni, S., Tassinari, P., Bonora, F., Barbaresi, A., Torreggiani, D., 2016. Efficacy of greenhouse natural ventilation: Environmental monitoring and CFD simulations of a study case. Energy and Buildings. 125, 276-286. https://doi.org/10.1016/j.enbuild.2016.05.014.

Boulard, T., Roy, J.C., Fatnassi, H., Kichah, A., Lee, I.-B., 2010. Computer fluid dynamics prediction of climate and fungal spore transfer in a rose greenhouse. Computers and Electronics in Agriculture. 74(2), 280-292. https://doi.org/10.1016/j.compag.2010.09.003.

Boulard, T., Roy, J.C., Lamrani, M.A., Haxaire, R., 1997. Characterising and Modelling the Air

562 Flow and Temperature Profiles in a Closed Greenhouse in Diurnal Conditions. IFAC
563 Proceedings Volumes. 30(26), 37-42. https://doi.org/10.1016/S1474-6670(17)41242-0.
564 Boulard, T., Wang, S., 2002. Experimental and numerical studies on the heterogeneity of crop
565 transpiration in a plastic tunnel. Computers and Electronics in Agriculture. 34(1-3), 173-190.
566 https://doi.org/10.1016/S0168-1699(01)00186-7.
567 Boulard, T., Roy, J.C., Pouillard, J.B., Fatnassi, H., Grisey, A., 2017. Modelling of
568 micrometeorology, canopy transpiration and photosynthesis in a closed greenhouse using
569 computational fluid dynamics. Biosystems Engineering. 158, 110-133.
570 https://doi.org/10.1016/j.biosystemseng.2017.04.001.
571 Bournet, P.-E., Boulard, T., 2010. Effect of ventilator configuration on the distributed climate of
572 greenhouses: A review of experimental and CFD studies. Computers and Electronics in
573 Agriculture. 74(2), 195-217. https://doi.org/10.1016/j.compag.2010.08.007.
574 Chen, J., Xu, F., Tan, D., Shen, Z., Zhang, L., Ai, Q., 2015. A control method for agricultural
575 greenhouses heating based on computational fluid dynamics and energy prediction model.
576 Applied Energy. 141, 106-118. https://doi.org/10.1016/j.apenergy.2014.12.026.
577 Cheng, X., Li, D., Shao, L., Ren, Z., 2021. A virtual sensor simulation system of a flower greenhouse
578 coupled with a new temperature microclimate model using three-dimensional CFD. Computers
579 and Electronics in Agriculture. 181, 105934. https://doi.org/10.1016/j.compag.2020.105934.
580 Fehér, T., 2006. Using Regression Trees in Predictive Modelling. Production Systems and
581 Information Engineering. 4, 115-124.
582 Haxaire, R., 1999. Caractérisation et modélisation des écoulements d'air dans une serre. Ph.D.
583 Thesis. Université de Nice, France.

He, X., Wang, J., Guo, S., Zhang, J., Wei, B., Sun, J., Shu, S., 2018. Ventilation optimization of solar greenhouse with removable back walls based on CFD. Computers and Electronics in Agriculture. 149, 16-25. https://doi.org/10.1016/j.compag.2017.10.001.

Hoxey, R.P., Richardson, G.M., 1983. Measurements of wind loads on full scale plastic greenhouse. J. Wind Eng. Ind. Aerodynam. 16, 57–83.

Katsoulas, N., Bartzanas, T., Boulard, T., Mermier, M., Kittas, C., 2006. Effect of vent openings and insect screens on greenhouse ventilation. Biosystems Engineering. 93(4), 427-436. https://doi.org/10.1016/j.biosystemseng.2005.01.001.

Kichah, A., Bournet, P.-E., Migeon, C., Boulard, T., 2012. Measurement and CFD simulation of microclimate characteristics and transpiration of an Impatiens pot plant crop in a greenhouse. Biosystems Engineering. 112(1), 22–34. https://doi.org/10.1016/j.biosystemseng.2012.01.012.

Kim, R.-w., Hong, S.-w., Norton, T., Amon, T., Youssef, A., Berckmans, D., Lee, I.-b., 2020. Computational fluid dynamics for non-experts: Development of a user-friendly CFD simulator (HNVR-SYS) for natural ventilation design applications. Biosystems Engineering. 193, 232-246. https://doi.org/10.1016/j.biosystemseng.2020.03.005.

Kim, R.-w., Kim, J.-g., Lee, I.-b., Yeo, U.-h., Lee, S.-y., Decano-Valentin, C., 2021. Development of three-dimensional visualisation technology of the aerodynamic environment in a greenhouse using CFD and VR technology, part 1: Development of VR a database using CFD, Biosystems Engineering. 207, 33-58. https://doi.org/10.1016/j.biosystemseng.2021.02.017.

Kim, R.-w., Lee, I.-b., Kwon, K.-s., 2017. Evaluation of wind pressure acting on multi-span greenhouses using CFD technique, Part 1: Development of the CFD model. Biosystems Engineering. 164, 235-256. https://doi.org/10.1016/j.biosystemseng.2017.09.008.

606 Kittas, C., Boulard, T., Bartzanas, T., Katsoulas, N., Mermier, M., 2002. Influence of an insect
607 screen on greenhouse ventilation. Transactions of the ASAE. 45.
608 https://doi.org/10.13031/2013.9940.
609 Li, T., Chang, J., Wei, M., Shi, G., Zhang, Y., Chen, D., 2018. Application situation and problem
610 analysis of ventilation facilities in solar greenhouse in Shandong province. Agricultural
611 Engineering and Technology. 38(16), 22-26. (In Chinese) https://doi.org/10.16815/j.cnki.11-
612 5436/s.2018.16.003.
613 Liu, R., Liu, J., Liu, H., Yang, X., Bienvenido Bárcena, J.F., Li, M., 2021. A 3-D simulation of leaf
614 condensation on cucumber canopy in a solar greenhouse. Biosystems Engineering. 210, 310-
615 329. https://doi.org/10.1016/j.biosystemseng.2021.08.008.
616 Liu, R., Li, M., Guzmán, J.L., Rodríguez, F., 2021. A fast and practical one-dimensional transient
617 model for greenhouse temperature and humidity. Computers and Electronics in Agriculture. 186,
618 106186. https://doi.org/10.1016/j.compag.2021.106186.
619 Majdoubi, H., Boulard, T., Fatnassi, H., Bouirden, L., 2009. Airflow and microclimate patterns in a
620 one-hectare Canary type greenhouse: An experimental and CFD assisted study. Agricultural and
621 Forest Meteorology. 149(6–7), 1050-1062. https://doi.org/10.1016/j.agrformet.2009.01.002.
622 MATLAB user's manual, R2021b. 2021.
623 Mistriotis. A., Bot, G.P.A., Picuno, P., Scarascia-Mugnozza, G., 1997. Analysis of the efficiency of
624 greenhouse ventilation using computational fluid dynamics. Agricultural and Forest
625 Meteorology. 85(3–4), 217-228. https://doi.org/10.1016/S0168-1923(96)02400-8.
626 Molina-Aiz, F.D., Fatnassi, H., Boulard, T., Roy, J.C., Valera, D.L., 2010. Comparison of finite
627 element and finite volume methods for simulation of natural ventilation in greenhouses.

628 Computers and Electronics in Agriculture. 72(2), 69-86.
629 https://doi.org/10.1016/j.compag.2010.03.002.
630 Nederhoff, E.M., van de Vooren, J., Udink ten Cate, A.J., 1985. A practical tracer gas method to
631 determine ventilation in greenhouses. Journal of Agricultural Engineering Research. 31(4), 309-
632 319. https://doi.org/10.1016/0021-8634(85)90107-6.
633 NY/T 1451-2018, 2018. Code for ventilation design of greenhouse. Ministry of Agriculture of the
634 PRC. P:7-8. (In Chinese)
635 Ould Khaoua, S.A., Bournet, P.E., Migeon, C., Boulard, T., Chassériaux, G., 2006. Analysis of
636 Greenhouse Ventilation Efficiency based on Computational Fluid Dynamics. Biosystems
637 Engineering. 95(1), 83-98. https://doi.org/10.1016/j.biosystemseng.2006.05.004.
638 Piscia, D., Montero, J.I., Baeza, E., Bailey, B.J., 2012. A CFD greenhouse night-time condensation
639 model. Biosystems Engineering. 111(2), 141-154.
640 https://doi.org/10.1016/j.biosystemseng.2011.11.006.
641 Rocha, G.A.O., Pichimata, M.A., Villagran, E., 2021. Research on the Microclimate of Protected
642 Agriculture Structures Using Numerical Simulation Tools: A Technical and Bibliometric
643 Analysis as a Contribution to the Sustainability of Under-Cover Cropping in Tropical and
644 Subtropical Countries. Sustainability. 13, 10433. https://doi.org/10.3390/su131810433.
645 Shalizi, C., 2006. Statistics 36-350: Data Mining. Lecture 10: Regression Trees.
646 https://www.stat.cmu.edu/~cshalizi/350-2006/.
647 Toparlar, Y., Blocken, B., Maiheu, B., van Heijst, G., 2019. CFD simulation of the near-neutral
648 atmospheric boundary layer: New temperature inlet profile consistent with wall functions.
649 Journal of Wind Engineering and Industrial Aerodynamics. 191, 91-102.

https://doi.org/10.1016/j.jweia.2019.05.016.

Tong, G., Che, Z., Bai, Y., Yamaguchi, T., 2008. Air exchange rate calculation for solar greenhouse using thermal balance method. Journal of Shenyang Agricultural University. 39(4), 459-462. (In Chinese) https://doi.org/10.3969/j.issn.1000-1700.2008.04.017.

Tong, G., Christopher, D.M., Zhang, G., 2018. New insights on span selection for Chinese solar greenhouses using CFD analyses. Computers and Electronics in Agriculture. 149, 3-15. https://doi.org/10.1016/j.compag.2017.09.031.

Van Buggenhout, S., Ozcan, S.E., Vranken, E., Van Malcot, W., Berckmans, D., 2007. Acoustical Ventilation Rate Sensor Concept for Naturally Ventilated Buildings. ASHRAE Transactions. 113(2), 192–199.

van Druenen, T., van Hooff, T., Montazeri, H., Blocken, B., 2019. CFD evaluation of building geometry modifications to reduce pedestrian-level wind speed. Building and Environment. 163, 106293. https://doi.org/10.1016/j.buildenv.2019.106293.

Villagrán, E.A., Baeza Romero, E.J., Bojacá, C.R., 2019. Transient CFD analysis of the natural ventilation of three types of greenhouses used for agricultural production in a tropical mountain climate. Biosystems Engineering. 188, 288-304. https://doi.org/10.1016/j.biosystemseng.2019.10.026.

Villagrán, E.A., Bojacá, C.R., 2019. Effects of surrounding objects on the thermal performance of passively ventilated greenhouses. Journal of Agricultural Engineering. 856, 20-27. http://hdl.handle.net/20.500.12010/8700.

Wu, G., Yang, Q., Zhang, Y., Fang, H., Feng, C., Zheng, H., 2020. Energy and optical analysis of photovoltaic thermal integrated with rotary linear curved Fresnel lens inside a Chinese solar

greenhouse. Energy. 197, 117215. https://doi.org/10.1016/j.energy.2020.117215.

Wang, S., Li, Z., Liu, S., Zhang, S., 2002. Effect of insect-proof screen on solar greenhouse ventilation. Transactions of the Chinese Society of Agricultural Engineering. 18(5), 123-125. https://en.cnki.com.cn/article_en/cjfdtotal-nygu200205023.htm.

Wang, X., Luo, J., Li, X., 2013. CFD Based Study of Heterogeneous Microclimate in a Typical Chinese Greenhouse in Central China. Journal of Integrative Agriculture. 12(5), 914-923. https://doi.org/10.1016/S2095-3119(13)60309-3.

Zhang, G., Fu, Z., Yang, M., Liu, X., Dong, Y., Li, X., 2019. Nonlinear simulation for coupling modeling of air humidity and vent opening in Chinese solar greenhouse based on CFD. Computers and Electronics in Agriculture. 162, 337-347. https://doi.org/10.1016/j.compag.2019.04.024.

Zhang, X., Wang, H., Zou, Z., Wang, S., 2016. CFD and weighted entropy based simulation and optimisation of Chinese Solar Greenhouse temperature distribution. Biosystems Engineering. 142, 12-26. https://doi.org/10.1016/j.biosystemseng.2015.11.006.

Appendix A

The developed regression trees model was connected to a one-dimensional greenhouse model that can predict the temperature and humidity (Fig. A1) (Liu et al., 2021). The energy source terms for the air in the greenhouse are associated with 5 sub-mechanisms: the ventilation energy, $q_v(t)$, W; the air leakage energy, $q_{lea}(t)$, W; the convective energy, $q_c(t)$, W; the water vapor-liquid transfer energy, $q_{liq}(t)$, W; and the plant energy, $q_p(t)$, W. The corresponding equation is given below:

694 $$\frac{dT(t)}{dt} = \frac{q_v(t)+q_{lea}(t)+q_c(t)+q_{liq}(t)+q_p(t)}{\rho*v*(c_p+c_{pw}*h(t))}$$

695 (A.1)

696 where, h is the indoor absolute humidity, kg kg^{-1}; t is time, s; ρ is the air density, (1.293)
697 kg m^{-3}; c_p is the specific heat capacity of the air, (1005) J kg^{-1} K^{-1}; c_{pw} is the specific
698 heat capacity of the water vapor, (1850) J kg^{-1} K^{-1}; and v is the greenhouse volume,
699 m^3. The greenhouse humidity source terms come from the ventilation humidity, s_v(t),
700 kg kg^{-1} s^{-1}; the air leakage humidity, s_{lea}(t), kg kg^{-1} s^{-1}; and the plant humidity, s_p(t), kg
701 kg^{-1} s^{-1}. The equation is given as follows,

702 $$\frac{dh(t)}{dt} = s_v(t) + s_{lea}(t) + s_p(t)$$

703 (A.2)

704 The application was presented and validated using a new group of measured climate
705 data collected on 20-26 Sept. 2019 from inside and outside of the greenhouse. The
706 greenhouse is the same size as Fig. 2, and it is located in Xiaotangshan, at the National
707 Precision Agriculture Demonstration Base (40°18’ N, 116°47’ E), Changping District,
708 Beijing, China. The outdoor climate data, including temperature, relative humidity,
709 solar radiation, wind speed, and direction, was measured every 15 mins to provide input
710 to the greenhouse model. The vents were opened from 7:00-18:00 during the
711 experimental days. The upper and lower opening area were respectively 30 m^2 and 5
712 m^2. The indoor temperature and humidity were measured every 15 mins to be validated
713 with the predictions using root mean squared error (RMSE). Note that the experimental
714 greenhouse has insect-proof net at the vents and the simulated ventilation rate is
715 multiplied by an attenuation coefficient. The ventilation rate is proved to significantly

716 decrease when an insect screen covered the vent (Kittas et al., 2002). The attenuation
717 coefficient normally depends on the characteristics of the insect-proof net and the
718 configuration of the vents, which is proved to be about 50% for the CSG with the
719 configuration of the same vents in this paper (Wang et al., 2002).

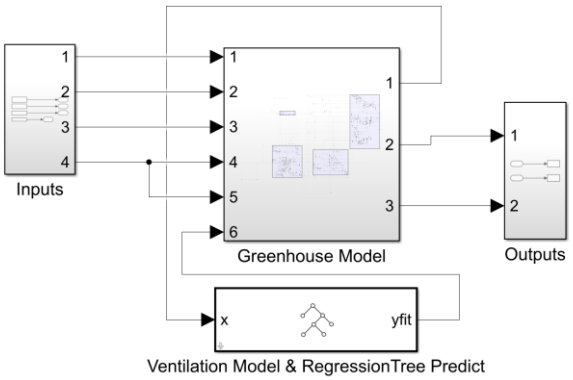

720

721 Fig. A1. Application of regression trees model.

722 Fig. A2 shows results obtained from a fast one-dimensional transient greenhouse model,
723 in which the regression trees ventilation model was included. Comparisons between
724 measurements and simulations are provided for September 20-26, 2019. The results
725 show that the model performs well as RMSE of temperature and relative humidity of
726 3.2 K and 9.8% respectively were found for a 7-day simulation.
727

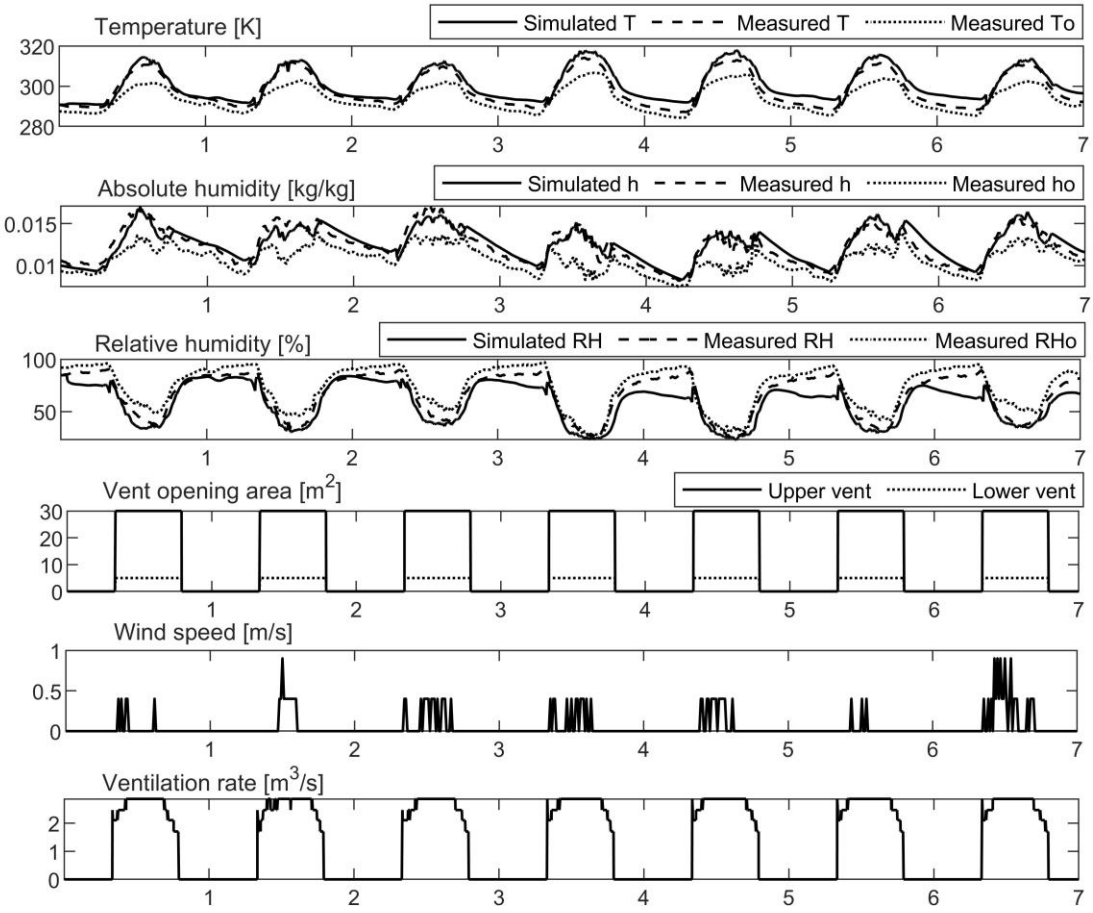

Fig. A2. Data set used for the model validation with the temperature and humidity on September 20-26, 2019. T is the averaged indoor temperature, K; T_o is the outdoor temperature, K; h is the averaged indoor absolute humidity, kg kg^{-1}; h_o is the outdoor absolute humidity, kg kg^{-1}; RH is the averaged indoor relative humidity, %; RH_o is the outdoor relative humidity, %.

2.2 Disease prediction in greenhouse

2.2.1 A model-based methodology for the early warning detection of cucumber downy mildew in greenhouses: An experimental evaluation

Research in this field is supported by the following journal publication:

Title	A model-based methodology for the early warning detection of cucumber downy mildew in greenhouses: An experimental evaluation
Authors	**R. Liu**, H. Wang, J. L. Guzmán, M. Li,
Journal	Computers and Electronics in Agriculture
Year	2022
Volume	194
Pages	106751
DOI	https://doi.org/10.1016/j.compag.2022.106751.
IF(JCR2022)	6.757
Categories	Horticulture (1/94) Q1 Computer Science Applications (38/747) Q1

Contribution of the Ph.D. Candidate

The Ph.D. candidate R. Liu is the main contributor and first author of this paper.

Computers and Electronics in Agriculture 194 (2022) 106751

Contents lists available at ScienceDirect

Computers and Electronics in Agriculture

journal homepage: www.elsevier.com/locate/compag

A model-based methodology for the early warning detection of cucumber downy mildew in greenhouses: An experimental evaluation

Ran Liu [a], Hui Wang [b], José Luis Guzmán [a,*], Ming Li [c,*]

[a] Department of Informatics, ceiA3, CIESOL, Ctra. Sacramento s/n, University of Almería, Almería, Spain
[b] Beijing Key Laboratory of Environment Friendly Management on Fruit Diseases and Pests in North China, Institute of Plant and Environment Protection, Beijing Academy of Agriculture and Forestry Sciences, Beijing 100097, China
[c] Information Technology Research Center, Beijing Academy of Agriculture and Forestry Sciences/National Engineering Research Center for Information Technology in Agriculture/National Engineering Laboratory for Agri-product Quality Traceability/Meteorological Service Center for Urban Agriculture, China Meteorological Administration- Ministry of Agriculture and Rural Affairs/Key Laboratory of Agri-informatics, Ministry of Agriculture, Beijing, China

ARTICLE INFO

Keywords:
Greenhouse climate
Mechanistic model
Downy mildew
Disease model
Weather forecast

ABSTRACT

This study introduces a new approach combining a mechanistic greenhouse climate model and a disease model for the forecast of diseases occurrence in greenhouses. The method was evaluated in NPADB (National Precision Agriculture Demonstration Base), Beijing, China using data collected from transplanting to the primary infection that occurred in the greenhouse, in the spring season of 2021. First, the dynamic model is used to predict the greenhouse indoor climate 72 h ahead. Then, this prediction is used as input to the disease model to detect disease occurrence in advance. The predictions for the greenhouse downy mildew were compared using real-time measured data for two months. After several false-positive reports, one positive report by both methods fitted the first observation in the greenhouse on April 24, 2021. Thus, the main contribution of this work is the early warning cucumber downy mildew via coupling climate and disease models, where only transient inputs from weather forecasts are required.

1. Introduction

The continuous rise in world population is paralleled by an increase in the area of bare land utilization for agriculture. Protected agriculture is of great significance because of its high efficiency, controllability, and advantages of land utilization. According to the latest statistics, the area of greenhouses worldwide was estimated at 3.64 million hectares (Guo et al., 2021). The warm air and sufficient water supply are obvious advantages of the protected cultivation, but it is also ideal for pest and fungal diseases (Cañadas et al., 2017). For example, downy mildew (*Peronospora sparsa*), botrytics (*Botrytics cinerea*), and powdery mildew (*Sphaerotheca pannosa*), which are three common fungal plant diseases in greenhouses, always result in damages on the foliage and fruit, bringing great economic losses (Mashonjowa et al., 2013).

The fungal epidemics in greenhouses begin with the introduction of infected plant material or by conidia blown from the outdoors (Linde and Shishkoff, 2003). The microconidia can also survive in the soil for an extended period or be spread on the hands and clothing of greenhouse workers (Linde and Shishkoff, 2003; Perez-Nadales et al., 2014). Even in a clean greenhouse, the occurrences of spores are inevitable. Without an artificial intervention, the disease will spread rapidly from the primary infection on a single leaf to the whole greenhouse.

On the premise of minimizing pathogens as far as possible, the optimum to prevent the occurrence of the disease is to avoid placing its host in a suitable environment for inoculation. This idea was widely used in fungal disease management, as it has a characteristic of rapidly spreading and extremely breakout when it meets medium temperature and high humidity conditions (Ojiambo et al., 2015; Yang et al., 2007). Once the infection is completed, the incubation period, which is the interval between inoculation and the appearance of disease symptoms, is determined by the temperature of surrounding air (Agrios, 2005; Yang et al., 2007). Notice that the control of environmental temperature cannot avoid the occurrence of symptoms after infection (Zhao et al., 2011). Consequently, most of the previous disease risk models pay attention to the prediction of the infection period.

Sufficient LWD (Leaf Wetness Duration) in hours and ideal temperature threshold (medium or high temperature) are considered as required conditions for several common fungal conidia infections by

* Corresponding authors.
E-mail addresses: joguzman@ual.es (J.L. Guzmán), lim@nercita.org.cn (M. Li).

https://doi.org/10.1016/j.compag.2022.106751
Received 26 October 2021; Received in revised form 15 January 2022; Accepted 24 January 2022
Available online 3 February 2022

Fig. 1. Experimental greenhouse and outdoor weather station (a); Leaf wetness sensor (b); Indoor weather station (c).

most previous studies (Zhao et al., 2011; Mashonjowa et al., 2013; Wang et al., 2019). In general, LWD can result from dew, fog, rain, and overhead irrigation (Hornero et al., 2017). In the greenhouse, LWD mainly comes from dew on the leaf surface and dew dripping down from the roof. From this point of view, one of the main meteorological problems in greenhouses is crop wetting caused by the interaction of high humidity and low temperature.

Monitoring and simulating LWD are two commonly used methods in current research (Hornero et al., 2017; Mashonjowa et al., 2013). The signal of the LWD sensor changes based on the electric resistance on the leaf surface, which can be disturbed by the surrounding environment. The LWD estimation models can be established by several methods, such as relative humidity threshold models (Zito et al., 2020; Zhao et al., 2011), dew point depression (DPD) models (Sentelhas et al., 2008; Mashonjowa et al., 2013) and machine learning models (Wang et al., 2019). Both of the monitoring or estimating ways rely on sensors sending out current signals to identify whether the leaf is wet or not and have limited abilities in sending warning massages for future LWD. The infection may have occurred when LWD appeared by monitoring or simulating.

For those reasons, data-based disease warning models were widely developed and applied in recent decades, including wheat stripe rust (El Jarroudi et al., 2017), rice blast (Wang et al., 2021), tomato and potato blight (Chelal et al., 2015; Andrade-piedra et al., 2005), etc. Some of these methods have been well applied in the open field condition by using weather forecasts (Kim et al., 2020). However, in greenhouses, the prediction lacks the link between the weather forecast and the infection model, which is given by the inside greenhouse climate, and thus, a greenhouse climate model is required. Most of the current greenhouse climate models require lots of inputs and parameters such as real-time wall temperature or heat flux (Sánchez-Molina et al., 2017), which makes it impossible to predict the future infection stage by only using weather forecast. Based on previous fungal disease models that correlate the infection risk or disease development to the greenhouse microclimate and farmer's practice, Katsoulas et al. (2021) introduced a web-based decision support system (DSS) that estimates the risk for the *Botrytis* disease development in a greenhouse. The DSS validated the simulation results that make use of outside climate forecast to predict the greenhouse microclimate conditions during a set of days, but it was not validated concerning the prediction of disease incidence (Katsoulas et al., 2021).

Therefore, this study aims to complete the validation of outdoor weather forecast accuracy, greenhouse microclimate prediction, and the early warning of primary infection date. In a previous study, a fast and practical one-dimensional greenhouse model was proposed, that includes a novel and easy-to-use wall temperature estimation method based on the energy balance (Liu et al., 2021). With the help of the embedded group of conservation equations, the greenhouse boundary temperatures can be simulated rather than having to measure the boundary temperature at each time step. Therefore, the number of model inputs is reduced, and the model can estimate the future greenhouse climate using only the current or predicted outdoor weather variables. In this work, taken cucumber downy mildew as an example, that greenhouse climate model is combined with a disease model, in such a way that future indoor climate can be predicted by weather forecast to provide necessary parameters (eg. LWD, temperature) for the infection and incubation period. As a result, disease occurrences can be detected 72 h in advance compared with classical methods. Experimental results are presented for a greenhouse located in Beijing (China), where the proposed approach was compared with the use of LWD sensors. The results show that the proposed methodology provides promising predictions and can be used as a tool to the early warm detection of diseases in greenhouses.

2. Materials and methods

2.1. Greenhouse facilities

The experimental greenhouse is a typical Chinese solar greenhouse (50 m*7 m, Fig. 1a), located at the National Precision Agriculture Demonstration Base (40°18′ N, 116°47′ E, annual average temperature: 11.8 °C, altitude: 39 m, local pressure: 101 kPa), Changping District, Beijing. The cucumber seedling 'Jingyan Mini II' was transplanted on March 4, 2021, in an average of 36 rows. Drip irrigation and fertilization under a plastic film were adopted. An integrated small weather station (Davis-6162, Davis Instruments, Hayward, USA, Fig. 1c) was installed in the center of the greenhouse to monitor air temperature (range, −40 - +65 °C; accuracy, ±0.5 °C), relative humidity (range, 0–100%; accuracy, ±3%) and leaf wetness duration (artificial leaf with electricity resistance, range, 0 dry – 15 saturated wetness, Fig. 1b) at a height of 1 m. Outdoor weather data was monitored by a weather station located in front of the greenhouse (Fig. 1a). The data were recorded at 15-minute intervals. To record the occurrence time of cucumber downy mildew, observations were recorded every day until it occurs.

2.2. Downy mildew model

The disease model used in this work includes two parts: infection and incubation periods. It was triggered two weeks after transplanting. In this model, for the infection periods, the prediction is positive when the

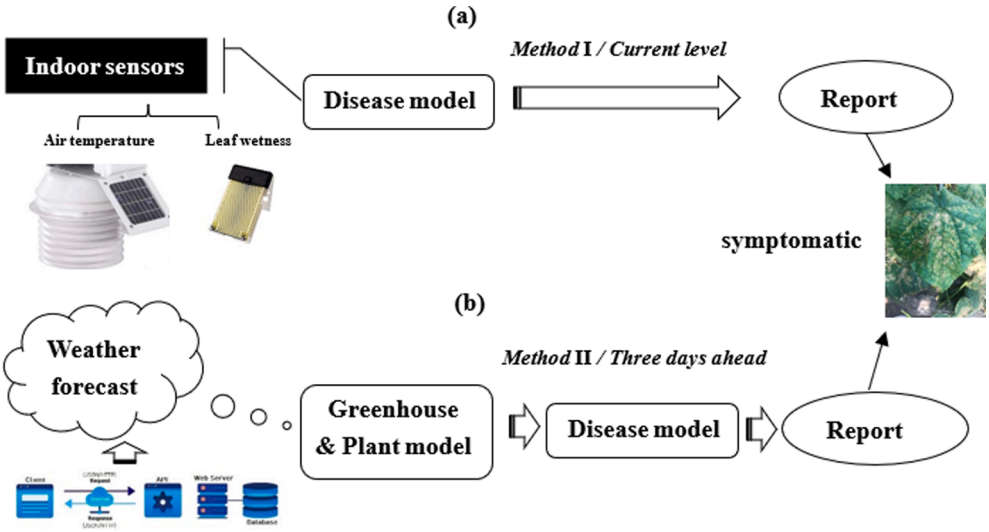

Fig. 2. Two methods to give early warning occurrence time of cucumber downy mildew.

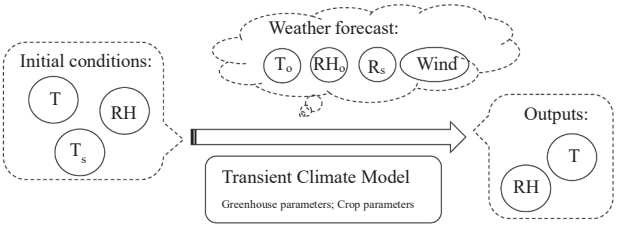

Fig. 3. Description of greenhouse climate prediction. T is indoor temperature, K; T_o is outdoor temperature, K; T_s is soil temperature, K; RH is indoor relative humidity, %; RH_o is outdoor relative humidity, %; R_s is solar radiation, W m^{-2}; Wind represents wind speed (m s^{-1}) and direction. The model includes a module converting relative humidity and temperature into absolute humidity, h.

product of leaf wetness duration (LWD, hour) and corresponding hourly temperature when leaves are wet (TLWD, °C), is bigger than 40 h*°C (Equation (1)), with a range of TLWD [5,30 °C] and LWD greater than 2 h conditions (Zhao et al., 2011). The LWD comes from the monitoring of an artificial leaf with electricity resistance (Fig. 1 (b)), or the continuous hours when the air relative humidity is higher than its threshold. Once the infection is done, the incubation period starts. It usually needs a couple of days when the incubation period finishes. It is an integration of hourly contribution rate (y, Equation (2)), which is calculated by an equation of hourly average temperature (T_h, °C). The deadline of the incubation period is the hour when the integration of $y \geq 1$, when leaves are predicted to be symptomatic. For example, if T_h is a constant value of 20 °C, the contribution rate y is 0.015 in each hour. The y takes 67 h to progress to 1.

$$LWD \times TLWD \geq 40h^{\circ}\mathrm{C}(LWD \geq 2h, 5^{\circ}C \leq TLWD \leq 30^{\circ}\mathrm{C}) \quad (1)$$

$$y = \frac{0.0165}{1 + 10389.2 \times exp(-0.5743 \times T_h)} \quad (2)$$

The disease model was used with two different approaches (Fig. 2). The traditional approach (Fig. 2a) was to estimate infection risk by using as inputs the real-time measured data from indoor sensors (e.g. artificial leaf wetness sensor, humidity, and temperature sensors) (Zhao et al., 2011; Wang et al., 2019). One of the disadvantages of this method is that sensor failure interrupts reports. Another disadvantage is that real-time monitoring is not able to avoid the infection stage when the leaf wetness is detected. In this method, LWD and TLWD were measured two weeks after transplanting to evaluate current infection risk.

The second approach was to follow the methodology proposed in this work, where the LWD and TLWD are simulated using the inside greenhouse climate data provided by the greenhouse model that considers weather forecast data for the next three days (Fig. 2b). The greenhouse microclimate (e.g. air humidity and temperature) was predicted three days in advance. The LWD was estimated based on a fixed threshold of predicted relative humidity (Li et al., 2010). Calibration is necessary to improve the model performance considering different conditions caused by local climate, crops, greenhouse structures, and facilities (Wang et al, 2019). In this study, LWD was estimated by two thresholds. One of the thresholds was optimized by the decision learning tree method (DLT) (Loh, 2008), using data from March to April 2021. Furthermore, another threshold of relative humidity of 90% used for Chinese greenhouse was documented by Zhao et al (2011). Thus, these two thresholds will be evaluated in this study.

2.3. Weather forecast model

For the weather forecast, a web-based model based on a REST API service provided by Weatherbit is used (WeatherBit, 2019). This model allows us to obtain weather forecasts in different geographical locations around the world. The Weatherbit service is based on the best available public forecast models, as well as radar, and station observations to offer the most accurate forecast possible. The resolution of the models ranges from 1 to 13 KM. The forecast sources are DWD ICON 7KM, GFS 13 KM, NAM 3KM, HRRR 1KM, ECMWF 9KM, SILAM, and EU CAMS models (see WeatherBit, (2019) for more information). For this work, that service was used to obtain weather forecasts 72 h ahead with an hourly sampling period. It is generally within 72 h from infection to the deadline of incubation. Thus, the 72 h prediction and climate control are adequate to avoid the occurrence of downy mildew. Temperature, humidity, wind speed, and solar radiation forecasts are obtained to be used as inputs to the proposed methodology. This web-based service requires basic parameters such as latitude, longitude, language, key, and number of hours for the forecast. The accuracy of the weather forecast is very high as it will be shown in Section 3.

To demonstrate the accuracy of the weather forecast, a local weather station located at the greenhouse facilities was used. Specifically, the Davis Vantage Pro2 Plus (Davis Instruments, Hayward, USA) weather station was installed on open land near the greenhouse, to measure the total solar radiation (range, 0–1800 W m^{-2}; accuracy, ±5%), wind speed (range, 0–67 m s^{-1}; accuracy, ±5%), air temperature, and relative humidity (see Fig. 1c). The weather forecast data was downloaded and

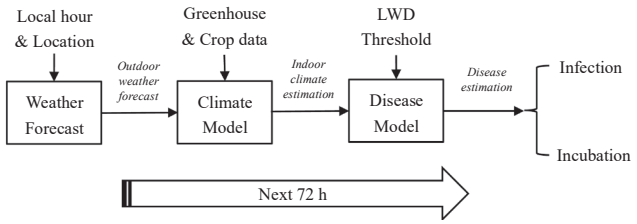

Fig. 4. Flow chart of the disease estimation methodology.

updated by every hour from 00:00 on April 25 to 00:00 on April 28, 2021. The RMSE (Root Mean Square Error) was used as a metric to evaluate the resulting accuracy.

2.4. Greenhouse climate model

In this section, the greenhouse climate model is briefly described (Fig. 3). The energy source terms for the air in the greenhouse belong to 5 sub-mechanisms: the ventilation energy source term, $q_v(t)$, W; the air leakage energy source term, $q_{lea}(t)$, W; the convective energy source term, $q_c(t)$, W; the water vapor liquidation energy source term, $q_{liq}(t)$, W; and the plant energy source term, $q_p(t)$, W. The greenhouses' energy budget has a combined effect on the indoor temperature and humidity. The corresponding equation is given below (Liu et al., 2021):

$$\frac{dT(t)}{dt}*\rho*c_p*v+h(t)*\rho*c_{pw}*v*\frac{dT(t)}{dt}=q_v(t)+q_{lea}(t)+q_c(t)+q_{liq}(t)+q_p(t) \quad (3)$$

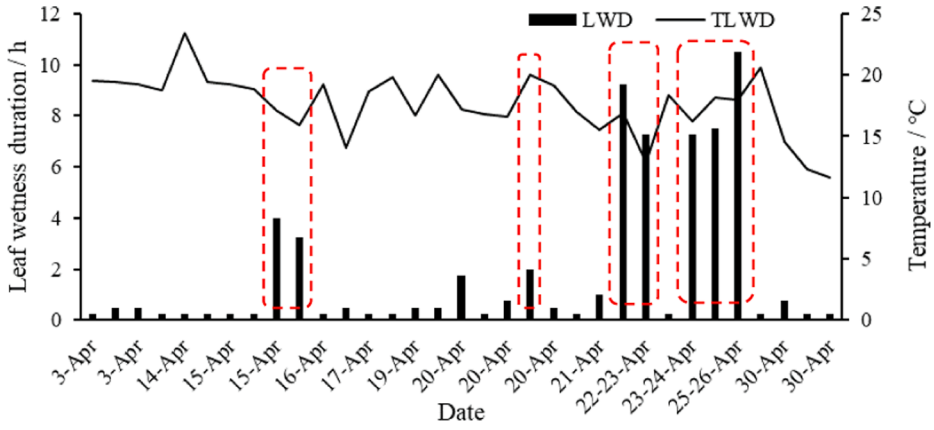

Fig. 5. Measurements of LWD and TLWD in the greenhouse from March 18-April 30, 2021. The red marked periods were ideal infection conditions. (For interpretation of the references to colour in this figure legend, the reader is referred to the web version of this article.)

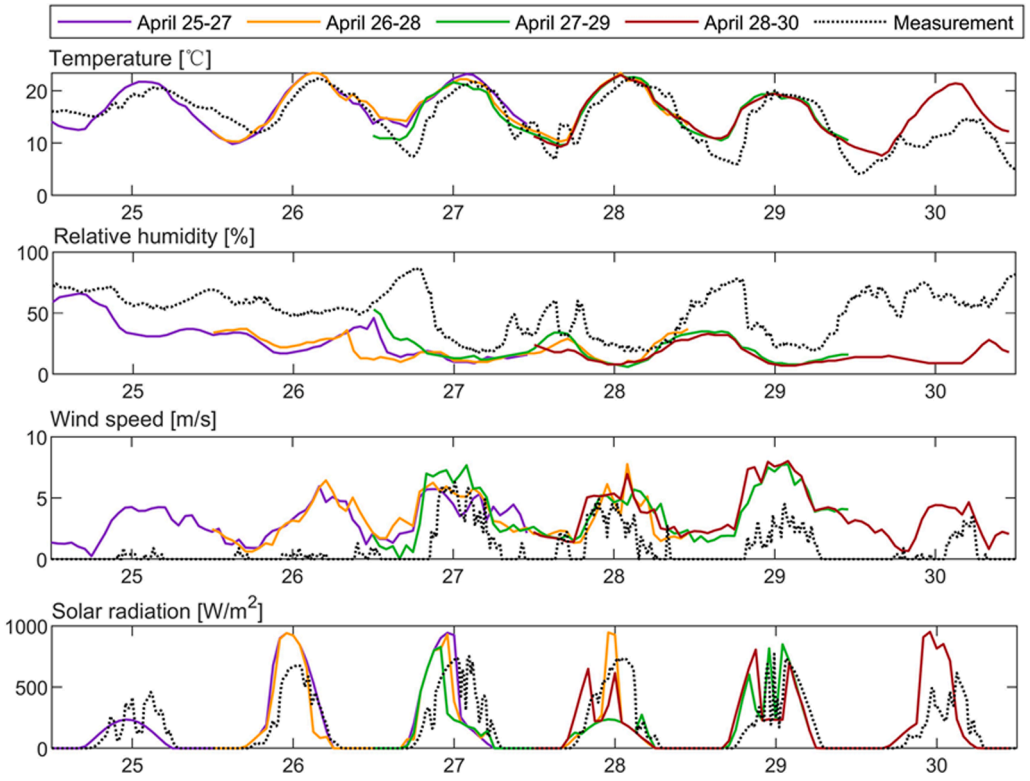

Fig. 6. Weather forecast data and outdoor measurements on April 25–30, 2021. Colors represent samples for the next 72 h collected at 00:00 on each day.

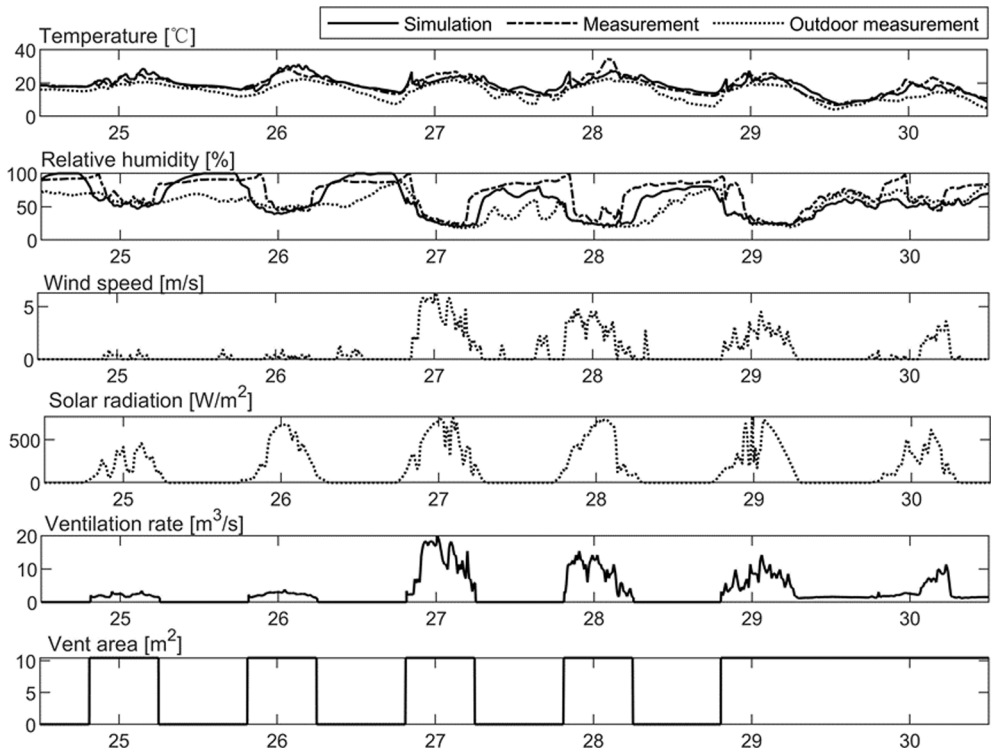

Fig. 7. Simulation of greenhouse temperature and humidity by inputting measured outdoor data on April 25–30, 2021.

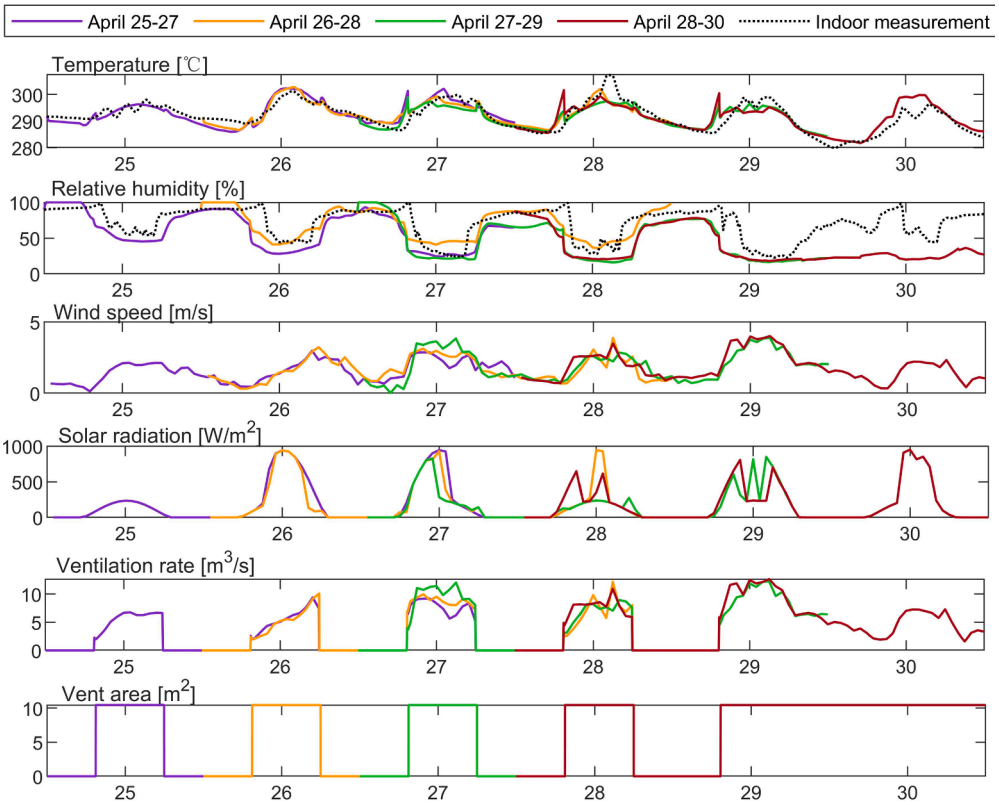

Fig. 8. Simulation of greenhouse temperature and humidity by inputting weather forecast data on April 25–30, 2021. Colors represent samples for the next 72 h collected at 00:00 on each day.

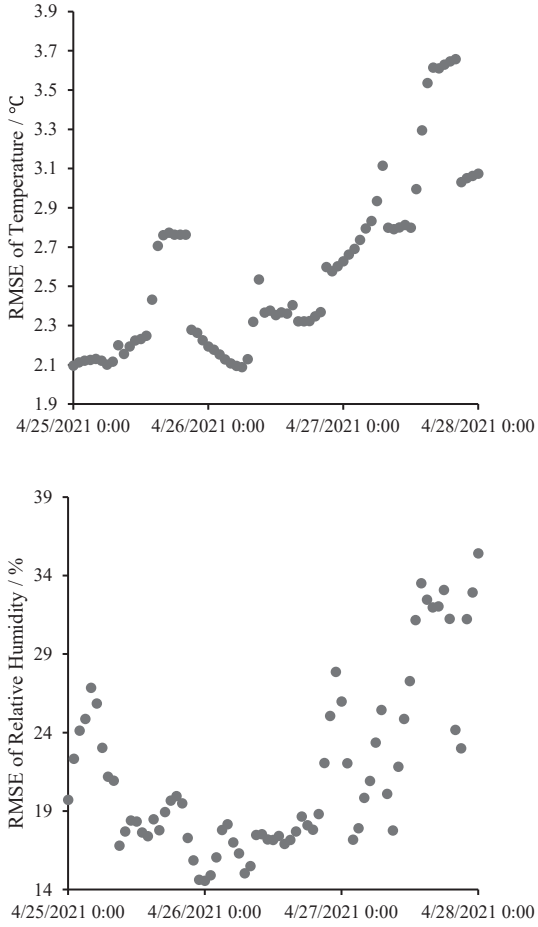

Fig. 9. RMSE of simulated temperature and humidity by inputting weather forecast data on April 25–30, 2021 of 73 samples.

which can be simplified as,

$$\frac{dT(t)}{dt} = \frac{q_v(t) + q_{lea}(t) + q_c(t) + q_{liq}(t) + q_p(t)}{\rho^* v^* (c_p + c_{pw}{}^* h(t))} \tag{4}$$

where, T is the indoor air temperature, K; h is the indoor absolute humidity, kg kg^{-1}; t is time, s; ρ is the air density, (1.293) kg m^{-3}; c_p is the specific heat capacity of the air, (1005) J kg^{-1} K^{-1}; c_{pw} is the specific heat capacity of the water vapor, (1850) J kg^{-1} K^{-1}; and v is the greenhouse volume, m^3.

The humidity equation was obtained by mass conservation. The greenhouses' humidity source terms come from the ventilation humidity source term, $s_v(t)$, kg kg^{-1} s^{-1}; the air leakage humidity source term, $s_{lea}(t)$, kg kg^{-1} s^{-1}; and the plant humidity source term, $s_p(t)$, kg kg^{-1} s^{-1}. The equation is given as follows,

$$\frac{dh(t)}{dt} = s_v(t) + s_{lea}(t) + s_p(t) \tag{5}$$

The boundary conditions and initial conditions were updated every hour automatically to predict greenhouse climate for the next 72 h. The probe sensor (Davis Instruments, Hayward, USA) was inserted into the soil at 0.5 m depth in the center of the greenhouse to measure soil temperature by every hour. The leaf area index (LAI) was measured manually before the simulation from five equidistant sampling points on the diagonal in the horizontal plane of the greenhouse, of which, four plants were taken from each sampling point. The mean value of LAI was taken as input and was considered as a constant value for the next 72 h. The measured indoor temperature and humidity were downloaded until the deadline of the weather forecast. The simulation was evaluated by using RMSE between simulated value and measured data on April 25–30. In addition, simulations using weather forecasts and measurements of outdoor data as inputs were compared.

2.5. Disease estimation methodology

This section summarizes the approach presented in this paper, where the greenhouse climate model and disease model are combined such as shown in Fig. 4. The location is the latitude and longitude of the greenhouse, and the local hour of weather forecast is updated every hour. The outputs of the model were the date and time for the infection and the deadline for the incubation period. The evaluation criteria were the comparison between the predicted deadline of the incubation period and the occurrence of real primary infection symptoms. Notice that the calculations under this model-based approach are repeated with a sampling period of one hour using a receding horizon approach. It means that every hour, predictions for infection and incubation for the next 72 h are obtained. Then, the next hour the weather forecast is obtained again and the infection and incubation predictions are repeated to account for weather forecast uncertainties and modeling errors.

3. Results and discussion

This section describes the main results for the proposed methodology, which are compared with traditional approaches for disease detection. First, the traditional method shown in Fig. 2a (method I) is used to detect the disease occurrence based on the leaf wetness sensor and the current measurements of greenhouse temperature and humidity. Afterward, the performance of the weather forecast service is analyzed. Then, the results for the proposed methodology (described in. Fig. 4) are presented and compared with the traditional approach.

3.1. Classical method based on indoor climate measurements and leaf wetness sensor

Fig. 5 shows the measured LWD and TLWD two weeks after transplanting. The LWD was detected throughout April. The repeated dates numbers on the x-axis of the figure indicate that there were multiple discontinuous LWDs on the same day. The red marked periods were ideal infection conditions. The first two ideal infection conditions were identified on April 15 and 16. However, they were proved to be false-positive predictions, because no symptoms were observed after the deadline of the predicted incubation periods. The third positive report began with an ideal infection condition on April 20, 20:15, of which, the inoculation period was finished on April 24, 11:15 during contribution rate (y, unitless, Equation (2)) reached 1. This met the first manual observation of downy mildew symptoms in the greenhouse on April 24. After two false-positive reports, the third positive report was true, which demonstrates that the disease model performed effectively by inputting real-time measured LWD and air temperature.

This primary infection model was also proved to have 68%-96% probability for the disease occurrence after a positive early warning, in the same experimental greenhouses from Xiaotangshan in the years of 2006 and 2007 (Zhao et al., 2011). The result agrees with Zhao et al (2011) that the disease model has relevant performance on warning cucumber downy mildew happened based on indoor climate data. In other publications, they also address the importance of hours of leaf wetness and day temperature to the warning model of cucumber downy mildew (Neufeld et al, 2017). They mentioned that the requirement of infection to occur is a minimum of 2 h of leaf wetness (Cohen, 1977; Neufeld and Ojiambo, 2012), being consistent with the model. Based on previous studies, early warnings can be provided two days before symptoms appear. However, the previous early warning system cannot avoid the primary infection, because the infection stage may have been completed when the LWD was detected or estimated by sensor

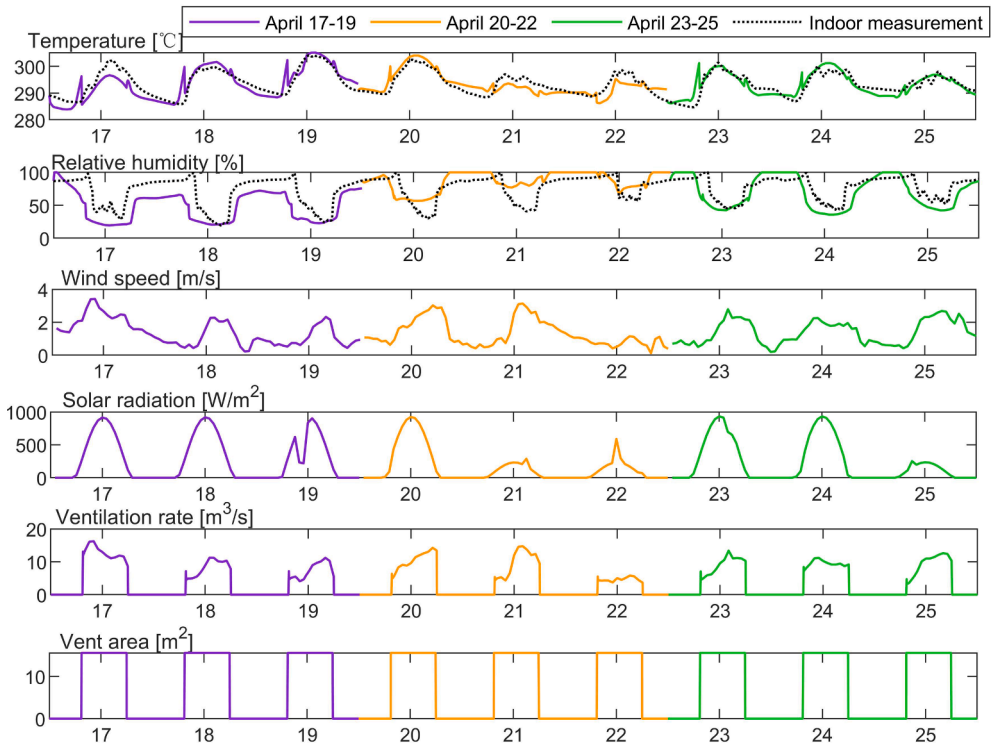

Fig. 10. Simulation of greenhouse temperature and humidity by inputting weather forecast in the future 3 days on April 17–25, 2021. The RMSE of temperature and relative humidity are respectively 3.0 °C and 26.5%; 4.2 °C and 15.7%; 1.9 °C and 17.0% in each simulation period.

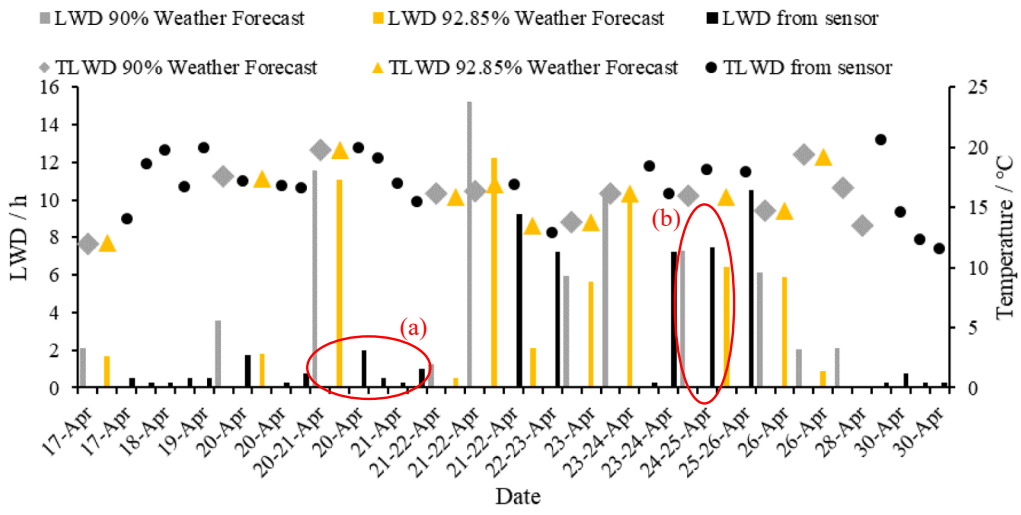

Fig. 11. Measurements and predictions of LWD and TLWD in the greenhouse, April 17–30, 2021.

measurement.

3.2. Proposed model-based methodology based on the climate greenhouse model and weather forecast

3.2.1. Performance of weather forecast

First, the performance of the weather forecast model is analyzed. The RMSE of temperature and relative humidity between the weather forecast and outdoor measurement were evaluated as range 2.5–4.5 °C and 25–37% in 73 samples on April 25–30. The temperature prediction was ideal and the weather forecast humidity was a little bit lower than the measurement (Fig. 6). The measured wind speed was lower than the weather forecast data, of which, the RMSE ranges 2.5–3 m s^{-1}, because the impacts on the wind speed of obstacles and height from the ground were not considered by the weather forecast. The RMSE of solar radiation forecast ranges 182–262 W m^{-2}. Both the measured and predicted solar radiation signals contain the attenuation by clouds. Anyway, the accuracy of the weather forecast was good enough for the objective of this work. To improve the accuracy, a receding horizon approach was used, where inputs to the greenhouse climate simulation were updated hourly, and new prediction for the next 72 h was obtained every hour.

3.2.2. Performance of greenhouse model by inputting measured outdoor climate or weather forecast

The climate greenhouse model was calibrated and validated based on measured real-time outdoor data and weather forecasts for the next three days, respectively. By inputting real-time measurements, RMSE of indoor air temperature and relative humidity were respectively 2.5 °C and 18.6% during consecutive six days (Fig. 7). The model by inputting measured outdoor data was also fully validated in the previous study by Liu et al., 2021. One of the advantages is that this model provides fair robustness under different operating conditions, requiring only five transient inputs, respectively, outdoor temperature and humidity, solar radiation intensity, wind, and vents configurations.

On the other hand, the performance of the model was also validated by inputting weather forecasts for the future three days are shown in Fig. 8. Colors in the figure indicate the set of three consecutive days performed for validation purposes. RMSE of simulated temperature ranged 2.1–3.7 °C and the mean value of 73 samples was 2.6 °C (Fig. 9). The RMSE of simulated relative humidity ranged 14.6%–35.4% and the mean value of 73 samples was 21.5%. The simulated indoor temperature performances were ideal with both measurement inputs and weather forecast inputs. The relative humidity performance with weather forecast inputs is not better than the measurement inputs on April 30, when the weather forecast lost its accuracy (Fig. 6). Besides, humidity simulation in the greenhouse is a challenge for researchers, where numerous studies can be found in the literature (He and Ma, 2010; Zou et al., 2017; Jung et al., 2020). Few fundamental models were reported for simulating greenhouse humidity. The gain or decrease of various humidity source terms, such as transpiration, air leakage, ventilation, soil evaporation, and condensation, must be fairly described by equations, and the interaction between them should be considered. Especially, in this study, part of the errors comes from the error of weather forecast. In general, by using weather forecast inputs, the simulation was conducted for the next three days, and the simulation was repeated and the result was corrected by every hour with the latest weather forecast data to avoid the large errors from estimation errors.

3.2.3. Warning result of cucumber downy mildew

Fig. 10 shows the predicted greenhouse temperature and humidity used to assess the risk of infection in this work (see Fig. 5 to see the relationship with the dates) and being the inputs to the disease model. The ideal accuracy ensures the feasibility of the disease evaluation. The predicted indoor relative humidity was used for estimating LWD based on a relative humidity threshold model. One of the RH thresholds adopted to estimate LWD in this study was 90% (Zhao et al., 2011) such as commented above, and the other one was 92.85%, which was calibrated by the DLT method using data from March and April 2021.

Fig. 11 shows the comparison between predictions by weather forecast (proposed approach, Fig. 2b) and measurements of LWD and TLWD (traditional approach, Fig. 2a) during April 17–30. Note that several discontinuous LWDs appeared on one day and samples were arranged on the x-axis according to the order of occurrence. The label day-day-Apr represents leaf wetting crossed 00:00. The measurements are often distributed discretely in a predicted leaf wetness period. Red mark (a) in Fig. 11 contains the predicted LWD of 11.5 h during 19:18–06:50 on April 20–21 (90% TR), the predicted LWD of 11 h during 19:35–06:38 on April 20–21 (92.85% TR), and four discontinuous periods by measurements (20:15–22:15, 22:30–23:00 on April 20 and 01:15–01:30, 05:00–06:00 on April 21). Their starting and total time are not fit exactly but they are very similar. Red mark (b) in Fig. 11 shows two predictions and one measurement: 7.3 h, 6.4 h, and 7.5 h, of which, the starting was respectively 23:04, 23:44, and 23:30 on April 24. In general, LWD and TLWD predictions show promising performances by the weather forecast for the future three days.

Using weather forecast, the first positive report for infection was in the morning on April 20 (Fig. 11 (90% TR)), and the predicted deadline of incubation was at 18:00 on April 23. It was one day earlier than the observation. By using 92.85% TR, the performance was better. The first positive report was in the night on April 20, and the predicted deadline of incubation was at 11:00 on April 24, which fits the first observation time and is very closed to the prediction by using real-time measured data (11:15, April 24). The results show that the prediction by inputting weather forecast data to the greenhouse model and by using 92.85% TR has a promising prediction for the primary infection of cucumber downy mildew.

4. Conclusion

This study proposed a new methodology to early warn cucumber downy mildew. Prediction of indoor climate data using weather forecast data for the next three days is used as inputs to the early warning model to perform estimations of disease occurrences. Combining the weather forecast service, the greenhouse climate model, and the primary infection and incubation model, the accuracy of positive prediction was validated. The proposed approach was compared with a classical primary infection and incubation model. It was proved that using weather forecasts for the early warning of greenhouse downy mildew has the same effect as using real-time indoor sensor data, but with the great advantage of providing the warning time in advance. Different from the traditional plant disease model studies, although this study evaluated the method in a short production season, the model gave an early warning to greenhouse managers. A period of two or three days is enough to make decisions to face the diseases and reduce the possibility of disease breakout. For instance, the proposed methodology can be combined with a hierarchical control approach, where climate control algorithms can modify the inside climate automatically to reduce the risk of disease occurrence.

Author contributions statement

Liu Ran was the responsible of conceptualization, methodology, formal analysis and writing. Wang Hui was responsible of formal analysis and supervision. J.L. Guzmán was the responsible of software, supervision and validation. Li Ming was the responsible of supervision and formal analysis.

Declaration of Competing Interest

The authors declare that they have no known competing financial interests or personal relationships that could have appeared to influence the work reported in this paper.

References

Andrade-Piedra, J.L., Hijmans, R.J., Forbes, G.A., Fry, W.E., Nelson, R.J., 2005. Simulation of Potato Late Blight in the Andes. I: Modification and Parameterization of the LATEBLIGHT Model. Phytopathology 95 (10), 1191–1199. https://doi.org/10.1094/PHYTO-95-1191.

Agrios, G.N., 2005. Plant Pathology, fifth ed. Elsevier Academic Press, USA. P. 89. https://doi.org/10.1016/B978-0-08-047378-9.50008-7.

Cañadas, J., Sánchez-Molina, J.A., Rodríguez, F., María del Águila, I., 2017. Improving automatic climate control with decision support techniques to minimize disease effects in greenhouse tomatoes. Informat. Process. Agric. 4 (1), 50–63. https://doi.org/10.1016/j.inpa.2016.12.002.

Cohen, Y., 1977. The combined effects of temperature, leaf wetness, and inoculum concentration on infection of cucumbers with Pseudoperonospora cubensis. Can. J. Bot. 55 (11), 1478–1487. https://doi.org/10.1139/b77-174.

Chelal, J., Al Masri, A., Hau, B., 2015. Modelling the interaction between early blight epidemics and host dynamics of tomato. Tropical Plant Pathol. 40 (2), 77–87. https://doi.org/10.1007/s40858-015-0021-0.

El Jarroudi, M., Kouadio, L., Bock, C.H., El Jarroudi, M., Junk, J., Pasquali, M., Maraite, H., Delfosse, P., 2017. A threshold-based weather model for predicting stripe rust infection in winter wheat. Plant Dis. 101 (5), 693–703. https://doi.org/10.1094/PDIS-12-16-1766-RE.

Guo, Y.u., Zhao, H., Zhang, S., Wang, Y., Chow, D., 2021. Modeling and optimization of environment in agricultural greenhouses for improving cleaner and sustainable crop production. J. Cleaner Prod. 285, 124843. https://doi.org/10.1016/j.jclepro.2020.124843.

He, F., Ma, C., 2010. Modeling greenhouse air humidity by means of artificial neural network and principal component analysis. Comput. Electron. Agric. 71, S19–S23. https://doi.org/10.1016/j.compag.2009.07.011.

Hornero, G., Gaitán-Pitre, J.E., Serrano-Finetti, E., Casas, O., Pallas-Areny, R., 2017. A novel low-cost smart leaf wetness sensor. Comput. Electron. Agric. 143, 286–292. https://doi.org/10.1016/j.compag.2017.11.001.

Jung, D.-H., Kim, H.S., Jhin, C., Kim, H.-J., Park, S.H., 2020. Time-serial analysis of deep neural network models for prediction of climatic conditions inside a greenhouse. Comput. Electron. Agric. 173, 105402. https://doi.org/10.1016/j.compag.2020.105402.

Katsoulas, N., Antoniadis, D., Nikitas, A., 2021. A web-based system for fungus disease risk assessment in greenhouses: System development. Comput. Electron. Agric. 188, 106326. https://doi.org/10.1016/j.compag.2021.106326.

Kim, H.-S., Do, K.S., Park, J.H., Kang, W.S., Lee, Y.H., Park, E.W., 2020. Application of numerical weather prediction data to estimate infection risk of bacterial grain rot of rice in Korea. Plant Pathol. J. 36 (1), 54–66. https://doi.org/10.5423/PPJ.OA.11.2019.0281.

Linde, M., Shishkoff, N., 2003. DISEASE | Powdery Mildew. In: Roberts, Andrew V. (Ed.), Encyclopedia of Rose Science. Elsevier, pp. 158–165. https://doi.org/10.1016/B0-12-227620-5/00068-9.

Liu, R., Li, M., Guzmán, J.L., Rodríguez, F., 2021. A fast and practical one-dimensional transient model for greenhouse temperature and humidity. Comput. Electron. Agric. 186, 106186. https://doi.org/10.1016/j.compag.2021.106186.

Li, M., Zhao, C., Qiao, S., Qian, J., Yang, X., 2010. Estimation model of leaf wetness duration based on canopy relative humidity for cucumbers in solar greenhouse. Trans. Chinese Soc. Agric. Eng. 26 (9), 286–291. https://doi.org/10.3969/j.issn.1002-6819.2010.09.047.

Loh, W.-Y., 2008. Classification and Regression Tree Methods. In: Ruggeri, Kenett, Faltin (Eds.), Encyclopedia of Statistics in Quality and Reliability. Wiley, pp. 315–323.

Mashonjowa, E., Ronsse, F., Mubvuma, M., Milford, J.R., Pieters, J.G., 2013. Estimation of leaf wetness duration for greenhouse roses using a dynamic greenhouse climate model in Zimbabwe. Comput. Electron. Agric. 95, 70–81. https://doi.org/10.1016/j.compag.2013.04.007.

Neufeld, K.N., Keinath, A.P., Ojiambo, P.S., 2017. A model to predict the risk of infection of cucumber by Pseudoperonospora cubensis. Microbial Risk Analysis. 6, 21–30. https://doi.org/10.1016/j.mran.2017.05.001.

Neufeld, K.N., Ojiambo, P.S., 2012. Interactive effects of temperature and leaf wetness duration on sporangia germination and infection of cucurbit hosts byPseudoperonospora cubensis. Plant Dis. 96 (3), 345–353. https://doi.org/10.1094/PDIS-07-11-0560.

Ojiambo, P.S., Gent, D.H., Quesada-Ocampo, L.M., Hausbeck, M.K., Holmes, G.J., 2015. Epidemiology and Population Biology of Pseudoperonospora cubensis: A Model System for Management of Downy Mildews. Annu. Rev. Phytopathol. 53 (1), 223–246. https://doi.org/10.1146/annurev-phyto-080614-120048.

Perez-Nadales, E., Almeida Nogueira, M.F., Baldin, C., Castanheira, S., El Ghalid, M., Grund, E., Lengeler, K., Marchegiani, E., Mehrotra, P.V., Moretti, M., Naik, V., Oses-Ruiz, M., Oskarsson, T., Schäfer, K., Wasserstrom, L., Brakhage, A.A., Gow, N.A.R., Kahmann, R., Lebrun, M.-H., Perez-Martin, J., Pietro, A.D., Talbot, N.J., Toquin, V., Walther, A., Wendland, J., 2014. Fungal model systems and the elucidation of pathogenicity determinants. Fungal Genet. Biol. 70, 42–67. https://doi.org/10.1016/j.fgb.2014.06.011.

Sentelhas, P.C., Dalla Marta, A., Orlandini, S., Santos, E.A., Gillespie, T.J., Gleason, M.L., 2008. Suitability of relative humidity as an estimator of leaf wetness duration. Agric. For. Meteorol. 148 (3), 392–400. https://doi.org/10.1016/j.agrformet.2007.09.011.

J. Sánchez-Molina M. Li F. Rodriguez J. Guzmán H. Wang X. Yang Development and test verification of an air temperature model for Chinese solar and Spanish Almeria-type greenhouse Int. J. Agric. Biol. Eng. 10 2017 66 76 10.25165/j.ijabe.20171004.2398.

Wang, H., Sanchez-Molina, J.A., Li, M., Rodríguez, D.F., 2019. Improving the Performance of Vegetable Leaf Wetness Duration Models in Greenhouses Using Decision Tree Learning. Water. 11 (1), 158. https://doi.org/10.3390/w11010158.

Wang, H., Mongiano, G., Fanchini, D., Titone, P., Tamborini, L., Bregaglio, S., 2021. Varietal susceptibility overcomes climate change effects on the future trends of rice blast disease in Northern Italy. Agric. Syst. 193, 103223. https://doi.org/10.1016/j.agsy.2021.103223.

WeatherBit, *WeatherBit API Guide*. https://www.weatherbit.io/api: WeatherBit, Inc., 2019.

Yang, X.T., Li, M., Zhao, C.J., Zhang, Z., Hou, Y.L., 2007. Early warning model for cucumber downy mildew in unheated greenhouses. N. Z. J. Agric. Res. 50 (5), 1261–1268. https://doi.org/10.1080/00288230709510411.

Zhao, C.J., Li, M., Yang, X.T., Sun, C.H., Qian, J.P., Ji, Z.T., 2011. A data-driven model simulating primary infection probabilities of cucumber downy mildew for use in early warning systems in solar greenhouses. Comput. Electron. Agric. 76 (2), 306–315. https://doi.org/10.1016/j.compag.2011.02.009.

Zito, S., Castel, T., Richard, Y., Rega, M., Bois, B., 2020. Optimization of a leaf wetness duration model. Agric. For. Meteorol. 291, 108087. https://doi.org/10.1016/j.agrformet.2020.108087.

Zou, W., Yao, F., Zhang, B., He, C., Guan, Z., 2017. Verification and predicting temperature and humidity in a solar greenhouse based on convex bidirectional extreme learning machine algorithm. Neurocomputing. 249, 72–85. https://doi.org/10.1016/j.neucom.2017.03.023.

2.3 Greenhouse control

2.3.1 Selective temperature and humidity control strategy for a Chinese solar greenhouse with an event-based approach

Research in this field is supported by the following journal publication:

Title	Selective temperature and humidity control strategy for a Chinese solar greenhouse with an event-based approach
Authors	**R. Liu**, J. L. Guzmán, F. García Mañas, M. Li
Journal	Revista Iberoamericana de Automatica e Informatica Industrial
Year	2022
Volume	Under review
Pages	--
DOI	--
IF(JCR2022)	1.250
Categories	Automation & Control Systems (62/82) Q4 Robotics (34/41) Q4

Contribution of the Ph.D. Candidate

The Ph.D. candidate R. Liu is the main contributor and first author of this paper.

Revista Iberoamericana de Automática e Informática Industrial

Revista Iberoamericana de Automática e Informática Industrial 00 (2022) 1–12

www.revista-riai.org

Estrategia de control selectivo de temperatura y humedad para un invernadero solar chino con un enfoque basado en eventos

Liu, R.[a], Guzmán, J.L.[a,*], García-Mañas, F.[a], Li, M.[b]

[a] *Departamento de Informática, ceiA3, CIESOL, Universidad de Almería, Ctra. Sacramento s/n, La Cañada de San Urbano, Almería, España.*
[b] *Information Technology Research Center, Beijing Academy of Agriculture and Forestry Sciences/ National Engineering Research Center for Information Technology in Agriculture/ National Engineering Laboratory for Agri-product Quality Traceability/ Meteorological Service Center for Urban Agriculture, China Meteorological Administration- Ministry of Agriculture and Rural Affairs/ Key Laboratory of Agri-informatics, Ministry of Agriculture, Beijing, China*

To cite this article: Liu, R., Guzmán, J.L., García-Mañas, F., Li, M., 2022. Selective temperature and humidity control strategy for a chinese solar greenhouse with an event-based approach. Revista Iberoamericana de Automática e Informática Industrial 00, 1-5. https://doi.org/XX.XXXX/riai.2022.XXXX

Resumen

Este artículo presenta la aplicación de un esquema de control selectivo de temperatura y humedad para invernaderos solares chinos, que son los más utilizados en las provincias del norte de China. En primer lugar, para controlar la temperatura, se propone un controlador PI con un enfoque basado en eventos. Tras la evaluación de varios valores de la banda de ocurrencia de eventos, se obtiene una solución que permite reducir en un 43,8 % el número de aperturas y cierres de las ventanas del invernadero, mientras que el error de temperatura se incrementa sólo en un 1,13 %. En segundo lugar, se ha diseñado un controlador para la humedad relativa y otro para la humedad absoluta. Los resultados muestran que el control de humedad relativa funciona adecuadamente cuando la consigna no es demasiado elevada. Sin embargo, la acción de control se deteriora cuando la consigna es superior al 70 %. En comparación, el control de humedad absoluta permite regular la humedad para referencias de cualquier valor, pero la precisión de control es menor. Finalmente, mediante un estudio en simulación, se demuestra la efectividad de la estrategia de control selectivo de temperatura con un esquema que da prioridad para controlar la humedad cuando ésta alcanza límites no deseados. Esta estrategia de control consigue mantener la humedad relativa por debajo del 80 % mientras que controla la temperatura en la consigna establecida, evitando así que la alta humedad dañe al cultivo.

Palabras clave: Control selectivo, Control PI, Control basado en eventos, Agricultura, Invernaderos.

Selective temperature and humidity control strategy for a chinese solar greenhouse with an event-based approach

Abstract

This paper introduces an application of a selective temperature and humidity control scheme for chinese solar greenhouses, which are the most widely used in the northern provinces of China. Firstly, a PI controller for temperature is studied with an event-based approach. After the evaluation of different event-generator thresholds, an optimum value is selected which significantly reduces the number of vent movements by 43.8%, while only increasing the temperature error by 1.13%. Secondly, a controller for relative humidity and another controller for absolute humidity were implemented. The results show that the controller for relative humidity performs adequately when the set-point is not high. However, the control action is deteriorated when the set-point is over 70%. The absolute humidity control allows to regulate the humidity for references of any value, but with less control precision. Finally, through a simulation study, the effectiveness is demonstrated for a selective temperature control strategy with a humidity priority control scheme. This control strategy keeps the relative humidity below 80% while controlling the temperature to the set-point, preventing high humidity from damaging the crop.

Keywords: Selective control, PI control, Event-based control, Agriculture, Greenhouses.

*Autor para correspondencia: joguzman@ual.es (Guzmán, J.L.);

1. Introducción

En los últimos años, con el crecimiento anual de la población mundial, el aseguramiento del suministro de alimentos ha recibido una atención cada vez mayor. La agricultura protegida es considerada como una de las soluciones por su alta productividad y aprovechamiento de los terrenos de cultivo. Según las últimas estadísticas, la superficie de invernaderos a nivel mundial se estima en 3,64 millones de hectáreas (Guo et al., 2021). En concreto, el área de cultivo en invernaderos en China se ha acercado a los 2 millones de hectáreas y, entre ellos, aproximadamente, 1,2 millones hectáreas están dedicadas a invernaderos de túnel de plástico, mientras que el área ocupada por los invernaderos solares chinos (*chinese solar greenhouses*, CSG) es de 0,6 millones de hectáreas (Wang et al., 2017).

Los CSG garantizan el suministro de hortalizas en las provincias del norte de China. A diferencia de los invernaderos tradicionales utilizados en el área del Mediterráneo, los CSG están diseñados para mejorar la utilización de la energía solar y minimizar las pérdidas térmicas, siendo esto último lo más importante. En las regiones del norte de China, la temperatura nocturna en invierno es inferior a 0 °C y la mayoría de los agricultores prefieren cubrir el techo transparente con una manta de aislamiento térmico, en lugar de quemar recursos energéticos para calefacción. Por tanto, debido a los factores geográficos y climáticos, la mayor diferencia entre los CSG y otros tipos de invernadero es el techo transparente en forma de abanico con una sola pendiente (véase la Figura 1). Destacar que esta estructura de invernadero da lugar a la obtención de gradientes muy elevados en las condiciones climáticas internas frente a cambios en las señales de control, siendo una de las principales diferencias dinámicas con respecto a invernaderos de la zona del Mediterráneo.

Figura 1: Invernadero solar en Pekín, China.

Actualmente, existen pocos estudios sobre la aplicación de técnicas de control automático en los CSG, como se resume a continuación. Wang y Zhang (2018) utilizaron un método de control adaptativo basado en lógica difusa para mantener la temperatura de un invernadero solar. Li et al. (2017) estudiaron un esquema de dos niveles con evaluación de riesgos para un uso óptimo de la energía solar en el invernadero. Xu et al. (2018a,b) presentaron un control óptimo y adaptativo, con dos escalas de tiempo y con horizonte deslizante aplicado al cultivo de lechuga en CSG.

Aparte de los citados trabajos, no se han reportado más estudios relevantes hasta el momento, y, particularmente, tampoco se ha estudiado el uso de controladores PID (Proporcional-Integral-Derivativo) para la regulación del clima dentro de los CSG. En la mayoría de las explotaciones comerciales, los agricultores confían en el control manual. En algunas instalaciones demostrativas de CSG, sí se suelen incorporar controladores convencionales para la regulación de consignas. No obstante, el control PID para regular la temperatura en el interior de los invernaderos ha sido ampliamente estudiado para invernaderos ubicados en otros lugares, como en Almería (Beschi et al., 2014; García-Mañas et al., 2021; Montoya-Ríos et al., 2020). Además, se han propuesto otros métodos de control, como el control basado en eventos, para disminuir el esfuerzo energético requerido para regular variables de interés (Pawlowski et al., 2016).

Los controladores PID requieren que los actuadores del invernadero respondan de manera continua y frecuente para mantener las variables climáticas controladas alrededor de una consigna, buscando reducir el error de control. Sin embargo, mantener la consigna regulada con una precisión de menos de 0,1 °C para el error de control podría provocar un mayor uso de los actuadores y un gasto excesivo en la energía que consumen. En este sentido, los esquemas de control basado en eventos reducen la actuación del sistema de control, reaccionando sólo cuando es estrictamente necesario, es decir, cuando el error de control se considera lo suficientemente grande. Por ejemplo, en comparación con el control PID clásico, Pawlowski et al. (2016) demostraron que si el número de actuaciones de un controlador basado en eventos para un invernadero tipo Almería se reduce en un 34 %, el error aumenta sólo en un 1 %; si el número de eventos se reduce en un 83 %, el error aumenta en un 19,8 %. Por lo tanto, este enfoque es una contribución importante para promover una producción agrícola más limpia, reduciendo el gasto de recursos.

En la literatura, la mayor parte de la investigación actual se dedica al control de la temperatura en invernaderos. Pocos trabajos consideran el control de la humedad, que es crucial para las funciones fisiológicas de muchos cultivos. Una humedad relativa alta reduce el número de semillas y, por lo tanto, tiene un efecto negativo en la polinización (Smit, 2005). Una humedad relativa demasiado baja (diferencia de presión de vapor alta) provoca estrés hídrico en la planta (Körner y Challa, 2003). La humedad de las hojas, causada por una humedad relativa alta y mantenida en el tiempo, daña los cultivos debido a diversas enfermedades fúngicas, como, por ejemplo, mildiú velloso, *Botrytis* y oídio (Liu et al., 2022). Rodríguez et al. (2008) presentaron un esquema de control de la humedad de un invernadero modificando las consignas de temperatura en función de la prioridad dada a la humedad relativa. La humedad relativa se controla mediante un límite superior e inferior dado, es decir, cuando la humedad está por encima de ese límite, la apertura de ventilación aumenta, y viceversa.

Pocas investigaciones previas presentan controladores PID específicos para invernadero, para humedad diurna y nocturna, así como temperatura, asegurando que el desempeño sea bueno para ambas variables. Un gran desafío de este problema es que la respuesta de la humedad es complicada y no lineal. Al aumentar la apertura de la ventilación del invernadero, la temperatura y el contenido de vapor de agua disminuyen simultáneamente, lo que tiene efectos y correlaciones respectivamente opuestos con la humedad relativa. Por lo tanto, en este trabajo se desarrollan y comparan dos métodos de control de la humedad.

El primero de ellos consiste en controlar directamente la humedad relativa en el interior del invernadero, pero el rendimiento no es el deseable, como se discute en la sección de resultados. El otro método consiste en adoptar una referencia dinámica de humedad absoluta, que depende de la temperatura en cada instante de tiempo y de una consigna fija para la humedad relativa. Este método se aplica por primera vez a invernaderos en este trabajo y los resultados obtenidos demuestran que puede ser una posible solución para controlar la humedad. En resumen, en este estudio se presenta un controlador PI basado en eventos, con un esquema de control selectivo aplicado para regular la temperatura y la humedad en un invernadero solar chino. Las principales contribuciones de este trabajo son las siguientes:

1. El control PI para la temperatura y la humedad se estudia por primera vez para invernaderos solares chinos.
2. El método de control basado en eventos reduce significativamente el número de eventos, es decir, el número de veces que los motores de las ventanas se accionan, lo que permite ahorrar energía y favorecer así una producción de cultivo más sostenible.
3. Se estudia en simulación una estrategia de control selectivo de temperatura y humedad con enfoque basado en eventos.

2. Materiales y métodos

En esta sección se describe el invernadero solar, la recopilación de datos, el modelado del invernadero y el diseño de los controladores para la temperatura y la humedad. Además, se expone el método de control basado en eventos y se presenta el esquema de control selectivo de temperatura y humedad.

2.1. Descripción del invernadero solar

El invernadero utilizado en este estudio es un invernadero solar chino, de estructura típica, con pendiente en forma de abanico (véase la Figura 1). Tiene 50 m de largo, 7 m de ancho, con una altura de cumbrera de 3,5 m, como se muestra en la Figura 2. El lateral orientado al norte es un muro de ladrillo de 0,6 m de espesor, y el techo (orientado al sur) está cubierto con una película de polietileno (PE) transparente. El suelo del invernadero está situado 0,5 m por debajo del nivel del suelo exterior para aumentar el aislamiento térmico. En primavera y otoño, se cultivan pepinos colocados en filas. Las tuberías de riego por goteo están enterradas en el suelo y cubiertas con una película de plástico transparente.

La ventilación natural se efectúa mediante actuadores encargados de enrollar la película de PE en las ventanas superior e inferior. El área máxima de apertura de las ventanas es de 30 m^2 (50 m × 0,6 m).

2.2. Datos experimentales

Los datos experimentales para este trabajo proceden de dos estaciones de medida instaladas en el invernadero anteriormente descrito. El periodo de los datos seleccionados es del 15 al 28 de abril de 2021.

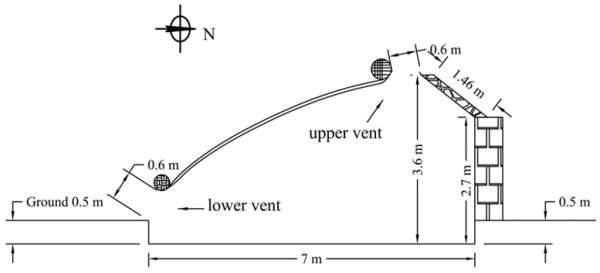

Figura 2: Estructura del invernadero experimental.

En el exterior, una estación meteorológica Davis Vantage Pro & Plus (Davis Instruments, Hayward, EE.UU.) se encarga de medir los datos meteorológicos cada 15 minutos: radiación solar (con rango 0 a 1800 $W \cdot m^{-2}$; precisión ±5 %), velocidad y dirección del viento (con rango 0 a 67 $m \cdot s^{-1}$; precisión ±5 %), temperatura del aire (con rango -40 a +65 °C; precisión, ±0,5 °C y humedad relativa (con rango 0 a 100 %; precisión, ±3 %). En el centro del invernadero se encuentra una estación meteorológica Davis-6162 (Davis Instruments, Hayward, EE.UU.) para medir la temperatura y humedad relativa del aire, y la temperatura del suelo a 0,5 m de profundidad.

La altura del cultivo y el índice de área foliar (*leaf area index*, LAI) se midieron manualmente en cinco puntos equidistantes en la diagonal en el plano horizontal del invernadero, tomando cuatro plantas por cada punto de medida.

2.3. Modelo del invernadero

En un estudio anterior (Liu et al., 2021), se diseñó, calibró y validó un modelo para el invernadero empleado en este trabajo. Se trata de un modelo dinámico, totalmente validado para simular la temperatura y la humedad del invernadero solar chino. Para ejecutar el modelo, se deben especificar las condiciones iniciales y las correspondientes condiciones de contorno transitorias (datos meteorológicos). El modelo es un conjunto de expresiones que representan transferencias de energía y balances de masa aire-vapor. Para el cálculo de la evolución de la temperatura del aire en el tiempo, t, se emplea la siguiente expresión:

$$\frac{dT(t)}{dt} = \frac{q_v(t) + q_{lea}(t) + q_c(t) + q_{liq}(t) + q_p(t)}{\rho \cdot V \cdot \left(c_p + c_{pw} \cdot h(t)\right)} \tag{1}$$

donde los términos $q(t)$ (W) representan transferencias térmicas: $q_v(t)$ por efecto de la ventilación, $q_{lea}(t)$ por pérdidas de aire a través de la cubierta, $q_c(t)$ por convección, $q_{liq}(t)$ por condensación del vapor de agua, y $q_p(t)$ por la transpiración del cultivo. La humedad absoluta se representa como $h(t)$ ($kg \cdot kg^{-1}$), ρ ($kg \cdot m^{-3}$) es la densidad del aire, c_p ($kg^{-1} \cdot K^{-1}$) es el calor específico del aire, c_{pw} ($J \cdot kg^{-1} \cdot K^{-1}$) es el calor específico del vapor de agua, T es la temperatura interior (K) y V (m^3) es el volumen del invernadero. Para calcular la humedad en el invernadero, se utiliza la siguiente expresión:

$$\frac{dh(t)}{dt} = s_v(t) + s_{lea}(t) + s_p(t) \tag{2}$$

donde los términos $s(t)$ ($kg \cdot kg^{-1} \cdot s^{-1}$) representan intercambios de masa aire-vapor: $s_v(t)$ por la ventilación, $s_{lea}(t)$ por pérdidas a través de la cubierta, y $s_p(t)$ por la transpiración del cultivo.

Cada uno de los términos que componen (1) y (2) se calculan a partir de un grupo de ecuaciones que son, en su mayoría, fuertemente no lineales. Por lo tanto, resulta complicado calcular un controlador usando este modelo. No obstante, es importante destacar que este modelo no lineal se utiliza como simulador del invernadero real en este trabajo.

2.4. Modelo lineal

Una forma sencilla de obtener un modelo lineal del invernadero es mediante el uso de polinomios que relacionen la salida con la entrada del sistema. Por ejemplo, utilizando técnicas de identificación de sistemas y haciendo uso del System Identification Toolbox de MATLAB es posible construir este tipo de modelos dinámicos a partir de datos experimentales.

Para este trabajo, utilizando el modelo no lineal descrito en el apartado anterior, se han aplicado una serie de señales de entrada como cambios aleatorios en la apertura de la ventilación del invernadero, generadas intencionadamente para provocar respuestas pronunciadas en la temperatura y la humedad relativa. El resto de entradas al modelo no lineal son datos meteorológicos reales. A partir de las respuestas de temperatura y humedad obtenidas, se realiza el procedimiento clásico de identificación de sistemas para determinar modelos polinómicos autoregresivos con entradas exógenas (*Auto Regressive with eXogenous inputs*, ARX) (Montoya-Ríos et al., 2020; García-Mañas et al., 2021).

Se han obtenido 14 modelos ARX, uno para cada día de las dos semanas de datos disponibles. Finalmente, se seleccionaron dos modelos (uno de la primera semana y otro de la segunda) para los días que mejor ajuste ofrecieron según la siguiente expresión:

$$FIT = \left(1 - \frac{||Y - \hat{Y}||}{||Y - \overline{Y}||}\right) \cdot 100 \tag{3}$$

donde Y son los datos medidos de la variable a modelar, e $\hat{Y}$ es la salida estimada por el modelo ARX. A partir de estos modelos lineales basados en datos, resulta más sencillo el cálculo de un controlador, como se expone en los siguientes apartados.

2.4.1. Modelo lineal de temperatura

Las ventanas del invernadero suelen mantenerse cerradas durante la noche, dado que la temperatura desciende por debajo de la consigna establecida. Por tanto, al considerar que la ventilación natural sólo actúa durante el día, para calcular un modelo ARX, se introducen cambios en la apertura de la ventilación durante el periodo diurno.

La Figura 3 muestra el esquema del modelo ARX que se obtiene al considerar como salida la temperatura del invernadero y como entrada la apertura de la ventilación natural. Se consideran como perturbaciones: la temperatura del aire exterior, la radiación solar y la velocidad del viento. La ecuación del modelo ARX en tiempo discreto, k, es la siguiente:

$$y(k) = \frac{B_1(z)}{A(z)}u(k) + \frac{B_2(z)}{A(z)}v_1(k) + \frac{B_3(z)}{A(z)}v_2(k) + \frac{B_4(z)}{A(z)}v_3(k) \tag{4}$$

donde y (°C) es la temperatura, u (%) es la apertura de la ventilación, v_1 (°C) es la temperatura exterior, v_2 (W·m^{-2}) es la radiación solar exterior, y v_3 (m·s^{-1}) es la velocidad del viento en el exterior.

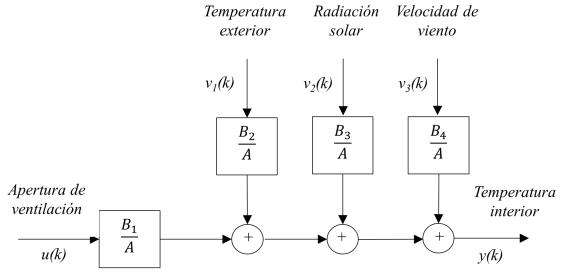

Figura 3: Esquema del modelo ARX que relaciona la temperatura del aire interior del invernadero con la apertura de la ventilación y con las perturbaciones.

2.4.2. Modelo lineal de humedad

Dado que en el presente trabajo se han comparado dos métodos para controlar la humedad, ha sido necesario calcular dos modelos ARX para dicha variable. Para el primer método, que consiste en controlar directamente la humedad relativa con la apertura de las ventilaciones, se han determinado modelos ARX para la humedad relativa diurna y nocturna, según el esquema de la Figura 4a.

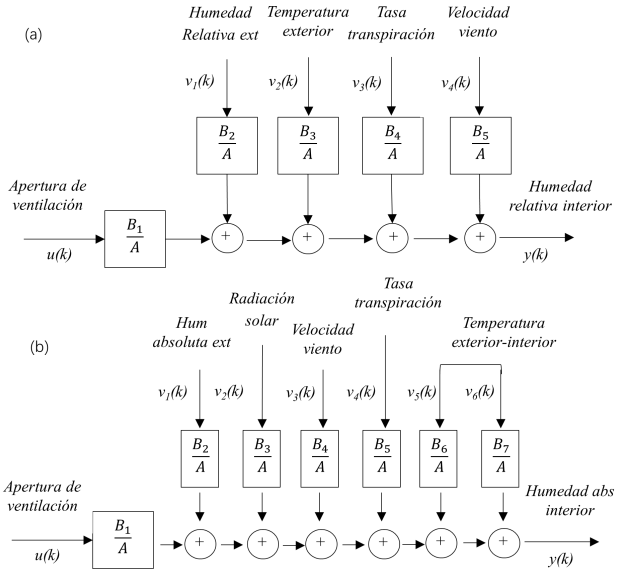

Figura 4: Esquemas de los modelos ARX que relacionan la humedad del aire interior del invernadero con la apertura de la ventilación y con las perturbaciones: (a) para la humedad relativa, (b) para la humedad absoluta.

Para el segundo método, que consiste en seguir una referencia cambiante de humedad absoluta, la salida del modelo ARX es la humedad absoluta (véase la Figura 4b) como cuantificación del contenido de vapor de agua en el invernadero, lo que está significativamente correlacionado con el intercambio climático interno-externo, la radiación y las funciones fisiológicas del cultivo. Como se aprecia en la Figura 4, las estructuras son similares, teniendo el segundo modelo más términos.

2.5. *Cálculo de las funciones de transferencia y de los controladores PID*

Una vez obtenidos los modelos alto orden tipo ARX, dichos modelos son simplificados con fines de control como funciones de transferencia de primera orden:

$$G(s) = \frac{k}{\tau s + 1} e^{-t_r s} \tag{5}$$

donde k es la ganancia estática, τ es la constante de tiempo, y t_r es el tiempo de retardo.

Para la simplificación de los modelos ARX, se han seguido las etapas y procedimientos expuestos por Montoya-Ríos et al. (2020) y García-Mañas et al. (2021). La idea principal se basa en aplicar un escalón de entrada a un modelo ARX y estudiar la respuesta en la salida para identificar un modelo mediante una función de transferencia de primer orden, para temperatura y para la humedad, respectivamente.

Los lazos de control se han diseñado mediante controladores PI para calcular la apertura de las ventanas en función del error existente entre la temperatura del invernadero (o la humedad) y el valor indicado como consigna (Montoya-Ríos et al., 2020). De esta forma, la ley de control vendrá dada por la siguiente expresión:

$$u(t) = k_p\, e(t) + \frac{k_p}{T_i} \int e(t)\, dt \tag{6}$$

siendo k_p la ganancia proporcional y T_i el tiempo integral. Aplicando la Transformada Laplace se obtiene:

$$C(s) = \frac{U(s)}{E(s)} = k_p \left(\frac{T_i s + 1}{T_i s} \right) \tag{7}$$

Para el diseño de los controladores se ha utilizado el método λ, cuyas reglas de sintonía son las siguientes (Åström y Hägglund, 2005):

$$T_i = \tau \tag{8}$$

$$k_p = \frac{\tau}{k(t_r + \lambda)} \tag{9}$$

En este trabajo, se ha fijado $\lambda = 0{,}3\tau$ para el controlador de temperatura, y $\lambda = \tau$ para el de humedad.

2.6. *Método de control basado en eventos*

El control basado en eventos es una metodología que permite adaptar y mejorar algoritmos de control tradicionales para encontrar un compromiso entre rendimiento y esfuerzo de control (o cambios en la señal de control) de forma relativamente sencilla. Su principal ventaja es la posibilidad de generar esfuerzo de control cuando realmente sea necesario y ventajoso para el proceso que se está controlando (Dormido et al., 2008). Un controlador PI estándar requiere que el actuador responda al error en cada instante de tiempo. Esto significa que el controlador mantiene una mayor precisión de control cambiando frecuentemente la señal de control para mantener la consigna deseada. En comparación, el control basado en eventos permite reducir el esfuerzo de control de forma drástica sin aumentar demasiado el error de realimentación. Existen multitud de variantes del control basado en eventos, pero la más sencilla es la basada en la estrategia del muestreo *Send-on-delta* simétrico (Pawlowski et al., 2016). De manera resumida, con este método, el controlador sólo se activa cuando el error supera unos límites concretos, $\pm\delta$. De lo contrario, el error se considera nulo. Este método se puede implementar con la inclusión de una zona muerta en el lazo de control, como se presenta en la Figura 5 mediante el bloque SSOD que representa el muestreo *Send-on-delta* simétrico sobre la señal de error.

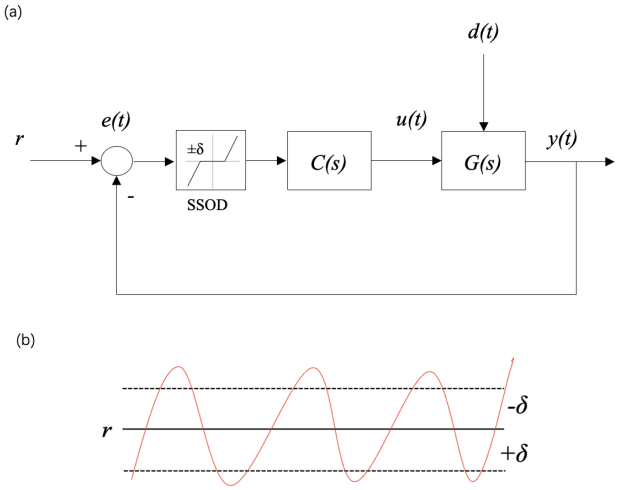

Figura 5: Esquema de control basado en eventos: (a) muestra el lazo de control, (b) presenta la referencia r con línea continua en negro, los límites superiores e inferiores con líneas negras punteadas, y la salida controlada en rojo.

Nótese que un valor de δ demasiado grande provocará la oscilación de la salida del proceso. Por el contrario, un valor de δ pequeño no supondría una reducción del esfuerzo de control. Para el caso de los CSG, el valor óptimo de δ no ha sido previamente estudiado. Por ello, en este trabajo se han evaluado diferentes valores de $\delta = [0\ \ 0{,}1\ \ 0{,}2\ \ 0{,}5\ \ 1]$, comprando el rendimiento entre el control basado en eventos y el control PI con el esquema clásico, según los siguientes índices:

1. Integral del error absoluto: $IAE = \sum |e(t)|$
2. ΔIAE en porcentaje: $(IAE - IAE_{\delta=0})/IAE_{\delta=0}$
3. Esfuerzo de control: $IAU = \sum |u(t) - u(t-1)|$
4. ΔIAU en porcentaje: $(IAU - IAU_{\delta=0})/IAU_{\delta=0}$
5. Número de eventos: E
6. ΔE en porcentaje: $(E_{\delta=0} - E)/E_{\delta=0}$

Destacar que los problemas de estabilidad de este algoritmo basado en SSOD relativo a la presencia de ciclos límite y fenómenos tipo Zenón han sido ampliamente estudiados en la literatura demostrado la estabilidad de este algoritmo tal y como se puede encontrar en (Beschi et al., 2013).

2.7. *Esquema de control de prioridad de humedad*

En este apartado se expone el método de control mixto para temperatura y humedad, considerando que normalmente sólo actúa el controlador PI de temperatura, pero, si fuera necesario, el método permite dar prioridad al control de la humedad para mantenerla regulada evitando unos rangos no deseados. En los CSG, no se suele presentar la humedad excesivamente baja, por lo que el objetivo de control se centra en evitar los valores elevados.

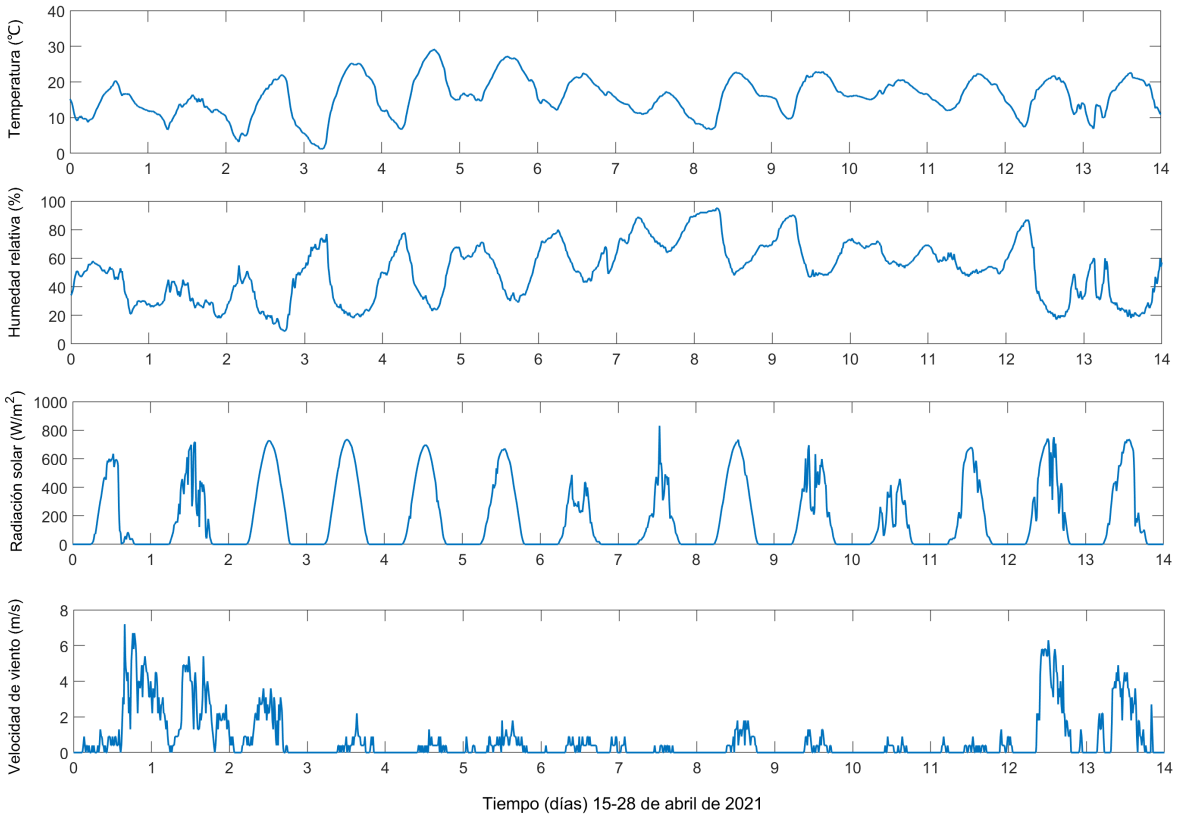

Figura 6: Datos del clima en el exterior del invernadero, medidos entre el 15 y el 28 de abril de 2021.

En este trabajo, la humedad relativa se controla mediante un límite superior dado, y cuando se encuentra por encima de ese límite, se aumenta la apertura de ventilación. En concreto, se ha establecido un 80 % de humedad relativa como límite superior y un 60 % como límite inferior. Cuando la humedad relativa está por encima del límite superior, el controlador PI de humedad se activa para tratar de reducirla al 60 %. Cuando la humedad relativa es menor del 60 %, el controlador de temperatura se reactiva para su control en la consigna establecida. Nótese que son dos casos diferentes los que ocurren. Cuando la humedad se mantiene en el rango [60, 80] %, el controlador de humedad no se activa. Cuando la humedad relativa supera el 80 %, el controlador de humedad se mantiene activado con prioridad sobre el de temperatura hasta que la humedad vuelva a ser inferior al 60 %.

3. Resultados y discusión

En esta sección se presentan los resultados del estudio de simulación para el control de temperatura y humedad con los métodos anteriormente descritos. Se compara el rendimiento del control de temperatura en un único día y en 14 días consecutivos, evaluando el método de control clásico y el basado en eventos. El mismo conjunto de datos se ha empleado para comprobar el desempeño de los controladores de humedad, tanto para la humedad absoluta como relativa. Finalmente, se presentan los resultados de simulación para el esquema de control selectivo de temperatura y humedad. En este caso, se utilizan los mismos 14 días consecutivos considerando la estrategia de control de prioridad de humedad. La Figura 6 muestra los datos meteorológicos utilizados para calcular los modelos ARX y realizar las simulaciones de control.

3.1. *Modelos ARX y funciones de transferencia*

Los modelos ARX fueron seleccionados en base a los que mejor ajuste presentaron para un día en cada semana de las dos disponibles. Debido a la extensión limitada de este artículo, sólo se presenta en (10)-(14) el modelo ARX para la temperatura, identificado para el día 19 de abril de 2021, con un ajuste del 85,49 % según (3).

$$A(z) = 1 - 2,41z^{-1} + 1,84z^{-2} - 0,15z^{-3} - 1,00z^{-4} + 1,60z^{-5} - 1,56z^{-6} + 0,96z^{-7} - 0,27z^{-8} \quad (10)$$

$$B_1(z) = 4,14 \cdot 10^{-5}z^{-7} - 8,28 \cdot 10^{-5}z^{-8} - 6,70 \cdot 10^{-5}z^{-9} \quad (11)$$

$$B_2(z) = 9,62 \cdot 10^{-3}z^{-7} - 8,70 \cdot 10^{-3}z^{-8} - 0,91 \cdot 10^{-3}z^{-9} \quad (12)$$

$$B_3(z) = 3,01 \cdot 10^{-4}z^{-7} - 3,81 \cdot 10^{-4}z^{-8} + 0,80 \cdot 10^{-4}z^{-9} \quad (13)$$

$$B_4(z) = -0,07z^{-7} + 0,14z^{-8} - 0,06z^{-9} \quad (14)$$

El ajuste de este modelo se puede apreciar gráficamente en la Figura 7. La identificación de los modelos ARX para la humedad se ha realizado distinguiendo entre aperturas de la ventilación durante el periodo nocturno y diurno, y entre la humedad absoluta y la humedad relativa.

Para ventilación en el periodo diurno, la Figura 8 presenta la respuesta del modelo ARX para la humedad relativa, con un ajuste del 79,35 %, y la Figura 9 presenta la respuesta del modelo ARX para la humedad absoluta, con un ajuste del 80,52 %.

Ambos modelos poseen un buen ajuste a los datos, lo que significa que representan de forma aceptable la respuesta del sistema para cambios en la apertura de las ventanas del invernadero y para las perturbaciones climáticas. Las expresiones de los modelos para la humedad no se muestran por ahorro de espacio ya que son de la misma forma que (10)-(14), aunque de distinto orden y valores.

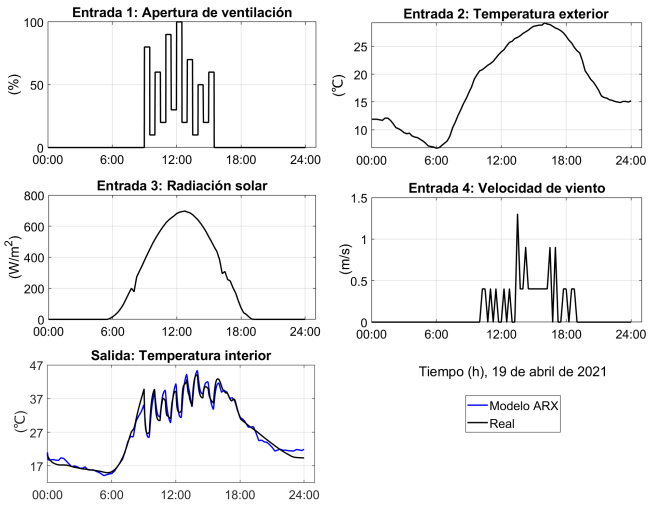

Figura 7: Modelo ARX identificado para la temperatura con datos del día 19 de abril de 2021.

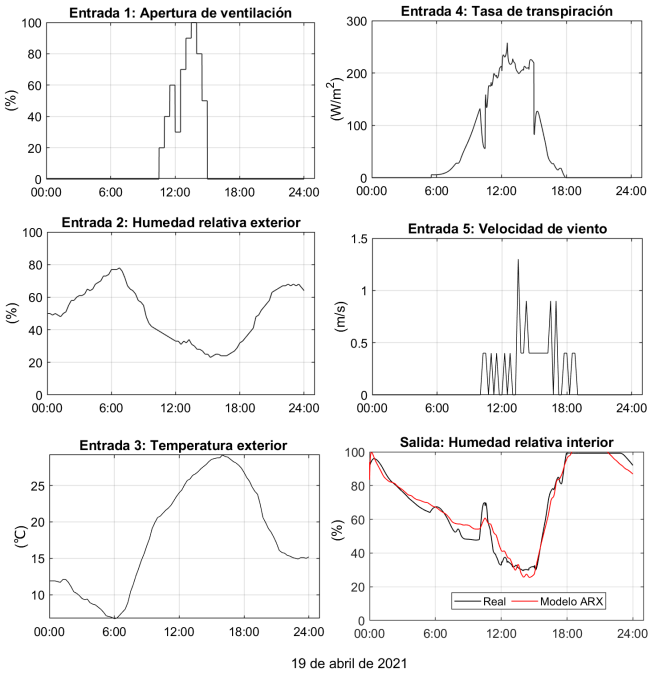

Figura 8: Modelo ARX para la humedad relativa con ventilación en el periodo diurno, identificado con datos del día 19 de abril de 2021.

Las Figuras 10 y 11 presentan la identificación de los modelos ARX de humedad pero para aperturas de la ventilación en el periodo nocturno, entre las 21:00 y las 05:00 horas del siguiente día. El modelo de la humedad relativa posee un ajuste del 81,32 %, y el de la humedad absoluta un ajuste del 86,61 %. Se puede apreciar que no suele haber viento durante la noche, por lo que la fuerza impulsora de la ventilación natural proviene de la diferencia de condiciones entre el interior y el exterior del invernadero, lo que produce una reducción de la humedad en el aire interior.

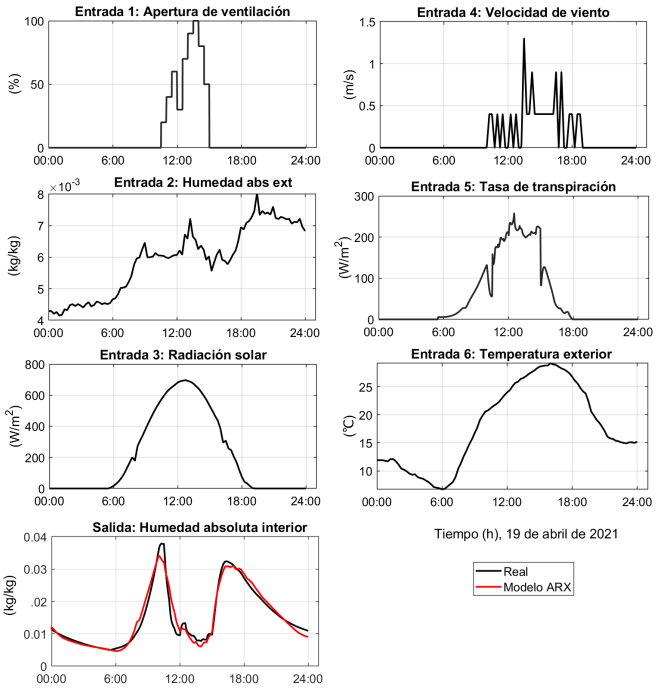

Figura 9: Modelo ARX para la humedad absoluta con ventilación en el periodo diurno, identificado con datos del día 19 de abril de 2021.

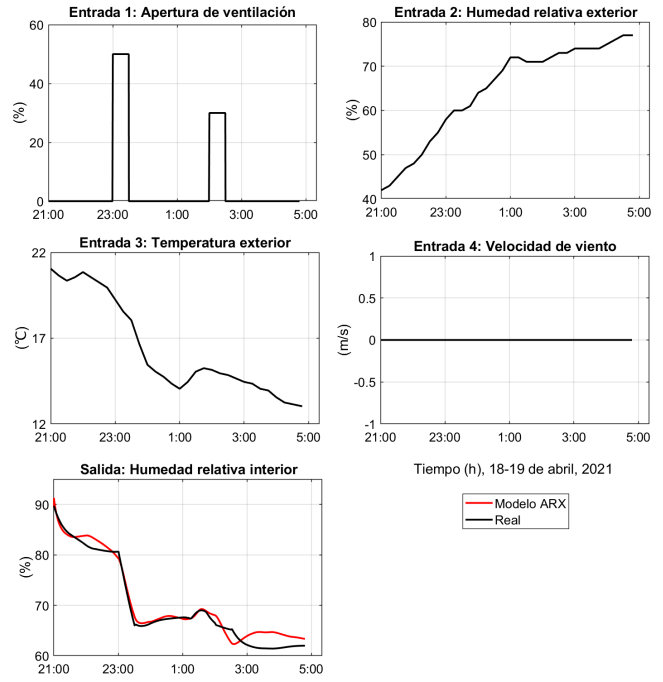

Figura 10: Modelo ARX para la humedad relativa con ventilación en el periodo nocturno, identificado con datos del día 19 y 20 de abril de 2021.

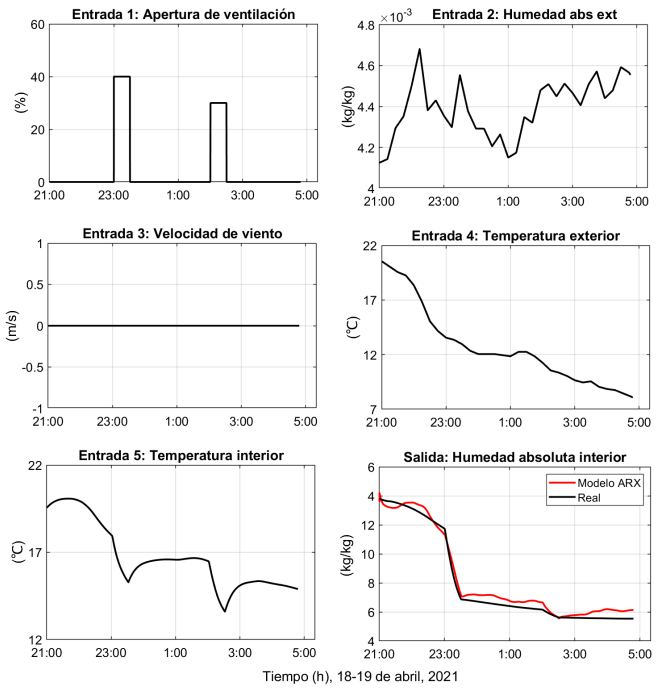

Figura 11: Modelo ARX para la humedad absoluta con ventilación en el periodo nocturno, identificado con datos del día 18 y 19 de abril de 2021.

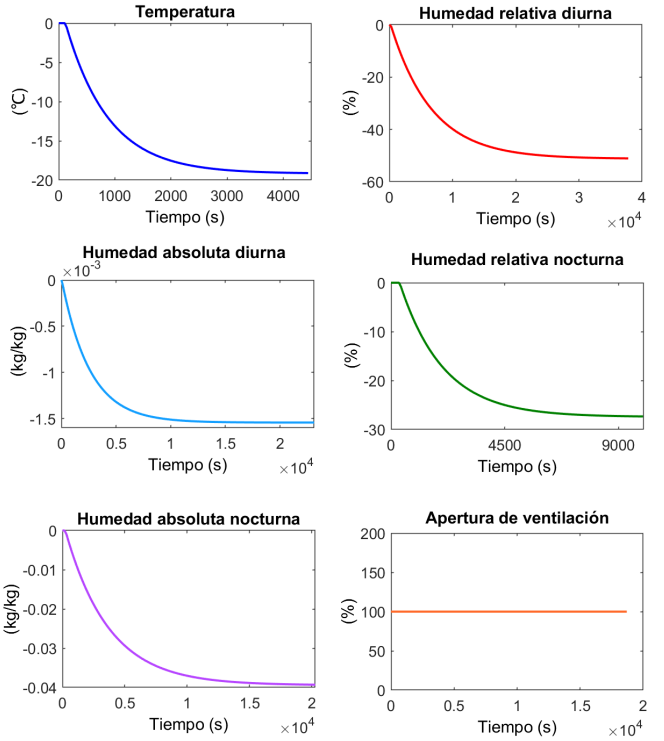

Figura 12: Respuestas de los modelos ARX para un escalón del 100 % en la entrada de ventilación.

Una vez calculados los modelos ARX, se procedió a determinar funciones de transferencia de primer orden para la temperatura, la humedad relativa y la humedad absoluta, mediante el procedimiento descrito en la sección 2.5.

En la Figura 12 se muestran las respuestas a un escalón de entrada para la ventilación, para las que las funciones de transferencia resultantes son las siguientes:

- Temperatura: $G_T(s) = \frac{-19{,}2}{765s+1}e^{-120s}$
- Humedad relativa diurna: $G_{HRd}(s) = \frac{-51{,}2}{6516s+1}e^{-205s}$
- Humedad relativa nocturna: $G_{HRn}(s) = \frac{-27{,}4}{1718s+1}e^{-342s}$
- Humedad absoluta diurna: $G_{HAd}(s) = \frac{-0{,}00154}{2574s+1}e^{-30s}$
- Humedad absoluta nocturna: $G_{HAn}(s) = \frac{-0{,}0394}{3494s+1}e^{-229s}$

Destacar los valores de las constantes de tiempo y especialmente de las ganancias estáticas obtenidas, que son drásticamente mayores a los valores típicos obtenidos en invernaderos de la zona del Mediterráneo. Este hecho es debido al tamaño reducido de los invernaderos solares chinos y al sistema de ventilación de los mismos, que da lugar a gradientes muy elevados frente a cambios en las señales de control. Este hecho ya fue observado en el desarrollo del modelo basado en primeros principios que se utiliza como base en este trabajo (Liu et al., 2021).

Cada una de estas funciones de transferencia se utilizan para determinar los respectivos controladores mediante el método λ (véase la sección 2.5). Dado que las ventanas del invernadero tienen una apertura restringida entre el 0 % y el 100 %, los controladores incorporan el mecanismo *anti-windup* para la desaturación del término integral, con una constante de seguimiento $T_t = \sqrt{T_i}$.

3.2. *Estudio comparativo de controladores basados en eventos para la temperatura*

Para examinar el rendimiento del control basado en eventos para la temperatura, es necesario adoptar diferentes valores para δ, ya que un valor demasiado grande o pequeño puede conducir, por ejemplo, a un aumento excesivo del error de control. Por tanto, en esta sección se analizan los resultados tras adoptar los siguientes valores: $\delta = [0\ \ 0{,}1\ \ 0{,}2\ \ 0{,}5\ \ 1]$.

Como se muestra en la Figura 13, el controlador PI ofrece un desempeño muy bueno para controlar la temperatura el día 20 de abril de 2021. Con $\delta = 0$ (que corresponde al caso clásico sin eventos) se observa que la señal de control provoca cambios constantemente en la apertura de la ventilación. Esto ofrece mayor precisión de control, al mantenerse la temperatura muy cerca de la consigna, pero, a su vez, causa un mayor desgaste de los motores de las ventanas y un mayor consumo de energía asociado. En la Tabla 1 se compara el desempeño para cada uno de los valores de δ con los que se ha simulado la estrategia de control. Se observa cómo el número de eventos (representado por E) se reduce significativamente a medida que se incrementa el valor de δ, cuyo valor óptimo será aquel que permita un balance entre ΔE y ΔIAU, y ΔIAE. Por ejemplo, si se incrementa δ de 0,5 a 1, ΔE aumenta de 43,8 % a 50,4 %, pero se duplica el valor de ΔIAE, pasando de 1,13 % a 2,29 %. Por otro lado, IAU representa el esfuerzo de control, por lo que reducir su valor se traduce en un ahorro en las veces en las que se accionan los motores de las ventanas y también en ahorro energético. Si se incrementa δ de 0,1 a 0,5, el valor de IAU se reduce considerablemente y se consigue triplicar ΔIAU, de 8,3 % a 25,6 %. Para valores de δ entre 0,5 y 1, ΔIAU cambia menos del doble de su valor. Esto significa que cambiar el valor

de δ por encima de 0,5 no es rentable debido al incremento del error. Por tanto, se deduce que un valor adecuado para δ en este caso es 0,5.

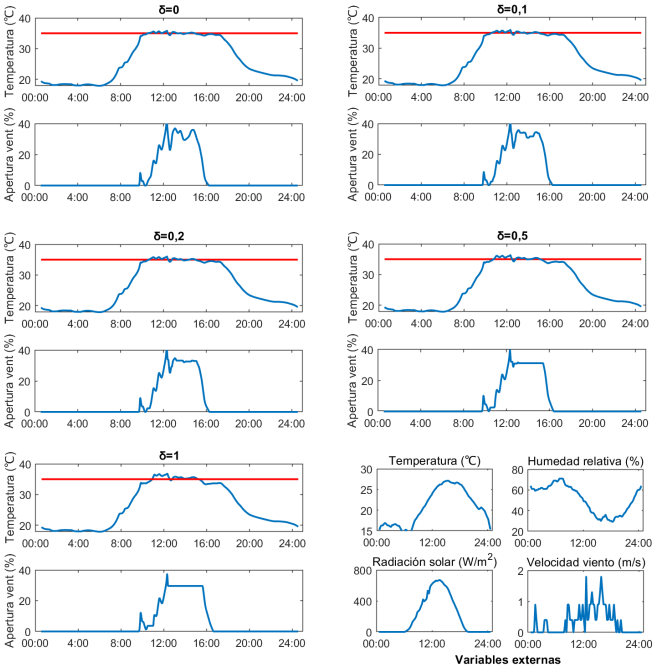

Figura 13: Control de temperatura con diferentes valores de δ para el 20 de abril de 2021.

Tabla 1: Desempeño del control de temperatura para diferentes valores de δ

δ	IAE (°C)	ΔIAE (%)	E	ΔE (%)	IAU
0	$7{,}7409{\cdot}10^5$	0	22968	0	156,0
0,1	$7{,}7593{\cdot}10^5$	0,24	19463	15,3	143,1
0,2	$7{,}7776{\cdot}10^5$	0,47	17287	24,7	132,6
0,5	$7{,}8286{\cdot}10^5$	1,13	12913	43,8	116,1
1	$7.9179{\cdot}10^5$	2,29	11395	50,4	105,4

3.3. *Estudio comparativo de dos métodos de control de la humedad*

En este apartado se discuten los resultados para comparar los dos métodos de control propuestos para regular la humedad.

El primero de ellos consiste en corregir directamente el error entre la humedad relativa y una referencia constante, con un esquema de control de realimentación clásico. El segundo método consiste en corregir el error entre la salida de humedad absoluta y una referencia dinámica, que se obtiene a partir de una referencia de humedad relativa constante y de la temperatura que se mide en el invernadero en cada instante de tiempo. Para ello, la referencia dinámica de humedad absoluta se genera mediante las siguientes expresiones:

$$P_w(t) = 610,78 \cdot \frac{r_{HR}}{100} \cdot e^{\left(\frac{T(t)-273,15}{T(t)-34,85} \cdot 17,2694\right)} \tag{15}$$

$$r_{HA}(t) = 0,622 \cdot \frac{P_w(t)}{P - P_w(t)} \tag{16}$$

donde P_w es la presión del vapor de agua, P es la presión atmosférica, r_{HR} es la referencia constante de humedad relativa, y r_{HA} es la referencia dinámica de humedad absoluta. Cabe destacar que, aunque se realiza un seguimiento de una referencia dinámica de la humedad absoluta, la consigna siempre es fija para la humedad relativa, lo cual resulta más sencillo de comprender para los agricultores que están más familiarizados con esta variable para detectar valores perjudiciales que puedan causar enfermedades en sus cultivos.

Atendiendo a los resultados que se presentan en la Figura 14, el primer método de control se comporta adecuadamente para consignas de humedad relativa bajas, como se observa para las consignas del 40 % y del 50 %. Sin embargo, cuando la consigna es del 60 %, la precisión del control disminuye, y para consigas por encima del 70 %, no se consigue controlar la humedad.

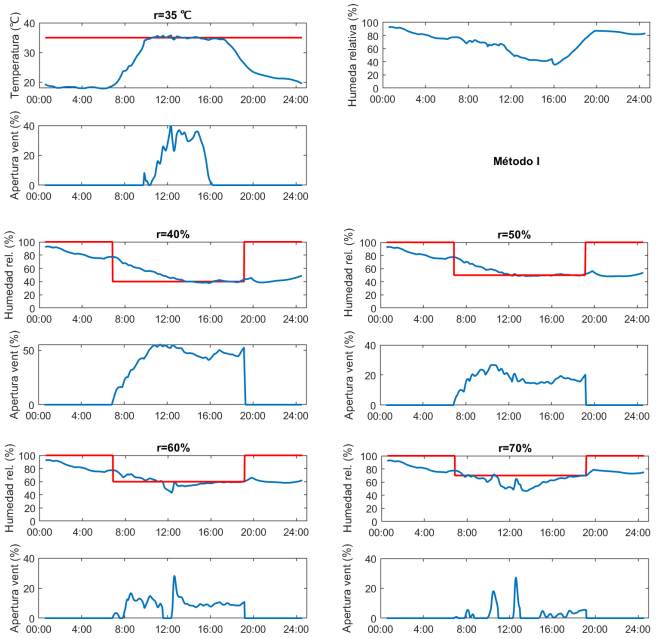

Figura 14: Comparación de resultados del primer método de control de humedad relativa para el día 20 de abril de 2021. Las gráficas situadas en la parte superior muestran la evolución de la humedad sin control (sólo de temperatura). Las gráficas inferiores muestran la respuesta de control para distintos valores de consignas.

En comparación, en la Figura 15 se aprecia que el segundo método es capaz de actuar y regular la humedad relativa con todos los valores de consignas, pero ofrece menor precisión de control que el primer método. Por lo tanto, se puede comprobar que es importante tener en cuenta en el control de la humedad relativa tanto el contenido de vapor de agua en el aire como la temperatura, aunque se recomienda escoger entre el primer o el segundo método según el escenario de aplicación y el rango de consignas a establecer.

3.4. *Control de temperatura en días consecutivos*

Una vez establecido el valor óptimo de δ, el rendimiento del control de temperatura se evaluó utilizando dos semanas consecutivas de datos considerando las condiciones climáticas expuestas en la Figura 6, y comparando el control basado en eventos con $\delta = 0,5$ frente a un control PI estándar, es decir,

con $\delta = 0$. Como se observa en la Figura 16, en ambos casos se obtienen unos resultados de control muy satisfactorios. Las desviaciones que se producen en la temperatura, por ejemplo, en los días 2, 8, 10, 12 y 13, se deben fundamentalmente a los cambios de radiación solar exterior (véase la Figura 6), que afecta como perturbación.

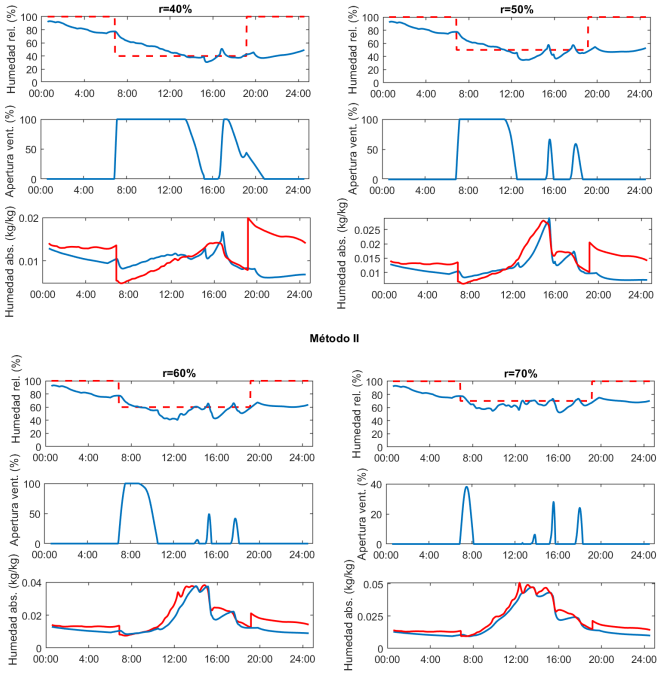

Figura 15: Resultados del segundo método de control de humedad relativa para el día 20 de abril de 2021.

Las fluctuaciones en la velocidad del viento tienen menos impacto en el rendimiento del control que la radiación solar. La temperatura exterior durante el día no presenta cambios notables, por lo que no es un factor clave que afecte el rendimiento del control.

Comparando los resultados que se muestran en la Tabla 2, el control basado en eventos permite reducir el número de eventos en un 33,85 %, produciéndose un incremento del error de tan sólo un 0,89 %. Además, consigue reducir el esfuerzo de control en un 18,8 %. Tanto ΔE como ΔIAU son menores para las dos semanas consecutivas que en un solo día, lo que significa que el método de control basado en eventos perdió efectividad en aquellos días en los que las perturbaciones fluctúan. No obstante, los resultados confirman que este método de control es adecuado para regular la temperatura ayudando a disminuir el uso de los motores de la ventilación.

3.5. *Funcionamiento del control selectivo con prioridad para la humedad*

El esquema propuesto en la sección 2.7 se ha ensayado para verificar que permite controlar la humedad evitando que tome valores altos mientras se mantiene una temperatura elevada. En la Figura 17 se muestran los resultados de control para dos semanas consecutivas de datos, en las que las consignas para las variables a controlar se mantuvieron fijas. Mantener la consigna de temperatura fija es una práctica habitual en invernaderos, que, en ocasiones, puede conllevar que la humedad relativa se incremente hasta valores que pueden ser perjudiciales para el cultivo, como se puede apreciar en los días 2, 7, 8 y 9. Para esos mismos días, el control de prioridad para la humedad actúa y evita que sobrepase el límite de 80 %, como se puede observar, especialmente, en el día 8, cuando se abren las ventanas del invernadero. Dicha apertura, sin embargo, provoca una reducción en la temperatura nocturna. Por tanto, sería interesante diseñar una estrategia independiente de reducción de humedad para un cultivo específico, dependiendo de la tolerancia a bajas temperaturas.

4. Conclusiones

En este trabajo se ha aplicado por primera vez el control PI para la temperatura y la humedad en invernaderos solares chinos. El método de control basado en eventos muestra un comportamiento adecuado que permite reducir el esfuerzo de control. Se espera poder aplicar este enfoque a distintos conjuntos de invernaderos y comprobar el ahorro en términos de movimientos realizados por los motores de las ventanas y de la energía que consumen. Además, este trabajo pone de manifiesto las dificultades y los desafíos de control de la humedad en invernaderos y propone un método factible para tratar de reducir el error de control de esta variable. Se demuestra que un control combinado de la temperatura y de la humedad es posible mediante un método que otorgue prioridad a mantener la humedad por debajo de niveles considerados demasiado elevados. De esta forma, se contribuye a mejorar la producción del cultivo y a la prevención en la aparición de enfermedades que puedan afectar al mismo. Como trabajos futuros se contemplará la implementación del algoritmo de control propuesto en un invernadero de China del centro NERCITA.

Agradecimientos

El autor Liu Ran agradece el apoyo económico brindado por el Consejo de Becas de China (*China Scholarship Council* , nº. 201909505002). El autor Francisco García-Mañas es beneficiario de una ayuda FPU del Ministerio de Ciencia, Innovación y Universidades.

Referencias

Åström, K. J., Hägglund, T., 2005. Advanced PID Control. ISA - The Instrumentation, Systems, and Automation Society, Research Triangle Park, NC 27709.

Beschi, M., Dormido, S., Sanchez, J., Visioli, A., 2013. Stability analysis of symmetric send-on-delta event-based control systems. In: 2013 American Control Conference. pp. 1771–1776.
DOI: 10.1109/ACC.2013.6580092

Beschi, M., Pawlowski, A., Guzmán, J. L., Berenguel, M., Visioli, A., 2014. Symmetric send-on-delta PI control of a greenhouse system. IFAC Proceedings Volumes 47 (3), 4411–4416.
DOI: 10.3182/20140824-6-ZA-1003.01028

Dormido, S., Sánchez, J., Kofman, E., 2008. Muestreo, control y comunicación basados en eventos. Revista Iberoamericana de Automática e Informática industrial 5 (1), 5–26.
DOI: 10.1016/S1697-7912(08)70120-1

García-Mañas, F., Guzmán, J. L., Rodríguez, F., Berenguel, M., Hägglund, T., 2021. Experimental evaluation of feedforward tuning rules. Control Engineering Practice 114, 104877.
DOI: 10.1016/j.conengprac.2021.104877

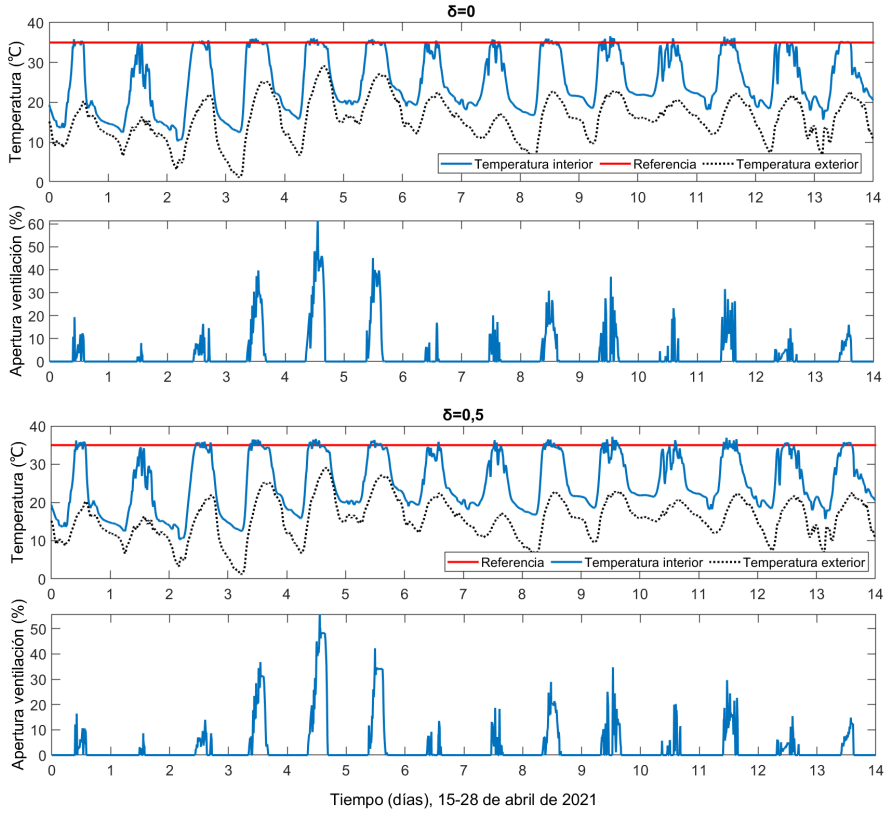

Figura 16: Resultados de control de temperatura para dos semanas consecutivas (del 15 al 28 de abril de 2021).

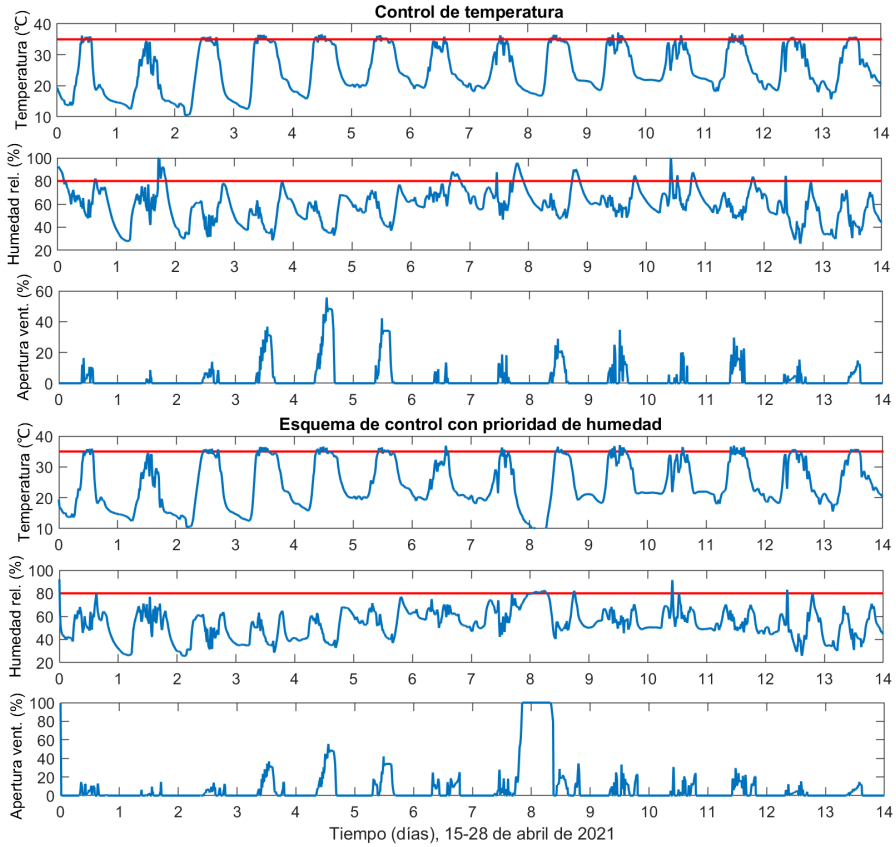

Figura 17: Comparación entre los resultados de controlar solamente la temperatura con $\delta = 0{,}5$ (gráficas de la parte superior) y de controlar la temperatura y la humedad con el esquema de control prioritario (gráficas de la parte inferior).

Tabla 2: Evaluación de resultados de control de temperatura con $\delta = 0$ y $\delta = 0{,}5$ durante los días consecutivos del 15 al 28 de abril de 2021.

δ	IAE (°C)	ΔIAE (%)	E	ΔE (%)	IAU	ΔIAU
0	$1{,}22{\cdot}10^7$	0	$2{,}53{\cdot}10^5$	0	2094,3	0
0,5	$1{,}23{\cdot}10^7$	0,89	$1{,}68{\cdot}10^5$	33,85	1700,4	18,8

Guo, Y., Zhao, H., Zhang, S., Wang, Y., Chow, D., 2021. Modeling and optimization of environment in agricultural greenhouses for improving cleaner and sustainable crop production. Journal of Cleaner Production 285, 124843.
DOI: 10.1016/j.jclepro.2020.124843

Körner, O., Challa, H., 2003. Process-based humidity control regime for greenhouse crops. Computers and Electronics in Agriculture 39 (3), 173–192.
DOI: 10.1016/S0168-1699(03)00079-6

Li, J., Li, L., Wang, H., Ferentinos, K. P., Li, M., Sigrimis, N., 2017. Proactive energy management of solar greenhouses with risk assessment to enhance smart specialisation in China. Biosystems Engineering 158, 10–22.
DOI: 10.1016/j.biosystemseng.2017.03.007

Liu, R., Li, M., Guzmán, J. L., Rodríguez, F., 2021. A fast and practical one-dimensional transient model for greenhouse temperature and humidity. Computers and Electronics in Agriculture 186, 106186.
DOI: 10.1016/j.compag.2021.106186

Liu, R., Wang, H., Guzmán, J. L., Li, M., 2022. A model-based methodology for the early warning detection of cucumber downy mildew in greenhouses: An experimental evaluation. Computers and Electronics in Agriculture 194, 106751.
DOI: 10.1016/j.compag.2022.106751

Montoya-Ríos, A. P., García-Mañas, F., Guzmán, J. L., Rodríguez, F., 2020. Simple tuning rules for feedforward compensators applied to greenhouse daytime temperature control using natural ventilation. Agronomy 10 (9), 1327.
DOI: 10.3390/agronomy10091327

Pawlowski, A., Beschi, M., Guzmán, J. L., Visioli, A., Berenguel, M., Dormido, S., 2016. Application of SSOD-PI and PI-SSOD event-based controllers to greenhouse climatic control. ISA Transactions 65, 525–536.
DOI: 10.1016/j.isatra.2016.08.008

Rodríguez, F., Guzmán, J. L., Berenguel, M., Arahal, M. R., 2008. Adaptive hierarchical control of greenhouse crop production. International Journal of Adaptive Control and Signal Processing 22 (2), 180–197.
DOI: 10.1002/acs.974

Smit, J N & Combrink, N. J. J., 2005. Pollination and yield of winter-grown greenhouse tomatoes as affected by boron nutrition, cluster vibration and relative humidity. South African Journal of Plant and Soil 22 (2), 110–115.
DOI: 10.1080/02571862.2005.10634691

Wang, L., Zhang, H., 2018. An adaptive fuzzy hierarchical control for maintaining solar greenhouse temperature. Computers and Electronics in Agriculture 155, 251–256.
DOI: 10.1016/j.compag.2018.10.023

Wang, T., Wu, G., Chen, J., Cui, P., Chen, Z., Yan, Y., Zhang, Y., Li, M., Niu, D., Li, B., Chen, H., 2017. Integration of solar technology to modern greenhouse in China: Current status, challenges and prospect. Renewable and Sustainable Energy Reviews 70, 1178–1188.
DOI: 10.1016/j.rser.2016.12.020

Xu, D., Du, S., van Willigenburg, G., 2018a. Adaptive two time-scale receding horizon optimal control for greenhouse lettuce cultivation. Computers and Electronics in Agriculture 146, 93–103.
DOI: 10.1016/j.compag.2018.02.001

Xu, D., Du, S., van Willigenburg, L. G., 2018b. Optimal control of chinese solar greenhouse cultivation. Biosystems Engineering 171, 205–219.
DOI: 10.1016/j.biosystemseng.2018.05.002

2.3.2 Hierarchical optimization control strategy for preventing fungal disease infections in a cucumber greenhouse

Research in this field is supported by the following journal publication:

Title	Hierarchical optimization control strategy for preventing fungal disease infections in a cucumber greenhouse
Authors	**R. Liu**, J. L. Guzmán, J.D Gill, M. Li
Journal	Journal of Cleaner Production
Year	2022
Volume	Under review
Pages	--
DOI	--
IF(JCR2022)	11.072
Categories	Building and Construction (4/211) Q1

Contribution of the Ph.D. Candidate

The Ph.D. candidate R. Liu is the main contributor and first author of this paper.

Hierarchical optimization control strategy for preventing fungal disease infections in a cucumber greenhouse

Ran Liu[a], José Luis Guzmán[a],*, Juan Diego Gil, Kaige Liu[b], Ming Li[b],*

[a]Department of Informatics, ceiA3, CIESOL, Ctra. Sacramento s/n, University of Almería, Almería, Spain

[b]Information Technology Research Center, Beijing Academy of Agriculture and Forestry Sciences/ National Engineering Research Center for Information Technology in Agriculture/ National Engineering Laboratory for Agri-product Quality Traceability/ Meteorological Service Center for Urban Agriculture, China Meteorological Administration- Ministry of Agriculture and Rural Affairs/ Key Laboratory of Agri-informatics, Ministry of Agriculture, Beijing, China

*Corresponding author: José Luis Guzmán (joguzman@ual.es); Ming Li (lim@nercita.org.cn)

Abstract

For climate control in greenhouses, increasing yield and preventing fungal diseases are contradictory processes, because fungal pathogens and hosts are necessarily stay in the same niche. The aim of this study is to maintain the optimum diurnal and nocturnal temperature for cucumber production, but give priority to disease control, using hierarchical optimization control strategy. The research line is conducted by three independent aspects. First, we investigated the infection mechanism of crop fungal diseases. Taking downy mildew as an example, a model was selected and evaluated to predict the infection and the onset date of downy mildew. Then we discussed the feasibility of using model prediction method to predict diseases in greenhouse. after the above work, we designed a PID actuator for controlling the greenhouse temperature. This controller keeps the greenhouse temperature within the optimum range for crop growth. However, many positive reports regarding to the infection risk of downy mildew were issued in the long season use of this control strategy. In order to eliminate these risks, a hierarchical control strategy is applied to the greenhouse. In the lower layer, the controller keeps the optimal temperature for crop

production. In the upper layer, the optimizer modifies the set-point when the positive report is issued. The cost function ensures the positive reports eliminated with the least heat loss.

Keyword: PID control; greenhouse; fungal disease; hierarchical control strategy; model prediction.

1. Introduction

1.1 Motivation of this study

Fungicide, climate control and biological control are the ways to reduce crop fungal disease (Elad et al., 1996; Keinath and Silva 2022). In recent years, environmental problems in Chinese solar greenhouse (CSG) have received increasing attention, relating to the intensive application of agrochemicals (Kalkhajeh et al., 2021). For cucumber production, the environmental risks are mostly related to excessive fertilizers (nitrogen, phosphorus and potassium), fungicides and pesticides inputs (Hu et al., 2017; Guan et al., 2022). A large amount of agrochemicals have accumulated in the soil with continuous cultivation year after year, due to imprecise crop management and imperfect promotion of soilless culture. The optimization control could be a solution to reduce agrochemicals.

At present, the applications of optimization control are mostly about improving the energy utilization. This approach has been studied in various greenhouses, including the Venlo, Almería type greenhouses and CSGs. They focus on higher productivity, better thermal utilization and lower economic consumption (Körner et al., 2004; Montoya et al., 2016; Xu et al., 2018a; Lin et al., 2020; Zhang et al., 2020). Much of the work designed to enhance productivity or energy efficiency has been done without considering its implications in making crops susceptible to diseases infections (Jewett and Jarvis, 2001). Few previous control approaches focus on plant fungal disease, which causes severe economic losses every year throughout the world, leading to

environmental pollution caused by fungicide. Because the host plant necessarily stays the same ecological niche as fungal pathogens, consciously control to avoid infection without damaging the host plant requires precise theoretical support.

In this study, taking greenhouse cucumber downy mildew as an example, a methodology of model predictive control (MPC) combined hierarchical optimization control strategy is demonstrated. The proposed constraints are about avoiding ideal infection conditions for *Pseudoperonospora cubensis*, a fungal pathogen of downy mildew. Meanwhile, the optimization climate control strategy ensures the accumulated temperature in the greenhouse and energy utilization efficiency.

1.2 Infection mechanism of cucumber downy mildew

Downy mildew (*Peronospora sparsa*), Botrytis (*Botrytis cinerea*) and Powdery mildew (*Sphaerotheca pannosa*) are three common fungal plant diseases in greenhouses, always result in damages on the foliage and fruit, bringing great economic losses (Mashonjowa et al., 2013). There are four common ways for fungal spores to get into the greenhouse: with the air flow through vents; carried through the clothes and shoes of the farmer; hidden in the soil for overwintering; infected plant tissue in the last cultivation remain in the greenhouse (Palti and Cohen, 1980). In fact, it is very difficult to completely remove spores in a greenhouse where fungal diseases have ever occurred. However, it is significant to avoid high humidity and moderate temperature in the greenhouse to reduce disease occurrence.

Avoiding infection is the key step to prevent disease. Without manual intervention, the germination of downy mildew spores on crop leaves results from leaf wetness, middle temperature and sufficient duration of the above two factors (Liu et al., 2022a). The lower environment limit for downy mildew infection is 20°C with 2 h of wetness (Cohen, 1977). The infection condition therefore depends on a favourable combination of LWD (Leaf Wetness Duration) and mean temperature in LWD (TLWD). Note that the rate of foliage growth and physiological age of the host bring uncertainty to the prediction, leading to false positive reports (Palti and Cohen, 1980). The infection model is expected to be further studied. Once the pathogen spores are successfully infected on the leaves of the plant, the disease is inevitable. The period from infection

to the onset of symptoms is called the incubation period. Its duration depends on the accumulated temperature, usually two to three days (Zhao et al., 2011).

1.3 Management of downy mildew in a greenhouse

The primary aim of disease control is to avoid leaf surface condensation caused by high humidity, one of the most common factors (Liu et al., 2021a). Excessive high absolute humidity, or low temperature that close to the dew point leads to high relative humidity. Currently, the LWD relating to high humidity is studied to be measured or estimated by models. LWD is estimated using relative humidity threshold, usually between 80% and 95%, depending on geographic location and climate (Wang et al., 2019). Or it is estimated using dew point depression method, relative to canopy temperature or greenhouse air temperature (Mashonjowa et al., 2013). The leaf wetness can be monitored in real time, using an artificial leaf sensor (Liu et al., 2022a). The drawback of measurement is that it is unable to predict the impending meteorological disaster. Using the weather forecast and the LWD estimation model, a developed web-based decision support system (DSS) that estimates the risk for the fungal disease infection is able to issue advanced early warning (Katsoulas et al., 2021; Liu et al., 2022a). A core technology of this DSS is the greenhouse climate model. Although a great number of greenhouse models have been published, more than 70 models were developed in the last decade (Katzin et al., 2022), most mechanism models require too many transient inputs and parameters besides weather forecast data, such as wall temperature and heat flux, so that few models can be used to predict future greenhouse climate.

1.4 Greenhouse climate model

Greenhouse model is a mathematical and logical relationship describing the internal and external environmental parameters of greenhouse, which is divided into dynamic or transient model and steady-state model. The earliest greenhouse model can be traced back to 1958 (Katzin et al., 2022). Most of the early models are systems composed of multiple equations. Their parameters are visible so that they are called mechanism models or white box models. With the improvement of computing power, black box models or time-series models are established by training multiple inputs and

outputs data (Guo et al., 2021). An easily determined one of the black box models is autoregressive models (Ljung, 1999). The ARX (auto-regressive with exogenous inputs) model is selected to simulate the greenhouse temperature (Montoya-Ríos et al., 2020; García-Mañas et al., 2021). The limitation of ARX model is that the training results of continuous sample data in long seasons are not accurate. Therefore, developers usually establish and adopt models for different time periods. In the 21st century, deep learning models and big data makes the prospect of complex nonlinear simulation optimistic (Jung et al., 2020; Moon and son, 2021). Although in the past 5 years, the deep learning model has gradually become the mainstream, one-third of the greenhouse models are NN (Neural Network) models, its application and promotion in agricultural greenhouses have made slow progress (Guo et al., 2021). This is because data loss caused by sensor failure is a common problem in agricultural environment. In addition, widely data collection, irregular and discontinuous sample data format is currently still a challenge. This shows that standardization for greenhouse is of great significance to the progress of an industry.

In our previous study, a fast mechanism model was proposed (Liu et al., 2021b). This model is designed to simplify user input. At each transient time step, the boundary conditions of the model, such as wall temperature, heat flux and net radiation gain, are calculated by groups of energy conservation equations. Finally, only five transient inputs that all included in any common weather forecast are required to run the model. The innovation of this model is that the greenhouse temperature and humidity can be predicted 72 hours ahead using weather forecast data, where receding horizon in hourly units ensures the timeliness of information.

1.5 Greenhouse climate control

In terms of managing crop diseases, various types of modern greenhouses are currently able to provide stable microclimate and prevent the temperature and humidity from exceeding the safe threshold (Körner and Challa, 2004; Chen and You 2021; Costantino et al., 2021). Körner and Challa applied a hierarchical optimization control strategy in a Dutch greenhouse, the set-point of humidity regime is optimized in the upper layer by simulating the greenhouse climate, energy consumption and

photosynthesis with different temperature regimes, rather than a conventional fixed set-point (2003). Rodríguez et al. put forward an adaptive hierarchical control strategy to keep humidity in a specific range through simulating with various temperature set-points (2008). Ramírez-Arias et al. addresses the problem of greenhouse crop growth through a hierarchical control architecture governed by a high-level multiobjective optimization approach to maximize profit, fruit quality, and water-use efficiency (2012).

Note that relative humidity threshold model for leaf wetting can be used as a reference for greenhouse humidity control, for example, maintaining the relative humidity below the threshold, which has been well applied in smart greenhouses (Wang et al., 2019). Few previous studies are devoted to a better humidity regime that is designed for a specific crop disease. This brings about two imperfections: first, unplanned dehumidification treatment (e.g. ventilation) sometimes leads to heat leakage, and the lower effective accumulated temperature has a negative impact on plant growth and production efficiency (Wang et al., 2022); second, the transpiration rate increased significantly under high vapour pressure deficit (VPD), which interferes with the hydraulic circle of crops (Medrano et al., 2005). Experiments show that maintaining high relative humidity significantly increased the production of greenhouse cucumbers and roses (Darlington et al., 1992; Bakker, 1988). Therefore, it is necessary to find the optimal set-point in each sample time. The set-point is a dynamic value in order to benefit both of productivity and disease control.

1.6 Automatic climate control in CSGs

Specifically, the CSG undertakes vegetable production in northern China, where cold weather with continuous rainy days always lead to intensive fungal disease, e.g. downy mildew, botrytis and powdery mildew. Relatively low economic profit forces farmers to choose natural ventilation, solar heating and thermal insulation blanket to control the greenhouse climate (Liu et al., 2021b). Farmers prefer to close vents for insulation in cold nights rather than ventilation and dehumidification, which sometimes has to damage crops. Even so, the CSG has an increasingly important position in horticultural production in northern China due to its energy saving and low operating cost.

Recently, a few smart CSGs have been demonstrated, its control is mostly conducted by hand, or conventional fixed set-point controllers (Xu et at., 2018a). Xu et al. embedded on-line parameter estimation to a two time-scale receding horizon optimal controller for lettuce crop production in a CSG, which improved the performance of the crop production system (2018b). Wang et al. applied an adaptive fuzzy control method to maintain a greenhouse temperature (2018). Li et al. studied a two-level scheme with risk assessment to make an optimal use of solar energy for the greenhouse (2017). No more studies relating to a hierarchical optimization control strategy for CSGs have been reported, and particularly the study of PID (Proportional-Integral-Derivative) controllers in CSG climate has not been fund. The energy consumption and economic profit were proved to be reduced by optimizing the step point of greenhouse temperature, humidity, CO_2, and then the fruit dry weight. The fungal disease infection is looked forward to being limited from the similar way.

1.7 Aim of this study

Weather indicated control measures not only help effective countermeasures, but also reduce the number of anti-disease treatments, in order to give better protection to the crops (Bourke 1970). Carlson demonstrated the use of Bayesian decision support and subjective probabilities predictions to provide optimal pesticide use actions for California peach growers in controlling peach brown-rot (1970). The above study is in field conditions, while in the greenhouses, MPC deserves better applications in reducing crop disease, due to the adjustable indoor climate.

The aim of this study is to apply hierarchical optimization control strategy for managing cucumber downy mildew in a CSG, where natural ventilation is used to cool and dehumidify the crops. The infection control has a short window of the minimum 2 hours in the case of cucumber downy mildew, and it takes time to heat up by solar radiation or dehumidify by natural ventilation (Zhao et al., 2011). Due to the time delay of the greenhouse climate response, when the leaf is detected to be wet by the sensor, the subsequent infection is inevitable. This problem could be solved by using MPC and hierarchical control strategy.

2. Materials and methods

2.1 Greenhouse and crop cultivation

The experimental greenhouse is located at the National Precision Agriculture Demonstration Base (40°18’ N, 116°47’ E, annual average temperature :11.8 °C), Changping District, Beijing. The CSG is a half fan-shaped tunnel greenhouse with a transparent polyethylene film roof facing south and brick walls on other sides. The length, width, ridge height are 50, 7 and 3.6 m. Natural ventilation is realized by rolling the film at the roof vent (upper vent) and side vent (lower vent). There is no additional heating except for solar radiation. The seedling of fruit cucumber 'Jingyan Mini II' was transplanted on March 4, 2021, in an average of 36 rows. A layer of plastic film was covered on the soil, and the drip irrigation belt was buried under the plastic film for irrigation and fertilization. The harvest season was ended on 7 July 2021.

Fig. 1. Photo of experimental greenhouse

2.2 Data collection

The greenhouse temperature (range, -40 - +65 ℃; accuracy, ±0.5℃) and relative humidity (range, 0-100%; accuracy, ±3%) were measured and recorded by every 15 minutes (Davis-6162，Davis Instruments, Hayward, USA). The outdoor weather data was predicted by a web-based model, based on a REST API service provided by Weatherbit (WeatherBit, 2019). This model allows to obtain weather forecasts in different geographical locations around the world. For this work, that service was used

to obtain weather forecasts 72 hours ahead with an hourly sampling period. Temperature, humidity, wind speed and solar radiation forecasts are obtained to be used as inputs to the proposed methodology. This web-based service requires basic parameters such as latitude, longitude, language, key and number of hours for the forecast. The accuracy of the weather forecast was validated by Liu et al. (2022a).

2.3 Observation and prediction model of downy mildew

A weekly observation of downy mildew was conducted since transplanted. Until the early symptoms of downy mildew appear (light yellow water-stained polygonal disease spots on the leaves, Fig. 2(b)), the observation frequency was changed to two times a week. The downy mildew symptom and lead area index (LAI) were observed at five fixed locations distributed in the greenhouse for every investigation, according the five-point sampling method (Liu et al., 2022b). Mildewed leaves were scored with a rating (r) of 0, 1, 3, 5, 7 or 9, denoting proportions of disease over the whole leaf area of 0, 1-5%, 6–10%, 11–25%, 26–50% and > 50%, respectively (Liang et al., 2005). Disease index was calculated according to the equation,

$$DI\% = \frac{\sum(n_r \times r)}{N \times 9} \times 100 \qquad (1)$$

where r is rating value; n_r is number of disease leaves with a rating of r; N = total number of investigated leaves.

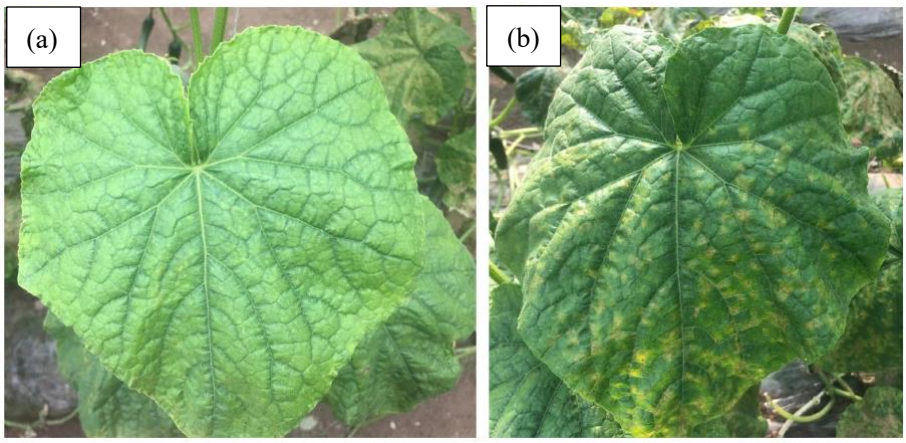

Fig. 2. Photos of downy mildew observations. (a) is asymptomatic and (b) is symptomatic.

Meanwhile, the infection state was predicted by the following equation, and positive reports were issued once the greenhouse environment fit the requirement,

$$IF = LWD \times TLWD \geq 40\ h℃\ (LWD \geq 2\ h, 5\ ℃ \leq TLWD \leq 30\ ℃) \quad (2)$$

where, LWD is leaf wetness duration, h; TLWD is hourly mean temperature in LWD, ℃. The LWD is estimated by a relative humidity threshold, where LWD is considered as the duration when the greenhouse relative humidity is above 95%. IF is the infection factor, h℃. The infection report is positive when IF is above 40 h℃.

Once a positive report for infection is issued, the following procedure is started to predict the time of symptom occurrence,

$$y = \frac{0.0165}{1+10389.2\times exp\ (-0.5743\times T_h)} \quad (3)$$

where y is an integration of hourly contribution rate, which is calculated by hourly average temperature (Th, ℃). The deadline of incubation period is the clock when the integration of $y \geq 1$, when leaves are predicted to be symptomatic. It usually takes about three days to progress to 1, which means that that symptoms appear.

2.4 Hierarchical optimization control for preventing infections

This section describes how to adjust the greenhouse climate through a hierarchical optimization control method, in order to keep the optimum temperature for cucumber production, but give priority to avoiding positive reports for downy mildew infection. From the previous literature review, it is known that the ongoing leaf wetting and disease infection are detected or simulated throw LWD models and primary infection models. When LWD appears, the greenhouse is suggested to conduct ventilation for dehumidification. However, this process leads to heat leakage and reduces the accumulated greenhouse temperature. The hierarchical optimization control strategy gives the best temperature set-point in each transient step. In the lower layer, a PID controller keeps the optimum temperature for cucumber production throw an expert supporting system (Fig. 3). In the upper layer, the optimizer gives a suggested set-point when disease infection is simulated by a three-day ahead weather forecast, to avoid the ongoing infection. The new set-point is calculated by a cost function, which ensures the

minimum integration of absolute error between the current set-point and the suggested set-point.

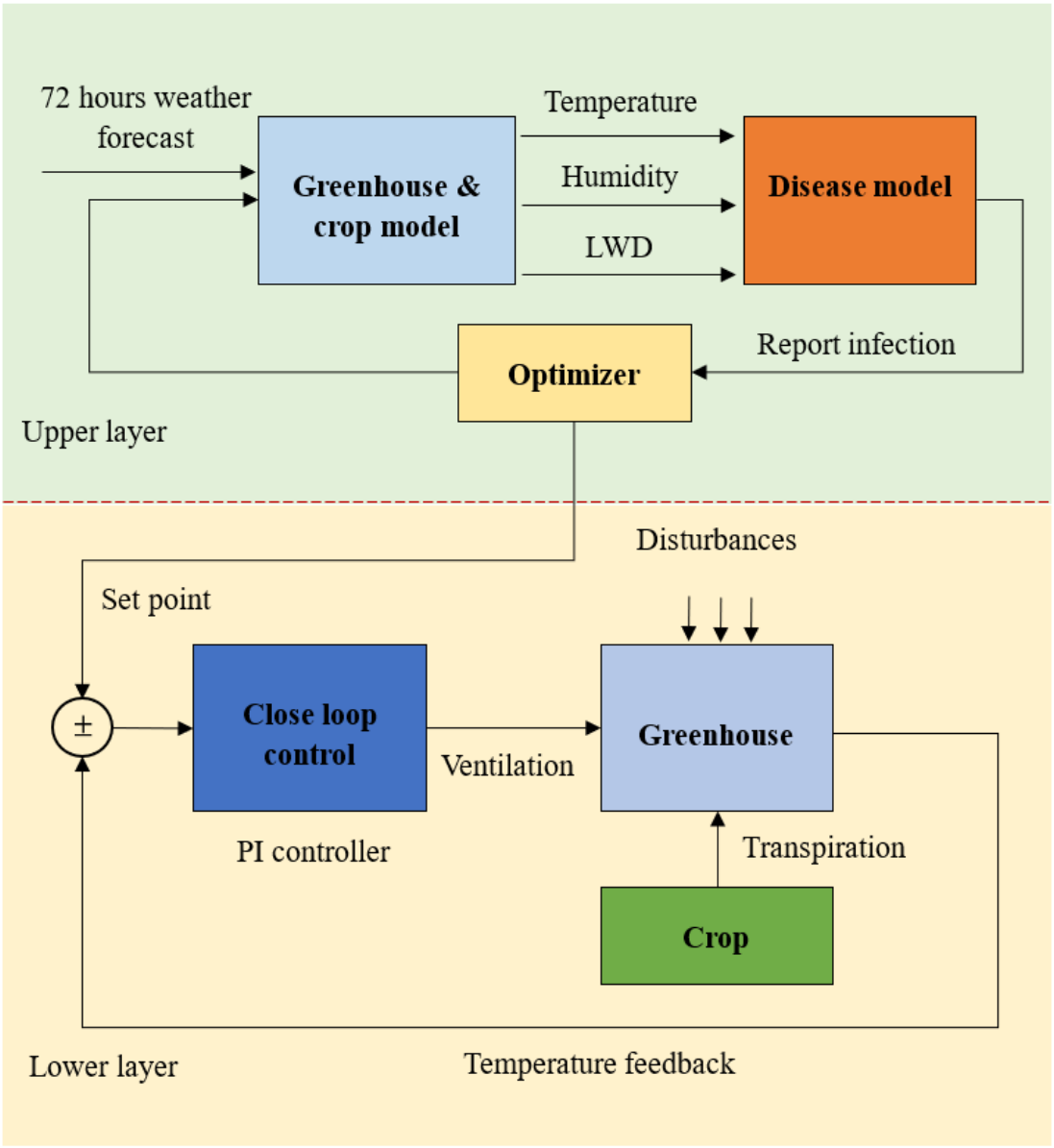

Fig. 3. Hierarchical control architecture of greenhouse disease.

2.4.1 Greenhouse and crop model

The outputs of greenhouse climate model are the air temperature and relative humidity. The transient model for temperature is an energy integrative equation,

$$\frac{dT(t)}{dt} = \frac{q_v(t)+q_{lea}(t)+q_c(t)+q_s(t)+q_p(t)}{\rho*v*(c_p+c_{pw}*h(t))} \quad (4)$$

where, T is the indoor air temperature, K; t is time, s; h is the indoor absolute humidity, kg kg^{-1}; t is time, s; ρ is the air density, kg m^{-3}; c_p is the specific heat capacity of the air,

J kg^{-1} K^{-1}; c_{pw} is the specific heat capacity of the water vapor, J kg^{-1} K^{-1}; and v is the greenhouse volume, m^3. $q_v(t)$ is the ventilation term, W; $q_{lea}(t)$ is the air leakage term, W; $q_c(t)$ is the convective term, W; $q_s(t)$ is the saturated water vapor term, W; and $q_p(t)$ is the leaves condensation term, W.

$$q_v(t) = L(t) * \rho * c_p * \left(T_o(t) - T(t)\right) \quad (5)$$

$$q_{lea}(t) = \frac{n_t}{3600} * \rho * c_p * v * \left(T_o(t) - T(t)\right) \quad (6)$$

$$q_c(t) = A_w * c_w(t) * \left(T_w(t) - T(t)\right) + A_r * c_r(t) * \left(T_r(t) - T(t)\right) + A_g * c_g(t) * \left(T_g(t) - T(t)\right) \quad (7)$$

$$q_s(t) = \gamma * (h(t) - h_s(T(t))) * v * \rho \quad (8)$$

$$q_p(t) = m_c(t) * \gamma * v_p \quad (9)$$

where, L is the total ventilation rate, m^3 s^{-1}; T_o is outdoor air temperature, K; n_t is the air leakage rate, h^{-1}; A_w, A_r, and A_g are the areas of the wall, roof and ground, m^2, respectively; c_w, c_r and c_g are the convective transfer coefficients on the internal surfaces of the opaque wall, the transparent roof and the ground, W m^{-2} K^{-1}, respectively; T_w, T_r, and T_g is the wall surface, roof surface and the ground temperature, K, respectively. γ is the water evaporation constant. $h_s(T)$ is the saturated absolute humidity under current temperature, kg kg^{-1}. m_c is the condensation rate on the canopy, kg m^{-3} s^{-1}, v_p is plant canopy volume, m^3.

Note that L, n_t, convective transfer coefficients, h_s and m_c are not constant. Wall and roof surface temperature should be simulated rather than being measured in order to predict the future greenhouse climate. Natural ventilation is a coupling effect of wind pressure and thermal pressure (Mistriotis et al., 1997). The air leakage rate also changes dynamically with the temperature difference and wind speed around the transparent roof (Ahamed et al., 2018). Including convective transfer coefficients, h_s, m_c, wall and roof surface temperature, they are dynamic in transient simulation. It makes the greenhouse model difficult to apply. See detailed description about solving complex parameters without using too many measurements in Liu et al. (2021b). Finally, it requires four transient inputs (outdoor temperature, outdoor humidity, solar radiation

and wind speed & direction) and three initial conditions (indoor temperature, indoor humidity, soil temperature) to run the model, that are include in any common weather forecast algorithm.

The model for humidity is a mass integrative equation about water vapor,

$$\frac{dh(t)}{dt} = s_v(t) + s_{lea}(t) + s_p(t) \quad (10)$$

where s_v is the ventilation term for humidity, kg kg^{-1} s^{-1}; s_{lea} is the air leakage term for humidity, kg kg^{-1} s^{-1}; s_p is the plant term for humidity, kg kg^{-1} s^{-1}.

$$s_v(t) = \frac{(h_o(t) - h(t)) * L(t)}{v} \quad (11)$$

$$s_{lea}(t) = \left(h_o(t) - h(t)\right) * \frac{n_t}{3600} \quad (12)$$

$$s_p(t) = \frac{(m_t(t) - m_c(t)) * v_p}{\rho * v} \quad (13)$$

where h_o is the outdoor absolute humidity, kg kg^{-1}. v_p is the volume of crop zone, m^3. m_t is the transpiration rate, kg m^{-3} s^{-1}. The crop transpiration is simulated in each transient step, see Boulard et al. for more information (2017).

2.4.2 Linear model

To view the response of the system is a way to obtain the transfer function, in order to design the PID controller. However, source terms of the mechanism greenhouse model are calculated from a group of heavy equations so that the integration of them could be complex and strongly nonlinear. It is an arduous task to design the controller by using this model. The linearization of the nonlinear model under zero initial condition helps to obtain and understand the system response.

The linear model could be a simple polynomial associated with multiple inputs. The polynomial ARX (Auto Regressive with Extra Input) models of the system identification toolbox (MATLAB®, Matlab, 2021) are adopted to perform the linear model from data (García-Mañas et al., 2021). In this work, the output of the linear ARX model is the greenhouse internal air temperature and the input is a set of randomly generated vent opening (Fig. 4). The training data therefore comes from the output if the mechanism greenhouse model. External air temperature, solar radiation and wind

speed are considered as disturbances. The equation is described below,

$$T(k) = \frac{B_1(z)}{A(z)}u(k) + \frac{B_2(z)}{A(z)}v_1(k) + \frac{B_3(z)}{A(z)}v_2(k) + \frac{B_1(z)}{A(z)}v_3(k) + e(k) \quad (14)$$

where u is the vent opening, %; v_1 is the first disturbance-outdoor temperature, °C; v_2 is the second disturbance-solar radiation, W m^{-2}; v_3 is the third disturbance-wind speed, m s^{-1}; e is error, °C. The best fits of 14 ARX models that are obtained to for each single day in two weeks during 15-29 April 2021 is selected to get the transfer function.

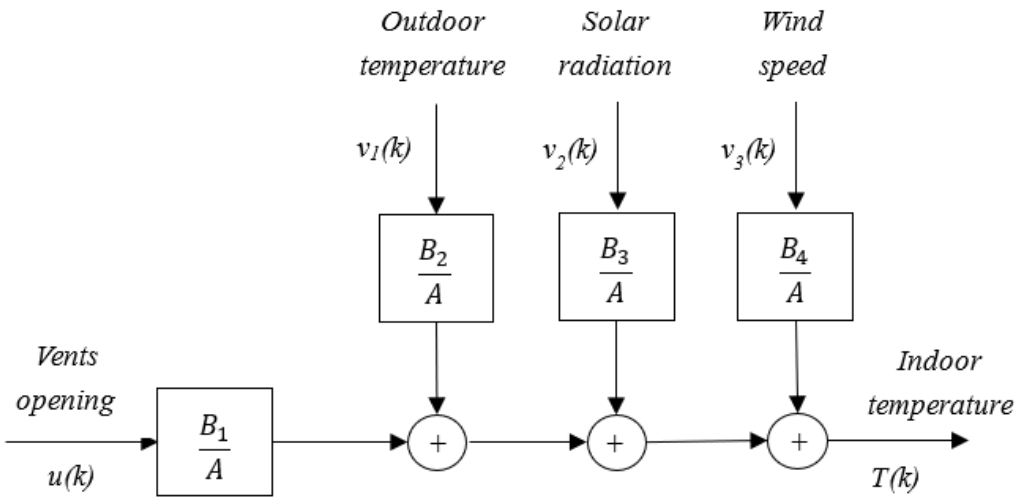

Fig. 4. ARX model for vents opening and internal air temperature with disturbances.

2.4.3 Design of transfer function and PID controller

The PID controller is a widely used feedback technique in greenhouses to calculate the vents opening depending on the greenhouse climate transfer function and the existing error between the current process output and the desired set-point (Montoya-Ríos et al., 2020). The output signal in each step is calculated as following equation,

$$u(t) = k_p e(t) + \frac{k_p}{T_i}\int e(t)dt \quad (15)$$

where k_p and k_p/T_i are respectively the proportional and integral parameters. Those parameters are obtained from transfer functions. The transfer functions are calculated with the λ tuning method (García-Mañas et al.,2021). Unit step was given to the ARX

model as input to identify a first-order transfer function model for temperature. The transfer functions of the system and the controller are given as Eq.16 and Eq.17. In each transient step, the C(s) gives a control signal u(t) based on current error e(t) (Fig. 5). The error is calculated by obtaining the difference between the reference value and the output of G(s).

$$G(s) = \frac{k}{\tau s+1} e^{-t_r s} \quad (16)$$

$$C(s) = k_p(\frac{T_i s+1}{T_i s}) \quad (17)$$

where k is the steady-state gain; τ is 63% of the time to reach the steady-state ($t_{63\%/y\infty}$) minus the delay time (t_r). The value of k_p and T_i are calculated by the following equations,

$$T_i = \tau \quad (18)$$

$$k_p = \frac{\tau}{k(t_r+\lambda)} \quad (19)$$

$$\tau = t_{63\%/y_\infty} - t_r \quad (20)$$

where λ is the tuning parameter, λ=0.3τ in this study.

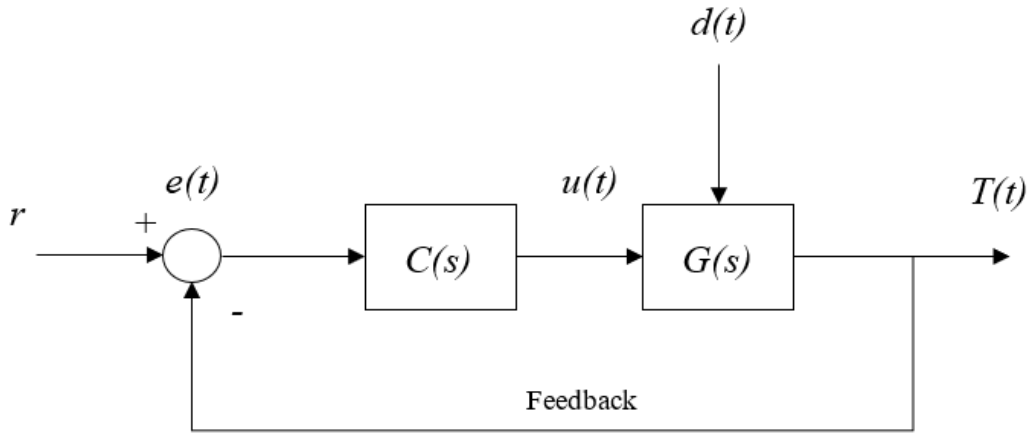

Fig. 5. Flow chart of control scheme. r is reference; e is error; u is vents opening; d is disturbances; y is internal greenhouse temperature.

2.4.4 Event-based control approach

The standard PID controller requires the actuator responses to the error in each transient step, which means that the controller keeps the highest accuracy and

frequently responses around the step-point. Event-based control schemes reduce the control system attention reacting only when it is strictly necessary, that is, when the control error is large enough. The event-based control method uses a parameter δ to reduce the control effort (Fig. 6). With this method, the controller is only triggered when the error is out of the limits, otherwise, the error is 0. The control method is realized by put the error between ±δ to a dead zone. In this study, a parameter |δ|=0.5 is adopted in the hierarchical optimization control system, which has been proved to significantly reduce the number of vent movements by 43.8%, while only increasing the temperature error by 1.13% (Liu et al., 2022c).

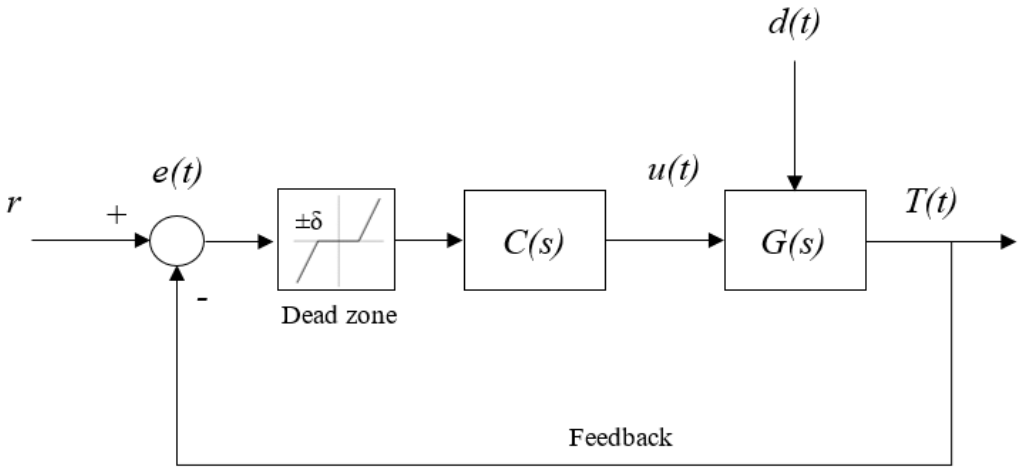

Fig. 6. Flow chart of the event-based control scheme.

2.4.5 Optimum temperature for cucumber production

Cucumber is a warm season crop, and the temperature is closely related to yield. At germination, average temperature is needed between 25-35 ℃. At growth stage, the optimum temperature is suggested by different researchers (Table 1). The minimum and maximum tolerable temperatures for cucumber are respectively 13 ℃ and 40 ℃ (Pal et al., 2020). In this study, the expert supporting system gives the diurnal temperature set-point as 30 ℃ and suggests closing the vents at night in order to keep the nocturnal temperature as high as possible. The outdoor nocturnal temperature in northern China is usually low. When a positive report for downy mildew is issued, the set-

point is modified by the optimizer. Besides, the lower and upper limits of the tolerable temperature for cucumber growth have the highest priority, that are set to 13 ℃ and 40 ℃ in this study. When the set-point given by the optimizer exceeds these two limits, it is changed to the closed boundary value.

Table 1. The optimum diurnal and nocturnal temperature for cucumber production suggested by different researchers.

Diurnal temperature	Nocturnal temperature	Literatures
27 ℃	23 ℃	Ding et al., 2019
30 ℃	20 ℃	Hui et al., 2003
28 ℃	≥18 ℃	Singh et al., 2017

3. Results and discussion

Section 3.1 presents the warning messages issued by the infection model and measured greenhouse climate data in a long production season over one hundred days. Then the disease infection and disease index were investigated to correlation between positive prediction and disease development. Section 3.2 shows the design of the PID controller, including the development of the ARX models, getting the transfer functions and using the λ tuning method to design the controller. Section 3.3 demonstrates the application of hierarchical control strategy to eliminate the positive reports along the production season, but keeps the optimal temperature for crop production.

3.1 Crop disease investigation and model prediction

Fig. 7 shows the disease index development at five sampling points, when this greenhouse is managed by the experience of farmers. The disease began to appear after April 20, and then the disease index increased rapidly. The farmers conducted two treatments respectively on May 7 and May 15. These treatments include the use of pesticides (spray of propamocarb hydrochloride, carbamate fungicide for downy

mildew) and the removal of diseased leaves.

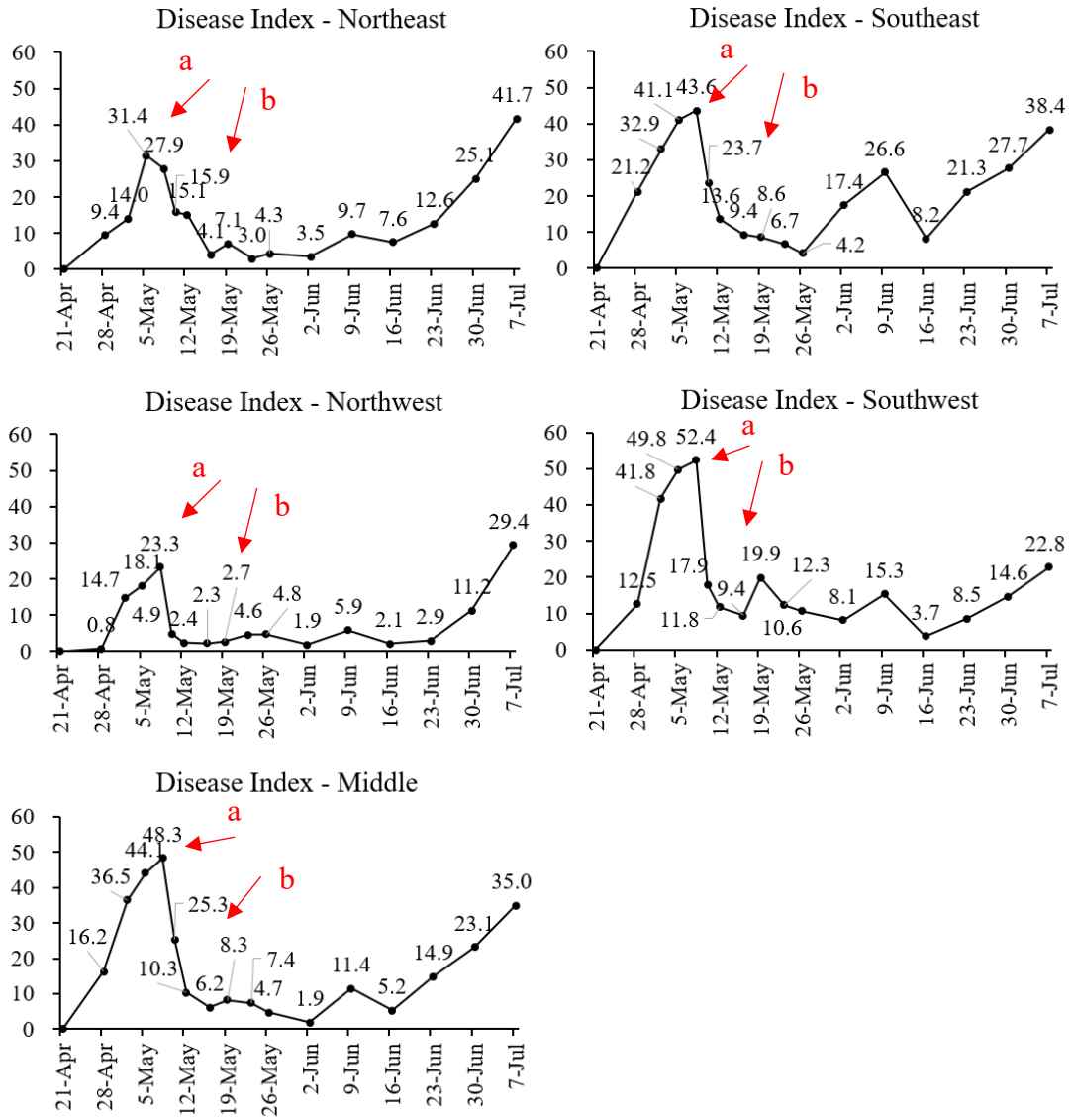

Fig. 7. Disease index at five sample point in the greenhouse. a is the first treatment and b is the second treatment.

Let's see the warning messages given by the primary infection model before the disease occurs. The blue bar in Fig. 8 shows the positive reports. If the infection factor over 40 h°C, which is calculated by Eq. 1. Then a positive report is issued. It usually takes three days to complete the incubation period after infection, and then symptoms appear. Multiple positive reports before April 23 are the first condition for the rapid development of the following disease index. Therefore, the aim is to remove all of the positive reports derived from the greenhouse climate, as well as keeping the optimum

temperature for cucumber production, through hierarchical control strategy. In this way, the crop disease is suppressed through climate control, not through fungicides, which is good for clean production.

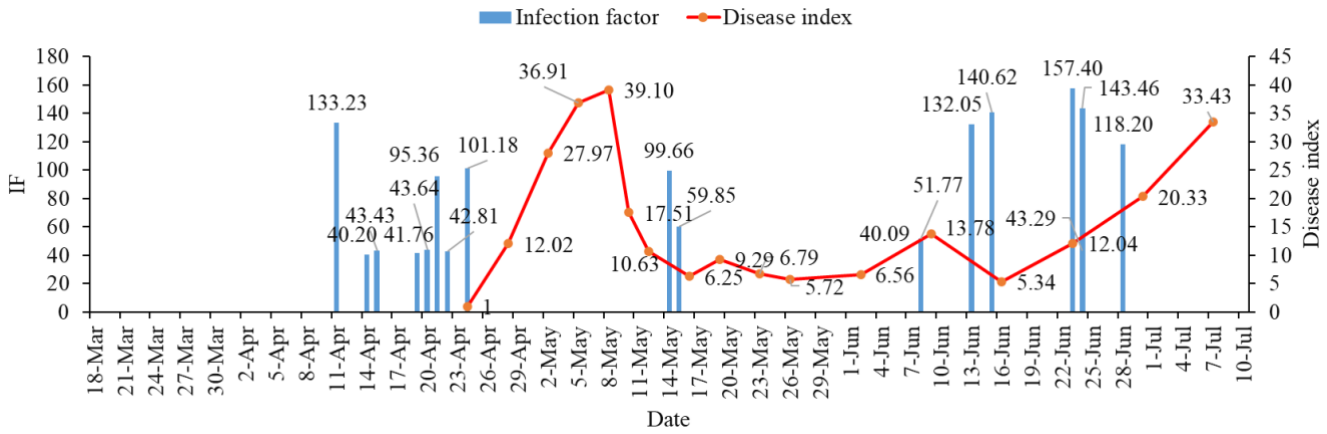

Fig. 8. Infection factor from model prediction of cucumber downy mildew and averaged disease index from investigation.

3.2 Design of PID controller in the lower layer

With the linear models, transfer functions for temperature and humidity are easily obtained from the step responses. The inputs and output data used for developing the ARX models are come from the measured weather data, a group of random ventilation opening and a virtual greenhouse. Fig. 9 shows the weather data in two weeks used to develop the ARX models and the best fit of a day in each week is selected as the system identification of the week.

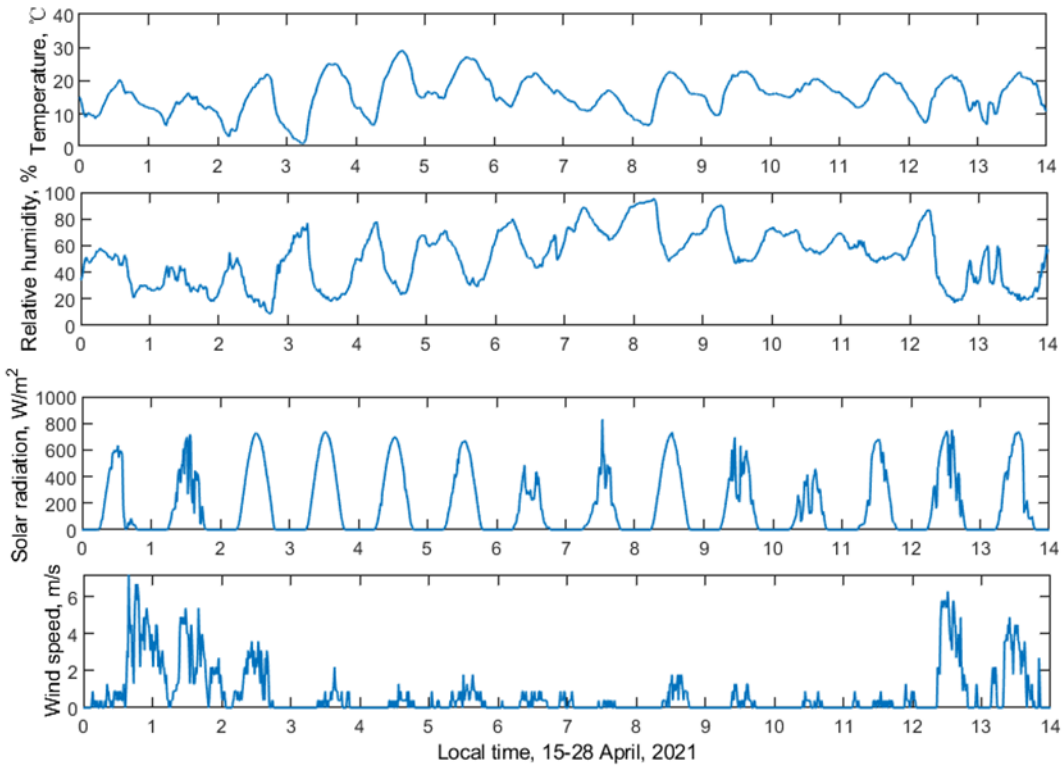

Fig. 9. External weather data on 15-28 April 2021.

The nocturnal temperature is no need to control, because it is far below the set-point. The ARX_837 for the diurnal temperature on 19 and 23 April is selected as the preparation for transfer functions, representing the temperature system identifications. Due to the limited space and similar process, only the system identification on 19 April is presented, with a FIT =85.49 (Fig. 10). The ARX_837 model is described below, where 8 is the order of polynomial A(z); 3 is the order of polynomial B(z); 7 is the input-output delay, s.

$$T(k) = \frac{B_1(z)}{A(z)}u(k) + \frac{B_2(z)}{A(z)}v_1(k) + \frac{B_3(z)}{A(z)}v_2(k) + \frac{B_1(z)}{A(z)}v_3(k) + e(k) \qquad (21)$$

where, T is the indoor temperature, ℃; u is the vent opening, %; v_1 is the outdoor temperature, ℃; v_2 is the solar radiation, W m^{-2}; v_3 is the wind speed, m s^{-1}; e is error, ℃.

$$A(z) = 1 - 2.413\,z\hat{}-1 + 1.839\,z\hat{}-2 - 0.1505\,z\hat{}-3 - 1.001\,z\hat{}-4 + 1.595\,z\hat{}-5 - 1.564\,z\hat{}-6 + 0.9603\,z\hat{}-7 - 0.2666\,z\hat{}-8 \qquad (22)$$

$$B1(z) = 4.144e-05\,z\hat{}-7 - 8.28e-05\,z\hat{}-8 - 6.702e-05\,z\hat{}-9 \qquad (23)$$

B2(z) = 0.009622 z^-7 - 0.008703 z^-8 - 0.0009135 z^-9 (24)

$B3(z) = 0.0003011\ z\text{^} - 7 - 0.0003806\ z\text{^} - 8 + 7.969e - 05\ z\text{^} - 9$ (25)

$B4(z) = -0.07244\ z\text{^} - 7 + 0.1366\ z\text{^} - 8 - 0.06414\ z\text{^} - 9$ (26)

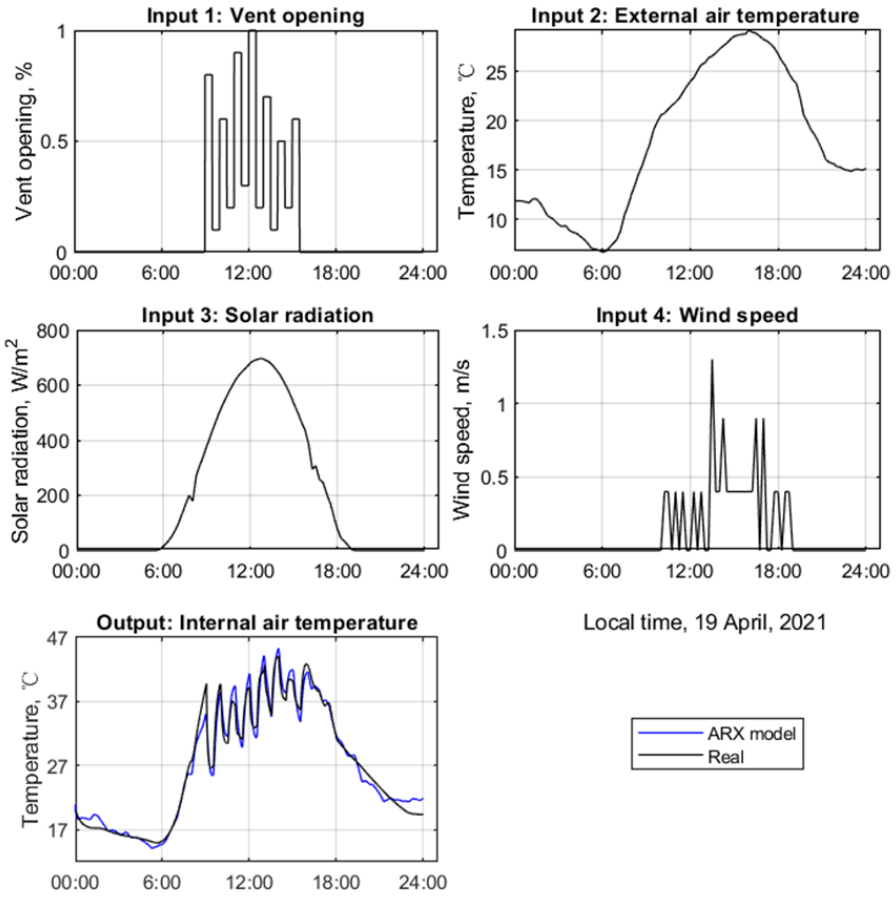

Fig. 10. ARX model identification for temperature with data from 19 April 2021.

The transfer functions are described below. A PI controller are derived respectively from each transfer functions, and the individual performance of each controller is demonstrated on a single day. The controllers are tuned by using a λ method. Moreover, controllers for temperature is combined with an anti-windup mechanism based on the back-calculation technique to reset the integrator when the actuator is saturated, with a tracking constant calculated as $T_t = \sqrt{T_i}$. The vents opening for natural ventilation is restricted to a range of 0%-100%.

$$G(s) = \frac{-19.2}{765s+1} e^{-120s} \quad (25)$$

3.3 Hierarchical control approach in reducing crop disease infections

Fig. 11 shows the closed-loop control in the lower layer. This control result keeps the greenhouse temperature around a constant set-point, which is the optimal temperature for cucumber production. However, it leads to high humidity in the greenhouse, because the vents are closed in order to keep the heat. Finally, two positive reports for the infection of downy mildew are issued in one day. This demonstrates that in the season of up to 100 days, control only based on crop growth will lead to many risk stages conducive to downy mildew infection.

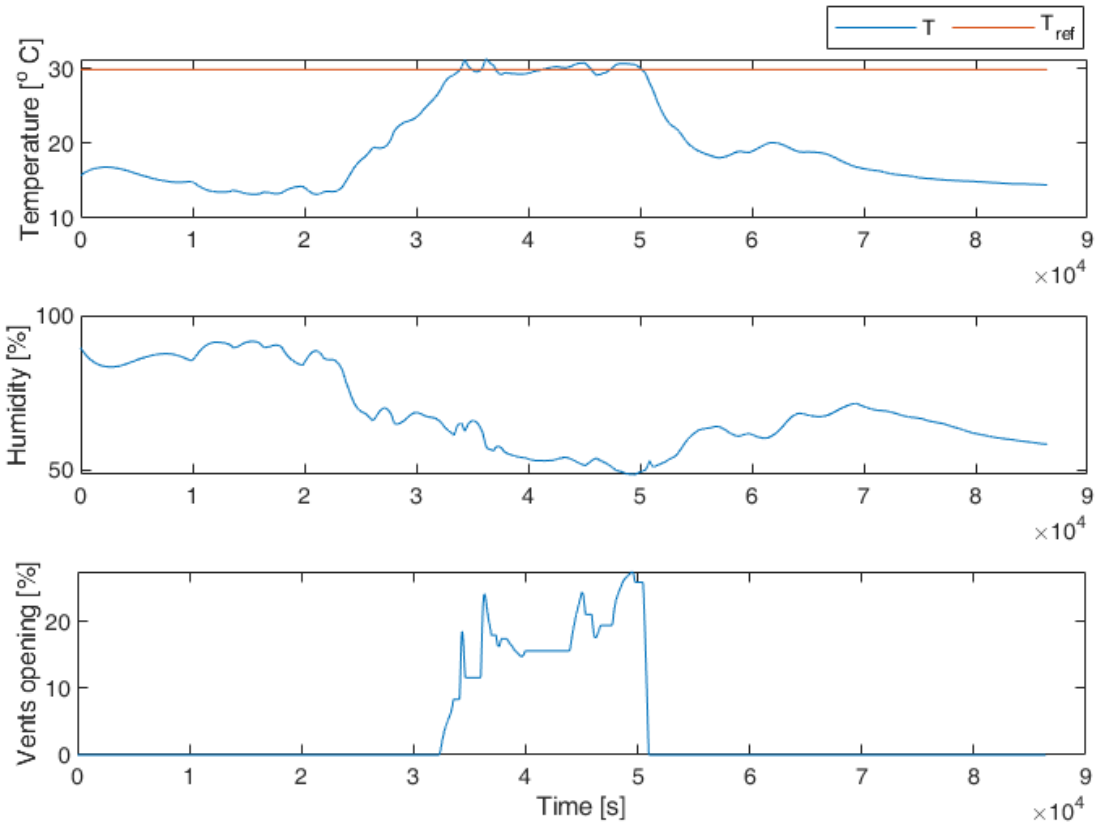

Fig. 11. Low level control for cucumber production.

Fig. 12 shows that the environmental factors that lead to downy mildew infections are eliminated by a hierarchical control strategy. The optimizer gives an independent optimal set-point by every hour. Then the horizon is moved forward for one hour and repeat the same procedure. The risk of infection can therefore be avoided and the set-

point always changes around the optimal temperature for crop growth. Compared with the control strategy of direct cooling and dehumidification to avoid disease, this method plays a game in production and safety, and finally gets the optimal solution.

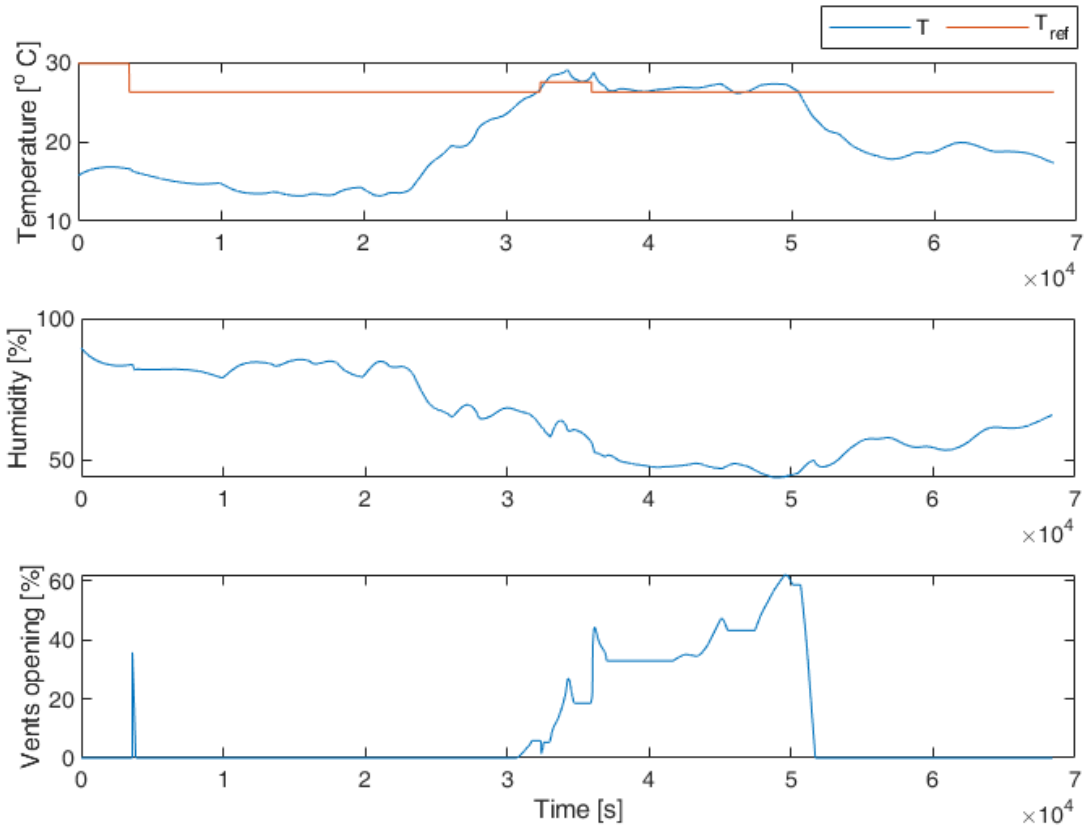

Fig. 12. Hierarchical control in order to keep the optimum temperature for cucumber production, but give priority to avoiding positive reports for downy mildew infection.

4. Conclusions

This study aims to reduce the occurrence of greenhouse crop diseases through climate control. The research line is conducted by three independent aspects. First, we investigated the infection mechanism of crop fungal diseases. Taking downy mildew as an example, a model was selected and evaluated to predict the infection and the onset date of downy mildew. Then we discussed the feasibility of using model prediction method to predict diseases in greenhouse. after the above work, we designed a PID actuator for controlling the greenhouse temperature. This controller keeps the

greenhouse temperature within the optimum range for crop growth. However, many positive reports regarding to the infection risk of downy mildew were issued in the long season use of this control strategy. In order to eliminate these risks, a hierarchical control strategy is applied to the greenhouse. In the lower layer, the controller keeps the optimal temperature for crop production. In the upper layer, the optimizer modifies the set-point when the positive report is issued. The cost function ensures the positive reports eliminated with the least heat loss.

References

Ran Liu, Hui Wang, José Luis Guzmán, Ming Li, A model-based methodology for the early warning detection of cucumber downy mildew in greenhouses: An experimental evaluation, Computers and Electronics in Agriculture, Volume 194, 2022a, 106751, https://doi.org/10.1016/j.compag.2022.106751.

Ran Liu, Jian Liu, Huiying Liu, Xinting Yang, José Fernando Bienvenido Bárcena, Ming Li, A 3-D simulation of leaf condensation on cucumber canopy in a solar greenhouse, Biosystems Engineering,Volume 210, 2021a, Pages 310-329, ISSN 1537-5110, https://doi.org/10.1016/j.biosystemseng.2021.08.008.

R. Liu, M. Li, J.L. Guzmán, F. Rodríguez, A fast and practical one-dimensional transient model for greenhouse temperature and humidity, Computers and Electronics in Agriculture, Volume 186, 2021b, 106186, ISSN 0168-1699, https://doi.org/10.1016/j.compag.2021.106186.

Yigal Elad, Nikolaos E. Malathrakis, Aleid J. Dik, Biological control of Botrytis-incited diseases and powdery mildews in greenhouse crops, Crop Protection, Volume 15, Issue 3, 1996, Pages 229-240, ISSN 0261-2194, https://doi.org/10.1016/0261-2194(95)00129-8.

Anthony P. Keinath, Felipe de Figueiredo Silva, Economic impacts of reduced fungicide efficacy against downy mildew on slicing cucumber, Crop Protection, Volume 155, 2022, 105934, ISSN 0261-2194, https://doi.org/10.1016/j.cropro.2022.105934.

Yusef Kianpoor Kalkhajeh, Biao Huang, Wenyou Hu, Chao Ma, Hongjian Gao, Michael L. Thompson, Hans Christian Bruun Hansen, Environmental soil quality and vegetable safety under current greenhouse vegetable production management in China, Agriculture, Ecosystems & Environment, Volume 307, 2021, 107230, ISSN 0167-8809, https://doi.org/10.1016/j.agee.2020.107230.

Wei-Han Chen, Fengqi You, Smart greenhouse control under harsh climate conditions based on data-driven robust model predictive control with principal component analysis and kernel density estimation, Journal of Process Control, Volume 107, 2021, Pages 103-113, ISSN 0959-1524, https://doi.org/10.1016/j.jprocont.2021.10.004.

O. Körner, H. Challa, Temperature integration and process-based humidity control in chrysanthemum, Computers and Electronics in Agriculture, Volume 43, Issue 1, 2004, Pages 1-21, ISSN 0168-1699, https://doi.org/10.1016/j.compag.2003.08.003.

O. Körner, H. Challa, Process-based humidity control regime for greenhouse crops, Computers and Electronics in Agriculture, Volume 39, Issue 3, 2003, Pages 173-192, ISSN 0168-1699, https://doi.org/10.1016/S0168-1699(03)00079-6.

Andrea Costantino, Lorenzo Comba, Giacomo Sicardi, Mauro Bariani, Enrico Fabrizio, Energy performance and climate control in mechanically ventilated greenhouses: A dynamic modelling-based assessment and investigation, Applied Energy, Volume 288, 2021, 116583, ISSN 0306-2619, https://doi.org/10.1016/j.apenergy.2021.116583.

Chun-Jiang Zhao, Ming Li, Xin-Ting Yang, Chuan-Heng Sun, Jian-Ping Qian, Zeng-Tao Ji, A data-driven model simulating primary infection probabilities of cucumber downy mildew for use in early warning systems in solar greenhouses, Computers and Electronics in Agriculture, Volume 76, Issue 2, 2011, Pages 306-315, ISSN 0168-1699, https://doi.org/10.1016/j.compag.2011.02.009.

Dan Xu, Shangfeng Du, L. Gerard van Willigenburg, Optimal control of Chinese solar greenhouse cultivation, Biosystems Engineering, Volume 171, 2018a, Pages 205-219, ISSN 1537-5110, https://doi.org/10.1016/j.biosystemseng.2018.05.002.

Dan Xu, Shangfeng Du, Gerard van Willigenburg, Adaptive two time-scale receding horizon optimal control for greenhouse lettuce cultivation, Computers and Electronics in Agriculture, Volume 146, 2018b, Pages 93-103, ISSN 0168-1699, https://doi.org/10.1016/j.compag.2018.02.001.

Dong Lin, Lijun Zhang, Xiaohua Xia, Hierarchical model predictive control of Venlo-type greenhouse climate for improving energy efficiency and reducing operating cost, Journal of Cleaner Production, Volume 264, 2020, 121513, ISSN 0959-6526, https://doi.org/10.1016/j.jclepro.2020.121513.

A.P. Montoya, J.L. Guzmán, F. Rodríguez, J.A. Sánchez-Molina, A hybrid-controlled approach for maintaining nocturnal greenhouse temperature: Simulation study, Computers and Electronics in Agriculture, Volume 123, 2016, Pages 116-124, ISSN 0168-1699, https://doi.org/10.1016/j.compag.2016.02.014.

Rodríguez, F., Guzmán, J. L., Berenguel, M., & Arahal, M. R. (2008). Adaptive hierarchical control of greenhouse crop production. International Journal of Adaptive Control and Signal Processing, 22(2), 180-197. https://doi.org/10.1002/acs.974.

A. Ramírez-Arias, F. Rodríguez, J.L. Guzmán, M. Berenguel, Multiobjective hierarchical control architecture for greenhouse crop growth, Automatica, Volume 48, Issue 3, 2012, Pages 490-498, ISSN 0005-1098,

https://doi.org/10.1016/j.automatica.2012.01.002.

P M A Bourke. Use of Weather Information in the Prediction of Plant Disease Epiphytotics. Annual Review of Phytopathology 1970 8:1, 345-370. https://doi.org/10.1146/annurev.py.08.090170.002021.

Gerald A. Carlson. 1970. A Decision Theoretic Approach to Crop Disease Prediction and Control. Volume52, Issue2, Pages 216-223. https://doi.org/10.2307/1237492.

Wang H, Sanchez-Molina JA, Li M, Rodríguez Díaz F. Improving the Performance of Vegetable Leaf Wetness Duration Models in Greenhouses Using Decision Tree Learning. Water. 2019; 11(1):158. https://doi.org/10.3390/w11010158.

Rong Wang, Zhaojun Sun, Dongyan Yang, Ling Ma, Simulating cucumber plant heights using optimized growth functions driven by water and accumulated temperature in a solar greenhouse, Agricultural Water Management, Volume 259, 2022, 107170, ISSN 0378-3774, https://doi.org/10.1016/j.agwat.2021.107170.

Evangelina Medrano, Pilar Lorenzo, María Cruz Sánchez-Guerrero, Juan Ignacio Montero, Evaluation and modelling of greenhouse cucumber-crop transpiration under high and low radiation conditions, Scientia Horticulturae, Volume 105, Issue 2, 2005, Pages 163-175, ISSN 0304-4238, https://doi.org/10.1016/j.scienta.2005.01.024.

Thomas Jewett, William Jarvis. Management of the greenhouse microclimate in relation to disease control: a review. Agronomie, EDP Sciences, 2001, 21 (4), pp.351-366. ⟨10.1051/agro:2001129⟩. ⟨hal-00886123⟩

A.B. Darlington, M.A. Dixon, M.J. Tsujita, The influence of humidity control on the production of greenhouse roses (Rosa hybrida), Scientia Horticulturae, Volume 49, Issues 3–4, 1992, Pages 291-303, ISSN 0304-4238, https://doi.org/10.1016/0304-4238(92)90165-9.

Bakker, J.C. (1988). THE EFFECTS OF HUMIDITY ON GROWTH AND PRODUCTION OF GLASSHOUSE CUCUMBERS, TOMATOES AND SWEET PEPPERS. Acta Hortic. 229, 159-164 https://doi.org/10.17660/ActaHortic.1988.229.13.

Mashonjowa, E., Ronsse, F., Mubvuma, M., Milford, J.R., & Pieters, J.G. (2013). Estimation of leaf wetness duration for greenhouse roses using a dynamic greenhouse climate model in Zimbabwe. Computers and Electronics in Agriculture. 95, 70-81. https://doi.org/10.1016/j.compag.2013.04.007.

Xilin Guan, Chuanyun Liu, Yan Li, Xiaozhong Wang, Yumin Liu, Chunqin Zou,

Xinping Chen, Wei Zhang, Reducing the environmental risks related to phosphorus surplus resulting from greenhouse cucumber production in China, Journal of Cleaner Production, Volume 332, 2022, 130076, ISSN 0959-6526, https://doi.org/10.1016/j.jclepro.2021.130076.

Wenyou Hu, Yanxia Zhang, Biao Huang, Ying Teng, Soil environmental quality in greenhouse vegetable production systems in eastern China: Current status and management strategies, Chemosphere, Volume 170, 2017, Pages 183-195, ISSN 0045-6535, https://doi.org/10.1016/j.chemosphere.2016.12.047.

Shanhong Zhang, Yu Guo, Huajian Zhao, Yang Wang, David Chow, Yuan Fang, Methodologies of control strategies for improving energy efficiency in agricultural greenhouses, Journal of Cleaner Production, Volume 274, 2020, 122695, ISSN 0959-6526, https://doi.org/10.1016/j.jclepro.2020.122695.

Cohen, 1977. Y. Cohen. The combined effects of temperature, leaf, wetness and inoculum concentration on infection of cucumbers with Pseudoperonospora cubensis. Canadian Journal of Botany, 55 (1977), pp. 1478-1487.

Wang, H., Sanchez-Molina J.A., Li M., Rodríguez Díaz F., 2019. Improving the Performance of Vegetable Leaf Wetness Duration Models in Greenhouses Using Decision Tree Learning. Water. 11(1), 158. https://doi.org/10.3390/w11010158.

Katsoulas, N., Antoniadis, D., Nikitas, A., 2021. A web-based system for fungus disease risk assessment in greenhouses: System development. Computers and Electronics in Agriculture. 188, 106326. https://doi.org/10.1016/j.compag.2021.106326.

David Katzin, Eldert J. van Henten, Simon van Mourik, Process-based greenhouse climate models: Genealogy, current status, and future directions, Agricultural Systems, Volume 198, 2022, 103388, ISSN 0308-521X, https://doi.org/10.1016/j.agsy.2022.103388.

Yu Guo, Huajian Zhao, Shanhong Zhang, Yang Wang, David Chow, Modeling and optimization of environment in agricultural greenhouses for improving cleaner and sustainable crop production, Journal of Cleaner Production, Volume 285, 2021, 124843, ISSN 0959-6526, https://doi.org/10.1016/j.jclepro.2020.124843.

Ljung, L. System Identification: Theory for the User, 2nd ed.; Prentice Hall PTR: Upper Saddle River, NJ, USA, 1999.

Montoya-Ríos, A.P.; García-Mañas, F.; Guzmán, J.L.; Rodríguez, F. Simple Tuning Rules for Feedforward Compensators Applied to Greenhouse Daytime Temperature Control Using Natural Ventilation. Agronomy 2020, 10, 1327. https://doi.org/10.3390/agronomy10091327.

F. García-Mañas, J.L. Guzmán, F. Rodríguez, M. Berenguel, T. Hägglund, Experimental evaluation of feedforward tuning rules, Control Engineering Practice, Volume 114, 2021, 104877, ISSN 0967-0661, https://doi.org/10.1016/j.conengprac.2021.104877.

Taewon Moon, Jung Eek Son, Knowledge transfer for adapting pre-trained deep neural models to predict different greenhouse environments based on a low quantity of data, Computers and Electronics in Agriculture, Volume 185, 2021, 106136, ISSN 0168-1699, https://doi.org/10.1016/j.compag.2021.106136.

Dae-Hyun Jung, Hyoung Seok Kim, Changho Jhin, Hak-Jin Kim, Soo Hyun Park, Time-serial analysis of deep neural network models for prediction of climatic conditions inside a greenhouse, Computers and Electronics in Agriculture, Volume 173, 2020, 105402, ISSN 0168-1699, https://doi.org/10.1016/j.compag.2020.105402.

Wang, L., Zhang, H., 2018. An adaptive fuzzy hierarchical control for maintaining solar greenhouse temperature. Computers and Electronics in Agriculture 155, 251-256, DOI: 10.1016/j.compag.2018.10.023

Jieyu Li, Li Li, Haihua Wang, Konstantinos P. Ferentinos, Minzan Li, Nick Sigrimis, Proactive energy management of solar greenhouses with risk assessment to enhance smart specialisation in China, Biosystems Engineering, Volume 158, 2017, Pages 10-22, ISSN 1537-5110, https://doi.org/10.1016/j.biosystemseng.2017.03.007.

Palti, J., Cohen, Y. Downy mildew of Cucurbits (Pseudoperonospora Cubensis): the Fungus and its hosts, distribution, epidemiology and control. Phytoparasitica 8, 109–147 (1980). https://doi.org/10.1007/BF02994506

WeatherBit, *WeatherBit API Guide*. https://www.weatherbit.io/api: WeatherBit, Inc., 2019.

Liu K, Zhang C, Yang X, Diao M, Liu H, Li M. Development of an Occurrence Prediction Model for Cucumber Downy Mildew in Solar Greenhouses Based on Long Short-Term Memory Neural Network. Agronomy. 2022b; 12(2):442. https://doi.org/10.3390/agronomy12020442

Liang, Y.C., Sun, W.C., Si, J. and Römheld, V. (2005), Effects of foliar- and root-applied silicon on the enhancement of induced resistance to powdery mildew in Cucumis sativus. Plant Pathology, 54: 678-685. https://doi.org/10.1111/j.1365-3059.2005.01246.x

Mistriotis. A., Bot, G.P.A., Picuno, P., Scarascia-Mugnozza, G., 1997. Analysis of the efficiency of greenhouse ventilation using computational fluid dynamics. Agricultural and Forest Meteorology. 85(3–4), 217-228. https://doi.org/10.1016/S0168-1923(96)02400-8.

Ahamed, M.S., Guo, H.Q., Tanino, K., 2018. Development of a thermal model for simulation of supplemental heating requirements in Chinese-style solar greenhouses. Computers and Electronics in Agriculture. 150, 235-244. https://doi.org/10.1016/j.compag.2018.04.025.

Boulard, T., Roy, J.C., Pouillard, J.-B., Fatnassi, H., Grisey, A., 2017. Modelling of micrometeorology, canopy transpiration and photosynthesis in a closed greenhouse using computational fluid dynamics. Biosystems Engineering. 158, 110-133. https://doi.org/10.1016/j.biosystemseng.2017.04.001.

MATLAB user's manual, R2021b, 2021.

Pal, A., Adhikary, R., Shankar, T., Sahu, A. K., & Maitra, S. (2020). Cultivation of cucumber in greenhouse. Protected Cultivation and Smart Agriculture; Sagar Maitra, DJGATS, Ed.; New Delhi Publishers: New Delhi, India, 139-145. DOI: 10.30954/NDP-PCSA.2020.14.

Ding, Xiaotao, Yuping Jiang, Dafeng Hui, Lizhong He, Danfeng Huang, Jizhu Yu, and Qiang Zhou. "Model Simulation of Cucumber Yield and Microclimate Analysis in a Semi-closed Greenhouse in China", HortScience horts 54, 3 (2019): 547-554, accessed Sep 11, 2022, https://doi.org/10.21273/HORTSCI13703-18.

Hui, Y.H., Ghazala, S., Graham, M. D., Murrel, K.D., Nip, W.K., (2003) Handbook of Vegetable Preservation and Processing. Technology and Engineering. CRC Press, Florida, United States.in both an open and a semi-closed greenhouse. Sci. Hort. 130,808-814.

Mahesh Chand Singh, J.P. Singh, S.K. Pandey, Dharinder Mahay and Varun Shrivastva. 2017. Factors Affecting the Performance of Greenhouse Cucumber Cultivation-A Review. Int.J.Curr.Microbiol.App.Sci. 6(10): 2304-2323. doi: https://doi.org/10.20546/ijcmas.2017.610.273.

Liu, R., Guzmán, J.L., García, F., Li, M., 2022c. Selective temperature and humidity control strategy for a Chinese solar greenhouse with an event-based approach. Revista Iberoamericana de Automática e Informática Industrial. Under review.

3 CONCLUSIONS AND FUTURE WORKS

3 Conclusions and future works

The contribution of this thesis can be grouped mainly in three aspects: development and evaluation of greenhouse microclimate models; prediction and model evaluation of greenhouse fungal diseases; greenhouse climate control for reducing fungal disease. Sections 3.1; 3.2; 3.3 respectively summarize the contributions in three aspects. Afterwards, sections 3.4 discusses the current problems and future solutions in this research field.

3.1 Conclusions on the greenhouses modelling

My Ph.D. thesis was completed in three years. In the first year, the supervisor asked me to build a fast one-dimensional transient greenhouse climate model for predicting temperature and humidity. Compared with the published models, the special ability for this mechanism model is that the inputs must be limited to the range that any common weather forecast can provide. This problem has been solved by two relevant innovations. First, embedded models are implemented within this system in order to simulate the parameters in each step. In this way, all of the dynamic parameters do not need to be measured and input at each time step, e.g. convective heat transfer coefficient, crop transpiration rate, ventilation rate, air leakage rate,…Second, the wall temperature and wall heat flux are simulated by solving a set of conservation equations at each transient step. Although the above two improvements have greatly increased the computing load (15 minutes per simulation day), it is within the acceptable range. Considering that the model can simulate the greenhouse climate just using weather forecast, these changes are worthwhile.

In the greenhouse climate model system, the ventilation rate estimation module requires a large number of professional parameters, such as coefficient of wind pressure, thermal pressure, etc. It is difficult for the farmers to measure these parameters. In this project, a regression trees natural ventilation model is developed using results from one thousand samples of virtual wind tunnel experiments. CFD method provides professional parameter support for wind tunnel experiments. Three-dimensional CFD simulation costs more than 30 hours to achieve convergence in each case, using an Intel Core I7 CPU and 16 GB RAM. Two-dimensional CFD simulation costs 5 mins in each case. It's time consuming but the ventilation rate obtained by this method is accurate. It took three months to get 1000 CFD samples, and finally they are trained into a regression tree model. Then, the users can get a dynamic ventilation rate in one second when using the proposed regression trees model. This model perfectly deals with the combined effect of wind pressure and thermal gradients. In addition, it can be embedded easily into the Simulink model system developed in the first part of the thesis.

Making further efforts, for the heterogeneity of greenhouse microclimate distribution, we developed three-dimensional and two-dimensional greenhouse temperature and humidity distribution models. Using user-defined functions, crops-

environment interactions are simulated. Then, the leaf condensation distribution is simulated based on the dynamic leaves temperature and air humidity distribution. In this process, we explored the way of creating high-quality boundary layer grid for arc roofs. The closed equations of heat convection, conduction and radiation between crops and environment are solved by user-defined functions based on C language. Finally, we set 15 temperature and humidity sampling points in a greenhouse with the same size to the model. Then the three-dimensional and two-dimensional greenhouse climate models are validated using these data.

3.2 Conclusions on the greenhouse fungal disease prediction

This work was mainly carried out in the second year of my Ph.D. We first reviewed the pathogenesis of fungal diseases and found that the important environmental parameters leading to infection were LWD and temperature. Later, we selected and evaluated a primary infection model for cucumber downy mildew in greenhouses. The problem of this kind of model is the delay of prediction, because the inputs are current LWD and TLWD. The infection may have occurred when the sensor in the greenhouse measures these parameters. Therefore, the main contribution of this work is to combine the greenhouse climate model, the weather forecast algorithm, and the disease infection model.

The use of weather forecast to predict future diseases has been widely used in the field condition (Kim et al., 2020). Similar applications are rare in greenhouse disease prediction, because weather parameters cannot represent the environment around crops in the greenhouse. The greenhouse model developed in this project can predict the greenhouse microclimate in the next few days only when the weather forecast is input. This model was adopted to evaluate the disease warning in a greenhouse in Beijing. After two false positive forecasts were issued, the date of occurrence predicted by one positive forecast was the same as the date of manual observation in April 2021, which indicates the feasibility of using weather forecast to predict greenhouse fungal diseases.

3.3 Conclusions on the greenhouse climate control for reducing fungal disease

The design of closed-loop controller is rare in Chinese solar greenhouses (CSGs). Therefore, firstly a PID controller was designed for greenhouse temperature and humidity. Moreover, an event-based control method is studied to reduce the control effort. Different values with $\delta = [0, 0.1, 0.2, 0.5, 1]$ relating to the event occurrence are tested. The results show that $\delta=0.5$ is the optimum value, which significantly reduces the number of vent movements by 43.8%, while only increasing the temperature error by 1.13%. Then, a mixed control application of temperature and humidity was demonstrated. Normally, only the temperature PI controller is activated. However, the humidity priority is given. The RH is controlled by given an upper limit, when the RH is over that limit, the vent opening is increased. This control strategy constantly keeps the relative humidity below 80% while controlling the temperature to the set-point, which not only prevents high humidity damaging the crops, but also greatly avoids the loss of energy.

However, the above strategy is still not the optimal one. For cucumbers, they are warm and wet loving crops. It is not recommended to ventilate and dehumidify coarsely, since in this way, excessive heat and water vapor are lost. Therefore, a hierarchical control strategy was proposed to provide a better management for greenhouse crop disease. In the upper layer, the fungal disease infection is predicted for the next three days by connecting weather forecast, the greenhouse climate model and a disease infection model for cucumber downy mildew. When a positive report is issued, the optimizer calculates the cost function to give the optimal temperature set-pot, which is an integrative equation of the absolute error between the optimal temperature for cucumber production and the suggested set-point to avoid fungal diseases. Finally, this strategy keeps the optimum temperature for cucumber production, as well as constantly avoiding positive reports for downy mildew infection in a long consecutive growing season that over one hundred days. This study is of great significance for clear production and efficient energy utilization.

3.4 Recommendations for future research

In the future research, the model must be mutually compensated by mechanism and experience. Many parameters in the mechanism model are dynamic variables, which are often based on empirical values. Therefore, using big data to train these parameters can improve the stability of the model. The development of neural network model is a promising field, but the current main problems are non-standard data format and discontinuous data collection. In the future, with the progress of sensor stability, the improvement of data storage systems, and the progress of computer computing power, the AI-based models are an interesting solution to be explored. This will be one of my research line in the future.

At present, many countries around the world are facing the problem of aging. The generation after 1990 is generally unwilling to engage in agricultural work. Therefore, the industrialization of agriculture is very important. At present, one of the main factors hindering the process of agricultural modernization is the lack of standards. If greenhouses are taken as an example, one can see that there are greenhouses in China with a single building area varies from 300 m^2 to 2000 m^2. Their constructions are also very casual. Generally, they are based on local conditions and local materials. This is unacceptable for those engaged in greenhouse modelling and automatic control. Therefore, the current greenhouse microclimate modelling only provides a method, which is still a long way from the large-scale promotion and application in the production process. The solution to this problem depends on the adjustment of national economic policies.

In terms of disease prediction in the greenhouse, the downy mildew infection model used in this project assumes that the number of spores in the greenhouse is sufficient and the crops are generally susceptible. Therefore, its inputs are environmental factors. This leads to the low specificity of the model, which is prone to false positive predictions. On the other hand, after the initial infection, the disease severity prediction model with the disease index as the output is still rare in the literature. At NERCITA in Beijing, research in this area is being conducted.

For greenhouse environmental control, the classical control system has been fully studied (Xu et al., 2018b). With the progress of computer power, the future research on greenhouse climate control will focus on three-dimensional models. It has been confirmed that the distribution of microclimate in the greenhouse is uneven at each transient step (Liu et al., 2021b). This distributed transient simulation is time-consuming, so it is unrealistic to run it with the control system in parallel. In the future, when the three-dimensional spatiotemporal distribution model output the current transient simulation results in sampling time of secons, it can provide the most comprehensive feedback information for the controller, including temperature distribution, humidity distribution, air velocity and flow pattern, etc. The controller will therefore calculate the most appropriate control signal according to the temporal and spatial distribution information, which will be a great improvement for the control efficiency.

4 REFERENCES

References

Andrade-piedra, J.L., Hijmans, R.J., Forbes, G.A., 2005. Simulation of Potato Late Blight in the Andes. I: Modification and Parameterization of the LATEBLIGHT Model. Phytopathology, 95 (10), 1191-1199. https://doi.org/10.1094/PHYTO-95-1191.

Ansys. 2010. Ansys Fluent User's guide. Ansys, Inc., Canonsburg, PA, USA ed.

Beschi, M., Pawlowski, A., Guzmán, J.L., Berenguel, M., Visioli, A., 2014. Symmetric send-on-delta PI control of a greenhouse system. IFAC Proceedings. 47 (3), 4411-4416. https://doi.org/10.3182/20140824-6-ZA-1003.01028.

Bouhoun Ali, H., Bournet, P.-E., Danjou, V., Morille, B., Migeon, C., 2014. CFD simulations of the night-time condensation inside a closed glasshouse: Sensitivity analysis to outside external conditions, heating and glass properties. Biosystems Engineering. 127, 159–175. https://doi.org/10.1016/j.biosystemseng.2014.08.017.

Boulard, T., Roy, J.C., Fatnassi, H., Kichah, A., Lee, I.-B., 2010. Computer fluid dynamics prediction of climate and fungal spore transfer in a rose greenhouse. Computers and Electronics in Agriculture. 74 (2), 280-292. https://doi.org/10.1016/j.compag.2010.09.003.

Boulard, T., Roy, J.C., Lamrani, M.A., Haxaire, R., 1997. Characterising and Modelling the Air Flow and Temperature Profiles in a Closed Greenhouse in Diurnal Conditions. IFAC Proceedings Volumes. 30 (26), 37-42. https://doi.org/10.1016/S1474-6670(17)41242-0.

Boulard, T., Roy, J.C., Pouillard, J.B., Fatnassi, H., Grisey, A., 2017. Modelling of micrometeorology, canopy transpiration and photosynthesis in a closed greenhouse using computational fluid dynamics. Biosystems Engineering. 158, 110-133. https://doi.org/10.1016/j.biosystemseng.2017.04.001.

Boulard, T., Wang, S., 2002. Experimental and numerical studies on the heterogeneity of crop transpiration in a plastic tunnel. Computers and Electronics in Agriculture. 34 (1-3), 173-190. https://doi.org/10.1016/S0168-1699(01)00186-7.

Bournet, P.-E., Boulard, T., 2010. Effect of ventilator configuration on the distributed climate of greenhouses: A review of experimental and CFD studies. Computers and Electronics in Agriculture. 74 (2), 195-217. https://doi.org/10.1016/j.compag.2010.08.007.

Bournet, P.-E., Brajeul, E., Truffault, V., Chantoiseau, E., Naccour, R., 2020. Impact of heating location, forced ventilation and screens on the energy efficiency and condensation risks inside a cucumber greenhouse. Acta Hortic. 1271, 25-32. https://doi.org/10.17660/ActaHortic.2020.1271.4.

Bournet, P.-E., Rojano, F., 2022. Advances of Computational Fluid Dynamics (CFD) applications in agricultural building modelling: Research, applications and challenges. Computers and Electronics in Agriculture. 201, 107277. https://doi.org/10.1016/j.compag.2022.107277.

Chen, J., Xu, F., Tan, D., Shen, Z., Zhang, L., Ai, Q., 2015. A control method for agricultural greenhouses heating based on computational fluid dynamics and energy prediction model. Applied Energy. 141, 106-118. https://doi.org/10.1016/j.apenergy.2014.12.026.

Chen, W-H., Mattson, N.S., You, F., 2022. Intelligent control and energy optimization in controlled environment agriculture via nonlinear model predictive control of semi-closed greenhouse. Applied Energy. 320 (119334). https://doi.org/10.1016/j.apenergy.2022.119334.

Cheng, X., Li, D., Shao, L., Ren, Z., 2021. A virtual sensor simulation system of a flower greenhouse coupled with a new temperature microclimate model using three-dimensional CFD. Computers and Electronics in Agriculture. 181, 105934. https://doi.org/10.1016/j.compag.2020.105934.

Chelal, J., Al Masri, A., Hau, B., 2015. Modelling the interaction between early blight epidemics and host dynamics of tomato. Tropical Plant Pathology. 40, 77–87. https://doi.org/10.1007/s40858-015-0021-0.

Cohen, Y., 1977. The combined effects of temperature, leaf wetness and inoculum concentration on infection of cucumbers with *Pseudoperonospora cubensis*. Canadian Journal of Botany. 55 (1977), 1478-1487.

De Halleux, D., 1989. Dynamic model of heat and mass transfer in greenhouses: theoretical and experimental study. PhD Thesis, Gembloux, Belgium.

Ding, X., Jiang, Y., Hui, D., He, L., Huang, D., Yu, J., Zhou, Q., 2019. Model Simulation of Cucumber Yield and Microclimate Analysis in a Semi-closed Greenhouse in China. HortScience horts. 54 (3), 547-554. https://doi.org/10.21273/HORTSCI13703-18.

El Jarroudi, M., Kouadio, L., Bock, C.H., El Jarroudi, M., Junk, J., Pasquali, M., Maraite, H., Delfosse, P., 2017. A threshold-based weather model for predicting stripe rust infection in winter wheat. Plant Disease. 101 (5), 693-703. https://doi.org/10.1094/PDIS-12-16-1766-RE.

FAO and IIASA, 2021 modified to comply with UN, 2021. https://www.fao.org/3/cb7654en/online/src/html/chapter-1-1.html.

García-Mañas, F., Guzmán, J.L., Rodríguez, F., Berenguel, M., Hägglund, T., 2021. Experimental evaluation of feedforward tuning rules. Control Engineering Practice. 114, 104877. https://doi.org/10.1016/j.conengprac.2021.104877.

Guan, X., Liu, C., Li, Y., Wang, X., Liu, Y., Zou, C., Chen, X., Zhang, W., 2022. Reducing the environmental risks related to phosphorus surplus resulting from greenhouse cucumber production in China. Journal of Cleaner Production. 332, 130076. https://doi.org/10.1016/j.jclepro.2021.130076.

Guan, Y., Lu, H., Jiang, Y., Tian, P., Qiu, L., Pellikka, P., Heiskanen, J., 2021. Changes in global climate heterogeneity under the 21st century global warming. Ecological Indicators. 130, 108075. https://doi.org/10.1016/j.ecolind.2021.108075.

Guo, Y., Zhao, H., Zhang, S., Wang, Y., Chow, D., 2021. Modeling and optimization of environment in agricultural greenhouses for improving cleaner and sustainable crop production. Journal of Cleaner Production. 285, 124843. https://doi.org/10.1016/j.jclepro.2020.124843.

Haxaire, R., 1999. Caractérisation et modélisation des écoulements d'air dans une serre. Ph.D. Thesis. Université de Nice, France.

Hornero, G., Gaitán-Pitre, J.E., Serrano-Finetti, E., Casas, O., Pallas-Areny, R., 2017. A novel low-cost smart leaf wetness sensor. Computers and Electronics in Agriculture. 143, 286-292. https://doi.org/10.1016/j.compag.2017.11.001.

Hoxey, R.P., Richardson, G.M., 1983. Measurements of wind loads on full scale plastic greenhouse. J. Wind Eng. Ind. Aerodynam. 16, 57–83.

Hu, W., Zhang, Y., Huang, B., Teng, Y., 2017. Soil environmental quality in greenhouse vegetable production systems in eastern China: Current status and management strategies. Chemosphere. 170, 183-195. https://doi.org/10.1016/j.chemosphere.2016.12.047.

Hui, Y.H., Ghazala, S., Graham, M. D., Murrel, K.D., Nip, W.K., 2003. Handbook of Vegetable Preservation and Processing. Technology and Engineering. CRC Press, Florida, United States. Sci. Hort. 130, 808-814.

Jewett, T., Jarvis, W., 2001. Management of the greenhouse microclimate in relation to disease control: a review. Agronomie, EDP Sciences. 21 (4), 351-366. https://doi.org/10.1051/agro:2001129.

Jung, D.-H., Kim, H.S., Jhin, C., Kim, H.J., Park, S.H., 2020. Time-serial analysis of deep neural network models for prediction of climatic conditions inside a greenhouse. Computers and Electronics in Agriculture. 173, 105402. https://doi.org/10.1016/j.compag.2020.105402.

Katzin, D., van Henten, E.J., van Mourik, S., 2022. Process-based greenhouse climate models: Genealogy, current status, and future directions. Agricultural Systems. 198, 103388. https://doi.org/10.1016/j.agsy.2022.103388.

Kalkhajeh, Y. K., Huang, B., Hu, W., Ma, C., Gao, H., Thompson, M.L., Bruun Hansen, H.C., 2021. Environmental soil quality and vegetable safety under current greenhouse vegetable production management in China, Agriculture. Ecosystems and Environment. 307, 107230. https://doi.org/10.1016/j.agee.2020.107230.

Kichah, A., Bournet, P.-E., Migeon, C., Boulard, T., 2012. Measurement and CFD simulation of microclimate characteristics and transpiration of an Impatiens pot plant crop in a greenhouse. Biosystems Engineering. 112 (1), 22–34. https://doi.org/10.1016/j.biosystemseng.2012.01.012.

Kim, H-S., Do, K.S., Park, J.H., Kang, W.S., Lee, Y.H., Park, E.W., 2020. Application of numerical weather prediction data to estimate infection risk of bacterial grain rot of rice in Korea. The Plant Pathology Journal. 36 (1), 54-66. https://doi.org/10.5423/PPJ.OA.11.2019.0281.

Kim, R.-w., Lee, I.-b., Kwon, K.-s., 2017. Evaluation of wind pressure acting on multi-span greenhouses using CFD technique, Part 1: Development of the CFD model. Biosystems Engineering. 164, 235-256. https://doi.org/10.1016/j.biosystemseng.2017.09.008.

Kimura, K., Yasutake, D., Yamanami, A., Kitano, M., 2020. Spatial examination of leaf-boundary-layer conductance using artificial leaves for assessment of light airflow within a plant canopy under different controlled greenhouse conditions. Agricultural and Forest Meteorology. 280, 107773. https://doi.org/10.1016/j.agrformet.2019.107773.

Körner, O., Challa, H., 2004. Temperature integration and process-based humidity control in chrysanthemum. Computers and Electronics in Agriculture. 43 (1), 1-21. https://doi.org/10.1016/j.compag.2003.08.003.

Li, T.H., Chang, J.M., Wei, M., Shi, G.Y., Zhang, Y.S., Chen, D.J., 2018. Application situation and problem analysis of ventilation facilities in solar greenhouse in Shandong province. Agricultural Engineering and Technology. 38 (16), 22-26. (In Chinese) https://doi.org/10.16815/j.cnki.11-5436/s.2018.16.003.

Liang, Y.C., Sun, W.C., Si, J., Römheld, V., 2005. Effects of foliar- and root-applied silicon on the enhancement of induced resistance to powdery mildew in Cucumis sativus. Plant Pathology. 54, 678-685. https://doi.org/10.1111/j.1365-3059.2005.01246.x

Lin, D., Zhang, L., Xia, X., 2020. Hierarchical model predictive control of Venlo-type greenhouse climate for improving energy efficiency and reducing operating cost. Journal of Cleaner Production. 264, 121513. https://doi.org/10.1016/j.jclepro.2020.121513.

Lin, D., Zhang, L., Xia, X., 2021. Model predictive control of a Venlo-type greenhouse system considering electrical energy, water and carbon dioxide consumption. Applied Energy. 298, 117163. https://doi.org/10.1016/j.apenergy.2021.117163.

Liu, K., Zhang, C., Yang, X., Diao, M., Liu, H., Li, M., 2022b. Development of an Occurrence Prediction Model for Cucumber Downy Mildew in Solar Greenhouses Based on Long Short-Term Memory Neural Network. Agronomy. 12 (2), 442. https://doi.org/10.3390/agronomy12020442.

Liu, R., Bournet, P.E., Guzmán, J.L., Li, M., 2022e. Numerical analysis of the wind field around greenhouse clusters and natural ventilation rate for the Chinese solar greenhouse. Computers and Electronics in Agriculture. Under review.

Liu, R., Guzmán, J.L., García, F., Li, M., 2022c. Selective temperature and humidity control strategy for a Chinese solar greenhouse with an event-based approach. Revista Iberoamericana de Automática e Informática Industrial. Accepted.

Liu, R., Guzmán, J.L., Gil, J.D., Liu, K., Li, M., 2022d. Hierarchical optimization control strategy for preventing fungal disease infections in a cucumber greenhouse. Journal of Cleaner Production. Under review.

Liu, R., Li, M., Guzmán, J.L., Rodríguez, F., 2021a. A fast and practical one-dimensional transient model for greenhouse temperature and humidity. Computers and Electronics in Agriculture. 186, 106186. https://doi.org/10.1016/j.compag.2021.106186.

Liu, R., Liu, J., Liu, H., Yang, X., Bienvenido Bárcena, J.F., Li, M., 2021b. A 3-D simulation of leaf condensation on cucumber canopy in a solar greenhouse. Biosystems Engineering. 210, 310-329. https://doi.org/10.1016/j.biosystemseng.2021.08.008.

Liu, R., Liu, J., Ren, A.X., Liu, H.Y., Guzmán, J.L., Bienvenido, J.F., Yang, X.T., Li, M., 2020. Simulation of night-time condensation on cucumber leaves in single slope solar greenhouse. Acta Hortic. 1296, 133-140. https://doi.org/10.17660/ActaHortic.2020.1296.18.

Liu, R., Wang, H., Guzmán, J.L., Li, M., 2022a. A model-based methodology for the early warning detection of cucumber downy mildew in greenhouses: An experimental evaluation. Computers and Electronics in Agriculture. 194, 106751. https://doi.org/10.1016/j.compag.2022.106751.

Ljung, L., 1999. System Identification: Theory for the User, 2nd ed.; Prentice Hall PTR: Upper Saddle River, NJ, USA.

Majdoubi, H., Boulard, T., Fatnassi, H., Bouirden, L., 2009. Airflow and microclimate patterns in a one-hectare Canary type greenhouse: An experimental and CFD assisted study. Agricultural and Forest Meteorology. 149 (6–7), 1050-1062. https://doi.org/10.1016/j.agrformet.2009.01.002.

Mashonjowa, E., Ronsse, F., Mubvuma, M., Milford, J.R., Pieters, J.G., 2013. Estimation of leaf wetness duration for greenhouse roses using a dynamic greenhouse climate model in Zimbabwe. Computers and Electronics in Agriculture. 95, 70-81. https://doi.org/10.1016/j.compag.2013.04.007.

MATLAB user's manual, R2021b. 2021.

Mirsadeghi, M., Cóstola, D., Blocken, B., Hensen, J.L.M., 2013. Review of external convective heat transfer coefficient models in building energy simulation programs: Implementation and uncertainty. Applied Thermal Engineering. 56 (1–2), 134-151. https://doi.org/10.1016/j.applthermaleng.2013.03.003.

Mistriotis, A., Bot, G.P.A., Picuno, P., Scarascia-Mugnozza, G., 1997. Analysis of the efficiency of greenhouse ventilation using computational fluid dynamics. Agricultural and Forest Meteorology. 85 (3–4), 217-228. https://doi.org/10.1016/S0168-1923(96)02400-8.

Molina-Aiz, F.D., Fatnassi, H., Boulard, T., Roy, J.C., Valera, D.L., 2010. Comparison of finite element and finite volume methods for simulation of natural ventilation in greenhouses. Computers and Electronics in Agriculture. 72 (2), 69-86. https://doi.org/10.1016/j.compag.2010.03.002.

Montoya, A.P., Guzmán, J.L., Rodríguez, F., Sánchez-Molina, J.A., 2016. A hybrid-controlled approach for maintaining nocturnal greenhouse temperature: Simulation study. Computers and Electronics in Agriculture. 123, 116-124. https://doi.org/10.1016/j.compag.2016.02.014.

Montoya-Ríos, A.P., García-Mañas, F., Guzmán, J.L., Rodríguez, F., 2020. Simple Tuning Rules for Feedforward Compensators Applied to Greenhouse Daytime Temperature Control Using Natural Ventilation. Agronomy. 10, 1327. https://doi.org/10.3390/agronomy10091327.

Moon, T., Son, J.E., 2021. Knowledge transfer for adapting pre-trained deep neural models to predict different greenhouse environments based on a low quantity of data. Computers and Electronics in Agriculture. 185, 106136. https://doi.org/10.1016/j.compag.2021.106136.

Ojiambo, P.S., Gent, D.H., Quesada-Ocampo, L.M., Hausbeck, M.K., Holmes, G.J., 2015. Epidemiology and Population Biology of Pseudoperonospora cubensis: A Model System for Management of Downy Mildews. Annual Review of Phytopathology. 53 (1), 223-246. https://doi.org/10.1146/annurev-phyto-080614-120048.

Ould Khaoua, S.A., Bournet, P.E., Migeon, C., Boulard, T., Chassériaux, G., 2006. Analysis of Greenhouse Ventilation Efficiency based on Computational Fluid Dynamics. Biosystems Engineering. 95 (1), 83-98. https://doi.org/10.1016/j.biosystemseng.2006.05.004.

Pal, A., Adhikary, R., Shankar, T., Sahu, A. K., Maitra, S., 2020. Cultivation of cucumber in greenhouse. Protected Cultivation and Smart Agriculture; Sagar Maitra, DJGATS, Ed.; New Delhi Publishers: New Delhi, India.139-145. https://doi.org/10.30954/NDP-PCSA.2020.14.

Papadakis, G., Frangoudakis, A., Kyritsis, S., 1992. Mixed, forced, and free convection heat transfer at the greenhouse cover. Journal of Agricultural Engineering Research. 51, 191-205. https://doi.org/10.1016/0021-8634(92)80037-S.

Pawlowski, A., Beschi, M., Guzmán, J.L., Visioli, A., Berenguel, M., Dormido, S., 2016. Application of SSOD-PI and PI-SSOD event-based controllers to greenhouse climatic control. ISA Transactions. 65, 525-536. https://doi.org/10.1016/j.isatra.2016.08.008.

Piscia, D., Montero, J.I., Baeza, E., Bailey, B.J., 2012. A CFD greenhouse night-time condensation model. Biosystems Engineering. 111 (2), 141–154. https://doi.org/10.1016/j.biosystemseng.2011.11.006.

Ramírez-Arias, A., Rodríguez, F., Guzmán, J.L., Berenguel, M., 2012. Multiobjective hierarchical control architecture for greenhouse crop growth. Automatica. 48 (3), 490-498. https://doi.org/10.1016/j.automatica.2012.01.002.

Rocha, G.A.O., Pichimata, M.A., Villagran, E., 2021. Research on the Microclimate of Protected Agriculture Structures Using Numerical Simulation Tools: A Technical and Bibliometric Analysis as a Contribution to the Sustainability of Under-Cover Cropping in Tropical and Subtropical Countries. Sustainability. 13, 10433. https://doi.org/10.3390/su131810433.

Rodríguez, F., Guzmán, J.L., Berenguel, M., Arahal, M.R., 2008. Adaptive hierarchical control of greenhouse crop production. International Journal of Adaptive Control and Signal Processing. 22 (2), 180-197. https://doi.org/10.1002/acs.974.

Roser, M., 2013. Future Population Growth". Published online at OurWorldInData.org. Retrieved from: https://ourworldindata.org/future-population-growth.

Sentelhas, P.C., Dalla Marta, A., Orlandini, S., Santos, E.A., Gillespie, T.J., Gleason, M.L., 2008. Suitability of relative humidity as an estimator of leaf wetness duration. Agricultural and Forest Meteorology. 148 (3), 392-400. https://doi.org/10.1016/j.agrformet.2007.09.011.

Singh, M.C., Singh, J.P., Pandey, S.K., Mahay, D., Shrivastva, V., 2017. Factors Affecting the Performance of Greenhouse Cucumber Cultivation-A Review. Int. J. Curr. Microbiol. App. Sci. 6 (10), 2304-2323. https://doi.org/10.20546/ijcmas.2017.610.273.

Sun, Y. C., Wang, H.T., Zhu, C.M., Lyu, H.Y., Zhang, X.H., Cao, Y.F., et al. 2022. Application performances of two greenhouses with new types of backwall in Yangling, China. Int J Agric & Biol Eng. 15 (3), 62–71. https://doi.org/10.25165/j.ijabe.20221503.6097.

Tong, G., Christopher, D.M., Li, B., 2009. Numerical modelling of temperature variations in a Chinese solar greenhouse. Computers and Electronics in Agriculture. 68 (1), 129-139. https://doi.org/10.1016/j.compag.2009.05.004.

Walton, G.N., 1983. Thermal Analysis Research Program Reference Manual, NBSSIR 83-2655. National Bureau of Standards.

Wang H, Mongiano G, Fanchini D, Titone, P., Bregaglio, S., 2021. Varietal susceptibility overcomes climate change effects on the future trends of rice blast disease in Northern Italy. Agricultural Systems. 193 (1), 103223. https://doi.org/10.1016/j.agsy.2021.103223.

Wang, H., Sanchez-Molina, J.A., Li, M., Rodríguez Díaz, F., 2019. Improving the Performance of Vegetable Leaf Wetness Duration Models in Greenhouses Using Decision Tree Learning. Water. 11 (1), 158. https://doi.org/10.3390/w11010158.

Wang, T., Wu, G., Chen, J., Cui, P., Chen, Z., Yan, Y., Zhang, Y., Li, M., Niu, D., Li, B., Chen, H., 2017. Integration of solar technology to modern greenhouse in China: Current status, challenges and prospect. Renewable and Sustainable Energy Reviews. 70, 1178-1188. https://doi.org/10.1016/j.rser.2016.12.020.

WeatherBit, WeatherBit API Guide. https://www.weatherbit.io/api: WeatherBit, Inc., 2019.

Wen, D., Wang, X., Sun, K.N., Wang, K.A., Yang, N., 2019. Development situation and prospects of mechanization for greenhouse vegetables in Shandong province. Agricultural Equipment & Vehicle Engineering. 57 (S1), 52-54. (In Chinese) https://doi.org/10.3969/j.issn.1673-3142.2019.S1.012.

Widmoser, P., 2009. A discussion on and alternative to the Penman–Monteith equation. Agricultural Water Management. 96 (4), 711-721. https://doi.org/10.1016/j.agwat.2008.10.003.

Xu, D., Du, S., van Willigenburg, G., 2018a. Optimal control of Chinese solar greenhouse cultivation. Biosystems Engineering. 171, 205-219. https://doi.org/10.1016/j.biosystemseng.2018.05.002.

Xu, D., Du, S., van Willigenburg, G., 2018b. Adaptive two time-scale receding horizon optimal control for greenhouse lettuce cultivation. Computers and Electronics in Agriculture. 146, 93-103. https://doi.org/10.1016/j.compag.2018.02.001.

Yue, Y., Quan, J., Zhao, H., Wang, H., 2018. The Prediction of Greenhouse Temperature and Humidity Based on LM-RBF Network. IEEE International Conference on Mechatronics and Automation. 1537-1541. https://doi.org/10.1109/ICMA.2018.8484456.

Zhang, C., Liu, R., Liu, K., Yang, X., Liu, H., Diao, M., Li, M., 2022. A CFD transient model of leaf wetness duration on greenhouse cucumber leaves. Computers and Electronics in Agriculture. 200, 107257. https://doi.org/10.1016/j.compag.2022.107257.

Zhang, S., Guo, Y., Zhao, H., Wang, Y., Chow, D., Fang, Y., 2020. Methodologies of control strategies for improving energy efficiency in agricultural greenhouses. Journal of Cleaner Production. 274, 122695. https://doi.org/10.1016/j.jclepro.2020.122695.

Zhang, X.D., Lv, J., Dawuda, M.M., Xie, J.M., Yu, J.H., Gan, Y.T., Zhang, J., Tang, Z.Q., Li, J., 2019. Innovative passive heat-storage walls improve thermal performance and energy efficiency in Chinese solar greenhouses for non-arable lands. Solar Energy. 190, 561-575. https://doi.org/10.1016/j.solener.2019.08.056.

Zhao, C.J., Li, M., Yang, X.T., Sun, C.H., Qian, J.P., Ji, Z.T., 2011. A data-driven model simulating primary infection probabilities of cucumber downy mildew for use in early warning systems in solar greenhouses. Computers and Electronics in Agriculture. 76 (2), 306-315. https://doi.org/10.1016/j.compag.2011.02.009.